The missing lnc:

long noncoding RNAs in neuroblast migration

A thesis submitted to the Department of Physiology, Anatomy and Genetics, in partial fulfilment of the requirements for the degree of

Doctor of Philosophy

By

Jemima Becker

Merton College, University of Oxford, United Kingdom

Michaelmas Term, 2025

Abstract

The Ventricular Subventricular Zone (V-SVZ) is the largest postnatal stem cell niche in the mammalian brain, it continuously generates Olfactory Bulb (OB) interneurons, but can also act as a source of glioblastomas. While there is a wealth of information regarding V-SVZ neural stem cell (NSC) proliferation, there is a relative dearth regarding how V-SVZ derived precursors migrate to their final destination. The site of maturation of V-SVZ derived progenitors is in the OB, therefore newly generated cells cannot function if they cannot migrate.

Long noncoding RNAs (lncRNAs) are RNA molecules that are greater than 200nt in length with minimal protein coding capacity. A large number of lncRNAs are specifically expressed in the V-SVZ. By comparing V-SVZ scRNAseq I found striking inconsistencies in methodology and reporting between studies. Despite these differences, trends in lncRNA expression in the V-SVZ were observed, which I analysed in a semi-quantitative manner and found several candidate lncRNAs for regulation of V-SVZ neurogenesis.

The lncRNA *2610307P16Rik* (also known as Cancer susceptibility 15, *Casc15*), is unusually well-conserved and is highly expressed in migratory V-SVZ neuroblasts. Through a combination of *in vitro* and *in vivo* studies I found that *Casc15* is a powerful regulator of neuroblast migration. However, OB interneurons that were depleted of *Casc15* exhibited defects in polarity, location, and structure. Unexpectedly, our transcriptomics revealed significant changes in a swathe of genes regulating cholesterol biogenesis.

In order to interrogate potential molecular mechanisms of *Casc15* on migration I focused on genes associated with cholesterol biosynthesis, as well as the upstream mevalonate pathway. I

found an inverse relationship between *Casc15* expression and the expression of *Srebp2*, the master regulator of cholesterol biosynthesis. RNA-immunoprecipitation (RIP) and chromatin immunoprecipitation (ChIP) revealed that *Casc15* physically interacts with the Polycomb Repressive Complex 2 (PRC2) and that PRC2 repressive activity at the *Srebp2* promoter is lost upon *Casc15* depletion. These data lead to the development of a novel circular mechanism in which *Casc15* regulates mevalonate and cholesterol pathway genes, and is in turn regulated by the product of the mevalonate pathway.

lncRNAs are frequently dismissed as transcriptional noise or even genomic "junk", but the profound migratory and metabolic changes observed upon loss of *Casc15* suggest that this is far from the truth.

Acknowledgements

I would like to first thank Dr Francis Szele, my primary DPhil supervisor. Francis has been a fantastic mentor and friend over the past four years, and has indulged my imagination and speculations, whilst simultaneously bringing me back to reality and helping refine my ideas.

I am grateful to all members of the Szele lab – particularly my fellow DPhil students Jun Ong and Mona Barkat, for their friendship and comradery, as well as support when experiments do (and don't) work. I am incredibly grateful to Ruby Mullens and Talia Vasaturo-Kolodner for their diligence and hard work in quantifying hundreds of near-identical green cells. I am also grateful for Professor Zoltan Molnar for his support.

I am very thankful to Dr Bin Sun for his support and expertise with electroporation, and for providing me with such a comprehensive catalogue of brains to work with.

I would like to thank Dr Martin Ducker, Dr Mega Suresh, Dr Luana Campos-Soares, and Dr Farah Alammari for their training and sharing of protocols and knowledge. Farah in particular, has been an invaluable support during the early stages of my DPhil, and helped me learn all of the fundamental techniques used in this project. Thank you greatly to Alan Tilley and Pete Appleford for their apparently bottomless patience when it comes to microscope (dys)function. I am also thankful for Angela Curran, Agata Stramek, Laura Thomas, and the whole BSB team for helping me care for my animals and supporting my experiments.

I am grateful for my collaborators, Dr Keith Vance, Dr Wilfried Haerty, and Professor Hiroko Isoda for their continued advice and feedback on my data over the last four years.

My research has only been possible due to the generous sponsorship of Hamish Magoffin and the Pranaiya and Arthur Magoffin foundation. I am deeply grateful to Hamish for granting me this opportunity, for his kind discussion and willingness to discuss research at any time of day.

Finally, I would like to thank my family and friends, who have supported me through every step of my DPhil, listening to every frustration and celebrating every success. To my dad, for whisking me away to the woods when I had had too much of the lab, my mum for bringing tea and hugs when experiments go awry. I am lucky to have my wonderful friends, Ab, Imi, Emily, and Robin who kidnap me to the pub when experiments have been running for too long. I am thankful for my sister Flora, who I am infinitely proud of, for letting me ring her with ridiculous ideas at all hours of the night. And finally, thank you to my wonderful partner Holly for her love, support, and sanity during this process.

Authorship statement

Unless otherwise specified, I performed all experiments, with advice and support from Assoc Prof Francis Szele when designing experiments.

Dr Bin Sun designed and electroporated the CRISPRi constructs used in Chapter 4, he dissected and sectioned these brains. I performed all further immunohistochemical studies and analyses using these brains. Dr Sun additionally validated the ASO knockdown constructs used in figures 4.2 and 5.3. Native RNA-IP and ChIP (Figure 5.3) was performed by Dr Sun, although I performed subsequent qPCR after immunoprecipitation (Figure 5.3, B).

In Chapter 4, **Ruby Mullens**, Biochemistry part II student, and **Talia Vasaturo-Kolodne**r, DPhil student, assisted with quantification of GFP+ cells in the OB after I had captured images.

Dr Michael Shapiro performed the alignment, pre-processing, and initial differential gene expression analysis of the bulk RNAseq data described in Figures 4.2 and 5.2.

Dr Kazunori Sasaki designed the experiments investigating RME described in Appendix 1, and performed administration of treatment and behavioural tests.

Dr Farah Alammari designed and performed the knockdowns of Paupar and Kap1 described in Appendix 3. I performed gene ontology and pathway analyses of raw data supplied by Novogene following bulk RNAseq.

All other experimental procedures, quantifications, and analyses were performed by myself, with the advice of colleagues and collaborators.

A note on statistics

For clarity, all descriptive statistics and the results of statistical tests have been reported in full in Tables 3.1 (for Chapter 3), 4.1 (for Chapter 4), 5.1 (for Chapter 5), A.1 (for Appendices) rather than in the body of the text or Figure legends. Each table corresponds to a specified results chapter, and the figures and Figure panels that each test describes are indicated. Significance is illustrated on graphs using the same scheme of $p>0.05$ (ns), $p<0.05$ (*), $p<0.01$ (**), $p<0.001$, $p<0.0001$ (****) in all figures.

List of Figures

Chapter 1: Introduction

Figure number	Content	Page
1.1	Gross anatomy of the V-SZ, RMS, and OB	3
1.2	Cytoarchitecture and lineage markers of the V-SVZ	5
1.3	Myriad roles of lncRNAs	16
1.4	lncRNA and PRC2	18
1.5	Schematic overview of the mevalonate pathway	22
1.6	Cholesterol production in the brain	25
1.7	Prenylation complexes and targets	29

Chapter 2: Materials and methods

Figure number	Content	Page
2.1	Anatomy for dissection	40
2.2	Schematic overview of the spheroid migration assay	43
2.3	Schematic overview of the explant migration assay	44
2.4	CRISPRi electroporation	46

Chapter 3: lncRNAs in the V-SVZ

Figure number	Content	Page
3.1	Overview of single cell sequencing	53
3.2	Developmental origins of the V-SVZ	56
3.3	Cumulative occurrences versus cell type	59
3.4	lncRNA in the aging V-SVZ	63
3.5	*Casc15* lncRNA in the V-SVZ	66
3.6	*Casc15* distribution in the whole mouse brain	67

Chapter 4: *Casc15* lncRNA and migration

Figure number	Content	Page
4.1	Aberrations in *Casc15* expression regulate cancer cell migration	73
4.2	*Casc15* regulates migration genes *in vitro*	78
4.3	Knockdown of *Casc15* increases the size of RMS spheroids	80
4.4	Effect of *Casc15* knockdown on an *ex vivo* explant assay	82

4.5	*In vivo* knockdown of *Casc15* increases cell density in the olfactory bulb	84
4.6	Knockdown of *Casc15* does not give rise to an overt V-SVZ phenotype	86
4.7	*Casc15* knockdown increases distance migrated by cells in the striatum	88
4.8	Knockdown of *Casc15* does not significantly alter proliferation in the V-SVZ or OB at 4 days post electroporation	91
4.9	Knockdown of *Casc15* does not significantly alter cell death in the V-SVZ or OB at 4 days post electroporation	92
4.10	Knockdown of *Casc15* causes GCL interneurons to show a misoriented morphology	94
4.11	*Casc15* knockdown causes an increase in cells maturing outside of the GL and GCL	96
4.12	*Casc15* knockdown causes truncation of GCL interneuron primary dendrites	97
4.13	*Casc15* CRISPRi knockdown does not alter dendritic spine density in the OB at 14dpe	99
4.14	A model for the generation of abnormal interneurons	113

Chapter 5: *Casc15* lncRNA and metabolism

Figure number	Content	Page
5.1	Pharmacological inhibitors of the mevalonate pathway and prenylation pathways	118
5.2	Further transcriptional effects of *Casc15* knockdown	122
5.3	*Casc15* interacts with PRC2 at the Srebp2 locus	126
5.4	Effects of simvastatin on neuroblast assays	129
5.5	Effect of modulating squalene synthesis and availability on an explant assay	131
5.6	Effect of prenylation inhibitors on an explant assay	134
5.7	Effect of a high dose prenylation inhibitor on neuroblast morphology	136
5.8	A possible mechanism of *Casc15* action	143

Chapter 6: Discussion

Figure number	Content	Page
6.1	Schematic for a *Casc15* conditional knockout mouse	146

Appendices

Figure number	Content	Page
A1.1	Effect of rosemary extract on Morris water maze test	162
A1.2	Effect of rosemary extract on cytogenesis in the SGZ	164
A2.1	Schematic for investigation in postpartum animals	166
A2.2	Impact of pregnancy on neural stem cells in the SGZ	167
A2.3	Impact of pregnancy in neurogenesis in the SGZ	168
A3.1	Transcriptional analysis of Paupar and Kap1 knockdowns	171
A4.1	A refined approach to drug administration	174
A4.2	Effect of simvastatin administration on grooming and social behaviour in female mice	175

List of Tables

Chapter 1: Introduction

Table	Description
Table 1.1	Evidence for prenylation of different GTPases

Chapter 2: Materials and methods

Table	Description
Table 2.1	Primers used for qPCR
Table 2.2	List of antibodies used
Table 2.3	Buffer recipes for CHIP-qPCR
Table 2.4	Ingredients list for key solutions
Table 2.5	Sequences of *Casc15* knockdown constructs

Chapter 3: lncRNAs in the V-SVZ

Table	Description
Table 3.1	**Descriptive statistics and test results**
Table 3.2	Features of scRNAseq papers in the V-SVZ
Table 3.3	lncRNA with CO>=4 in NSCs, TAPs, and Nbs
Table 3.4	lncRNA that accumulate in qNSCs in the aging V-SVZ
Table 3.5	Transcription factors with binding sites overrepresented in the promoters of lncRNAs in Table 3.4
Table 3.6	Indirect gene ontology - transcription factor ontologies

Chapter 4: *Casc15* lncRNA and migration

Table	Description
Table 4.1	**Descriptive statistics and test results**
Table 4.2	*Casc15* and Cancer cell migration literature search
Table 4.3	Differentially expressed genes
Table 4.4	Gene Ontology Analysis

Chapter 5: *Casc15* lncRNA and metabolism

Table	Description
Table 5.1	**Descriptive statistics and test results**
Table 5.2	Enzyme inhibitors used in this study

Table 5.3	IPA analysis
Table 5.4	Upstream regulator analysis

Appendices

Table	Description
Table A.1	**Descriptive statistics and test results**
Table A.2	Kap1 knockdown differentially expressed genes
Table A.3	Kap1 knockdown gene ontology
Table A.4	Kap1 knockdown pathway analysis
Table A.5	Kap1 knockdown predicted upstream regulators
Table A.6	Paupar knockdown differentially expressed genes
Table A.7	Paupar knockdown gene ontology
Table A.8	Paupar pathway analysis

Abbreviations

Abbreviation	Definition
3P	3-Photon
AD	Alzheimer's Disease
ASO	Antisense Oligonucleotide
BDNF	Brain derived neurotrophic factor
BLAST	Basic Local Alignment Search Tool
BP	Biological process
Bv	Blood Vessel
CAM	Cell Adhesion Molecule
Casc15	Cancer Susceptibility Candidate 15
CC	Corpus Callosum
ChIP	Chromatin Immunoprecipitation
CNS	Central Nervous System
CO	Cumulative Occurrences
CP	Choroid Plexus
CRISPR (i)	CRISPR inhibition
CSF	Cerebrospinal Fluid
dCas9	dead (catalytically inactive) Cas9
DEG	Differentially expressed gene
DMSO	Dimethyl Sulphoxide
dpe	Days post electroporation
E	Ependymal cell
E (e.g. E10.5)	Embryonic day (E.g. Embryonic day 10.5)
ECM	Extracellular Matrix
ECT	Electroconvulsive Therapy
EGF	Epidermal Growth Factor
EZ	Ependymal Zone
FACS	Fluorescence Activated Cell Sorting
FDR	False Discovery Rate
FGF	Fibroblast Growth Factor
FTase	Farnesyl Transferase
FTI	Farnesyl Transferase Inhibitor
GABA	Gamma-Aminobutyric Acid
GBM	Glioma/Glioblastoma Multiforme
GCL	Granule Cell Layer
GFP	Green Fluorescent Protein
GGTase	Geranylgeranyl Transferase
GGTI	GeranylGeranyl Transferase Inhibitor
GL	Glomerular Layer

GO	Gene Ontology
GWAS	Genome Wide Association Study
HBSS	Hank's Balanced Salt Solution
HMT	Histone Methyltransferase
IP	Immunoprecipitation
IPA	Ingenuity Pathway Analysis
IPL	Inner Plexiform Layer
ISH	In situ hybridisation
KD	Knockdown
KO	Knockout
LGE	Lateral Ganglionic Eminence
lncRNA	Long noncoding RNA
LV	Lateral Ventricle
MC	Mitral Cell
MCL	Mitral Cell Layer
Mg	Microglia
MGE	Medial Ganglionic Eminence
MWM	Morris Water Maze
Nb	Neuroblast
NBA+	Neurobasal A+
NCAM	Neural Cell Adhesion Molecule
NHS	National Health Service
NSC	Neural Stem Cell
NSPC	Neural Stem/Progenitor Cell
OB	Olfactory Bulb
OE	Over-Expression
ONL	Olfactory Nerve Layer
ONP	Oxford nanopore
OPL	Outer Plexiform Layer
P (e.g. P4)	Postnatal day (e.g. Postnatal day 4)
PCA	Principle Component Analysis
PGC	Periglomerular Cell
Pol-II	RNA Polymerase II
PRC2	Polycomb Repressive Complex 2
PSA	Polysialic Acid
PSA-NCAM	Polysialated Neural Cell Adhesion Molecule
qPCR	Quantitative PCR
RGL	Radial Glia-Like
RIP	RNA immunoprecipitation
RME	Rosemary Extract
RMS	Rostral Migratory Stream
RT	Room temperature

RT-qPCR	Reverse Transcription-quantitative Polymerase Chain Reaction
SAMP8	Senescence accelerated mouse prone 8
SAMR1	Senescence accelerated mouse resistant 1
scRNAseq	Single cell RNA sequencing
Sep	Septum
SEZ	Subependymal Zone (aka V-SVZ, SVZ)
SGZ	Subgranular Zone
SMRT	Single molecule real-time
SNPs	Single nucleotide polymorphisms
snRNAseq	Single nucleus RNA sequencing
Sp	Subpallium
SQSD	Squalene synthase deficiency
SRE	Sterol response element
SSRI	Selective Serotonin Reuptake Inhibitor
Str	Striatum
SVZ	Subventricular Zone (aka V-SVZ, SEZ)
TAC	Transit Amplifying Cell (aka TAP)
TAP	Transit Amplifying Progenitor (aka TAC)
TBI	Traumatic Brain Injury
TC	Tufted cell
tdTom	tdTomato
TF	Transcription Factor
UMAP	Uniform Manifold Approximation and Projection
V-SVZ	Ventricular-Subventricular Zone (aka SVZ, SEZ)
VZ	Ventricular Zone

Table of Contents

Abstract ..... *i*

Acknowledgements ..... *iii*

Authorship statement ..... *v*

A note on statistics ..... *vii*

List of Figures ..... *viii*

List of Tables ..... *xi*

Abbreviations ..... *xiii*

Chapter 1: Introduction *1*

1.1 Introduction to the V-SVZ and postnatal neurogenesis **1**

1.1.i Postnatal and adult neurogenesis from the V-SVZ 1

1.1.ii Adult neurogenesis in health and disease 6

1.1.iii Mechanisms of neuroblast migration 7

1.2 Long-noncoding RNAs **11**

1.2.i Conservation and expression 12

1.2.ii General characteristics and types of mechanism 13

1.3 Mevalonate pathway and cholesterol biosynthesis **19**

1.3.i Mevalonate pathway layout 19

1.3.ii Cholesterol biosynthesis in the brain 23

1.3.iii Prenylation pathway 26

1.4 Investigating the missing link between the V-SVZ, cholesterol, and lncRNA **30**

Chapter 2: Materials and Methods *32*

2.1 Computational work **32**

2.1.i Graphs and figures 32
2.1.ii Qualitative meta-analysis 32
2.1.iii Bulk RNAseq 34
2.2 Molecular Techniques 35
2.2.i RNA extraction 35
2.2.ii cDNA synthesis 36
2.2.iii RT-qPCR 36
2.2.iv ChIP-qPCR 37
2.3 *In vitro* and *ex vivo* models 39
2.3.i Neurosphere assay 39
2.3.ii Spheroid migration assay 41
2.3.iii Explant migration assay 43
2.4 *In vivo* work 45
2.4.i Electroporation 45
2.5 Immunohistochemistry 47
2.5.i In free floating sections 47
2.5.ii *In vitro* 48
2.6 Imaging and image analysis 49
2.6.i Epifluorescent imaging 49
2.6.ii Brightfield imaging 49
2.6.iii Live imaging 49
2.6.iv Quantification and analysis 49
Chapter 3: lncRNAs in the V-SVZ 51
3.1 Introduction 51
3.1.i Overview 51
3.1.ii scRNAseq techniques 51

3.1.iii Patterns of lncRNA expression 53

3.1.iv V-SVZ heterogeneity 55

3.2 Results 56

3.2.i There is limited consistency in methodology between studies 56

3.2.ii Many studies show consistent enrichment patterns of lncRNA expression 57

3.2.iii lncRNAs abound in the V-SVZ 59

3.2.iv Indirect gene ontology analysis of lncRNA expression in the ageing V-SVZ 60

3.2.v *Casc15* lncRNA is enriched in neural progenitors 63

3.3 Discussion 67

3.3.i How far can we rely on aggregate lncRNA expression data? 67

3.3.ii Cell type specific enrichment does not confer function 68

3.3.iii lncRNA in the ageing V-SVZ 68

3.3.iv *Casc15* is poised to regulate neurogenesis 69

3.4 Conclusions 70

Chapter 4: Casc15 lncRNA and Migration 71

4.1 Introduction 71

4.1.i Long noncoding RNA in migration and metastasis 71

4.1.ii *Casc15* lncRNA 71

4.1.iii Migration assays 74

4.2 Results 75

4.2.i *Casc15* regulates migration genes *in vitro* 75

4.2.ii Knockdown of *Casc15* increases the size of RMS spheroids 79

4.2.iii *Casc15* suppresses migration of neuroblasts *ex vivo* 80

4.2.iv *Casc15* supresses neurogenesis *in vivo* 83

4.2.iv *Casc15* knockdown does not give rise to an overt V-SVZ phenotype *in vivo* 84

4.2.v *Casc15* knockdown *in vivo* noes not significantly alter proliferation or cell death 88

4.2.vii *Casc15* modulates the orientation of newborn OB interneurons *in vivo* 92

4.2.vi *Casc15* modulates the location of mature newborn OB interneurons *in vivo* 94

4.2.viii *Casc15* modulates the structure of newborn OB interneurons *in vivo* 97

4.2.ix *Casc15* knockdown does not impact dendritic spine density in the OB 98

4.3 Discussion 100

4.3.i Transcriptional changes upon *Casc15* depletion 100

4.3.ii *Casc15* lncRNA restrains V-SVZ neurogenesis 102

4.3.iii *Casc15* lncRNA knockdown does not give rise to an overt V-SVZ phenotype 108

4.3.iv Structural defects 109

4.4 Conclusions 114

Chapter 5: Casc15 lncRNA and metabolism 115

5.1 Introduction 115

5.1.i lncRNA in metabolic regulation 115

5.1.ii Prenylation 115

5.1.iii Pharmacological inhibitors of mevalonate and prenylation enzymes 115

5.2 Results 119

5.2.i *Casc15* regulates mevalonate pathway genes *in vitro* 119

5.2.ii *Casc15* interacts with PRC2 to target the *Srebp2* locus 123

5.2.iii Effect inhibiting of HMGCR on neuroblast assays 127

5.2.iv Effect of modulating squalene synthesis and availability on RMS explants 129

5.2.v Effect of modulating prenylation on RMS explants 131

5.3 Discussion 137

5.3.i Transcriptional impact of *Casc15* depletion 137

5.3.ii PRC2 targeting to the *Srebp2* locus 139

5.3.iii Blocking with statins 140

5.3.iv Modulation of squalene synthesis and availability 140

5.3.v Modulation of prenylation 141

5.4 Conclusion 142

5.4.i Model 142

Chapter 6: Discussion 144

6.1 Overview 144

6.1.i lncRNAs in the V-SVZ 144

6.1.ii *Casc15* lncRNA and migration 147

6.1.iii *Casc15* lncRNA and metabolism 150

6.2 Limitations 152

6.2.i Technical 152

6.2.ii Species 154

6.3 Future directions 154

6.3.i Mouse functional outcomes 154

6.3ii Long term survival of newborn neurons 157

6.3.iii *CASC15* in the human brain 157

6.3.ii Cholesterol and metabolomics 158

6.3 Final overview 158

Appendices 160

Appendix 1: Nutraceuticals and cytogenesis in a model of Alzheimer's Disease 160

Appendix 2: Impact of pregnancy on hippocampal neurogenesis 165

Appendix 3: *Paupar* lncRNA and KAP1 regulation of the V-SVZ 169

Appendix 4: Refined animal handling for administration of simvastatin 172

References 176

Chapter 1: Introduction

1.1 Introduction to the V-SVZ and postnatal neurogenesis

1.1.i Postnatal and adult neurogenesis from the V-SVZ

The ventricular subventricular zone (V-SVZ), alternatively known as the subventricular zone (SVZ) and subependymal zone (SEZ) is the largest postnatal stem cell niche in the mammalian brain (Alvarez-Buylla and García-Verdugo, 2002). It's homeostatic role is in the continuous production of new GABAergic interneurons in the olfactory bulb (OB). These interneurons contribute to olfactory learning and plasticity in rodents, as well as social and maternal behaviour (Breton-Provencher et al., 2009; Chaker et al., 2023; Feierstein et al., 2010). The V-SVZ is also an accessible and robust system with which to investigate principles and mechanisms of brain development and plasticity.

Neurogenesis also occurs in the subgranular zone (SGZ), located in the hippocampal dentate gyrus (DG) (Kempermann et al., 2015).

Gross anatomy of the V-SVZ

The V-SVZ is a thin layer of cells lining the lateral ventricles, with conserved anatomical location between mouse (Figure 1.1, A) and human (Fig 1.1, B) (Sunkin et al., 2013). Neural progenitors are born in the V-SVZ (shown in pink in Fig 1.1), and migrate rostrally via the Rostral Migratory Stream (RMS) (Fig 1.1, C, illustrated in green) towards the Olfactory Bulb (OB) (Altman, 1969). Upon arrival at the OB, cells take a sharp turn and migrate radially from the RMS outwards. The majority of postnatally generated interneuron precursors derived from

the V-SVZ then differentiate with their cell body in the Granule Cell Layer (GCL) or Glomerular Layer (GL) of the olfactory bulb (Fig 1.1, D) (Altman, 1969).

GCL interneurons account for the majority (>95%) of cells generated from the postnatal rodent V-SVZ (Winner et al., 2002). These GABAergic interneurons form dendrodendritic synapses with lateral dendrites of Mitral Cells (MCs) and Tufted Cells (TCs), which are the primary output neurons and project to distinct regions of the olfactory cortex via the lateral olfactory tract (Shepherd et al., 2007; Zeppilli et al., 2021). GCL interneurons can be subdivided based on dendritic morphology, position within the GCL, as well as gene expression patterns (Takahashi et al., 2018). Alternatively, progenitors can migrate through the GCL, Inner Plexiform Layer (IPL), Mitral Cell Layer (MCL), and Outer Plexiform Layer (OPL), finishing their journey in the GL where they differentiate to form periglomerular cells (PGCs) (Figure 1.1, D). Like GCL interneurons, PGCs also form dendrodendritic synapses with excitatory MCs and TCs (Orona et al., 1984). A key difference between GCL and GL GABAergic interneurons is the point at which they make contact with excitatory output cells – GCL interneurons synapse with lateral dendritic projections in the external plexiform layer, whereas PGCs synapse within the olfactory glomeruli (Orona et al., 1984). There are multiple molecularly distinct subtypes of postnatally generated PGCs (Whitman and Greer, 2007).

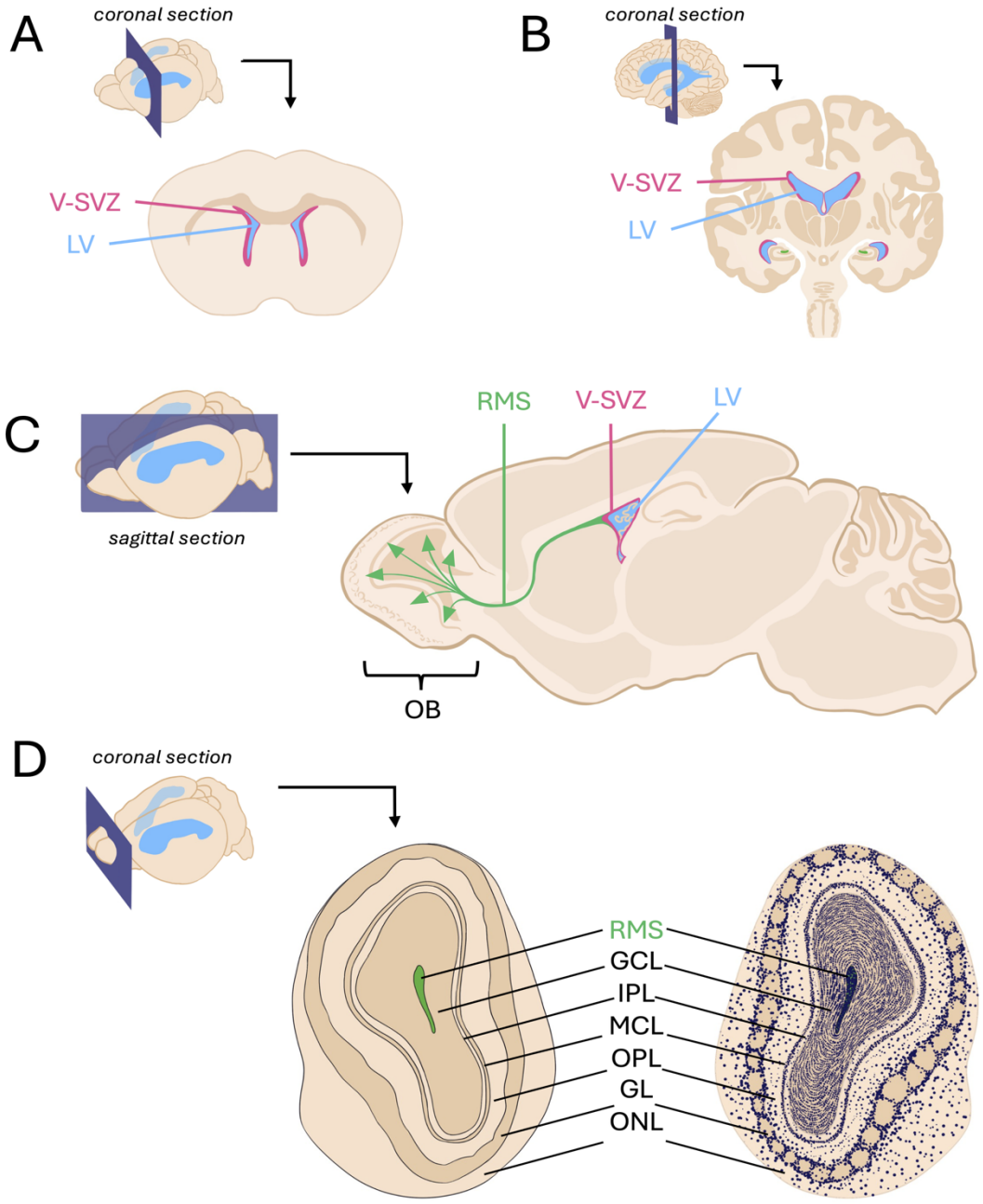

Figure 1.1 Gross Anatomy of the V-SVZ, RMS, and OB. ***A)*** *Mouse brain shown in coronal section to highlight LV (blue) and V-SVZ (pink).* ***B)*** *Human brain shown in coronal section to highlight LV (blue) and V-SVZ (pink).* ***C)*** *Mouse brain shown in sagittal section to highlight the RMS (green).* ***D)*** *Anatomy of the murine main OB with layers shown on the left and approximate nuclear densities on the right.*

Abbreviations: V-SVZ - Ventricular subventricular zone; LV – Lateral ventricles; RMS – Rostral migratory stream; GCL – Granule cell layer; IPL - Inner plexiform layer; MCL – Mitral cell layer; OPL – Outer plexiform layer; GL – Glomerular layer; ONL – Olfactory nerve layer. Illustrations drawn in Adobe Procreate. Not to scale.

On lineage progression in the V-SVZ

The V-SVZ has a characteristic cytoarchitecture, illustrated in Figure 1.2, A (Ihrie and Álvarez-Buylla, 2011). Neural stem cells (NSCs, or B cells) are Radial Glia-like (RGL) stem cells, which contact both the cerebrospinal fluid (CSF) in the lateral ventricles, as well as blood vessels (Doetsch et al., 1997, 1999; Ihrie and Álvarez-Buylla, 2011). These NSCs proliferate and give rise to Transit Amplifying Progenitor (TAPs, or C cells) which are able to proliferate and migrate locally (Doetsch et al., 1997). These differentiate to form Neuroblasts (Nbs, or A cells) which then migrate via the RMS to the OB, before differentiating into GABAergic interneurons. As illustrated in Fig1.2, A, the V-SVZ contains a large number of distinct cell types in a small spatial range (Ihrie and Álvarez-Buylla, 2011). When investigating the V-SVZ experimentally, state-specific protein markers are used to differentiate cell types (Fig1.2, B). Typically, markers are used in combination as there are no clear cell-type unique markers available (Mamber et al., 2013). These markers can be combined with analysis of cell morphology to distinguish cell-types.

Proliferation of NSCs in the V-SVZ can be regulated by a plethora of inputs. The V-SVZ is highly vascularised and NSCs make contact with both CSF of the lateral ventricles as well as with local blood vessels, allowing integration of a large number of cues. For example, dopaminergic signalling at the border between the striatum and the V-SVZ can promote proliferation of NSCs in both rodents and primates (Freundlieb et al., 2006; O'Keeffe et al., 2009). In addition, growth factors such as brain derived neurotrophic factor (BDNF), epidermal growth factor (EGF), and fibroblast growth factor (FGF) all increase proliferation in the V-SVZ when continuously infused into the ventricles (Kuhn et al., 1997; Pencea et al., 2001).

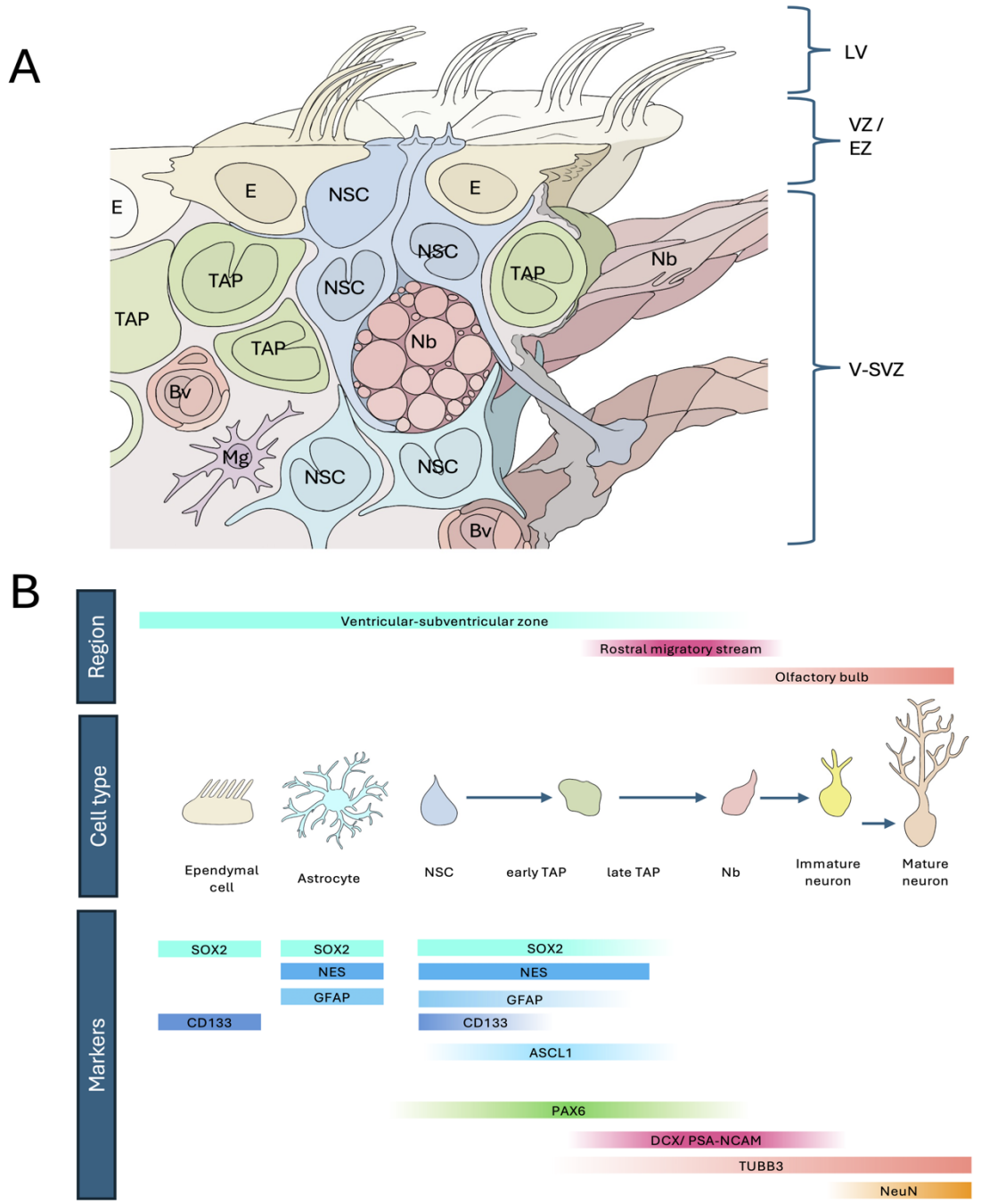

Figure 1.2 Cytoarchitecture and lineage markers of the V-SVZ. A) *Illustration of the cellular architecture of the V-SVZ, adapted with permission from Ihrie and Alvarez-Buylla (2011).* ***B)*** *Approximate expression of marker proteins in different cell types of the V-SVZ, RMS, and OB. Adapted with permission from Mamber et al (2013).*

Abbreviations: LV – Lateral ventricles; VZ – Ventricular zone; EZ – Rpendymal zone; V-SVZ – Ventricular subventricular zone; E – Ependymal cell; NSC – Neural stem cell; TAP – Transit amplifying progenitor; Nb – Neuroblast; Bv – Blood vessel; Mg – Microglia. Illustrations drawn in Adobe Procreate.

1.1.ii Adult neurogenesis in health and disease

Defects and alterations in V-SVZ neurogenesis have been found to contribute to- and ameliorate disease phenotypes.

In animal models of traumatic brain injury (TBI), proliferation in the V-SVZ increases rapidly (Szele and Chesselet, 1996). Some rodent studies have found that DCX+ cells from the V-SVZ are able to migrate to the region of injury, deviating from their usual course in the RMS (e.g. Miyamoto et al., 2025; Saha et al., 2013), while others have found no effect (e.g. Szele and Chesselet, 1996). The method and location of injury, and means of assessing migration differ significantly between studies, perhaps accounting for the differing results (Chang et al., 2016). Pharmacological interventions such as treatment with diterpenoids are able to improve V-SVZ response to injury and increase the number of mature NeuN+ neurons at the site of injury (Pardillo-Díaz et al., 2025).

Glioblastomas (GBM) are the most common form of adult brain cancers, associated with poor prognosis and a median survival of less than two years after diagnosis (Tan et al., 2020). It has been found that GBMs can be derived from cells in the human V-SVZ (Lee et al., 2018), and that glioblastomas that contact the V-SVZ may be more invasive than GBMs that originate in other brain regions (Lim et al., 2007). The role of the V-SVZ in GBM initiation has been illustrated in murine models carrying common GBM driver mutations such as alterations in the *Idh1* gene (Bardella et al., 2016). Principles of proliferation and migration in the brain could be investigated using the V-SVZ, and later applied to GBM treatments to limit metastasis.

V-SVZ neurogenesis has been found to be suppressed in rodent models of depression and chronic stress (e.g. Hitoshi et al., 2007; Lau et al., 2007). However, the effect of typical

interventions for depression on V-SVZ neurogenesis varies. This may be context dependent – Ohira et al (2011) found that the Selective Serotonin Reuptake Inhibitor (SSRI) fluoxetine suppressed proliferation in the V-SVZ of rats in the absence of any other interventions; whereas in stroke models fluoxetine increases neurogenesis (Ohira and Miyakawa, 2011; Sun et al., 2015). Other interventions such as physical exercise and electroconvulsive therapy (ECT) have been found to promote neurogenesis in the V-SVZ, but similarly to fluoxetine, further clarity is needed in disease contexts (Inta et al., 2013; Luo et al., 2014).

1.1.iii Mechanisms of neuroblast migration

"Neurogenesis" encompasses multiple stages and processes, from the division of a stem cell in the V-SVZ to neuroblast migration through the RMS and finally their differentiation in the OB. Much study of V-SVZ neurogenesis for therapeutic applications has focussed on harnessing the self-renewal properties of stem cells in order to generate more neurons. However, these cells mature and integrate into neural circuits far from their original birthplace. In order to harness the full therapeutic potential of V-SVZ neurogenesis, we need to be able to understand and exogenously regulate neuroblast migration.

Guiding neuroblasts to the OB

Neuroblasts derived from the V-SVZ migrate via the RMS to the OB. This migration is guided by chemorepellent, chemoattractant, and cell intrinsic cues. While the V-SVZ itself does not secrete repulsive cues, juxtaposition of explants from the V-SVZ with other brain regions has revealed that the septum and choroid plexus (CP) secrete chemorepulsive factors (Hu, 1999; Hu and Rutishauser, 1996). The chemorepulsive nature of the CP is dependent on secretion of SLIT2, ligand for the ROBO receptor (Hu, 1999). Interestingly, the OB itself is dispensable for migration of neuroblasts along the RMS. Kirschenbaum and colleagues found that after surgical removal of the OB, neuroblasts continued to migrate along the RMS and accumulated

at the point where they would typically enter the OB – suggesting that migration via this route is not determined by a chemoattractant secreted from the OB (Kirschenbaum et al., 1999). Furthermore, this gradient of chemorepellent from the septum/CP is conditional, highlighted by patterns of migration of cells from the V-SVZ through the corpus callosum and into the cortex upon brain injuries (Miyamoto et al., 2025). This exemplifies how cells can deviate from their typical routes of migration under conditions of disease or injury.

The RMS is dispersed through the walls of the lateral ventricles, cells then coalesce from the dorsal horn of the V-SVZ, where cells initially move ventrally before their route curves dorsally again (Fig 1.1, C) (Nam et al., 2007). This route and these features of neuroblast migration cannot be accounted for by a simple monomodal model of repulsion, suggesting that there are more regulatory features at play.

Another potential mechanism for guiding neuroblasts is via the extracellular matrix (ECM). Because the RMS is exceptionally dense in migrating cells, it may have a specialised ECM that could facilitate directed migration. The ECM can act as a regulator of migration by the localised accumulation of otherwise diffusible molecules that drive migration (Maeda, 2015). However, neuroblasts are able to migrate in the absence of the ECM, although without any particular direction – highlighted by the development of methods such as a spheroid assay of neuroblast migration, in which robust migration can be assessed after the enzymatic digestion of the ECM (Ducker et al., 2020a). Interactions between the ECM and neuroblasts are essential for neuroblast migration *in vivo*, highlighted by the impact of mutations in molecules that mediate these interactions (Mobley and McCarty, 2011). Furthermore, interactions between cells, mediated by cell adhesion molecules (CAMs), are essential for brain development and some have been extensively studied in the context of V-SVZ neuroblast migration. One key CAM is

neural cell adhesion molecule (NCAM) that has been modified by the posttranslational additional of polysialic acid (PSA) to form PSA-NCAM, frequently used as a marker of neuroblasts (see Fig 1.2, B). Knockout of *Ncam* has been found to reduce OB neurogenesis sufficiently to cause a decrease in the volume of the OB, an effect which is phenocopied by the enzymatic removal of the PSA moiety from NCAM (Cremer et al., 1994; Ono et al., 1994). Moreover, cortical injury induces PSA-NCAM expression, correlating with increases in neurogenesis (Szele and Chesselet, 1996).

Initially it was thought that RMS migration was dependent on ensheathing of the RMS by glial cells, or that cells were perhaps guided by radial glial fibres, but these ideas have been disproved (Kishi et al., 1990; Wichterle et al., 1997). Blood vessels are also able to guide migration, although this mechanism does not account for all features of neuroblast migration (Bovetti et al., 2007).

Neuroblast migration

Cells migrating from the V-SVZ to the OB have two phases of migration: the first phase is from the V-SVZ to the OB where cells migrate in chains, and the second is within the OB where cells detach from these chains and migrate radially through the layers of the OB to their final destinations in the GL or GCL (Lois and Alvarez-Buylla, 1994). While the net movement of cells is from the V-SVZ to the OB, some cells may change direction and turn back on themselves (Martinez-Molina et al., 2011). Within the RMS neuroblasts can adopt both bipolar and multipolar morphologies, and heterogeneous speeds of migration (Nam et al., 2007).

When these neuroblasts reach the OB they will disperse and shift towards a radial mode of migration, while little is understood about the transition from chain to radial migration in the

RMS/OB, some signals have been identified. One such signal is Reelin (encoded by the gene *Reln*), a large matrix glycoprotein which signals the switch between chain migration in the RMS to radial migration in the OB, although it does not act as a directional cue (Hack et al., 2002). Reelin was first identified through a spontaneously arising mutation which gave rise to mice with severe gait and balance defects – named "reeler" mice due to their characterising "reeling" gait (D'Arcangelo et al., 1995; Falconer, 1951). Homozygous *Reln*-/- mice show defects in OB morphology (Hack et al., 2002; Wyss et al., 1980), while their heterozygous counterparts *Reln*+/- show poor performance in olfactory discrimination tasks (Larson et al., 2003) – both of these phenotypes are characteristic of disrupted OB neurogenesis. Conversely, when *Reelin* is overexpressed, cells prematurely disperse and migrate radially out from the RMS (Courtès et al., 2011). While Reelin is undoubtedly important for OB neurogenesis, this is not its only role, illustrated by cases of lissencephaly in humans driven by mutations in the *RELN* gene (Hong et al., 2000). Human mutant phenotypes in combination with the broad neurological defects of the Reeler mice indicate that Reelin plays a broader role in brain development than simply regulating the shift from chain to radial migration in the RMS.

The features of RMS migration discussed here suggest that migration is a generic cell-intrinsic feature of neuroblasts, while the specificity and directionality of migration is a non-cell autonomous feature of V-SVZ neurogenesis. While there is some knowledge regarding the movement of cells on a molecular basis, there is a relative dearth concerning the specificity of migration. Migration of cells from the V-SVZ to the OB is incredibly specific, although this specificity is conditional – as illustrated by TBI case studies. It is likely that the route taken by V-SVZ derived neuroblasts is guided by all of the inputs discussed here, as well as many more that have yet to be identified.

There are many unresolved questions regarding the route of neuroblast migration, including: what determines which layer of the OB a neuroblast will differentiate in? What prevents neuroblasts from migrating into the cortex under "normal" conditions? The V-SVZ has multiple embryonic origins, do these diverse origins give rise to diverse neuroblasts in the adult?

1.2 Long-noncoding RNAs

A missing piece in our understanding of the overall process of V-SVZ neurogenesis may be the functions of long noncoding RNAs (lncRNAs). LncRNAs are a group of regulatory RNA molecules defined as being over 200 nucleotides in length and lacking significant protein coding capacity (Mattick et al., 2023). Due to the broadness of this definition, there are a range of functional molecules that can be classed as "lncRNA", these can be subcategorised by additional features such as genomic location or mechanism of action. Despite the human genome containing approximately 95,000 annotated lncRNAs, relatively little is known about their significance in development and disease compared to protein coding regions (Li et al., 2022). Candidate gene studies have highlighted that there are many lncRNAs which can regulate brain development and brain pathologies (Safari et al., 2019; Sauvageau et al., 2013). There are a large number of lncRNAs that are expressed with exceptionally high specificity in the V-SVZ, although little is known about their function in this context (Ramos et al., 2013a).

Ramos et al (2013) combined poly(A) enriched RNAseq data from the V-SVZ, OB, and dentate gyrus (DG) to identify lncRNA that were enriched in neural progenitors. They used an *ab initio* annotation approach, so that the data was not limited by what was already annotated in gene expression databases. This analysis revealed 8,992 lncRNAs expressed in the neurogenic

niches 2,108 of which were uniquely expressed in either the V-SVZ, OB, or DG. Many of the lncRNA identified by this study were completely novel and unannotated in any examined database (76.5% unannotated in RefSeq, 56.1% unannotated in UCSC, 40.9% unannotated in Ensembl). This data provides a broader view than candidate gene studies and tells us that there are a huge number of lncRNAs that are poised to regulate neurogenesis.

The overwhelming majority of well characterised lncRNAs are those generated by RNA Polymerase II (Pol-II), which closely resemble protein coding mRNA and feature 5' capping, splicing, and 3' polyadenylation (poly(A)) (Cabili et al., 2011). These features have allowed these Pol-II lncRNAs to be studied with greater ease, as many sequencing techniques enrich for poly(A) transcripts thus allowing lncRNAs to be studied in previously published datasets that focus on protein coding mRNAs. Some subclasses of lncRNA such as those encoded in intergenic regions are transcribed by Pol-II but are less commonly polyadenylated and spliced (Schlackow et al., 2017). lncRNAs can also be generated by the action of RNA polymerases I and III, although the study of these lncRNAs is relatively neglected (Mattick et al., 2023).

1.2.i Conservation and expression

lncRNAs are typically expressed at lower levels and with greater cell-type and tissue specificity on average than protein coding mRNAs (Derrien et al., 2012a), and have slightly shorter half-lives (Clark et al., 2012). For many lncRNAs, it can be hypothesised that overall structure and 3D folding underpins their function, rather than precise sequence; this is supported by the identification of structural motifs within lncRNA genes, as well as the observation that lncRNA function can be conserved even when the underlying DNA sequences are different (Hezroni et al., 2015). The combination of highly specific expression and shorter half-life makes lncRNAs very good drug targets. Targeting a lncRNA using siRNA, for example, may confer therapeutic

benefits with limited off-target effects when comparing to small molecule inhibitors of more broadly expressed proteins.

1.2.ii General characteristics and types of mechanism

Due to the nonspecific definition of a lncRNA there are a range of potential mechanisms that they can function through, and many lncRNAs act via multiple mechanisms, some of which are illustrated in Figure 1.3. The mechanisms of action can be broadly divided into transcription-dependent effects – i.e. the act of transcribing the lncRNA gene provides the function, rather than the RNA molecule itself; and transcript-dependent effects where function is conferred by physical interactions between the lncRNA and other molecules. It is possible for the same lncRNA to exert function through a combination of transcription- and transcript-dependent effects. lncRNAs can be found in both linear and circular forms, depending on alternative splicing and can have drastically different roles depending on which form is taken (Zhang et al., 2018, 2016).

The act of transcription alone

lncRNAs can act as transcriptional regulators for other genes not through the functional RNA, but through the act of being transcribed – termed transcriptional interference - which can be achieved is through competition for active RNA Pol-II complexes (Shuman, 2020). Many lncRNAs are encoded antisense to a protein coding gene, and high levels of transcription of the lncRNA can inhibit transcription of its protein coding counterpart by competing for Pol-II complexes. This is one of the mechanisms documented for the repressive action of the *Airn* lncRNA at the *Igf2r* locus, where high levels of *Airn* transcription limit Pol-II recruitment to the *Igf2r* promoter, thus suppressing its expression independently from the mature *Airn* transcript itself (Latos et al., 2012). Transcriptional interference has been suggested to underpin the function of many lncRNAs such as *Snhg14*, *Kcnq1ot1*, and *Nespas* (Mancini-DiNardo et

al., 2006; Meng et al., 2013; Tibbit et al., 2015). The importance of the act of transcribing a lncRNA is highlighted by patterns of conservation along lncRNA genes: on average, a lncRNA promoter is relatively highly conserved whereas the body of the gene is more divergent (Derrien et al., 2012a; Guttman et al., 2009).

lncRNA protein complexes

While transcriptional interference is likely a mechanism adopted by a large proportion of lncRNAs, it cannot account for all of their regulatory activities. lncRNAs are thought to fold in 3D to form complex and specific structures, and are able to interact with both proteins and RNA in the nucleus and cytoplasm (Chillón and Marcia, 2020). Such interactions can result in the targeted recruitment of transcription factors, such as the lncRNA *Paupar* which may recruit a complex of PAX6 and KAP1, facilitating changes in gene expression by bringing transcription factors and chromatin into close proximity (Pavlaki et al., 2018a; Vance et al., 2014). Beyond transcriptional regulation when associated with chromatin, lncRNA can also bind transcription factors and thus sequester them as is the case for the lncRNA *Gas5* which acts as a molecular decoy for the glucocorticoid receptor and prevents it from binding DNA (Kino et al., 2010).

lncRNA multiplexes with DNA

lncRNAs are able to contribute to the formation of- or recruitment of proteins to- several types of RNA:DNA multiplexes, namely R-loops (or heteroduplexes), RNA-DNA triplexes, and DNA-DNA G-quadruplexes (Leisegang et al., 2024). R-loops are a triple stranded nucleic acid structure comprised of an unannealed DNA strand and an RNA:DNA hybrid (Thomas et al., 1976), they can form in a variety of contexts and are associated with actively transcribed regions of chromatin although they can contribute to DNA damage (Aguilera and García-Muse,

2012). Through complimentary base pairing with single stranded DNA, lncRNAs can contribute to the formation and stabilisation of R-loops. The lncRNA *Tarid* forms an R-loop by hybridising to DNA at the *Tcf21* promoter, facilitating increased levels of *Tcf21* transcription via recruitment of DNA demethylases to this site (Arab et al., 2019). RNA-DNA triplexes can form when a single stranded lncRNA invades the DNA double helix to form a three-stranded structure, this can repress or activate genes in *cis* in a context-dependent manner. This is a known mechanism for several well conserved lncRNAs such as *Kcnq1ot1* and *Meg3*. In the case of *Meg3*, the lncRNA forms part of a triplex with a GA-rich DNA binding domain and recruits Polycomb Repressive Complex 2 (PRC2) to the site of triplex formation in order to repress targets of the TGF-beta signalling pathway (Mondal et al., 2015).

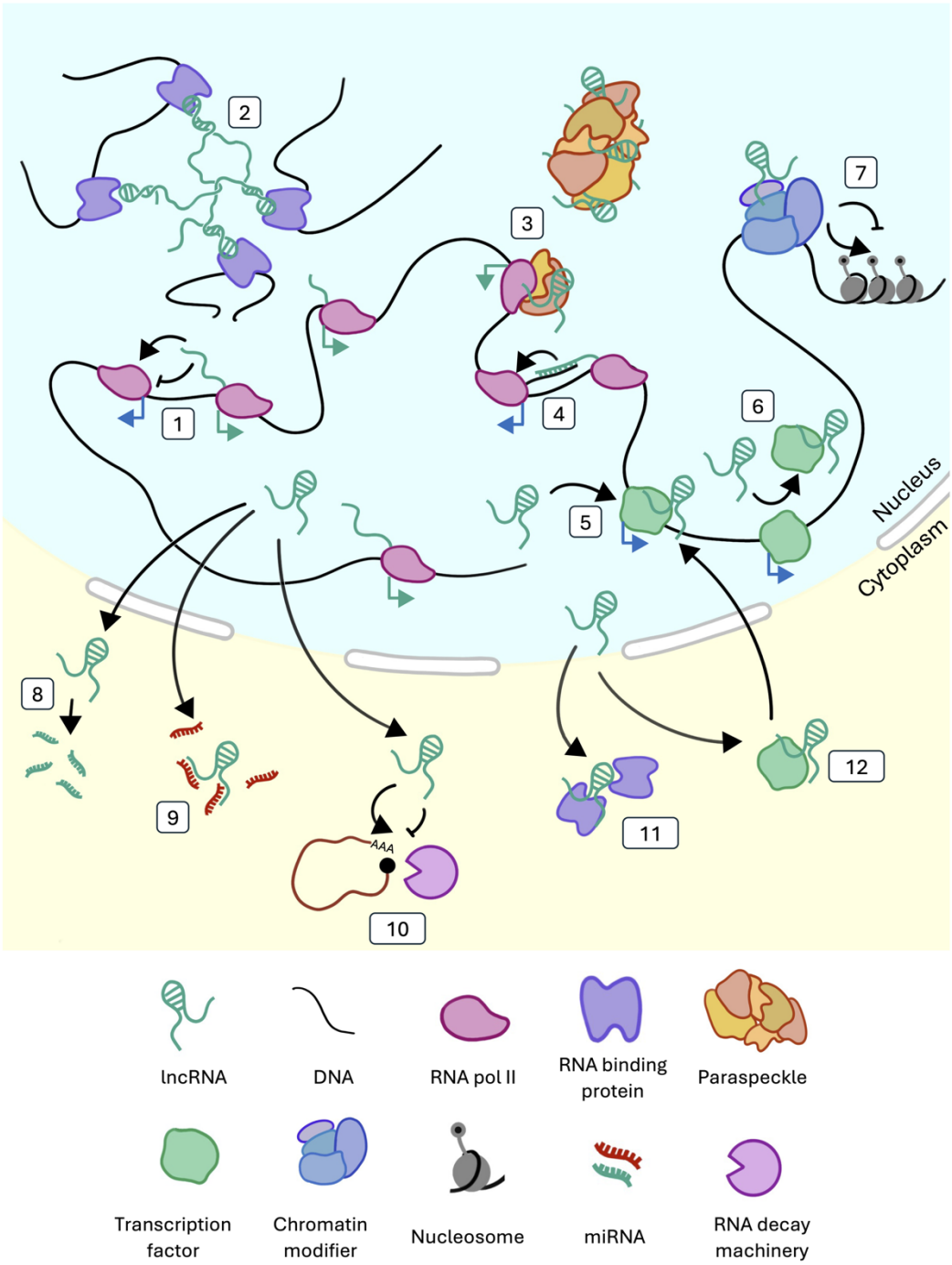

Figure 1.3 Myriad Roles of lncRNA*. Illustrated are a number of mechanisms that have been found for the ways in which lncRNAs act as molecular regulators.* ***1)*** *Transcriptional regulation such as regulation by transcriptional interference.* ***2)*** *Mediation of long range inter-chromosomal interactions.* ***3)*** *Formation of phase separated nuclear domains and paraspeckles.* ***4)*** *Formation of R-loops.* ***5)*** *As a guide for the recruitment od transcription factors.* ***6)*** *As a decoy for transcription factors.* ***7)*** *As a scaffold for the recruitment of chromatin modifiers.* ***8)*** *As a source of miRNAs.* ***9)*** *As a sponge for miRNAs.* ***10)*** *Modulating the rate of cytoplasmic mRNA decay.* ***11)*** *Regulating RNA binding protein sequestration.* ***12)*** *Regulating transcription factor localisation. Adapted with permission from Marchese et al (2017). Illustration drawn in Adobe Procreate.*

lncRNAs and PRC2

In a similar vein, lncRNAs can medicate changes in chromatin architecture by recruitment of epigenetic regulators to target sites in the genome: the interaction between lncRNAs and the polycomb repressive complex 2 (PRC2) has been illustrated with multiple lncRNAs in various cell types and developmental stages, and is a common mechanism of lncRNA action. This is thought to be achieved by a combination of lncRNA-protein interaction, and lncRNA-DNA interaction, thus bridging the gap between PRC2 and its target sites.

The Polycomb Repressive Complex 2 (PRC2) is a repressive epigenetic modifier. It deposits mono, di, or tri-methylation (Me1, Me2, Me3) on Lysine 27 (K27) of Histone protein H3, denoted H3K27Me1, H3K27Me2, or H3K27Me3. The core holoenzyme is composed of subunits Enhancer of Zeste 1/2 (EZH1/2), Embryonic Ectoderm Development (EED), and Suppressor of Zeste 12 (SUZ12), which is the minimal core that confers Histone Methyltransferase (HMT) activity. In addition to these core subunits, there are a number of facultative subunits that associate with the complex with varying stoichiometries such as Jumonji and AT-rich interactive domain 2 (JARID2) (Chammas et al., 2020). Different PRC2 components show different patterns of expression through the V-SVZ neurogenic lineage, data generated by Dr Bin Sun revealed that PRC2 enzyme EZH2 has restricted expression which is highest in DCX/PSA-NCAM + neuroblasts (Figure 1.4) (Sun et al., 2018).

Dysregulated interactions between lncRNAs and PRC2 can cause fundamental developmental failures, such as is the case lncRNA *Fendrr* whose loss causes embryonic lethality due to disrupted PRC2 activity (Grote et al., 2013). There are multiple proposed mechanisms as to exactly how lncRNAs are able to regulate PRC2 recruitment, such as acting as a molecular scaffold between DNA and PRC2 (Fig 1.4)

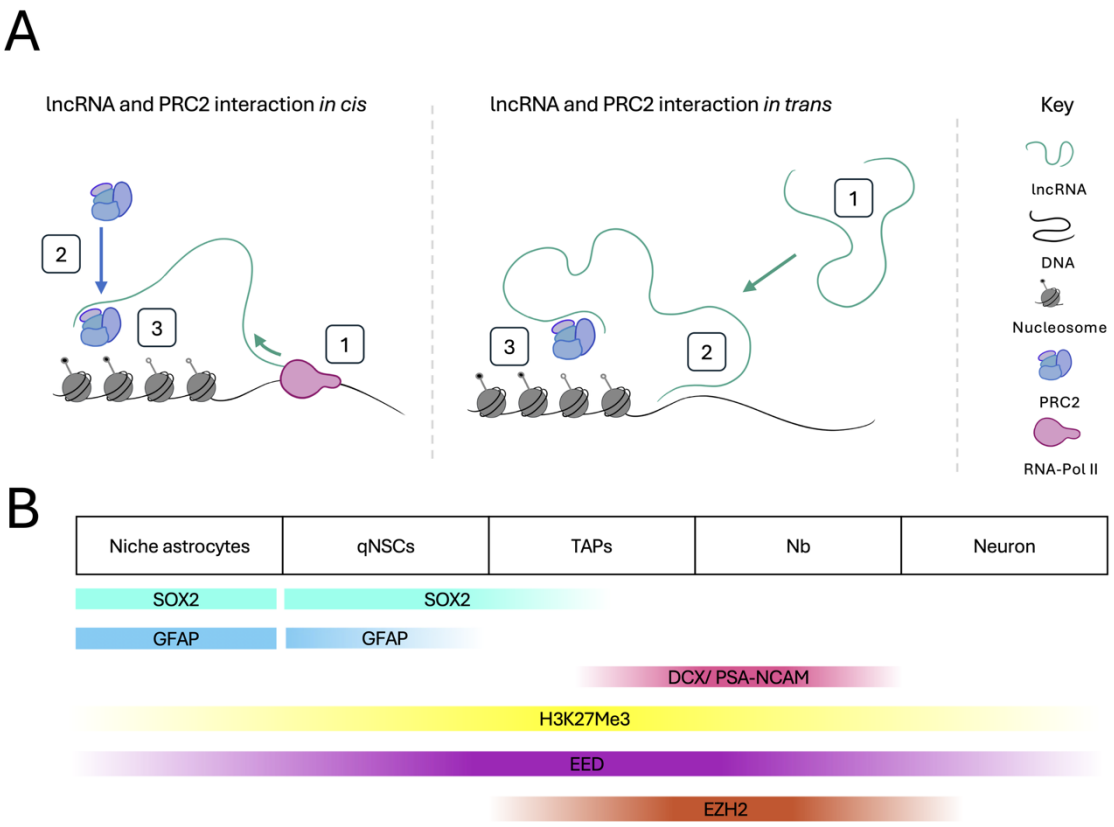

***Figure 1.4 lncRNAs and PRC2**. **A)** Illustration of potential cis and trans interactions of lncRNA and PRC2. In the left panel a lncRNA is transcribed at (1), and PRC2 interacts with the nascent lncRNA transcript at (2), bringing PRC2 into close proximity with the locus that is being transcribed from (3). Alternatively lncRNA and PRC2 can interact in trans, with the lncRNA transcribed elsewhere in the nucleus (1), but forms interactions at one end with DNA at (2), while the other end interacts with PRC2 (3), bringing it into close proximity with the locus where this lncRNA interacts with DNA. **B)** Distribution of expression of PRC2 subcomponents and neurogenic lineage markers, adapted from Sun et al (2018) with permission.*

Abbreviations: PRC2 – Polycomb Repressive Complex 2; qNCSs – Quiescent neural stem cells; TAPs – Transit amplifying progenitors; Nb – Neuroblast. Illustrations drawn in Adobe Procreate.

Structural roles

Some lncRNAs are additionally able to exert effects on the structural organisation of chromatin, such as in the looping of chromatin and in formation of phase-separated domains within the nucleus. A well-documented example is that of *Neat1*, which is an essential structural component for the formation of nuclear paraspeckles (Clemson et al., 2009; Wang et al., 2020).

lncRNA and interaction with other RNAs

Beyond chromatin modification there are many roles that can be played by lncRNA. Another mode of action that has been illustrated for multiple lncRNAs is binding of small RNAs – both miRNA and lncRNA are single stranded RNA molecules, and as such bind if they have complementary sequences, thus sequestering the miRNA and effectively neutralising it (Yan et al., 2020; Yao et al., 2020). A mature lncRNA transcript can also be processed to give rise to miRNA, such as *H19* giving rise to *miR-675* (Dey et al., 2014; Keniry et al., 2012).

lncRNAs are a poorly understood class of diverse regulatory molecules, many of which are highly expressed in the V-SVZ. While many may represent transcriptional noise, there are many lncRNAs that are poised to regulate V-SVZ neurogenesis and may represent novel therapeutic targets.

1.3 Mevalonate pathway and cholesterol biosynthesis

Another unanswered question in the V-SVZ is what is the role, if any, of cholesterol biosynthesis in neurogenesis?

1.3.i Mevalonate pathway layout

The mevalonate pathway (alternatively called the isoprenoid pathway or HMG-CoA reductase pathway) is a well-characterised metabolic pathway that generates the precursors for cholesterol and steroids, among others (Holstein and Hohl, 2004). This pathway is highly conserved and is fundamental in eukaryotes, archaea, and some bacteria (Lombard and Moreira, 2011). An overview of the pathway in Eukaryotes is illustrated in Figure 1.5, (Miziorko, 2011). Two Acetyl-CoA are condensed to acetoacetyl-CoA by acetyl-CoA acetyltransferase 1 /2 (ACAT1/2), which is then used by HMG-CoA synthase 1 /2

(HMGCS1/2) to generate HMC-CoA. 3-hydroxy-3-methylglutaryl coenzyme A reductase (HMGCR) next catalyses the conversion of HMG-CoA to mevalonic acid; this is the rate limiting step of this pathway and HMGCR is the target for statins, a class of cholesterol-lowering drugs (Hajar, 2011). Mevalonic acid is then used to generate isopentyl-5-PP via Mevalonate kinase (MVK) and phosphomevalonate kinase (PMVK). Isopentyl-5-PP can be reversibly isomerised by isopentenyl-diphosphate delta isomerase 1 / 2 (IDI1/2) to generate Dimethylallyl-PP. Downstream from Isopentyl-5-PP and dimethylallyl-PP, geranylgeranyl pyrophosphate synthase 1 (GGPS1) and Farnesyl disphosphate synthase (FDPS) generate Farnesyl-PP. Squalene synthase (SQS) then generates Squalene, the key precursor for cholesterol and steroids (Buhaescu and Izzedine, 2007; Miziorko, 2011). SQS represents the first committed and irreversible step towards cholesterol biosynthesis.

The expression of many enzymes of the mevalonate pathway are regulated by the transcription factor Sterol Regulatory Element-Binding Protein/Factor 2 (SREBP2 or SREBF2), including the rate limiting enzyme HMGCR (ENCODE Project Consortium, 2004; Horton et al., 2003). SREBP2 binds Sterol Responsive Elements (SREs) in the promoters of target genes to activate gene expression (Osborne et al., 1988; Südhof et al., 1987). In the pathway illustrated in Fig 1.5, SREBP2 targets are highlighted in red. Having a single master transcriptional regulator for a large number of enzymes, including the rate limiting enzyme HMGCR, allows efficient and coordinated regulation of the entire pathway.

The importance of this pathway in development can be highlighted by murine studies examining homozygous knockout (KO) animals. Global KO of the rate limiting enzyme *Hmgcr* is pre-implantation lethal in mice (Ohashi et al., 2003). KO of both *Mvk* and *Sqs* in mice are embryonic lethal, but at later stages of development than that of *Hmgcr* (Fig 1.5) (Horvat et al.,

2011). Loss of functional *SQS* in humans gives rise to the developmental disorder Squalene Synthase Deficiency (SQSD), characterised by neonatal onset seizures, characteristic craniofacial features, and profound global developmental delay (Coman et al., 2018). Thus far only three case studies have been reported: a pair of siblings and an unrelated child. In all three cases, hypoplasia of the corpus callosum and white matter loss were reported, as well as polymicrogyria in the unrelated patient (Coman et al., 2018). Notably, both polymicrogyria and corpus callosum hypoplasia are associated with defective cell migration and axon outgrowth in the developing brain (Kato, 2015; Raymond et al., 1995; Stutterd and Leventer, 2014).

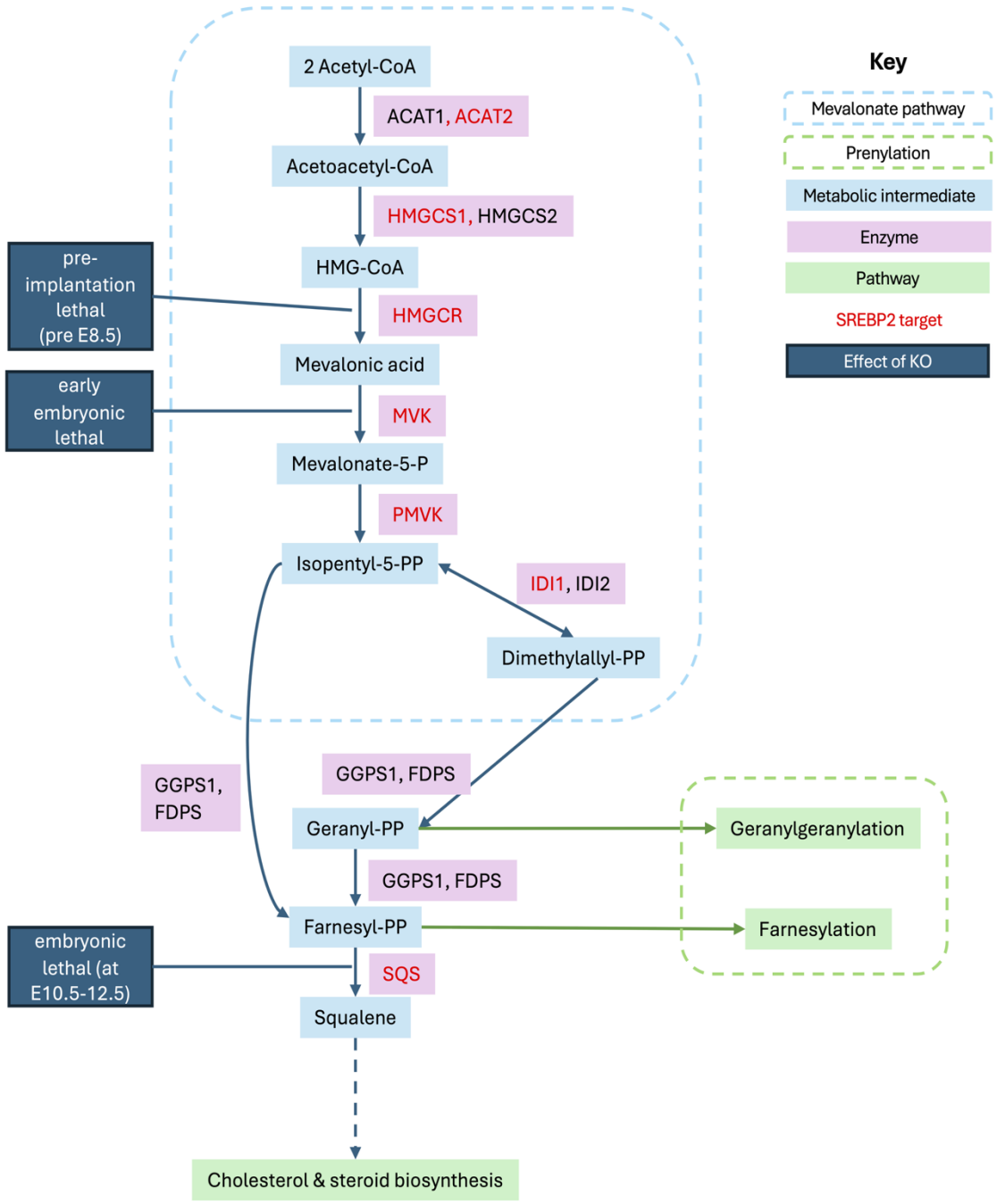

Figure 1.5 Schematic overview of the mevalonate pathway. *Pink boxes indicate enzymes and proteins; light blue boxes indicate metabolic intermediates; green boxes represent broad pathways and processes; red text shows enzymes that are directly regulated by SREBP2; and navy blue boxes indicate lethal mutant phenotypes in mouse models (Ohashi et al, J Biol Chem 2003).*

Abbreviations: KO - knockout; E (e.g. E10.5) – Embryonic day.

1.3.ii Cholesterol biosynthesis in the brain

Output from the mevalonate pathway is used for cholesterol biosynthesis and prenylation (Figure 1.5). Mammals contain two pools of cholesterol: peripheral (the body) and central (central nervous system). Despite accounting for only 2% of human body mass, the brain contains ~20% of the body's total cholesterol (Quan et al., 2003). Patterns of cholesterol concentration in the body appear to be conserved within mammals, with the highest concentration found in the brain, closely followed by the adrenal glands and lungs (Figure 1.6, A). The bulk of brain cholesterol is found in myelin, while ~30% is metabolically active (Dietschy and Turley, 2004; Quan et al., 2003). The total amount of brain cholesterol in mice increases with age, although the rate of cholesterol synthesis differs between developmental stages with the highest rate of cholesterol synthesis in mice at approximately two weeks of age (Fig 1.6, B, C) (Quan et al., 2003). Brain cholesterol levels in mice have been shown to be independent of plasma cholesterol levels (Quan et al., 2003). The majority of cholesterol biosynthesis in the brain is performed by oligodendrocytes and other glial cells, with a smaller amount of cholesterol produced by neurons (Nieweg et al., 2009). Cholesterol synthesis in neurons occurs uniquely in the cell body, unlike other membrane lipids which can be synthesised in axons (Vance et al., 1994).

The relationship between cholesterol biosynthesis and neurogenesis is very poorly understood, with a particular dearth of studies looking at the V-SVZ. There are a number of studies examining the impact of statin treatment on glioblastoma cell survival and death, which can be derived from the V-SVZ as previously discussed (e.g. Afshordel et al., 2015; Larner et al., 1998; Wu et al., 2009). Many functional studies of cholesterol and postnatal neurogenesis use statins as experimental tools. A key issue with this approach is that statins target HMGCR, so alterations in cholesterol biosynthesis will never be the only downstream effects, as the

pathway will branch before the generation of cholesterol, so farnesylation and geranylgeranylation may also be affected by statin streatment (see Figure 1.5). A more effective method to block cholesterol production in cells would be to administer an inhibitor of the enzyme SQS, which represents the first reaction in the committed synthesis of cholesterol.

Membranes and lipid rafts

Cholesterol is a component of all eukaryotic cell membranes, and is used to regulate cell membrane fluidity. One consequence of higher membrane fluidity is greater movement of transmembrane proteins, which has been linked to increased metastasis of cancer cells (Gonda et al., 2010; Zeisig et al., 2007). Cholesterol additionally is needed for the formation of highly dynamic domains within cell membranes called Lipid rafts (Karnovsky et al., 1982). Lipid rafts are important structural domains of eukaryotic cell membranes and can act as a focus for signalling. The posttranslational modification palmitoylation, for example, increases the affinity of modified proteins for lipid rafts, allowing these proteins to be concentrated into select membrane domains (Levental et al., 2010; Lorent et al., 2017). Palmitoylation alone, however, is not sufficient for raft association. Particularly pertinent examples of lipid raft-associated proteins include ephrin receptors. Ephrin receptors are a class of receptor tyrosine kinases that play a fundamental role in growth cone survival during neuronal development and axon guidance. EphrinA5 (*Epha5*), for example is restricted to lipid rafts in the axonal growth cone (Davy et al., 1999). Through restriction of cholesterol availability in SGZ neuronal precursors it has been found that continuous availability of cholesterol is essential for EPHA5-mediated growth cone collapse (Fünfschilling et al., 2012).

As a chemical precursor

Cholesterol may not be the final functional product generated from the action of the mevalonate and cholesterol biosynthetic pathways. Importantly, cholesterol is the precursor for all steroid hormones such as oestrogen and testosterone, as well as being the precursor for vitamin D. Oestrogen in particular is a strong regulator of V-SVZ neurogenesis (Ponti et al., 2018; Suzuki et al., 2007). Sex steroids derived from cholesterol are also able to act as neuroactive steroids, and regulate neuronal excitability. Allopreganolone (marketed as zuranolone) is an example of a cholesterol-derived neuroactive steroid that regulates both GABAergic signalling and SGZ neurogenesis (Deligiannidis et al., 2021; García-Baos et al., 2022). Allopregnanolone is now prescribed for the treatment of postpartum depression (PPD) as a rapidly acting intervention, and is the first PPD-specific drug treatment (Deligiannidis et al., 2021).

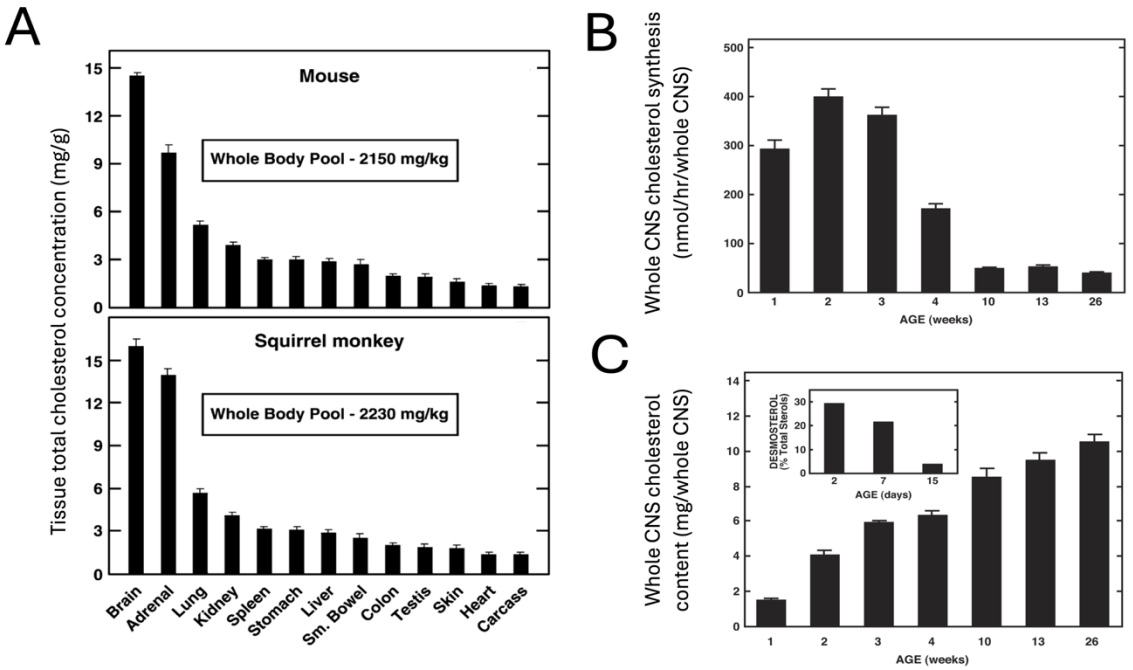

Figure 1.6 Cholesterol production in the brain. ***A)*** *Tissue total cholesterol concentration in the adult mouse (top) and squirrel monkey (bottom).* ***B)*** *Rate of cholesterol synthesis in the murine brain vs weeks of age.* ***C)*** *Total murine CNS cholesterol content vs weeks of age.*

A) is reproduced from Dietschy & Turley (2004) with permission from Elsevier, B) & C) are adapted from Quan et al (2003) with permission from Elsevier. Abbreviations: CNS – Central nervous system

1.3.iii Prenylation pathway

Instead of being used in cholesterol and steroid biogenesis, intermediates from the mevalonate pathway can be used for prenylation. Prenylation refers to the addition of a prenyl group as a C-terminal posttranslational modification (Wang and Casey, 2016). Prenylation is an umbrella term that includes farnesylation – the addition of a farnesyl group – and geranylgeranylation – the addition of a geranylgeranyl group. There are four known eukaryotic prenylation complexes: Farnesyltransferase (FTase), and Geranylgeranyltransferases I-III (GGTase-I, GGTase-II, GGTase-III) (Wang and Casey, 2016). These complexes have both common and unique subunits, illustrated in Fig 1.7, as well as some overlapping protein targets.

Prenylation by these different complexes is dependent on the presence of a CaaX C-terminal amino acid motif, where C is cysteine, aa are any two aliphatic residues, and X represents any C-terminal amino acid (Roberts et al., 2008). Variability in the precise residues of the CaaX motif confers specificity of modification by the different prenylation complexes (Roberts et al., 2008). However, many GTPases of the Ras, Rap, and Rho families can be either geranylgeranylated or farnesylated, indicating that the sequence of the CaaX box alone is not sufficient to confer unique modification by one prenylation complex over another (Whyte et al., 1997) (see Fig1.7, Table 1.1). Prenylation of peptides is an evolutionarily ancient process with a small number of prenylated proteins detected in bacteria, although there does not appear to be a consensus target sequence such as the CaaX motif in eukaryotes (Krute et al., 2015).

Prenyl groups are lipophilic, thus the functional outcome of prenylation is that proteins are targeted to membranes (Kato et al., 1992; Solski et al., 2002). This can be either the plasma membrane or intracellular membranes. This anchoring to the internal side of the plasma

membrane is vital for the function of many GTPases, illustrated by functional experiments that mutate the CaaX box or deplete prenylation complexes (Kato et al., 1992).

The majority of prenylated proteins are Ras-superfamily GTPases, a large family of small GTPases with fundamental roles in cell morphology, cell proliferation, nuclear transport, and vesicular transport (Figure 1.7) (Nobes and Hall, 1995; Wang and Casey, 2016). Different prenylation complexes and the Ras-superfamily GTPases that they modify are illustrated in Figure 1.7, and supporting citations are listed in Table 1.1. There are a number of prenylated Ras-superfamily GTPases with important roles in brain development and neuroblast migration due to regulation of the cytoskeleton and growth cone dynamics. For example the highly conserved GTPase RAC1 regulates axon and dendrite outgrowth, and this regulation is dependent on prenylation (Banka et al., 2022; Scott-Solomon and Kuruvilla, 2020).

Beyond the swathe of Ras proteins that are prenylated are other targets such as pre-lamins A and B, both of which are targeted by FTase (Sinensky et al., 1994; Wolda and Glomset, 1988). These structural proteins regulate the shape of the nucleus, and are dynamically modified during cell division to allow dissolution of the nuclear envelope (Worman et al., 2009). Indeed, farnesylation of lamin B1 is essential for neuronal migration in the developing brain – mutating the CaaX box of lamin B1 in mice leads to severe neurodevelopmental defects and premature death (Jung et al., 2013).

The most recently discovered prenylation complex, GGTase-III, geranylgeranylates F-box/LRR-repeat protein 2 (FBXL2) and YKT6 v-SNARE homolog (YKT6) (Kuchay et al., 2019; Shirakawa et al., 2020). FBXL2 is a ubiquitin ligase, and geranylgeranylation targets it to membranes where it is able to polyubiquitinate membrane-associated proteins (Kuchay et

al., 2019). FBXL2 notably lacks the CaaX motif that is typically required for prenylation by other complexes.

Prenylation represents a potent mechanism for regulating the activity of small GTPases without changes in gene expression. In turn, these GTPases regulate myriad processes that can influence V-SVZ neurogenesis and neuroblast migration.

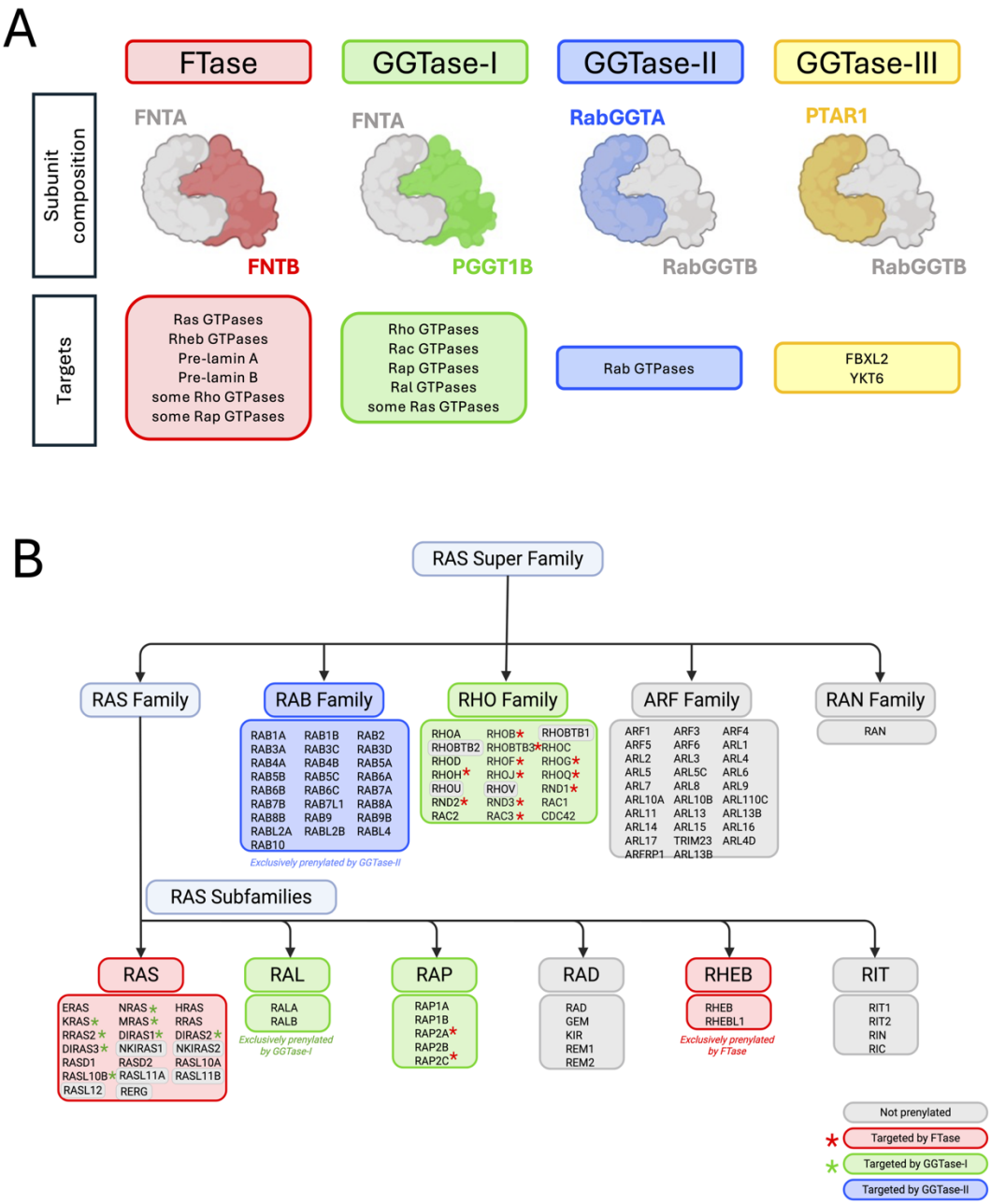

Figure 1.7 Prenylation complexes and targets**. **A)** The four currently known eukaryotic prenylation complexes and their subunits are illustrated. Each complex has a unique subunit, and one subunit that is shared with another complex; unique subunits are coloured. An overview of the targets of each complex is listed below. **B)** Illustration of the RAS Super Family, coloured by the prenylation complexes that target each member. Proteins in grey boxes are not known to be prenylated. Those in a red box or with a red asterisk are farnesylated by FTase. Those in a green box or with a green asterisk are geranylgeranylated by GGTase-I. Targets of GGTase-II are shown in blue boxes. **See Table 1.1 for evidence regarding each of these.

Abbreviations: FTase – Farnesyltransferase; GGTase – Geranylgeranyltransferase. Image generated using BioRender.

1.4 Investigating the missing link between the V-SVZ, cholesterol, and lncRNA

My overarching goal for this research was to examine the cohort of lncRNAs expressed in the V-SVZ, identify a candidate for regulating neuroblast migration, and then interrogate that candidate functionally and mechanistically.

Aim 1: Characterisation of lncRNAs in the V-SVZ

Building off of the results generated by Ramos et al (2013), I wanted to leverage data from newly developed scRNAseq approaches to understand patterns of lncRNA expression. Through this analysis I aimed to identify a list of candidate lncRNAs that were highly and specifically expressed in NSCs, TAPs, and migratory neuroblasts derived from the V-SVZ. I collated open-access data that examined cell type-specific enrichment and evaluated how many different studies had found the same results. Based on these results I then chose a specific lncRNA for functional investigations: *2610307P16Rik (aka Casc15).* This aim is addressed in "Chapter 3: LncRNAs in the V-SVZ".

Aim 2: Functional investigation of a candidate lncRNA

I then planned to evaluate the role of my chosen lncRNA in V-SVZ neurogenesis. I achieved this using multiple different methods of lncRNA depletion both *in vivo* and *in vitro*. I interrogated the *Casc15* knockdown phenotype in terms of cell migration, proliferation, death, and a myriad of structural and morphological phenotypes. This data is discussed in "Chapter 4: *Casc15* lncRNA and migration"

Aim 3: Molecular mechanisms of *Casc15*

My final goal was to investigate the mechanism by which *Casc15* lncRNA influences migration of V-SVZ-derived neuroblasts and the morphology of mature neurons. This was achieved by examining bulk RNAseq data to identify pathways that change in their expression. I then validated these inferences by using small molecule inhibitors to block different enzymes of the mevalonate and cholesterol biosynthetic pathways and by supplementing squalene in cell culture media. This revealed a strong influence of both cholesterol production as well as prenylation on migration in V-SVZ derived cells and resulted in the development of a potential mechanism for further interrogation. These data and mechanism are discussed in "Chapter 5: *Casc15* lncRNA and metabolism".

Chapter 2: Materials and Methods

2.1 Computational work

2.1.i Graphs and figures

All generated using GraphPad Prism 9 for macOS, GraphPad Software, San Diego, California USA, www.graphpad.com. Unless otherwise stated illustrations were drawn in Adobe Procreate. Some components of figures were generated using BioRender.

2.1.ii Qualitative meta-analysis

A literature search was conducted to identify research articles that made use of single cell RNA sequencing in the V-SVZ using the following searches in Scopus (Elsevier): (TITLE-ABS-KEY ("V-SVZ" OR svz OR sez OR "subventricular zone" OR "subependymal zone") AND TITLE-ABS-KEY ("scRNAseq" OR "single cell sequencing")) and in GEO DataSets: ((V-SVZ OR SVZ OR subventricular OR subependymal OR SEZ)) AND "mus musculus"[Organism]. The majority of papers identified document the murine V-SVZ, 14 of these were chosen for analysis (del Águila et al., 2022; Basak et al., 2018; Belenguer et al., 2021; Cebrian-Silla et al., 2021a; Kalamakis et al., 2019; Kriska et al., 2021; Llorens-Bobadilla et al., 2015; Mizrak et al., 2019, 2020; Shi et al., 2018; Xie et al., 2020; Zamboni et al., 2020). Eight of these were chosen for further study because in depth results of their analyses were available. Papers and data were chosen that examined healthy brains in the absence of any treatment, genetic manipulation or pathology.

Data available as supplementary spreadsheets from each study was first taken that examined enrichment in a selected cell type (NSCs, Nbs, TAPs) relative to all other cell types in the dataset. Each dataset was filtered to identify every occurrence in which a lncRNA was enriched

with an adjusted P value <0.05. The number of datasets in which a gene fit this criteria was summed to give "Cumulative occurrences" (CO) for each category of comparison. The Ensembl database was accessed via R to annotate the gene biotype of each gene and allow subsetting of data to isolate lncRNAs (Howe et al., 2021). Assessment of conservation was carried out using a combination of sequence-based searches (BLAST and discontinuous megaBLAST) and examination of conservation of synteny (Kent, 2002; Ma et al., 2002) . This strategy was chosen to accommodate the fact that while a given lncRNA may be functionally conserved, the sequence conservation of lncRNAs is frequently poor. The papers used for the analysis are listed in Table 3.2.

Transcription factor binding motifs that were overrepresented within the promoters of murine lncRNAs were identified using the web tool PSCAN and the mouse genome reference database in a window from +450 upstream to -50 bp downstream from the annotated transcriptional start site for each gene (Zambelli et al., 2009a). Transcription factors (TFs) whose binding sites were over-represented within the cohort of sequences relative to a random control sequence with p<0.05 were taken to examine gene ontology. Gene ontology (GO) analysis was conducted for the cohort of TFs (with binding sites that were statistically enriched in the supplied list of lncRNA promoters) via EnrichR in R with an adjusted P value cut-off of <0.05 (Kuleshov et al., 2016; Xie et al., 2021).

Conservation of sequences and binding motif ontologies

2610307P16Rik (Casc15) was initially identified as the murine homolog of human *CASC15* by using NCBI BLAST (Altschul et al., 1990) to perform a discontiguous megaBLAST (Ma et al., 2002) for related but dissimilar sequences; identifying a locus on human Chromosome 6 as

having a similar sequence. A more stringent BLAT (Kent, 2002), run via the Ensembl BLAST tool, confirmed *CASC15* as the human homolog (Howe et al., 2021).

2.1.iii Bulk RNAseq

Quality control and preprocessing was performed at the Oxford Genomic Centre by Jerome Nicod. Pre-processed data were provided and then analysed by Dr Michael Shapiro (Vance Lab, University of Bath) using the following pipeline. All code used is deposited on GitHub https://github.com/JemimaBecker/DPhil .

Analysis was performed in the Elements cIDE for Linux. Paired end fastq files were trimmed using Trim Galore. The resulting files were then combined using Fast Length Adjustment of SHort reads (FLASH), these were then aligned to the mm10 genome using Bowtie to generate sam files (Langmead et al., 2009). These were turned into bam files using the picard tool (Broad Institude, 2019). DESeq2 (Love et al., 2014) was then used to combine bam files with sample info to generate a summarized experiment, a DESeq data set and a DESeq object. The regularized log transform was used produce transformed data for a heat map (Kolde, 2019) and PCA plot and MA plot of the data for the control and both experimental conditions. Subsets of the data were used to produce summarized experiments DESeq data sets and DESeq objects for the control and each of the experimental conditions and these were used to produce MA plots and tables of significantly up- or down-regulated genes for the control vs. each of the experimental conditions.

From this point I performed all analysis using the output from the DEseq analysis generated by Michael Shapiro. Significantly changed Gene Ontologies were calculated using the Python package GoEnrich accessed via DICE (Pomaznoy et al., 2018a; Rudolph, 2023). Pathway analysis was conducted using Ingeuinty Pathway Analysis (IPA) software from Qiagen .

2.2 Molecular Techniques

2.2.i RNA extraction

RNA was extracted using the RNeasy Mini kit (Quiagen 74104) according to manufacturer instructions. Briefly, cells were lysed with 600µL buffer RLT and homogenised by centrifugation in a QIAshredder column (Quiagen 79656). 600µL 70% EtOH was added and mixed by pipetting. 700µL of this mix was transferred to an RNeasy spin column and centrifuged for 15s at >=8000g. An on-column DNase digestion was performed by washing with 350µL buffer RW1, then centrifuged for 15s at >=8000g. 10µL DNase stock (Quiagen 79254) diluted in 90µL buffer RDD was added to the spin column membrane and incubated for 15 minutes at RT. 350µL buffer RW1 was added, then centrifuged for 15s at >=8000g. The spin column membrane was then washed to remove all EtOH by adding 500µL buffer RPE to the column, then centrifuging for 15s at >=8000g, then adding a further 500µL buffer RPE to the column, then centrifuging for 2 minutes at >=8000g. Then 1 minute centrifuge at full speed. The RNA was then eluted from the spin column membrane into a 1.5mL collection tube with 30µL nuclease-free water (Quiagen 129114) and centrifuging for 1 minute at >=8000g. With the exception of the first and final steps, the flow through is discarded.

RNA purity and quality were assessed using NanoDrop™ Lite Spectrophotometer (Thermofisher, NDNDLPRUSCA). A cutoff of DNA contamination (A_{260}/A_{280}) of 1.8 was applied for all samples.

2.2.ii cDNA synthesis

RNA was diluted with nuclease-free water (Quiagen 129114) to a concentration of 1µg/11µL. cDNA was generated using the SuperScript III First-Strand synthesis system (Life technologies 18080051). 1µg RNA in 11µL nuclease free water was combined with 1µL of 250µg/µL random primers and 1µL 10mM dNTP, and incubated for 5 minutes at 65°C then put on ice for >1 minute. To each reaction 4µL first strand buffer 5x, 1uL 0.1M DTT, 1uL RNase OUT inhibitor, 1µL superscript reverse transcriptase was added. This mixture was incubated at 25°C for 5 minutes, then 55°C for 1 hour, then 70°C for 15 minutes. A 1:10 dilution of the resulting cDNA was made in nuclease-free water.

2.2.iii RT-qPCR

Primer design was carried out using the Primer3 algorithm via the NCBI Primer BLAST tool (Ye et al., 2012). Three primer pairs were designed to target each of the cDNA sequences. These were then tested using the qPCR protocol below on serial dilution of cDNAs derived from V-SVZ neurospheres, and whole mouse brain. Primers were ordered from Thermofisher as dried desalted DNA oligos (Thermofisher A15612). See Table 2.1 For Primer sequences.

qPCR for gene expression was performed by combining 10µL Luna universal qPCR master mix (NEB M3003L) with 0.5uL 10µM forward primer, 0.5µL 10µM reverse primer, 1µL cDNA, and 8µL nuclease-free water. 20µL of this reaction mixture was used per well in a 96-well PCR plate (Life technologies 4346906) and sealed with film (Life technologies 4311971). qPCR was performed using a Quantstudio 5 real-time PCR instrument (Applied biosystems A28568) with the following programme: Denaturation (95°C 60 seconds, 1 cycle), Denaturation and extension (95°C 15 seconds, 60°C 30s, for 40-45 cycles), and melt curve (60-

95°C for one cycle). Beta actin was used as a control housekeeping gene relative to which target gene expression was normalised.

Relative expression calculation was performed using the $\Delta\Delta C_q$ method in Excel:

$$\Delta C_q = C_q[target] - C_q[control] \quad (1)$$

$$\Delta\Delta C_q = \Delta C_q[sample] - \Delta C_q[reference] \quad (2)$$

$$Normalised\ expression = 2^{-\Delta\Delta C_q} \quad (3)$$

2.2.iv ChIP-qPCR

Chromatin immunoprecipitation followed by qPCR (ChIP-qPCR) was performed with the advice of Dr Keith Vance and the help of Dr Bin Sun. Dr Sun performed the first steps of ChIP, and I performed the primer design, DNA fragment purification, and qPCR.

The cell suspension was centrifuged at 1500rpm/5mins/at room temperature (RT). The pellet was then washed with 20ml PBS 1X (Sigma, P4417-100TAB) and spun at 1500rpm/5mins/RT three times. Disuccinimodyl glutarate (Thermofisher, 20593) was added to a final concentration of 2mM and mixed immediately. The mix was then incubated on a rotating wheel at RT for 45 minutes at maximum speed (8-10rpm). Samples were then centrifuged at 1500rpm/10mins/RT. The cell pellet was washed with 20ml PBS 1X and spun at 1500rpm/5mins/RT three times. The pellet was resuspended in 20ml PBS 1X and 540µl of 37% formaldehyde (Merck Millipore, 8187081000) was added and mixed immediately. Samples were incubated rotating for 15mins at RT. The reaction was quenched with 1ml of 2.5M glycine (Sigma , G8898-1KG). Samples were then incubated rotating for 10mins at RT. Samples were centrifuged at 1500rpm/5mins/4ºC, then kept on ice. The supernatant was

removed and the pellet was washed 3 times with ice-cold PBS 1X and was spun down at 1500rpm/5mins/4ºC after each wash.

2ml (per immunoprecipitation (IP)) cold hypotonic buffer was added and the sample was dounced 10 times and incubated on ice for 10 minutes. Samples were dounced a further 10 times and then spun down at 3500rpm/5min/4ºC. The nuclear pellet was then resuspended in 200µl (per IP) sonication buffer. Samples were then sonicated to an average size of 200bp (+/-50bp) using a Bioruptor Pico: 30on/30off – 6 cycles. Sonicated chromatin was centrifuged to pellet the cell debris at 14000rpm/10min/4 ºC. The supernatant was diluted 1:10 on ice with IP dilution buffer, and 1% was retained as input. Samples were immunoprecipitated using 5µg of antibody (see table) or non-specific IgG (Millipore, PP64B) overnight at 4°C on a rotating wheel.

The next day, the IP samples (antibody-bound) were added to the blocked beads (after removing supernatant) and incubated for 4 hours on a rotating wheel at 4°C. Samples were next centrifuged at 14000rpm/30sec/4°C, and unbound material was retained for qPCR. 50µl of Dynabeads (Invitrogen, 10001D) (per IP) were added in a LoBind tube with 1ml of blocking solution. Beads were collected using a magnetic stand and the supernatant aspirated. This was step was repeated 2 more times before resuspending the beads in 1ml blocking solution and incubating overnight rotating at 4°C. The beads were washed with 500µl from each of the wash buffers I, II and III for 5mins rotating. They were then washed twice with TE buffer pH 8 (See Table 2.3). The beads were then transferred to a new LoBind tube.

250µl of ChIP elution buffer was added to elute crosslinked chromatin, and samples were rotated at RT for 15 minutes. The beads were then spun down and the supernatant collected using the magnetic stand. Crosslinking was reversed by adding RNAse A (DNAse-free Roche, cat# 13689800) and NaCl (Thermofisher, 59625-1KG) to a final concentration of 0.25M. Samples were then incubated overnight at 65 ºC. 2.5 volumes of 100% EtOH (Sigma, 32221-

2.5L-M) were added to samples and incubated overnight at -20°C. The next day, samples were centrifuged at 13000rpm/20mins/4°C. DNA was next washed with 400µl of 70% ethanol and then resuspended in 100µl of water. 25µl of Proteinase K buffer was added to each sample and incubated for 1-2hours at 42°C. DNA fragments were then purified using the QIAquick PCR purification kit (Quiagen, 28104). See Table 2.1 for primer sequences for qPCR, Table 2.2 for antibodies used, Table 2.3 for buffer and solution content.

2.3 *In vitro* and *ex vivo* models

2.3.i Neurosphere assay

Generation of secondary neurospheres

4 to 7 wild type (C57BL6) pups aged between postnatal days (P) P2 and P4 were euthanised via intraperitoneal overdose of pentobarbital, with confirmation of death by cervical dislocation. The brains were removed on ice and sliced into 350µm sections using the McIlwain Tissue Chopper (Model TC752). Sections were dissected under dissection hood using two 27G needles in NB-A+ (see Table 2.4) supplemented with 20ng/mL EGF/FGF (Sigma E9644-2MG, Qkine Qk052-0050) to isolate a thin strip of tissue containing the lateral V-SVZs from both sides of 4-5 sections. The anatomy for dissection is illustrated in Figure 2.1 The dissection media was aspirated and the tissue triturated with 700U/mL Accutase (Thermofisher A1110501) and then incubated for 15 minutes at 37°C to generate a single cell suspension. One volume of NB-A+ was added and the cells pelleted by centrifugation at 1.2rpm for 10 minutes. Cells were resuspended in warmed NB-A+ to a concentration of 75,000 cells/mL and plated into 6-well non-tissue culture treated plates (SLS 351146). Cells were incubated at 37°C for 7 days, then passaged by pelleting cells by centrifugation, trituration and incubation with Accutase for 15 mins at 37°C, one volume of NB-A+ added, and the number of viable cells estimated using a Trypan blue assay (Merck T8154-100ML), any culutres with a live cell percentage of less than

85% were not used. Cells were then pelleted and any Accutase remaining aspirated off. Single cells were resuspended in NB-A+ at a density of 50-60,000 cells/mL in poly-HEMA (Merck 529265-5G) coated t75 TC flasks (Corning 430641U).

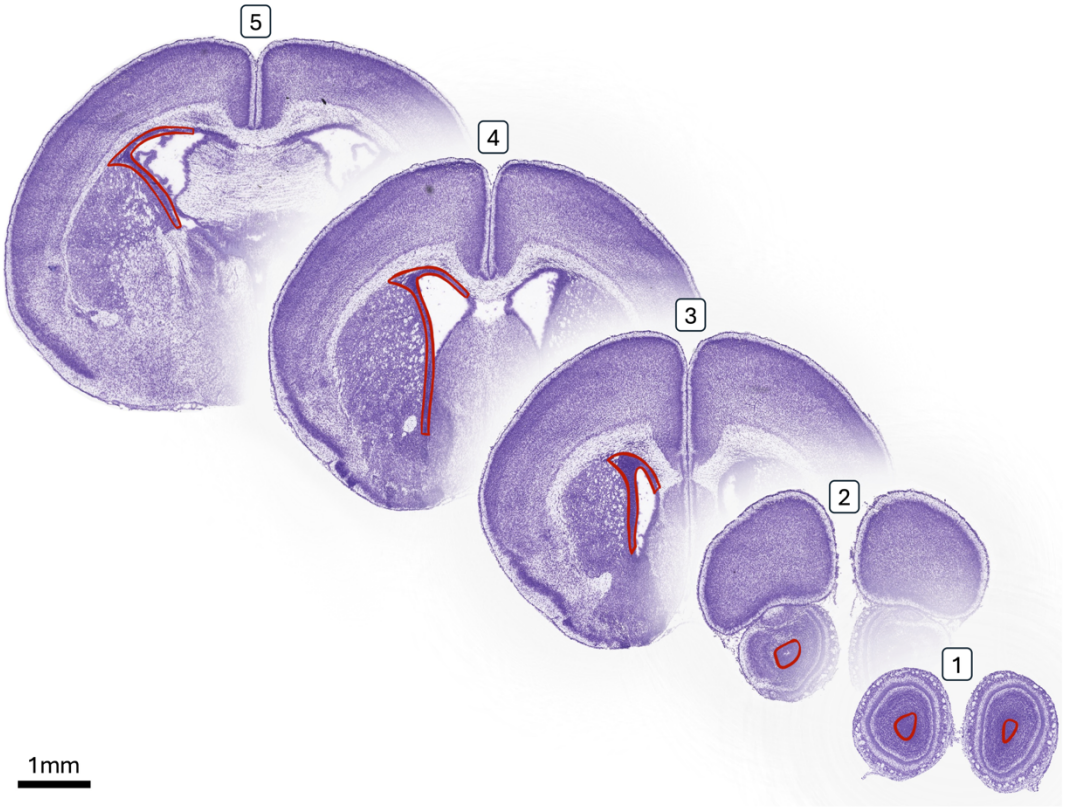

Figure 2.1 Anatomy for dissection. *P4 mouse brain coronal sections with Nissl staining from the Allen Brain Atlas developing mouse brain atlas. Red outlines show the area for dissection. Areas indicated in slices 1 and 2 are for explant migration or spheroid migration assays. Areas highlighted in 3, 4, and 5 indicate tissue for generation of proliferative neurospheres. Scale bar represents 1mm.*

Abbreviations: P4 – postnatal day 4. Illustration made in Adobe Procreate.

Nucleofection of neurospheres

Nucleofection was performed using the Mouse Neural Stem Cell Nucleofector™ Kit (Lonza VPG-1004). Secondary V-SVZ-derived neurospheres were dissociated with 2mL Accutase (Thermofisher A1110501) for 15 minutes at 37°C. Accutase was neutralised with 2mL NB-A and cells were counted using trypan blue (Merck T8154-100ML). Cells were pelleted at 1.2rpm for 10 minutes and the supernatant aspirated off. 5-6x10^6 cells per sample were resuspended in 100µL nucleofector solution with 2µL 200nM of either knockdown or control siRNA with 2µL

0.5 µg/µl GFP plasmid stock solution (Supplied with Mouse Neural Stem Cell Nucleofector™ Kit). siRNA constructs used were either *Silencer*™ Select Negative Control No. 1 siRNA (Life technologies 4390843) or *Silencer*™ Select Pre-Designed siRNA against *2610307P16Rik* (Life technologies 4392420). See Table 2.5 for sequences

Cells were nucleofected in Amaxa-certified cuvettes using the programme A-33 in an Amaxa Nucleofector I device. Cells were spun down 1.2rpm for 10 minutes and the nucleofector solution aspirated. Cells were resuspended in NB-A+ and put into 6-well non tissue-culture treated plates at a density of $1x10^6$ cells/well. Cells were left to re-form neurospheres for three days before RNA extraction. Successful nucleofection was confirmed by the presence of GFP+ cells within neurospheres.

2.3.ii Spheroid migration assay

The spheroid migration assay was performed following the protocol of (Ducker et al., 2020b) with modification and advice from Dr Martin Ducker. A schematic overview of this assay is shown in Figure 2.2.

The brains of P0-P2 C57BL6 pups were removed and sliced into 300-mm sections using a McIlwain Tissue Chopper (Model TC752). The OB and the anterior-most two to three sections containing the RMS were collected in ice-cold Hanks Balanced Salt Solution (HBSS) (Life Technologies 14170070), and 27G syringe used to needles dissect RMS in HBSS on ice, the anatomy for dissection is illustrated in Figure 2.1. HBSS was aspirated and cells resuspended in Accutase (Thermofisher A1110501), and incubated for 15 minutes at 37°C. The accutase was diluted out by adding 2 mL of the cells to 8 mL of NB-A+ medium (see Table 2.5). The cell suspension was transferred through 40-µm cell strainer (Corning 352340) into a 50-mL

Falcon tube and washed with a further 10-mL of NB-A+. Cells were spun down at 1.2rpm for 10 minutes. The pellet was resuspended in 4mL NBA+ and cells counted using trypan blue (Sigma, T8154-100ml) and a haemocytometer. The cell suspension was split into 15mL falcon tubes containing $1x10^6$ cells each. The cells were spun down at 300 x g for 5 min and supernatant aspirated.

Nucleofection was performed using the Amaxa® Mouse Neural Stem Cell Nucleofector® Kit (Lonza, VPG-1004) following manufacturer instructions. Cells were resuspended in 100µL of 50% nucleofector solution diluted in HBSS with 2µL of 200nM control/knockdown construct and 3µL GFP plasmid (0.5µg/µl in 10 mM Tris pH 8.0). The cell suspension was transferred into an Amaxa certified cuvette and then into an Amaxa® Nucleofector® I machine and program G-13 used. 500µL of NBA+ was added to the cuvette, and the supplied pipette was used to transfer cells into 1mL NBA+. Cells were spun at 300xg for 5 minutes and the supernatant aspirated. Cells were resuspended in 4mL NBA+ and plated in a single well per condition in a non-tissue culture treated 6-well plate (Corning, 351146) and left to recover at 37°C for four hours.

Cells were diluted to a concentration of 50,000 cells per mL of NBA+, and 5,000 cells (100µL) of this suspension was added to each well of a 96-well Ultra Low Attachment round bottom plate (Greiner, 650970). The plate was sealed with a gas-permeable seal (Kisker Biotech, 4TI 044850) and incubated overnight at 37°C, 5% CO_2.

The next day the spheroid plate was removed from the incubator and left to cool to room temperature. Matrigel (Corning, 356231) was diluted to 50% in ice-cold NB-A+ medium. The spheroid plate was briefly chilled on ice and the seal removed. 25µL of diluted Matrigel was

trickled down the side of each well and the plate returned to ice while the Matrigel settled. The plate was resealed and then left for 3 minutes to return to room temperature, and then returned to the incubator.

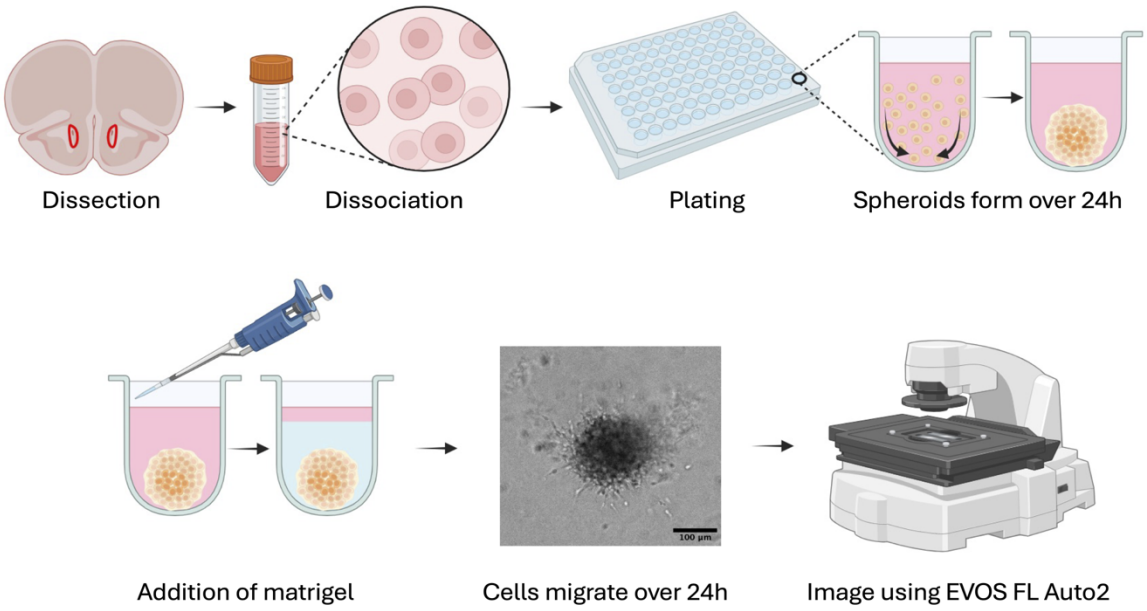

Figure 2.2 Schematic overview of the spheroid migration assay*. The RMS is dissected (see Figure 2.1 for more detail on anatomy) and dissociated. Dissociated cells are placed into 96 well ultra low attachment plates and allowed to form spheroids overnight for 24h. After 24h ice-cold matrigel diluted in NBA+ is trickled down the side of the wells, and is allowed to solidify around the spheroid. After a further 24h cells have migrated out into matrigel and are imaged in an Evos FL Auto 2 microscope in brightfield.*

Schematic adapted from Ducker et al 2020, generated using BioRender

2.3.iii Explant migration assay

2 to 4 wild type (C57BL6) pups aged between P4 and P5 were euthanised via intraperitoneal overdose of 20% w/v pentobarbital (Animalcare, XVD132), with confirmation of death by cervical dislocation. The brains were removed on ice and sliced into 350µm sections using the McIlwain Tissue Chopper (Model TC752). The rostral migratory stream (RMS) of the most rostral coronal sections in the OB was dissected using two 27G needles on ice-cold Hanks balanced salt solution (Life Technologies 14170070) (See Figure 2.1 for dissection anatomy). Explants were then immersed in 6mg/mL Matrigel (Corning, BD 356231) diluted in NBA+.

10µL of Matrigel containing a single explant was taken up in a pipette and then transferred to a 24-well tissue culture plate (Corning, 3526) and incubated at 37°C 5% CO_2 for 30 minutes to allow Matrigel to solidify in a 3D droplet. 1mL NBA+ was added to each well. Over the following 48h cells migrate into the Matrigel. A schematic of this protocol is shown in Figure 2.3, A. Images of cells at the point of embedding in Matrigel (time T_0) and after 48 hours (Time T_{48}) were captured, and the ratio of the surface areas covered by cell bodies was used as a metric for migration. See Figure 2.3,B for an illustration of this calculation.

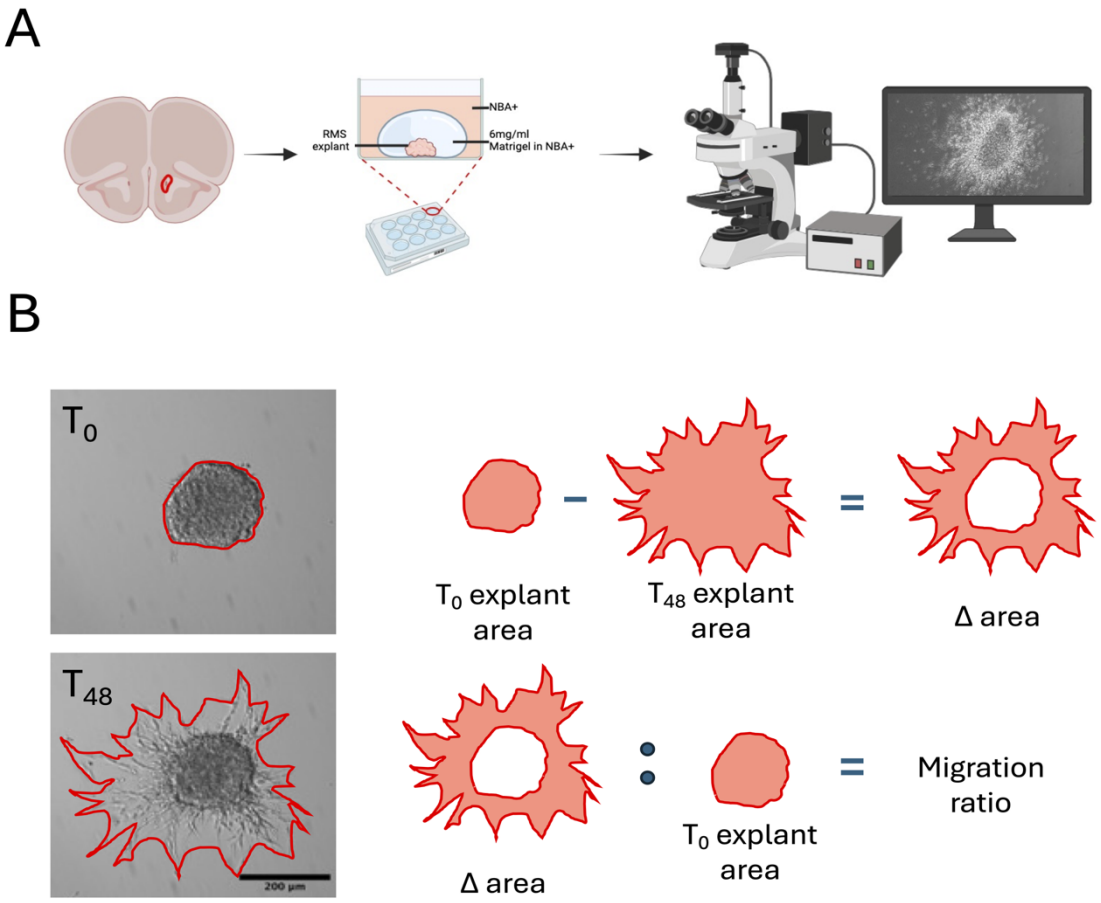

Figure 2.3 Schematic overview of the explant migration assay. ***A)*** *The RMS is dissected (see Figure 2.1 for more detail on anatomy). Small explants of the RMS are embedded in a 3D droplet of matrigel and covered with NBA+ after matrigel has solidified. Cells are allowed to migrate for 48h either whilst being continuously imaged in a Nikon Eclipse ti microscope, or are imaged once at the end of the 48h using an EVOS Fl Auto2.* ***B)*** *Schematic of how migration ratio is calculated, using the area of the explant when it is first removed from the brain (T0) and the area that cells spread into over 48 hours (T48).*

Schematic generated using BioRender. Abbreviations: RMS – Rostral Migratory Stream. Scale bar indicates 200µm.

2.4 *In vivo* work

2.4.i Electroporation

All *in vivo* electroporations were performed by Dr Bin Sun. Plasmids used for postnatal electroporation were prepared by Endofree Plasmid Maxi Kit (Quiagen, 12362). CRISPRi knockdown constructs were prepared by Dr Bin Sun, using CRIPSRi guide RNAs (sequences in Table 2.2) inserted into a dCas9 KRAB plasmid (Figure 2.4, A). Marker plasmids encoding a myristoylated tdTomato and H2B-GFP fusion were a kind gift from the laboratory of Dr Shankar Srinivas.

Before use, 1% fast green (Sigma, F7252-25G) in PBS (Sigma, P4417-100TAB, filtered through a 0.22µm filter (Millipore, SLGP033R5) was mixed with the plasmid solution as 1:10 for tracing. For the postnatal electroporation procedure, P0-P2 pups were anesthetized by hypothermia. ~2µl of plasmid solution (4µg/µl) was injected into the lateral ventricle via a pulled glass capillary. Pups were then subjected to electrical pulses (-100V, 50ms ON with 850ms intervals for 5 cycles) (BTX ECM 830) by tweezer electrodes coated with conductive gel (Boutin et al., 2008; Chesler et al., 2008; Fernández et al., 2011). After surgery, pups were kept in a 37°C warming box for recovery and then returned to the dam. Pups were then kept for 4 to 14 days post electroporation (dpe) before perfusion fixation and removal of the brains (Fig 2.4, B).

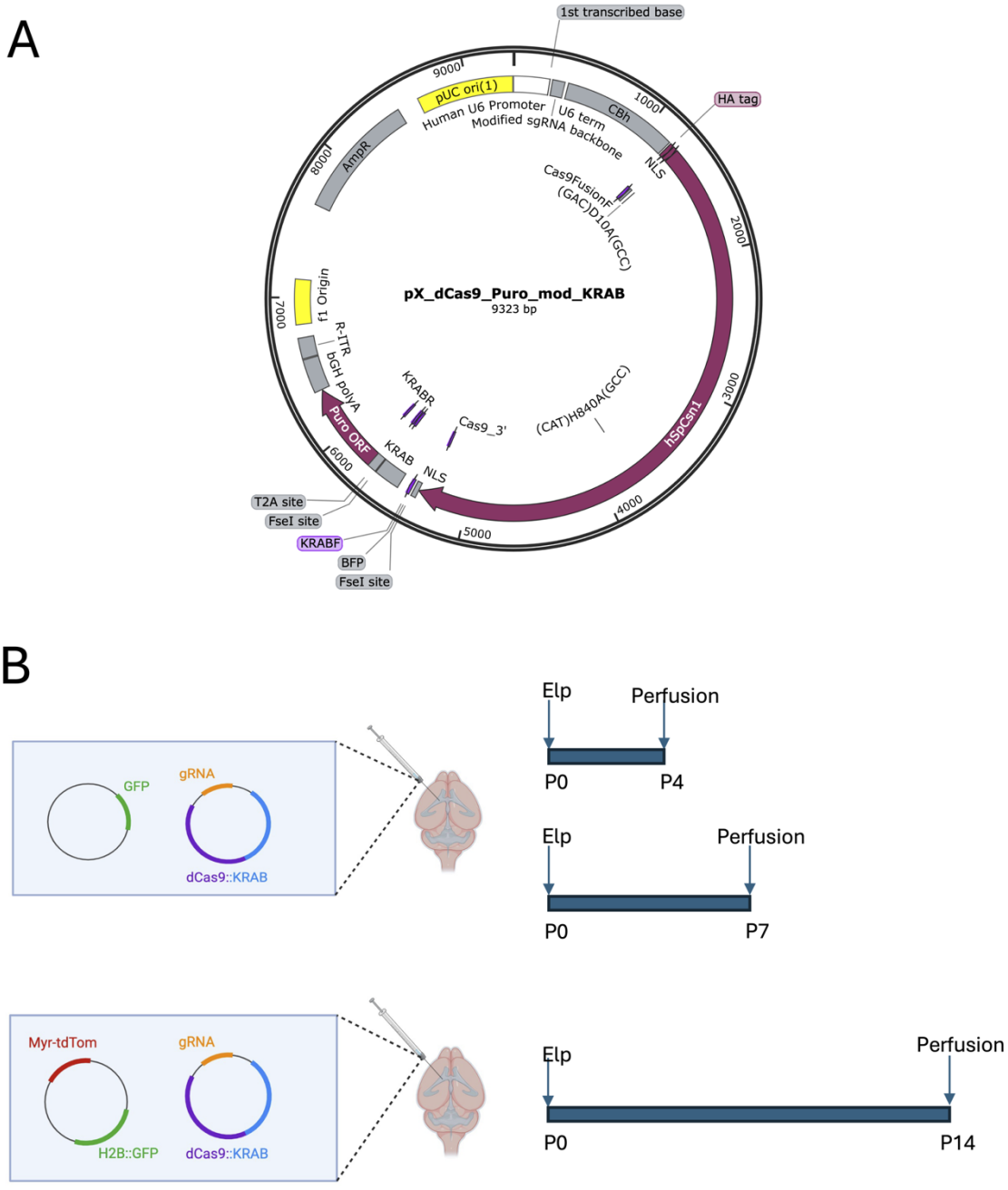

Figure 2.4 CRISPRi electroporation. ***A)*** *Schematic overview of the plasmid used to deplete Casc15 in vivo. Image generated in SnapGene.* ***B)*** *Timeline of electroporation – a GFP expression plasmid was co-electroporated at P0 with the knockdown plasmid into the lateral wall of the V-SVZ and animals allowed to recover for either 4 or 7 days before perfusion. Alternatively, the knockdown plasmid was co-electroporated with a plasmid expressing myristoylated tdTomato and H2B-GFP at P0, and animals were allowed to recover for 14 days before perfusion.*

Abbreviations: Elp – Electroporation; P0P4/P7/P14 – Postnatal day 0/4/7/14. Schematic in B generated using BioRender.

2.5 Immunohistochemistry

2.5.i In free floating sections

Sectioning

Mice were sacrificed by intraperitoneal injection of 20% w/v pentobarbital (Animalcare, XVD132), followed by transcardiac perfusion with 1X PBS (Sigma, P4417-100TAB) and 4% PFA (ChemCruz SC-281692). Brains were dissected and kept in 4% PFA overnight at 4°C, and then transferred into 30% w/v sucrose (Sigma, 16104-1KG) for 48 hours at 4°C. Brains were removed from sucrose solution, after confirmation of equivalent density to sucrose solution by their sinking to the bottom of the solution. Brains were then placed into dry ice to freeze, they were sectioned on Microtome a (Leica, Model SM2000R) to 30µm thick free-floating sections stored in cryoprotectant at -20°C (See Table 2.4).

Immunohistochemistry

Sections were removed from cryoprotectant with brushes and washed 3x10minutes in 1X PBS (Sigma, P4417-50TAB), 15 minutes in 50mM glycine (Sigma, G8898-1KG), then 3x10 minutes 1X PBS. Sections were blocked for 60 minutes in PBS+T (See Table 2.4), and then incubated overnight at 4°C in primary antibody solutions in PBS+. Sections were then washed 3x10 minutes in PBS, from here sections were kept covered from light. Sections were then incubated for 1 hour in secondary antibody in PBS+T. Sections were washed for a further 3x10 minutes in PBS, then 10 minutes in 10mg/mL DAPI stock (LifeTechnologies, D1306) diluted 1:1000 in PBS. Finally, sections were washed 3x10 minutes in 0.1M PB (See Table 2.4), then mounted onto slides (VWR, 631-0911) and Four drops of FluorSave reagent (Sigma, 345789-20mL) were added and coverslips added (VWR, 631-0147). Slides were sealed with clear nail varnish and stored at 4°C until imaging. For antibodies see Table 2.2.

For samples in which HCl antigen retrieval was performed there were two extra steps before the initiation of the standard immunohistochemistry protocol. Firstly, sections were removed from cryoprotectant with brushes and washed 3x10 minutes in PBS. Then sections were incubated for 1 hour at 37°C in 2M HCl (Sigma, 248649). Then the immunohistochemistry protocol was continued as described above. This method was used for stains examining BrdU or H3K27Me3.

2.5.ii *In vitro*

For immunohistochemistry *in vitro* cells were fixed in 4% Paraformaldehyde (Thermofisher Scientific, 15434389) for 15 minutes, and then permeabilised for a further 15 minutes with 0.5% Triton-X100 (Sigma, X100-100ML) in PBS (Sigma, P4417-50TAB). The permeabilization buffer was aspirated and cells were then blocked with PBS+T. The blocking buffer was aspirated and samples were then incubated overnight in primary antibody solution in PBS+T at 4°C. The next day primary antibody solutions were aspirated, and samples were washed with PBS for 5 minutes. PBS was aspirated and samples were then incubated for 1h at room temperature with secondary antibodies and 1:1000 10mg/ml DAPI (LifeTechnologies, D1306) in PBS+T. Samples were washed for 5 mins with PBS before aspirating and filing the well with FluorSave (Sigma, 345789-20mL). For antibodies see Table 2.2. Samples were stored in the dark at 4°C until imaging.

2.6 Imaging and image analysis

2.6.i Epifluorescent imaging

Sections were imaged using a Nikon Eclipse Ti microscope at 10x, 40x, and 100x magnification. 100x images were captured using an oil immersion lens. For each stain the same parameters (magnification, exposure, gain, laser intensity) were used for all image acquisition.

2.6.ii Brightfield imaging

Brightfield imaging for spheroid migration assays was performed using an Evos Fl Auto 2 microscope at 4x and 10x magnification.

2.6.iii Live imaging

Live imaging of explant migration assays was performed using the Nikon Eclipse Ti microscope using an OkoLab stage top incubator. Live imaging was run over a period of 48h with continuous supply of 5% CO_2 in humidified air and the chamber temperature was maintained at 37°C. Z stacks were captured of each explant with 25 z-planes at 30 minute intervals using Volocity.

2.6.iv Quantification and analysis

Microscope images were exported to tiffs where they were imported to ImageJ Fiji. Each image was assigned a random number using the following code in R, which generates a random number:

```{r}
runif(1, min = 0, max = 1000)
```

Images were then quantified using the random number and un-blinded when quantification was complete. Analysis of differences between groups was performed in GraphPad Prism.

Chapter 3: lncRNAs in the V-SVZ

3.1 Introduction

3.1.i Overview

The V-SVZ has been previously identified as a region that is particularly rich in lncRNA expression (Ramos et al., 2013b). Moreover, there is a precedent for the regulation of V-SVZ neurogenesis by lncRNAs (e.g. Fan et al., 2020; Ng et al., 2013; Pavlaki et al., 2018). In order to identify lncRNAs that could be suitable candidates for the regulation of V-SVZ neurogenesis and migration. I pooled single-cell RNA sequencing (scRNAseq) data and compared their results (Becker et al., 2022). I chose to repurpose open-access scRNAseq data examining the V-SVZ to identify candidate genes enriched in the V-SVZ as there are many descriptive scRNAseq studies performed in the V-SVZ, several of which are near-replicates of each other. Due to the high cell density and large number of interspersed cell types in the V-SVZ, scRNAseq is currently the best way to efficiently profile large numbers of cells in parallel.

3.1.ii scRNAseq techniques

The first sequencing technology was pioneered by Fred Sanger (Sanger et al., 1977), which was based on a chain termination method using differently labelled nucleotides. This sequencing-by-synthesis method was then refined into Illumina/Solexa sequencing, which is one of the most widely used DNA sequencing technologies (Canard and Sarfati, 1994; Meyer and Kircher, 2010). The principle is very similar to that of Sanger sequencing, with the key difference being the incorporation of fluorescently labelled nucleotides. The labelled nucleotides using in this method are not chain terminating, allowing larger sequences to be analysed in shorter periods of time, without the need to separate fragments based on size. This concept has subsequently been expanded upon to develop “next generation” sequencing

technologies, such as Single Molecule Real Time (SMRT) sequencing and Oxford Nanopore (ONP) sequencing, both of which sequence a single DNA molecule at high resolution (Udaondo et al., 2021).

As sequencing technologies have evolved, the tissue requirements have gradually reduced. This allows for incredibly small inputs to be used, with single-cell and even sub-cellular resolution now possible. A timeline for scRNAseq technology development is highlighted in Figure 3.1, A with an example scRNAseq pipeline in Figure 3.1, B.

scRNAseq, like all technologies is fallible, but it does give high resolution insight into large numbers of cells allowing identification of highly specialised cell types and transcriptional programs. Many lncRNAs show very high degrees of cell type specificity of expression but are frequently expressed at lower levels than protein coding genes, and thus biologically meaningful patterns of expression may be missed in bulk RNAseq experiments (Derrien et al., 2012b).

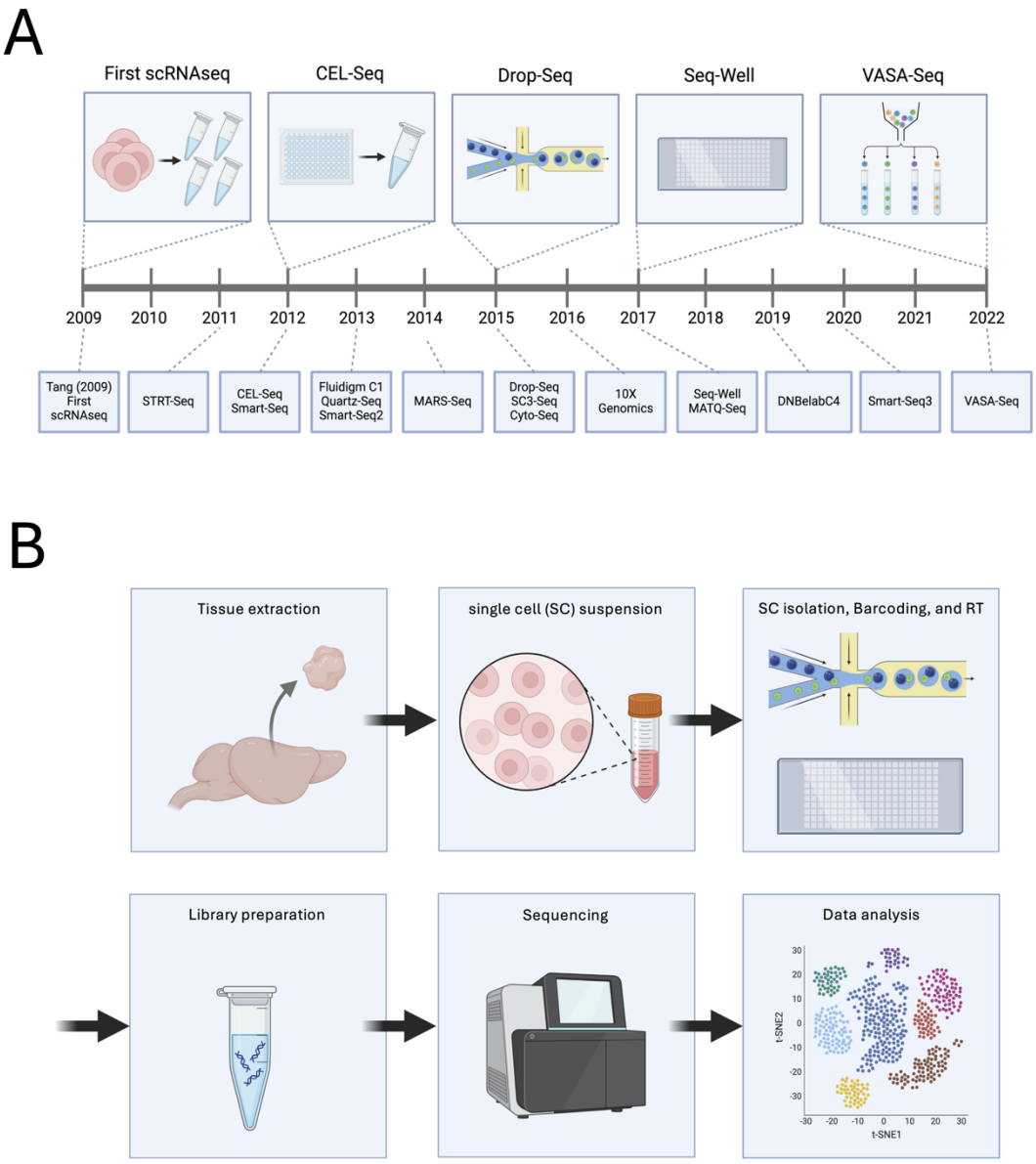

Figure 3.1 Overview of single cell sequencing. ***A)*** *Timeline of single cell RNAseq technical development from first description by (Tang et al., 2009) to the development of VASA-Seq.* ***B)*** *Process of single cell RNAseq from tissue isolation to data analysis, adapted from (Wu et al., 2018) with permission from Elsevier. Figure generated in BioRender.*

Abbreviations: scRNAseq – single-cell RNA sequencing; CEL-seq – Cell expression by linear amplification and sequencing; VASA-seq – Vast transcriptome analysis of single cells by dA-tailing; STRT-seq – Single-cell tagged reverse transcription; MARS-seq – Massively parallel RNA single-cell sequencing framework; MATQ-seq – Multiple annealing and dC-tailing-based quantitative single-cell RNAseq; RT – Reverse transcription

3.1.iii Patterns of lncRNA expression

LncRNAs are typically Pol-II products similar to protein coding mRNAs, and thus show many of the same features such as polyadenylation (Mattick et al., 2023). Because of this, sequencing

data that are enriched for poly(A) transcripts will also provide information regarding lncRNA expression. However, there are some intrinsic features of lncRNAs that may increase the challenges associated with their study.

Many lncRNAs are vulnerable to being filtered out of datasets during bioinformatic analysis, due to low expression levels which are typically lower than that of protein-coding mRNAs (Derrien et al., 2012). Most (if not all) RNA sequencing quality control pipelines will include a step in which transcripts that are expressed at very low levels are filtered out; as such this may obscure biologically meaningful changes in lncRNA levels. An additional complication of low levels of lncRNA expression is that they may be more likely to be mis-identified by bioinformatic methods to be statistically enriched in given cell types, (Derrien et al., 2012b). Differential gene expression analysis typically takes into account fold-change of gene expression, as well as the absolute change in the number of detected transcripts; for some pipelines this may lead to skewing of data for very low expressed genes (Hao et al., 2024). Additionally, random genomic sequences may show consistent patterns and signatures of regulation independently of conservation or function, and therefore we must be wary when drawing conclusions about lncRNA functionality based off of expression or regulation alone (de Boer et al., 2020; Eddy, 2013; Mutschler et al., 2018).

For some lncRNAs, cell-type regulation and changes in functionality are achieved not through changes of the total cellular lncRNA levels, but through changes in the levels of individual isoforms (Wright et al., 2022a). Therefore, unless a particular study uses long-read sequencing to identify isoform-specific expression changes, biologically meaningful changes in transcript levels may be missed or not reported.

Given these potential confounding factors that are specific to lncRNA, it seems prudent to compare expression signatures across a wide range of available papers. This allows us to examine whether the same patterns can be observed despite differences in platform and methodology – this might indicate a more significant or biologically meaningful signature. Furthermore, it has been suggested that up to 90% of RNA pol II transcription is simply "noise", therefore consistency of results between studies might indicate a biological effect that extends beyond background noise (Struhl, 2007).

3.1.iv V-SVZ heterogeneity

Many recently published papers describing gene expression and transcriptomic signatures in the V-SVZ reveal an unanticipated degree of heterogeneity within relatively small spatial and developmental timeframes; this could be attributed in part to different developmental origins of different regions of the V-SVZ, illustrated in Figure 3.2. Variability in gene expression within the V-SVZ has been identified with sex (Mizrak et al., 2019), age (Shi et al., 2018; Xie et al., 2020), position along dorso-ventral axis (Borrett et al., 2020; Cebrian-Silla et al., 2021a), and position along medio-lateral septal-lateral axis (Mizrak et al., 2019).

Due to this heterogeneity, as well as the high cell density within the V-SVZ, I chose to analyse multiple single cell RNAseq datasets together to allow identification of those lncRNAs that are specifically enriched in the neurogenic lineage. These lncRNAs therefore are positioned to act as regulators of neurogenesis.

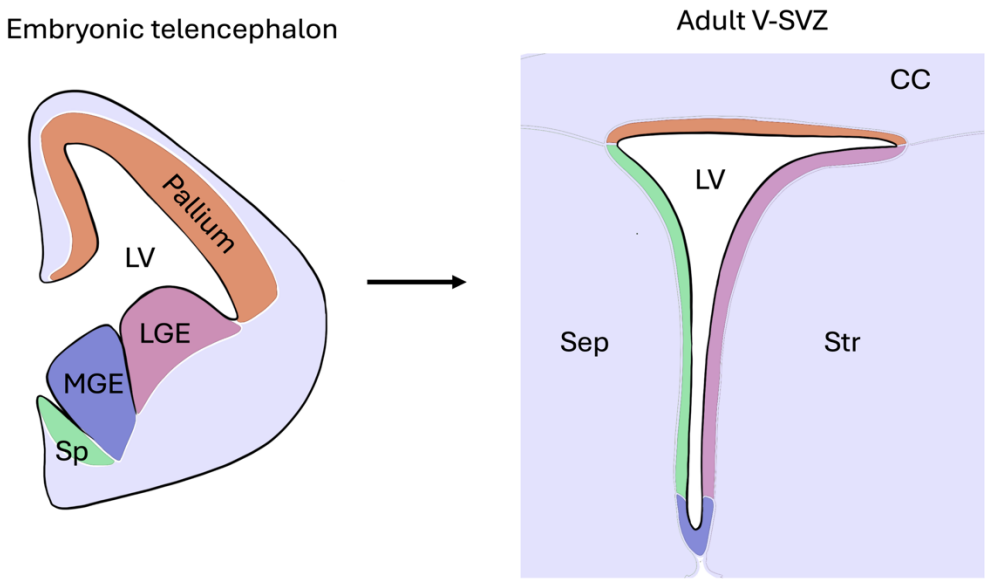

Figure 3.2 Developmental origins of the V-SVZ. *Colours correspond to the tissue of origin, for example the pallium gives rise to subcallosal V-SVZ, and are both coloured orange to illustrate this.*

Abbreviations: LV – lateral ventricle; LGE – lateral ganglionic eminence; MGE – medial ganglionic eminence; Sp – subpallium; CC – corpus callosum; Sep – septum; Str – Striatum. Illustration adapted with permission from (Chaker et al., 2016). Illustration drawn in Adobe Procreate.

3.2 Results

3.2.i There is limited consistency in methodology between studies

In order to find data describing the expression patterns of lncRNA in the V-SVZ I conducted a structured literature search. This revealed a large number of studies that performed scRNAseq analysis in the murine V-SVZ. I then manually removed papers that examined specific genotypes or disease models, as well as those that were not transparent regarding data release and reporting. This left 14 studies that performed descriptive scRNAseq of the murine V-SVZ (del Águila et al., 2022; Basak et al., 2018; Belenguer et al., 2021; Cebrian-Silla et al., 2021a; Kalamakis et al., 2019; Kriska et al., 2021; Llorens-Bobadilla et al., 2015; Mizrak et al., 2019, 2020; Shi et al., 2018; Xie et al., 2020; Zamboni et al., 2020).

I started with a detailed examination of the materials and methods for each study, to identify parameters that would confound quantitative comparisons between datasets. Biological parameters that I examined were: age, strain, and sex of animals; as well as region of the V-SVZ used. I also examined the technical parameters: average number of genes covered per cell; the number of cells profiled; the average number of reads per cell; sequencing platform and library generation methods. These results are summarised in Table 3.2. This table highlights that even superficially similar studies have striking differences in terms of basic background of the animals, as well as in sample generation, preparation, and sequencing. Despite many of these studies examining the same biological question, every single one used different methodology.

3.2.ii Many studies show consistent enrichment patterns of lncRNA expression

In order to rapidly and qualitatively identify lncRNAs that are enriched in particular cell types of the V-SVZ, notably neural stem cells (NSCs), Transit amplifying progenitors/cells (TAPs/TACs) and Neuroblasts (Nbs) I focussed on data generated for each study when annotating cell types, using data generated from each of the 14 studies listed in Table 3.2.

The Seurat function FindAllMarkers examines all cells in a dataset, and hierarchically clusters them based on similarity of the transcriptome of each cell (Hao et al., 2021, 2024). The most highly and specifically expressed genes in each cluster can then be used as "markers" to identify the specific cell type. This reveals canonical markers of these cell types such as Doublecortin (*Dcx*) for neuroblasts, as well as non-canonical marker genes such as lncRNAs that are uniquely enriched within a given cell cluster.

I took the results of these analyses from each paper and for each cell type (NSCs, TAPs, Nbs) assigned a value of 1 for each time a given lncRNA had been identified by FindAllMarkers as being enriched within one of these cell types with a significance $p<0.05$. Across 14 papers this meant that the maximum score for any lncRNA would be 14 – if all 14 papers had identified it as being a marker for the same cell type – and a minimum score would be 0. I named this score "cumulative occurrences" (CO) for the total number of occurrences of a lncRNA as a marker. lncRNAs with CO>=4 are listed in Table 3.3 for NSCs, TAPs, and Nbs.

This revealed that a large number of murine lncRNAs had a CO of 0 or 1, indicating that they had only been found to have significant cell-type enrichment in one (or zero) studies (Figure 3.3). However, a small proportion showed consistent cell type enrichment patterns with CO of up to 9, indicating that 9 independent studies had found them to show statistically significant enrichment in a particular cell type. Maternally expressed gene 3 (*Meg3*) for example, was found to be significantly enriched in neuroblasts in 9 out of 14 studies, giving it a CO score of 9 for neuroblasts. There was no lncRNA that was enriched with a CO of 14 across all studies.

Taken together, these results suggest that a large number of lncRNA are expressed in the V-SVZ, although only a small proportion of these show reproducible patterns of expression across studies.

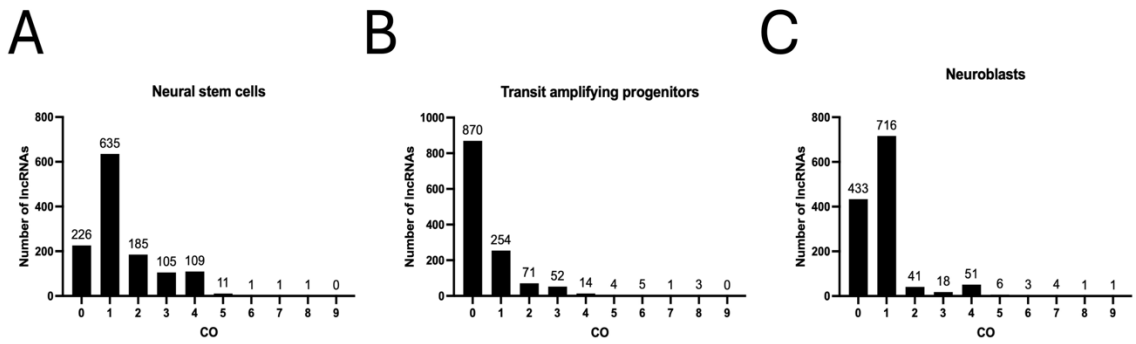

Figure 3.3 CO vs cell type. A-C) *CO vs number of lncRNAs for different cell types in the V-SVZ. These plots show the number of lncRNAs that had each value for CO in* ***A)*** *Neural stem cells,* ***B)*** *Transit amplifying progenitors,* ***and C)*** *Neuroblasts. These plots highlight that irrespective of cell cluster, most lncRNAs only show cell-type specific expression in 1 or 0 studies.* ***See Table 3.3 for more details.***

Abbreviations: CO – Cumulative Occurrences

3.2.iii lncRNAs abound in the V-SVZ

Of the lncRNA that show high scores for CO, a small number have been functionally investigated, but even fewer have been studied in the context of healthy V-SVZ neurogenesis. Because of this lack of annotation, it is not possible to conduct gene ontology (GO) analyses for these lncRNAs to reveal patterns of functionality. However, examination of lncRNAs on a gene-by-gene basis reveals that many lncRNAs which show high values for CO have documented roles in neurodevelopment and stem cell maintenance.

POU3F3 adjacent non-coding transcript 1 (*Pantr1* aka *LINC-BRN1A, LINC-POU3F3, LINC01158*) has the highest CO in NSCs (CO NSCs = 8), and its inhibition leads to premature differentiation of V-SVZ-derived NSCs, and global loss of *Pantr1 in vivo* leads to abnormal cortical lamination (Carelli et al., 2019; Sauvageau et al., 2013). Another NSC enriched (CO NSC = 5) lncRNA, Erythroid differentiation regulator 1 (*Erdr1* aka *Gm21887*, *Gm55594*), has been found to be dysregulated in multiple different models of neurodevelopmental disorders (Ling et al., 2014; Trent et al., 2014; Winkler et al., 2020).

LncRNA downstream of Cdkn1b (*Lockd* aka *1190002F15Rik*) was enriched in TAPs in the largest number of studies (CO TAPs = 8), and has been found to regulate the proliferation and regeneration of myoblasts, but hasn't been studied in a neural stem cell context (Chen et al., 2022). EGFR long non-coding downstream RNA (*Eldr* aka *FABL, LINC01156*) was also consistently enriched in TAPs (CO TAPs = 5), and correlates with markers of neural progenitors, it is frequently increased in copy number in glioblastomas (Carelli et al., 2019; Sur and Ray, 2021; Sur et al., 2020).

Maternally expressed 3 (*Meg3* aka *GTL2, LINC00023, NCRNA00023, ONCO-LNCRNA-83*) is a highly conserved and well characterised lncRNA with a range of different roles in different cell types and disease contexts. It was enriched in NBs in 9 different studies (CO NBs = 9), and has been found to play a role in neural differentiation of both human and murine stem cells (Mo et al., 2015; Ya-Ping et al., 2018). Growth arrest specific 5 (*Gas5* aka *NCRNA00030*, *SNHG2*) was also found to be enriched in neuroblasts in multiple studies (CO NBs = 5). In vitro examination has found that *Gas5* contributes to the survival of neurons via regulation of NOTCH1 signalling following ischaemic stroke in mice (Chen et al., 2018).

While I can't conclusively conduct a gene ontology analysis, specific enrichment of lncRNAs that are known to regulate brain development and stem cells suggests that at least some of the lncRNAs identified here may be regulating neurogenesis in the V-SVZ.

3.2.iv Indirect gene ontology analysis of lncRNA expression in the ageing V-SVZ

The neurogenic capacity of the V-SVZ declines with age, and there are several scRNAseq studies documenting the expression patterns of lncRNAs with age (Luo et al., 2006; Shi et al., 2018; Xie et al., 2020). I wanted to determine which lncRNAs may be contributing to the

increased resistance with age of quiescent neural stem cells (qNSCs) to activation. I chose to perform this analysis using data from qNSCs as a "proof-of-concept" for multiple reasons: 1) There are known transcriptional alterations that occur in these cells with aging; 2) Availability of quality data with clear reporting; 3) Mechanisms by which qNSCs become increasingly resistant to activation over time are currently unclear. I therefore aimed to clarify how lncRNAs are regulated as part of the aging process in the V-SVZ.

I took a list of lncRNAs that significantly increased their expression with age in qNSCs of the V-SVZ and analysed their promoters to see what processes they may be contributing to. Most lncRNA genes are not functionally annotated so a direct gene ontology analysis was not possible. Therefore, I needed to develop my own approach to examine whether there were any patterns in the types of lncRNAs that were being expressed, a schematic for which is outlined in Figure 3.4 A.

For this analysis I used a dataset from Kalamakis et al., 2019 comparing the V-SVZ of 2 and 23 month old male C57BL6/J mice. After filtering to those lncRNA that are annotated in both NCBI and Ensembl databases, I was left with 48 lncRNAs whose expression increased in qNSCs of the ageing V-SVZ (Table 3.4) (Dyer et al., 2025; Sayers et al., 2025). I removed those lncRNA that were annotated only in one of these two databases, as these were sequences that had been previously identified as predicted genes, but did not have sufficient sequencing-based support for their existence.

I started by using PSCAN (Zambelli et al., 2009b), a tool which examines sequences of co-regulated gene promoters and identifies whether there are any transcription factor binding sites that are statistically enriched across the list of provided sequences. This allows insight not into

gene function *per se*, but into common themes of regulation. By comparing a window 450bp upstream and 50bp downstream of the annotated transcriptional start site for all of these lncRNA in parallel PSCAN was able to identify 38 binding sites that were enriched across all of these promoters ($p<0.05$) (Table 3.5).

In order to identify common themes and processes that these transcription factors were part of, I ran a Gene Ontology (GO) analysis via GOnet (Pomaznoy et al., 2018b). GOnet is a webtool built on the python goenrich package (Rudolph, 2023). This returned a list of 62 GO terms that were significantly (FDR adjusted $p<0.05$) associated with the list of transcription factors that I supplied (Table 3.6). As anticipated when running GO on a list of transcription factors, 22/62 terms were associated with transcription and RNA biogenesis. 24/62 were associated with metabolism and biosynthesis, 12/62 with oxidative stress and hypoxia, and the remaining 4/62 with cell cycle and development among other processes (Fig 3.4, B).

This indirect analysis suggests that lncRNAs which accumulate in age in qNSCs may be regulated in concert with genes that are involved with regulation of metabolism and responses to hypoxia and oxidative stress. This same approach could be applied to multiple cell types and systems to gain insight into genes without annotated function.

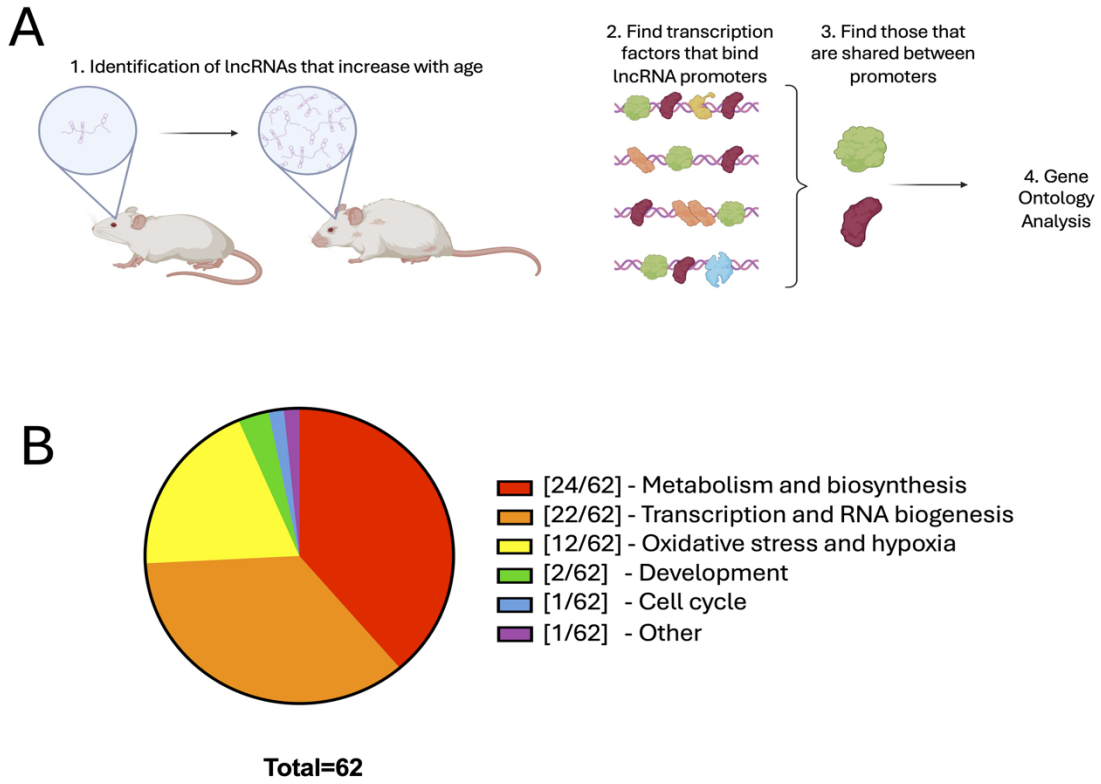

Figure 3.4 lncRNA in the aging V-SVZ. *Analysis of lncRNAs that accumulate with age in the qNSCs.* ***A)*** *schematic for indirect gene ontology analysis of lncRNAs that accumulate with age in the qNSCs of the V-SVZ. Firstly lncRNA that increase with age are identified, then the common transcription factors that are shared between their promoters are identified, then gene ontology analysis is run on those transcription factors.* ***B)*** *Overview of gene ontology terms significantly ($p<0.05$) associated with the list of transcription factors generated in A. Panel A generated in BioRender.* ***See Tables 3.4, 3.5, and 3.6 for more detail.***

3.2.v *Casc15* lncRNA is enriched in neural progenitors

In search of novel regulators of V-SVZ neurogenesis I turned next to migratory neuroblasts, as there is little known about the function of lncRNAs in this context. I examined the list of lncRNAs that had high values of CO in neuroblasts, and chose to focus on RIKEN cDNA 2610307P16 gene (*2610307P16Rik*, Ensembl Id ENSMUSG00000085936, Genbank GeneID 72518) a particularly long and conserved lncRNA, identified as enriched in neuroblasts in four of the scRNAseq studies examined (Cebrian-Silla et al., 2021b; Mizrak et al., 2019, 2020; Xie et al., 2020). BLAST search identified this as the murine homolog of the Human Cancer susceptibility 15 (*CASC15*); *2610307P16Rik* will be referred to as *Casc15* from here. Using

the mouse *Casc15* sequence to conduct a BLAST search across all genomes in the Genbank database revealed striking sequence similarity between species, with conservation of both sequence identity and synteny across amniote genomes (Altschul et al., 1990). This is illustrated in Figure 3.5, A. In all cases, *Casc15* is present as a large multiexonic locus encoded between the *Sox4* and prolactin loci. *Casc15* was an appealing gene for study as it was highly conserved, expressed in neuroblasts in multiple studies, and had never been studied outside of disease models, making it a good candidate for gleaning novel insights into V-SVZ neurogenesis.

Plotting scRNAseq data from Cebrian-Silla et al (2021) (Fig 3.5, B) highlights expression patterns of *Casc15* (*2610307p16rik*) vs different marker genes used for lineage analysis in the V-SVZ (Cebrian-Silla et al., 2021a). I plotted *Casc15* (*2610307P16Rik*) against the following markers: Achaete-scute homolog 1 (*Ascl1*, aka *Mash1*) expressed in neural stem/progenitor cells (Casarosa et al., 1999); Doublecortin (*Dcx*) expressed in neuroblasts (Yang et al., 2004); Glial fibrillary acidic protein (*Gfap*) expressed in radial-glia like stem cells and astroctyes (Doetsch et al., 1999); marker of proliferation Kiel 67 (*Mki67*), a marker of the mitotic cell cycle (Scholzen and Gerdes, 2000); Oligodendrocyte transcription factor (*Olig2*) expressed in oligodendrocyte progenitors and some neuronal progenitors (del Águila et al., 2022; Marshall et al., 2005); Paired Box 6 (*Pax6)* a transcription factor expressed neural stem/progenitor cells of the developing nervous system (Strachan and Read, 1994; Talamillo et al., 2003); SRY-related HMG-box 4 (*Sox4*) predominantly expressed in neural progenitors (Cheung et al., 2000; Foronda et al., 2014); and S100 calcium-binding protein B (*S100b*) a marker of mature astrocytic and ependymal cells (Raponi et al., 2007).

Examining the overlap between these different genes and *Casc15* expression reveals high expression in cell clusters that correspond to proliferative neuroblasts (*Dcx*+ and *mKi67*+ cells). Additionally, there is a population of *S100b*+ ependymal cells that express *Casc15* at a lower level.

I then confirmed *Casc15* expression in the V-SVZ relative to the cortex by RT-qPCR following manual dissection of the cortex, striatum, Olfactory Bulb, and V-SVZ of P4 mice finding that *Casc15* was indeed significantly enriched in the V-SVZ (Fig 3.5, C).

Taken together, the scRNAseq data from Cebrian-Silla *et al* (2021) and my own RT-qPCR suggest that *Casc15* is highly expressed in the V-SVZ and V-SVZ-derived cells.

I next confirmed this enrichment by examining spatial transcriptomic data of the whole mouse brain from Yao et al (2023) (Yao et al., 2023). Summarised in Figure 3.6, this data reveals highly restricted patterns of *Casc15* expression. Confirming the results from scRNAseq data in Figure 3.5, *Casc15* is most highly expressed in the V-SVZ and RMS (Fig 3.6, A-C). In the olfactory bulb, *Casc15* is expressed in the most anterior portion of the RMS, as well as in the mitral cell layer and glomerular layer (Fig 3.6, A). Looking further posterior, *Casc15* is enriched in the choroid plexus, and also is expressed to a lower extent in the thalamus (Fig 3.6, D, E). In the hippocampus *Casc15* is also highly expressed in the SGZ of the dentate gyrus (Fig 3.6, E).

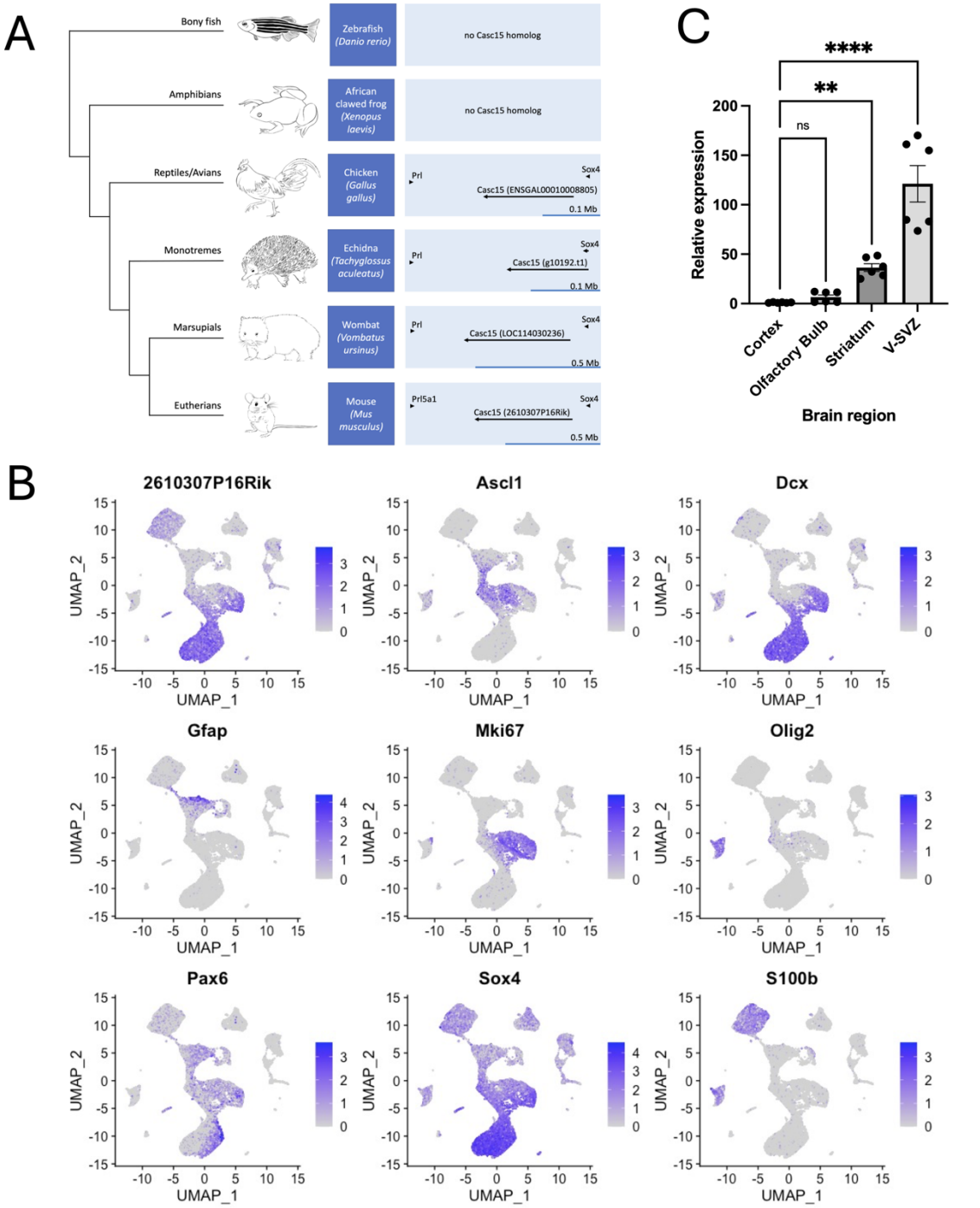

Figure 3.5 Casc15 lncRNA in the V-SVZ *Casc15 is conserved in amniotes and is expressed in neuroblasts.* ***A)*** *schematic of Casc15 conservation across vertebrate lineages, with an illustration of locus structure in the right panels.* ***B)*** *Expression of 2610307P16Rik (Casc15) and various markers (Ascl1, Dcx, Gfap, Mki67, Olig2, Pax6, Sox4, S100b) in scRNAseq data from Cebrian-Silla et al., 2021. Darker blue colour indicates higher expression and pale/grey indicates lower expression.* ***C)*** *Expression of Casc15 relative to β-actin in different microdissected brain regions as detected by qPCR indicates significant enrichment in the V-SVZ.* ***See Table 3.1 for details of statistical tests.***

Error bars represent SEM. Animal illustrations drawn in Adobe Procreate.

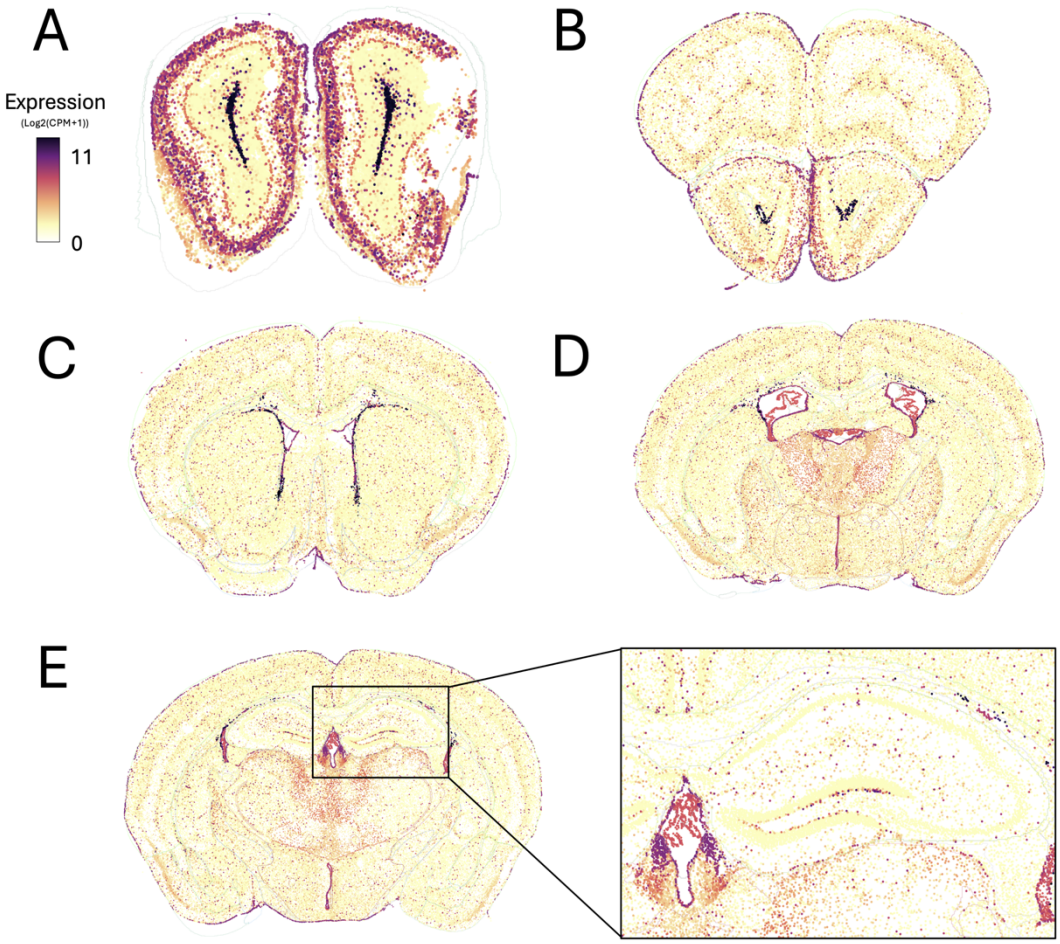

Figure 3.6 Casc15 distribution in the whole mouse brain. *Spatial transcriptomics from Yao et al (2023) reveal distribution of Casc15 in the mouse mouse brain.* ***A) – E)*** *show coronal sections from anterior to posterior in the brain, highlighting high expression in the neurogenic niches. The same scale of expression is used in all panels.*

3.3 Discussion

3.3.i How far can we rely on aggregate lncRNA expression data?

While the scRNAseq-derived cell type specific enrichment of most lncRNAs is not consistent across studies, there are some that show very strong patterns of expression that can be seen across multiple studies. This indicates that these select lncRNAs may represent biologically meaningful patterns of expression, and could act as regulators of neurogenesis. This approach of aggregating the results from multiple papers is very prone to false negatives, and it is likely

that there are many lncRNAs that genuinely do regulate V-SVZ neurogenesis that have been excluded. Despite this risk of missing potentially relevant lncRNAs, this is a relatively rapid and low computational input of identifying trends across datasets without the need for programming expertise or high-performance computing. Neither high-performance computing nor programming expertise are needed, as would be the case with a quantitative meta-analysis. Multiple lncRNAs that are highly conserved and already known to regulate neurogenesis such as *Sox2ot, Meg3*, and *Kcnq1ot1* were identified by this approach, lending support to inferences about lncRNAs that have not yet been investigated in this context such as *Casc15* (*2610307p16rik*).

3.3.ii Cell type specific enrichment does not confer function

While many lncRNAs were identified by this process as being enriched in specific cell types within the V-SVZ, this does not necessarily mean that they have a conserved functional role in the V-SVZ. This is exemplified by the lncRNA *Visc-2* (*C130071C03Rik*), which I found in 5 different scRNAseq studies to be specifically and significantly enriched in V-SVZ NSCs. However, disruption of this lncRNA did not give rise to an overt phenotype in the OB (Oliver et al., 2015).

3.3.iii lncRNA in the ageing V-SVZ

As an animal ages, the qNSCs of the V-SVZ become increasingly resistant to activation. In conjunction, there are evolutionarily conserved age-related changes that occur in the brain in terms of metabolism, as well as cellular responses to hypoxia and oxidative stress (Bishop et al., 2010). On this basis I investigated whether lncRNAs that accumulate with age in the qNSCs may be contributing to this phenomenon, using an indirect approach to Gene Ontology (GO) analysis. This indirect analysis suggested that those lncRNA which increase with age may be

regulated in conjunction with wider changes to oxidative stress, hypoxia, and metabolic changes. While this doesn't prove function for those lncRNA, this approach does highlight that this cohort of lncRNA likely aren't "random" noise but rather a part of a wider shift in the transcriptional landscape. Furthermore, the consistency between GO categories identified through this indirect approach and analyses of protein-coding genes that change with age suggests that this method may be a viable insight in cases such as this when functional data regarding the function of a list of genes is not available.

3.3.iv *Casc15* is poised to regulate neurogenesis

Based on the comparison of V-SVZ scRNAseq datasets, the lncRNA *Casc15* (*2610307p16rik*) may be a suitable candidate for the investigation of lncRNA regulation of V-SVZ neurogenesis for a number of reasons. Firstly, it is highly and specifically expressed in neuroblasts in scRNAseq data (Cebrian-Silla et al., 2021b; Mizrak et al., 2019, 2020; Xie et al., 2020). I next showed by qPCR that *Casc15* is enriched in the postnatal murine V-SVZ, although it is not possible to show cell-type specific enrichment when manually dissecting without cell sorting as I did. This is because of the high cell density in the V-SVZ – many different cell types exist within a very small volume so it is not possible to separate them without the use of Fluorescence-activated cell sorting (FACS) or an equivalent technique. Spatial and cell-type specificity of *Casc15* expression could be confirmed by RNA in-situ hybridisation (ISH), overlaid with RNA ISH for selected marker genes such as *Dcx*.

According to scRNAseq data *Casc15* is expressed highly in neuroblasts and is expressed at a lower level in ependymal cells, making it a good candidate to study in the V-SVZ as electroporation of constructs in the early postnatal mouse target the neural lineage, whereas electroporation in the adult predominantly targets the ependymal cells – this may allow dissection of differing roles in these different cell types. Key information that is missing from

the available data is which splice variants of *Casc15* are expressed – at the time of writing there are 242 isoforms of *Casc15* annotated in the Ensembl catalogue with varying degrees of transcript support (Dyer et al., 2025). For this to be addressed the RNAseq would need to be performed using long reads at a high read depth as exemplified by Wright et al (Wright et al., 2022a).

Casc15 is very well conserved both in terms of sequence and synteny, potentially indicating an important role. Finally, the human locus, Cancer susceptibility 15, contains 29 different single nucleotide polymorphisms (SNPs), which predispose the carrier to highly metastatic cancers, again implying a role for *Casc15* in regulation of cell migration/metastasis (Buniello et al., 2019; Cerezo et al., 2025).

3.4 Conclusions

Many lncRNAs show consistent and highly specific patterns of expression despite significant methodological differences between scRNAseq papers, and these patterns can be identified in a qualitative way without the need for high performance computing (Becker et al., 2022). Of the lncRNAs that showed consistent patterns of cell type enrichment, *Casc15* (*2610307p16rik*) stood out as a candidate for the regulation of neurogenesis on the basis of its conservation and the impact of variants in this locus on human disease phenotypes.

Chapter 4: *Casc15* lncRNA and Migration

4.1 Introduction

4.1.i Long noncoding RNA in migration and metastasis

There is a reasonable amount of information supporting the role of various lncRNA in the migration and metastasis of cells within the CNS. A large proportion of this data however focusses on regulating the migration of tumour-derived cells, rather than examining how migration is regulated in the absence of pathology. Cancers and metastases, by definition, show aberrant patterns of migration and cell division. While data from tumour cells and immortalised cell lines can inform research on migration, migration from the V-SVZ to the OB is highly specific and tightly regulated. Thus, it is likely that particular lncRNAs may play different roles in migration regulation between health and disease.

4.1.ii *Casc15* lncRNA

Cancer susceptibility 15 (*Casc15*) is a long noncoding RNA that is highly expressed in the V-SVZ neurogenic lineage and shows several unusual features. lncRNAs typically show relatively poor sequence-based conservation and evolve more rapidly than protein coding sequences, furthermore, an estimated 30% of lncRNAs in the human genome are primate specific (Derrien et al., 2012a).

Casc15 is highly conserved at the level of both sequence and synteny in all amniote species examined, and is present in all cases as a complex multi-exonic locus encoded between the genes for *Sox4* and Prolactin (or the Prolactin cluster, in the case of mice). On average, a mature human lncRNA transcript is comprised of two exons with a total median length of 592 bases,

whereas the canonical *CASC15* transcript is made up of 8 exons with a total length of 1351 bases (Derrien et al., 2012a). The conservation of such a large and complex *CASC15* gene suggests that there may be selective pressure to maintain such a locus.

Genome Wide Association Study (GWAS) data reveals a strong relationship between variations in the *CASC15* sequence and various traits and pathologies (Buniello et al., 2019) (Figure 4.1, A). *CASC15* variants are associated with a range of different cancers, suggesting a role in tumorigenesis that is not cell-type or tissue specific. Functional data have found that *CASC15* regulates migration in a range of different cancers (Summarised Fig 4.1, B and Table 4.2). In most types of cancer, *CASC15* was found to promote migration (Figure 4.1, B). In neuroblastoma however, all available data suggested that *CASC15* acted as a suppressor of migration. Expanding examination of *CASC15* expression in human neuroblastoma using scRNAseq data reveals a clear overlap between *CASC15* expression, the neuroblastoma marker *MLLT11*, and the neuroblast marker *DCX* (Fig 4.1, C) (Bonine et al., 2024; Oskouian et al., 2024). This pattern of overlapping expression of *Casc15*, *Mllt11*, and *Dcx* is repeated in the V-SVZ of mice (Fig 4.1, D). Indeed in the developing human brain there is a strong positive correlation between *CASC15* and *DCX* expression (R=0.735), and a weaker positive correlation between *CASC15* and *MLLT11* (R=0.41) (Sunkin et al., 2013). This shared pattern of expression of these three genes suggests that there is some degree of shared identity between neuroblastoma cells and neuroblasts of the V-SVZ, despite neuroblastomas typically forming outside of the brain. It is therefore likely that data obtained examining the effects of *Casc15* on V-SVZ neuroblast migration will be most similar to the neuroblastoma data. Some genes may play different roles in different cellular and developmental context, which may drive the differing effects of *CASC15* on migration in different types of cancer.

The high degree of conservation of *Casc15* in conjunction with a broad-reaching and non-tissue specific effects suggests that it is poised to be a highly important regulator of migration and development.

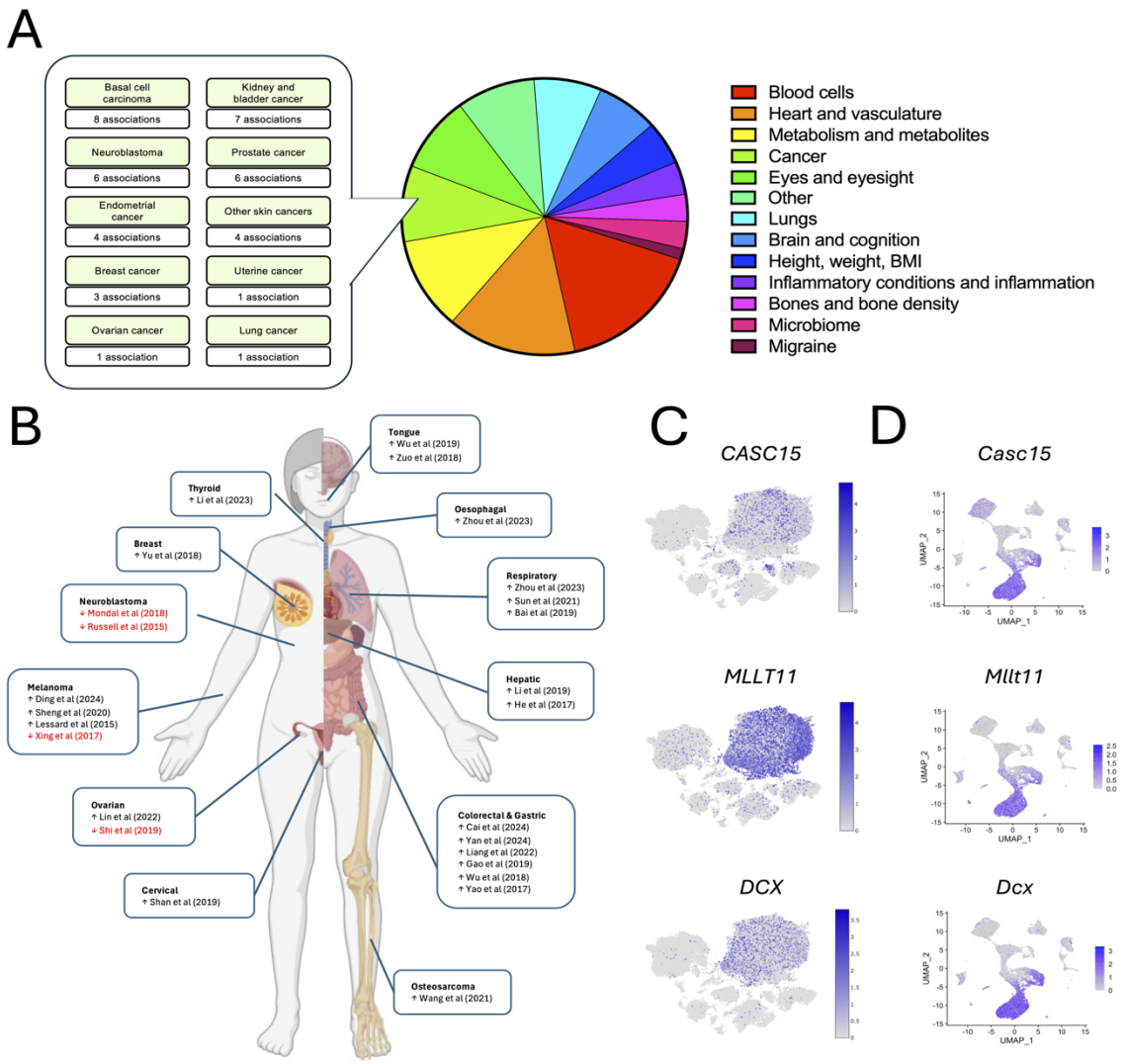

Figure 4.1 Aberrations in Casc15 expression regulate cancer cell migration A) *GWAS data of CASC15 associations in humans, with section on cancer expanded.* ***B)*** *This figure illustrates the impact of Casc15 on migration in different types of cancers. ↑ indicates cancers in which Casc15 promotes migration, and ↓ indicates cancers in which Casc15 suppresses migration. See Table 4.2 for details of each study.* ***C)*** *UMAP plots of CASC15, MLLT11, and DCX in human neuroblastoma samples highlight correlated patterns of expression (Bonine et al., 2024).* ***D)*** *UMAP plots of Casc15 (2610307P16rik), Mllt11, and Dcx in murine V-SVZ samples highlight correlated patterns of expression (Cebrian-Silla et al., 2021).* ***See Table 4.2 for more detail.***

Illustration in Panel B generated using BioRender.

4.1.iii Migration assays

There are a range of different migration assays that can be applied to study neuroblast migration in V-SVZ-derived cells. They differ vastly in terms of scalability and their ability to replicate *in vivo* migration. The scalability is determined by whether cells are cultured after removal from the animal – an explant migration assay for example, has a finite number of explants that can be generated from a single animal; whereas a neurosphere migration assay can have huge numbers of parallel replicates derived from a single animal as cells can be cultured with EGF/FGF to promote proliferation. Whether cells are migrating on a 2-dimensional plane or on a 3-dimensional matrix can have a large impact on results, as cells may have radically different migration dynamics depending on the substrate that they migrate through, and in 3D assays the first cells to migrate through a matrix may modify it (Lemmon et al., 2009). Cells typically migrate in 3D *in vivo* rather than along a plane or surface, so this may be a more accurate model for studying cell migration.

Another consideration is whether cells will be dissociated and diluted to a set concentration. Dissociation allows tighter control of cell numbers and can ensure the same number of cells starting in each replicate, and when used in conjunction with FACS sorting for example can allow isolation of the desired cell type. However, dissociation is destructive and can lead to cell death as well as destroying extracellular matrix features, disrupting cell-cell interactions, and disrupting chemokine gradients that may be influencing migration. It is important to note that chemoattractant gradients are not necessary for V-SVZ neuroblast migration, and cells will continue to migrate along the RMS even in the absence of the OB (Kirschenbaum et al., 1999). There are additional chemorepellent factors such as SLIT proteins present in the V-SVZ (Wu et al., 1999). However, dissociated cells from the RMS will continue to migrate - albeit without

particular direction - suggesting that neuroblast migration is dependent on both cell intrinsic and extrinsic factors.

As with any techniques studying a given process, all of these migration assays fall along a spectrum from higher throughput but poor representation of *in vivo* processes (e.g. neurosphere migration assay), to low throughput but highly representative (e.g. intravital 3-photon live imaging). Using a combination of methods and comparing trends in their results allows the separation of meaningful biological effects and the quirks of a particular assay.

4.2 Results

4.2.i *Casc15* regulates migration genes *in vitro*

In order to identify biological processes that may be regulated by *Casc15*, bulk RNA sequencing was performed *in vitro* on tertiary neurospheres derived from the murine V-SVZ. Two different antisense oligonucleotide (ASO) constructs, denoted ASO147 and ASO899 were used to significantly reduce *Casc15* expression (Figure 4.2, A). Initial library generation and sequence alignment was performed by Dr Bin Sun and Dr Michael Shapiro.

Dimensionality reduction and principle component analysis suggest that the construct ASO899 is most different from the control, and that construct ASO147 is more similar to the control (Fig 4.2, B). This similarity can be visualised again by plotting a heatmap of regularised log transformed values, which shows that samples treated with ASO899 clustering separately whilst ASO147 and control samples are more similar (Fig 4.2, C). Knockdown of *Casc15* with ASO147 lead to the upregulation of 107 genes and the downregulation of 79 genes (Fig 4.2, D, Table 4.3). Knockdown with ASO899 lead to the upregulation of 291 genes and the

downregulation of 371 genes (Fig 4.2, E, Table 4.3). There was an overlapping cohort of 95 genes that were up- or downregulated by both constructs (Fig 4.2, F, Table 4.3).

Differential gene expression analysis revealed that there are 95 genes that were significantly differentially expressed in the same direction after *Casc15* knockdown with both ASO147 and ASO899 (Fig 4.2, F). Key downregulated genes with known roles in cell migration and brain development and include A disintegrin and metalloproteinase with thrombospondin motifs 9 (*Adamts9*), (Carver et al., 2021); Jagged1 (*Jag1*) (Ables et al., 2011); Roundabout homolog 2 (*Robo2*) (Andrews et al., 2008); and Sonic hedgehog (*Shh*) (Lai et al., 2003).

Examining Biological Process (BP) gene ontology (GO) analysis results (Fig 4.2, G, Table 4.4) for genes that are differentially regulated ($p<0.05$, $l2fc>2$) for both ASO constructs reveals a significant enrichment for terms associated with cell migration and neuronal morphogenesis, the 20 most significant of which are plotted in Fig 4.2, G. This suggests that *Casc15* may be regulating gene networks that control the rate of cell migration and morphogenesis in neural precursor cells. The four most significantly changed gene ontology terms are all regarding the negative regulation of movement and motility: GO:0040013 (Negative regulation of locomotion, FDR adj p= 4.381E-04), GO:0030336 (negative regulation of cell migration, FDR adj p= 4.381E-04), GO:2000146 (negative regulation of cell motility, FDR adj p= 4.539E-04), GO:0051271 (negative regulation of cellular component movement, FDR adj p= 1.005E-03). The method used for calculating GO, GOnet, takes into account the directionality of expression change for each gene, but the output highlights dysregulated ontologies, rather than up- or downregulated ontologies. This approach allows for assessment of changed gene ontologies in which the expression of multiple related genes is altered due to loss of regulation control, rather than the induction of specific regulatory mechanisms.

These data suggest that ASO-mediated depletion of *Casc15* lncRNA triggers transcriptional changes associated with the regulation of cell migration in neurospheres. Analysis of this dataset is expanded upon to examine directional changes and broader pathways in Chapter 5 (Figure 5.2, Table 5.3).

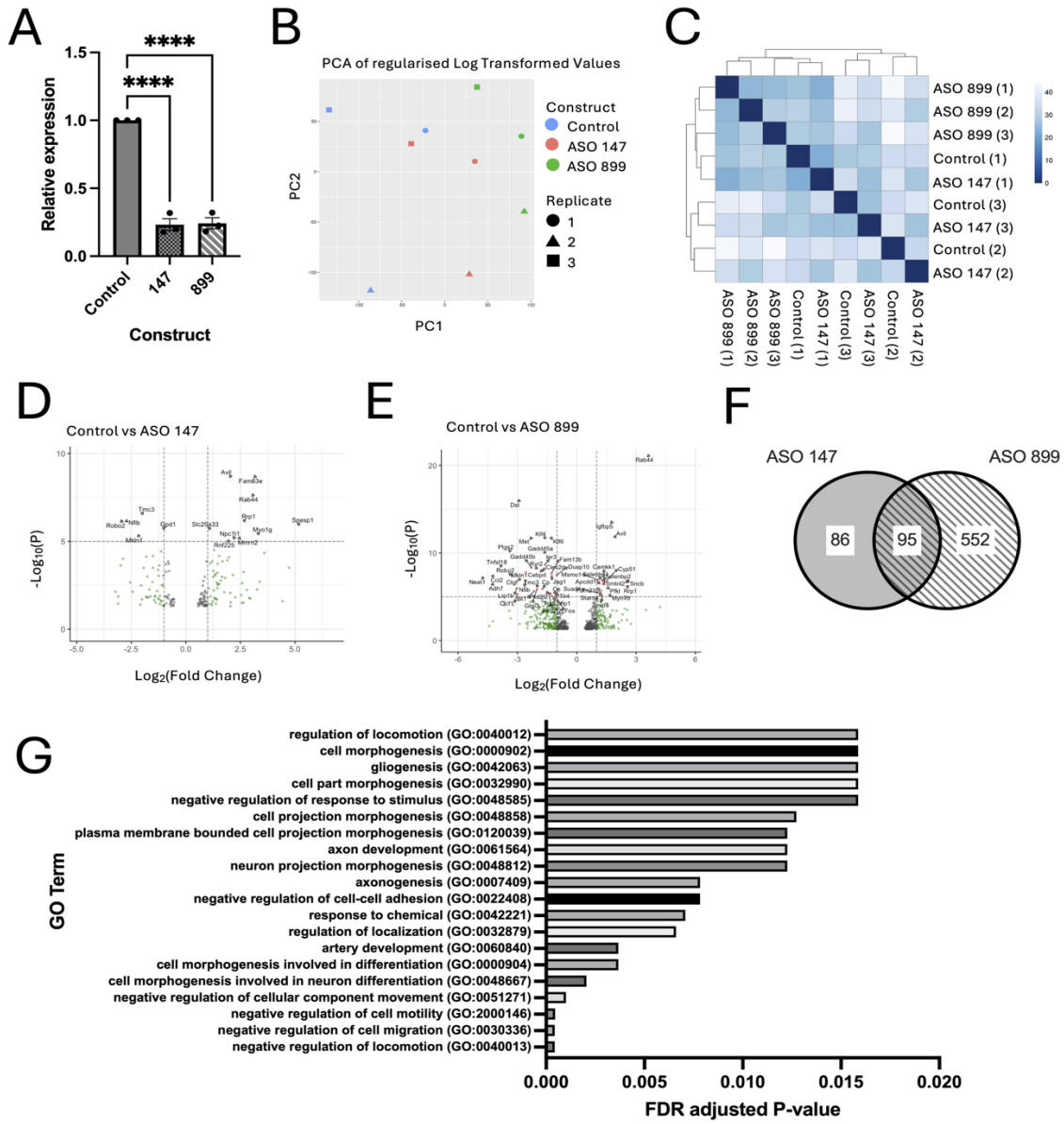

Figure 4.2 Casc15 regulates migration genes* in vitro** ***A) *Casc15 relative expression in tertiary neurospheres with control construct, ASO 147, or 899. Two different ASO constructs were used to significantly reduce Casc15 expression* ***B)*** *PCA of regularised log transformed values for Casc15 bulk RNAseq in neurospheres.* ***C)*** *Heatmap of regularised log transformed values for Casc15 bulk RNAseq knockdown.* ***D)*** *Volcano plot for differential gene expression of ASO 147 vs control, filtered to show only genes with padj<0.05.* ***E)*** *Volcano plot for differential gene expression of ASO 899 vs control, filtered to show only genes with padj<0.05.* ***F)*** *Venn diagram illustrating the number of differentially expressed genes relative to controls. A total of 181 genes are differentially expressed upon ASO 147 treatment, and 647 genes are differentially regulated by ASO 899 treatment. There is a cohort of 95 genes that change in expression upon treatment by either construct* ***G)*** *Top 20 enriched biological process gene ontology terms for genes that show differential regulation in both ASO 147 and ASO 899 samples relative to control.* ***See Tables 4.3 and 4.4 for more detail.***

Error Bars = SEM. Abbreviations: ASO – Antisenseo; PCA – Principle component analysis; GO – Gene Ontology

4.2.ii Knockdown of *Casc15* increases the size of RMS spheroids

In order to confirm whether the effect of *Casc15* on migration-related genes was functional I next used an *in vitro* assay of V-SVZ neuroblast migration using primary RMS neuroblasts.

Casc15 lncRNA was depleted using two different siRNA constructs of differing strengths so that dose-dependent responses could be studied. Constructs were validated by co-electroporation with a GFP+ plasmid into tertiary neurospheres and quantification by RT-qPCR 72h after electroporation. siRNA12 and siRNA11 significantly reduced *Casc15* expression in neurospheres to approximately 40% and 11% of control levels, respectively. (Figure 4.3, A).

Knockdown siRNA constructs were electroporated into dissociated RMS-derived neuroblasts, which were subsequently embedded in Matrigel. After 24h these spheroids were imaged in brightfield and their largest cross-sectional area was quantified (Ducker et al., 2020a). The reduction of *Casc15* expression caused a significant increase in the volume occupied by neuroblasts relative to controls with both siRNA12 and siRNA11, (Fig 4.3, B). Example images of spheroids electroporated with each construct are shown in Fig 4.3 C, where the increased cross sectional area of spheroids treated with siRNA11 is clear. However, from this assay alone is it unclear whether this difference in spheroid area is due to changes in cell migration, proliferation, survival, or a combination of all three.

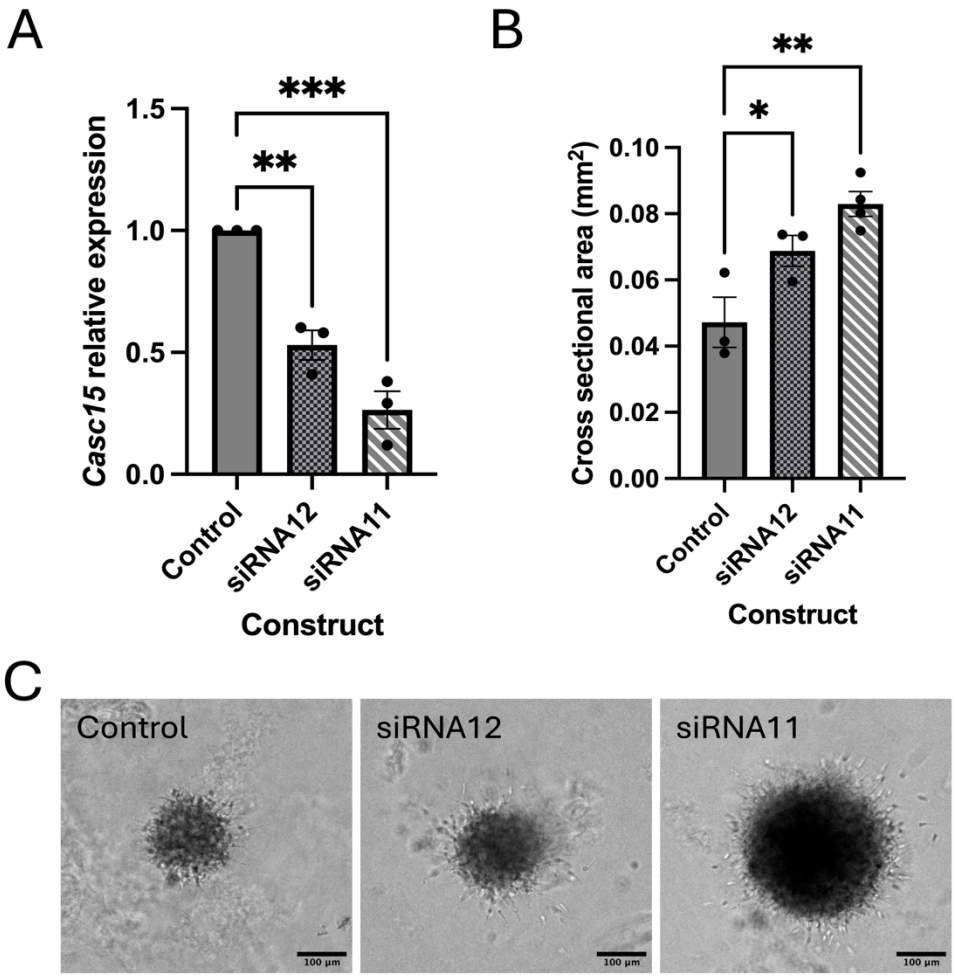

Figure 4.3 Knockdown of Casc15 increases the size of RMS spheroids. ***A)*** *Relative expression of Casc15 in neurospheres as determined by RT-qPCR with control or knockdown (siRNA12, siRNA11) constructs nucleofected.* ***B)*** *Cross-sectional area of RMS spheroids when nucleofected with each siRNA construct.* ***C)*** *Example brightfield images at 10x of RMS spheroids after 24h migration into matrigel, images show a single Z plane.* ***See Table 4.1 for details of statistical tests.***

Scale bars represent 100µm, error bars represent SEM.

4.2.iii *Casc15* suppresses migration of neuroblasts *ex vivo*

I next used an *ex-vivo* model of migration using explants taken from the RMS. These are cells taken from the same region as those used for spheroids previously, but the extracellular matrix is not disrupted by dissociation. In order to maintain the integrity of the explants I exposed them to siRNA constructs in the Matrigel that they were embedded in without dissociating and electroporating the constructs. The efficacy of simply suspending these constructs in cell

culture media without electroporating was confirmed in a single-cell suspension of tertiary neurospheres. This showed that *Casc15* expression was significantly reduced by siRNA12 to ~12% and siRNA11 to ~2% relative to control samples after 24h of exposure to constructs in media (Figure 4.4, B).

In order to quantify changes in the rate of migration upon treatment with *Casc15* knockdown siRNAs I measured the surface area covered by neuroblasts 48h after treatment (Denoted T48, Fig 4.4, A'). this area will be influenced by the original size of the explant, so I calculated a value "migration ratio" that accounted for this difference. Firstly, I calculated the overall change in the area covered by cell bodies, Δ(Area), by subtracting the original area of the explant (T_0(Area), Fig 4.4 A) from the area covered at 48h (T_{48}(Area), Fig 4.4 A') (equation 1, Fig 4.4 A''). I then divided this by the original area of the explant to give the migration ratio (equation 2, Fig 4.4, A'').

$$[1]\ \Delta(Area) = T_{48}(Area)\ -\ T_0(Area)$$

$$[2]\ Migration\ Ratio = \frac{\Delta(Area)}{T_0(Area)}$$

Analysis of explants treated with siRNA11 and siRNA12 suggested that they both increased the migration ratio relative to control. siRNA11 significantly increased migration ratio, while siRNA12 did not give rise to a statistically significant change (Fig 4.4 C). While I have termed this metric "migration ratio" it is important to consider that there may be other factors that can influence the surface area occupied by cell bodies; an increase in proliferation, for example, could cause an increase in the number of cells that migrate out from an explant, thus increasing the "migration ratio" without having a direct effect on the rate of migration.

I then confirmed the identity of the cells that migrated out of the explants using the markers GFAP (astrocytes) and TUBB3 (neuronal progenitors), Fig 4.4, E. As has been seen in previous studies of RMS explant migration, there were some GFAP+ astrocytic processes extending out of the core of the explant, but all cells that had fully migrated out from the explant were TUBB3+ (Wichterle et al., 1997). This assay additionally was able to recapitulate characteristic features of V-SVZ neuroblast migration such as chain migration, which was present across all treatment groups.

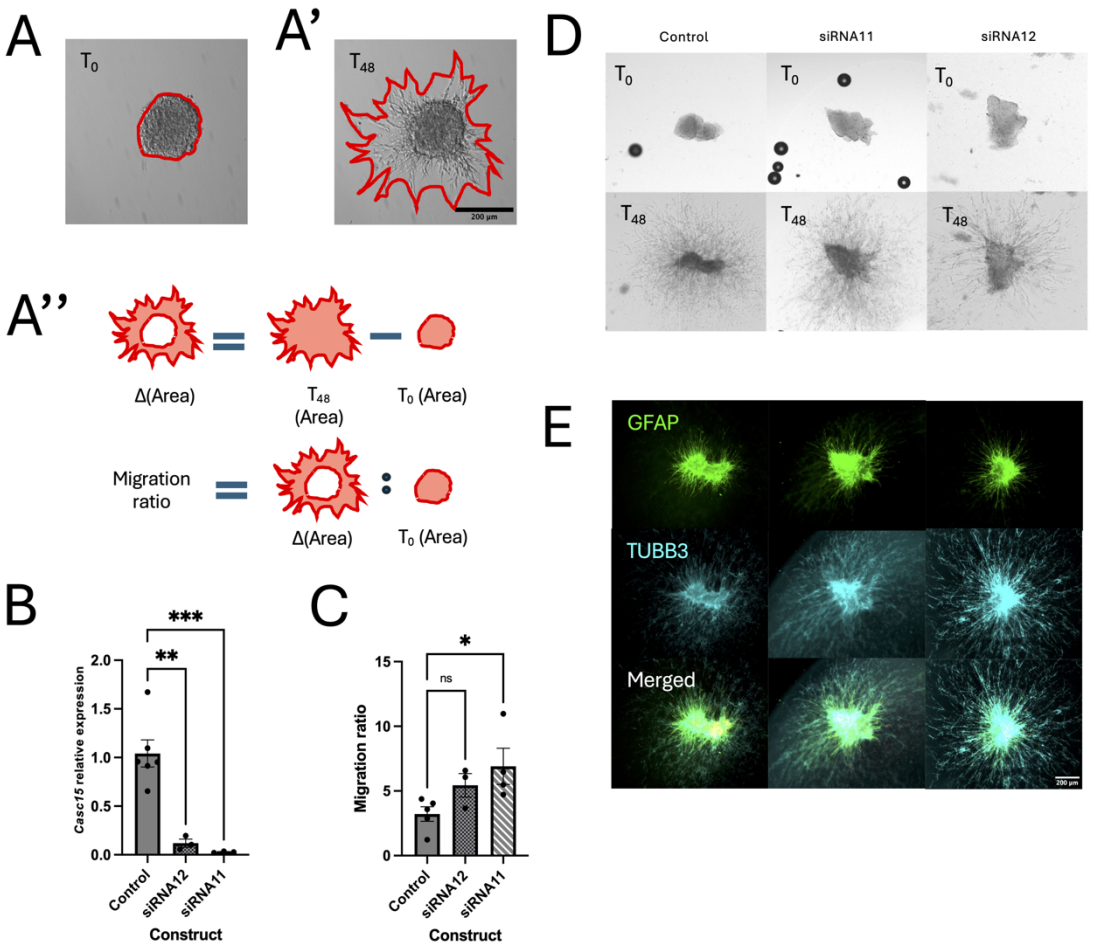

Figure 4.4 Effect of Casc15 knockdown on an ex vivo explant assay A) *Visual illustration of calculation of migration ratio.* ***A)*** *explant at T0,* ***A')*** *the same explant at T48,* ***A'')*** *illustration of how migration ratio is calculated using outlines from* ***A*** *and* ***A'. B)*** *Impact of knockdown constructs after 24h on Casc15 expression in tertiary neurospheres without electroporation* ***C)*** *Migration ratio for explants treated with either control or knockdown constructs in the media* ***D)*** *Brightfield images of representative explants at 0 (T0) and 48h (T48) after dissection* ***E)*** *Immunohistochemistry of representative explants showing GFAP (green), TUBB3 (cyan) and merged images at 48h after dissection.* ***See Table 4.1 for details of statistical tests.***

Error bars= SEM, the same scale is used for panels D and E, scale bar = 200µm.

4.2.iv *Casc15* supresses neurogenesis *in vivo*

In order to assess the impact of *Casc15* depletion on neurogenesis *in vivo*, two plasmids were co-electroporated into the V-SVZ of P0 pups. The first plasmid was a kind gift from the laboratory of Professor Shankar Srinivas, and encoded a histone2B-GFP fusion to mark nuclei, and a myristoylated tdTomato which marks cell membranes (Trichas et al., 2008). The second plasmid consisted of a CRISPRi guide RNA (gRNA) and a dCas9-KRAB fusion, which possesses the same sequence specific targeting ability as Cas9, but transcriptionally represses the target site rather than cleaving DNA (Figure 4.5, A). Generation, validation, and electroporation of plasmid constructs were performed by Dr Bin Sun, a former member of the Szele Lab. CRISPRi constructs targeting the *Casc15* locus were used, denoted 58i and 59i, to significantly reduce the expression of *Casc15* when electroporated into V-SVZ-derived neurospheres (Fig 4.5, B).

Constructs were electroporated into cells lining the lateral wall of the V-SVZ, therefore all cells expressing knockdown constructs that are found in the OB will have migrated there from the V-SVZ. I found that knockdown of *Casc15* with CRISPRi significantly increased the density of GFP+ nuclei within the OB of animals at 14 days post electroporation (Figure 4.5, C). Examination of GFP+ cell density in the OB of animals at 4 and 7 days post electroporation revealed a trend towards increased density, but this did not reach statistical significance (data not shown). Notably, at 4 days post electroporation almost all cells are still located within the RMS and have not yet begun the radial phase of migration through the OB nor have they started to differentiate. Radial migration but not differentiation was observed in cells at 7 days post electroporation. These observations are consistent with the timeline of olfactory interneuron differentiation described by Petreanu & Alvarez-Bullya (2002).

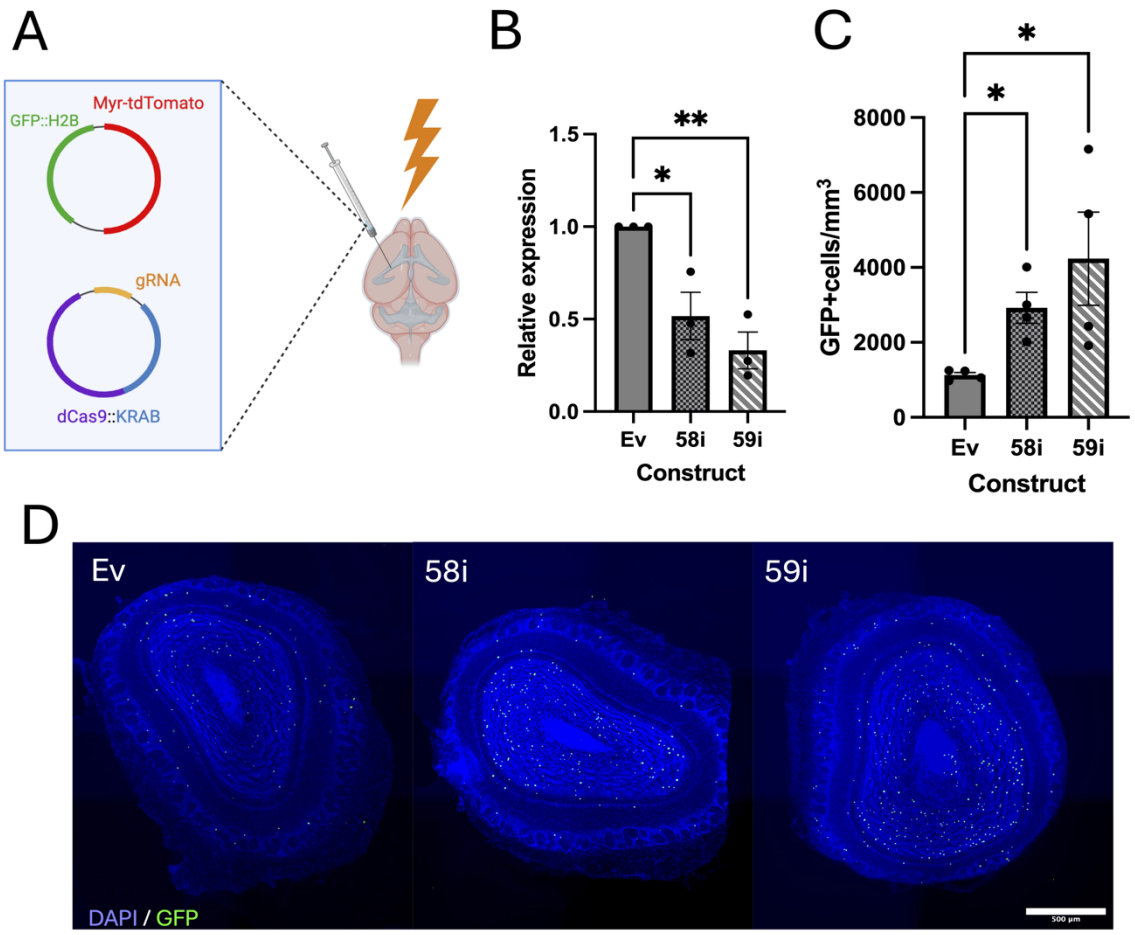

Figure 4.5 In vivo knockdown of Casc15 increases cell density in the olfactory bulb A) *schematic of marker and knockdown construct plasmids used for electroporation* ***B)*** *RT-qPCR shows that knockdown constructs 58i and 59i were able to significantly reduce Casc15 expression* ***C)*** *mean density of GFP+ cells in the OB at 14dpe is increased significantly in 58i and in 59i treated brains.* ***D)*** *example tilescans of OB sections at 14dpe and 20x magnification, highlighting GFP+ cells.* ***See Table 4.1 for details of statistical tests.***

Error bars = standard error of the mean, scale bar = 500µm. Abbreviations: OB (olfactory bulb), 14dpe (14 days post electroporation), GFP (green fluorescent protein)

4.2.iv *Casc15* knockdown does not give rise to an overt V-SVZ phenotype *in vivo*

Increases to the number of GFP+ cells reaching the OB after knockdown could be due to a number of factors, such as increased proliferation of progenitors in the V-SVZ prior to migration or a decrease in the rate of apoptosis. In order to examine whether there is an effect of *Casc15* lncRNA on *in vivo* cell division or survival, a construct expressing a CRISPR inhibition (CRISPRi) construct was electroporated into the lateral ventricles of P0 mice.

Animals were then allowed to recover for 4, 7, or 14 days. CRISPRi knockdown constructs for 4 and 7 day recovery groups were co-electroporated with a GFP expressing plasmid, and constructs for 14 day group were co-electroporated with a plasmid encoding a GFP::H2B fusion and a myristoylated tdTomato (described in Methods section).

The density of GFP+ cells in the V-SVZ did not change significantly between groups at 4 days post electroporation (Figure 4.6, A), 7 days post electroporation (Fig 4.6, B), or 14 days post electroporation (Fig 4.6, C). This suggests that the change in the number of GFP+ cells in the OB at 14 days post electroporation cannot be attributed to differences in electroporation efficiency or the number of GFP+ cells in the V-SVZ. Despite there being no statistically significant effects, there does appear to be a trend towards increased GFP+ cells in the V-SVZ of CRISPRi animals at 4 days post electroporation; whether this could be due to differences in cell death or proliferation is addressed in Figures 4.8 and 4.9.

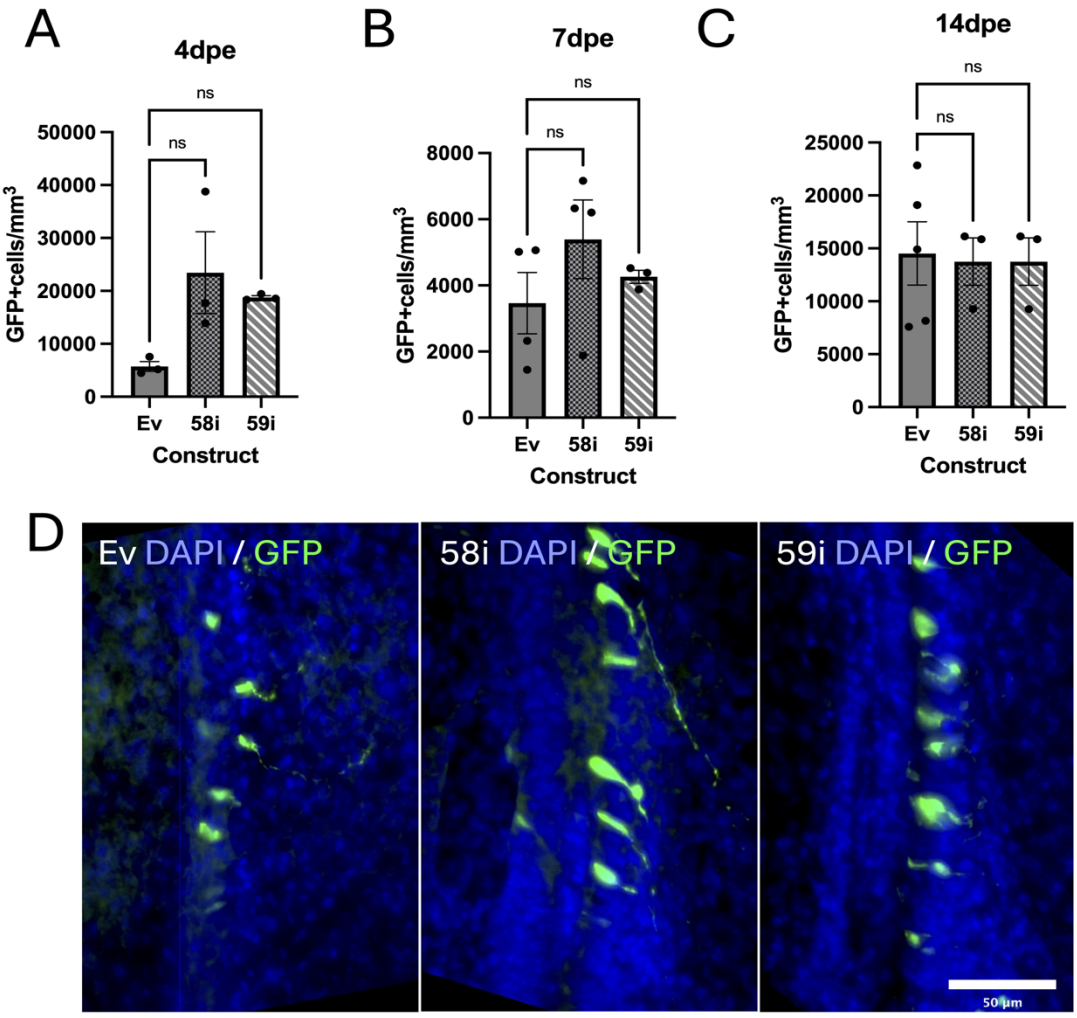

Figure 4.6 Knockdown of Casc15 does not give rise to an overt V-SVZ phenotype A) *mean density of GFP+ nuclei in the V-SVZ at 4dpe.* ***B)*** *mean density of GFP+ nuclei in the V-SVZ at 7dpe.* ***C)*** *mean density of GFP+ nuclei in the V-SVZ at 14dpe.* ***D)*** *Representative images of the V-SVZ in 4dpe animals, showing DAPI (blue) and GFP (green).* ***See Table 4.1 for details of statistical tests.***

Abbreviations: V-SVZ - Ventricular-subventricular zone; dpe - Days post electroporation. Error bars = SEM, scale bars = 50µm

The question then remains whether this increase cell density within the OB upon *Casc15* knockdown is specific to the RMS, or a could be due to an increase in migration of V-SVZ derived progenitors. The postnatal V-SVZ also generates a small number of glial cells that migrate into the striatum (Al-Dalahmah et al., 2020; Levison and Goldman, 1993). Therefore I examined the striatal V-SVZ in coronal sections and classified each cell as being "V-SVZ associated" – i.e. within 1 cell width of the cell-dense V-SVZ; or "striatal" i.e. one or more

cells width from the V-SVZ. This revealed no significant increase in the proportion of cells migrating from the V-SVZ into the striatum (Figure 4.7, A).

However, measuring the distance between each individual striatal cell and the closest part of the V-SVZ suggested that cells that enter the striatum are migrating further in animals treated with the 59i knockdown construct, although no significant difference was found between controls and the weaker knockdown construct 58i (Fig 4.7, B). The morphology of these cells (shown in Fig 4.7, C) is characteristic of striatal astrocytes (Soto et al., 2023; Torigoe et al., 2015). This suggests that the impact of *Casc15* in the postnatal brain is not restricted to the neuronal lineage.

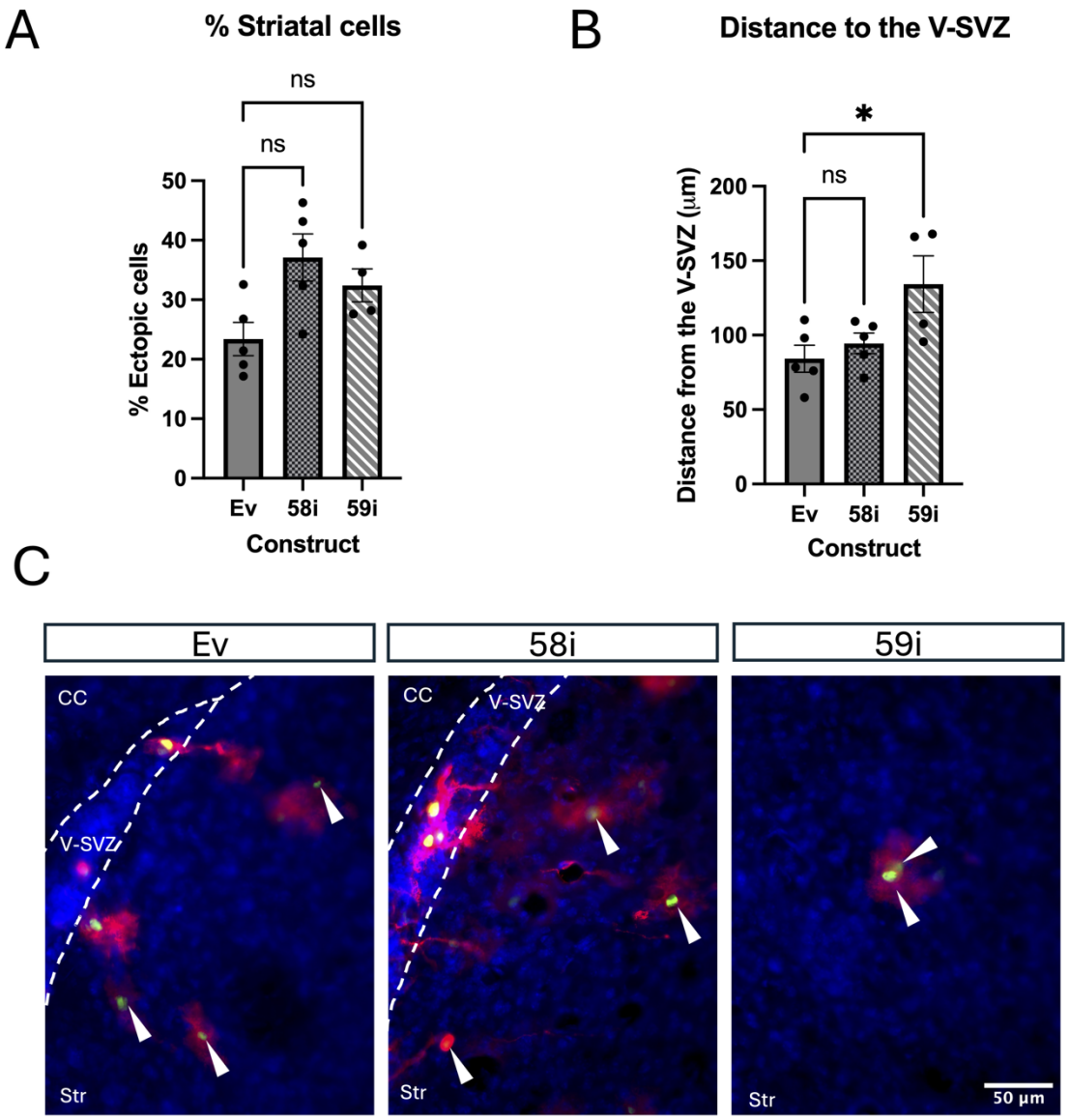

Figure 4.7 Casc15 knockdown increases distance migrated by cells in the striatum A) *Percentage of GFP+ cells at 14dpe that are found in the striatum.* ***B) A****verage distances for striatal cells from the V-SVZ (μm).* ***C)*** *Expression of construct (H2B-GFP / myr-tdTomato) at 14dpe in the V-SVZ and striatum, with the edge of the striatum highlighted by the dashed line.* ***See Table 4.1 for details of statistical tests.***

Error bars = SEM, scale bars = 50μm. Abbreviations: CC – Corpus Callosum; V-SVZ – Ventricular-subventricular zone; Str – Striatum.

4.2.v *Casc15* knockdown *in vivo* noes not significantly alter proliferation or cell death

An increase in the number of cells reaching the olfactory bulb upon *Casc15* knockdown could be due to either increased proliferation or decreased cell death independent from changes in

the rate of migration. I therefore examined the number of cells that expressed both the GFP+ knockdown constructs and the mitotic marker mKi67 (mKi67), and the marker of apoptosis cleaved Caspase-3 (Casp3) (Riss et al., 2004; Scholzen and Gerdes, 2000).

If alterations in proliferation are the underlying cause in the increase of neural progenitors reaching the OB then we would expect an increase in the percentage of GFP+ cells that express mKi67 after *Casc15* knockdown. Examining the percentage of GFP-construct labelled cells in the V-SVZ that co-expressed mKi67 did not reveal any significant difference between constructs, with ~2% of GFP+ being mKi67 + under all conditions (Figure 4.8, A). Examining the density of GFP+ mKi67 + cells in the V-SVZ reveals a slight trend towards increase with *Casc15* knockdown, although this does not reach statistical significance (Fig 4.8, B). This suggests that the majority of GFP labelled cells in the V-SVZ at 4dpe are not actively undergoing mitosis.

V-SVZ-derived neuroblasts are able to proliferate 2-3 times en-route to the OB (Ponti et al., 2013), so I next examined the overlap of GFP and mKi67 in the anterior RMS/posterior OB. This revealed a statistically insignificant trend towards an increase in % GFP+mKi67 cells upon *Casc15* depletion, (Fig 4.8 D). Similarly the density of GFP+mKi67+ in the OB at 4 days post electroporation did not very significantly between groups (Fig 4.8, E). Very notably, the percentage of GFP+ cells that expressed mKi67 in the anterior RMS of Ev animals was 0% in all animals examined, in contrast to 0.8232% +/-0.5 and 1.293% +/- 0.5217 in 58i and 59i treated animals respectively. This suggests that *Casc15* knockdown may have a very subtle effect on the proliferation of these neural precursors.

I next examined expression of the marker of apoptosis cleaved Caspase-3 (CASP3), as decreased rates of cell death in *Casc15* knockdown groups could cause the increased number of GFP+ cells reaching the OB. Examining the density of GFP+ cells that were also Caspase-3+ in the V-SVZ at 4 days post electroporation did not reveal any significant differences between Ev control and 58i or 59i knockdown constructs (Figure 4.9, A). Furthermore, examination of the proportion of total GFP+ cells in the V-SVZ that were expressing Caspase-3 also did not reveal any significant effect of *Casc15* knockdown (Fig. 4.9 B). Example immunohistochemistry showing Caspase-3 staining in the V-SVZ is shown in Fig 4.9, C.

I next examined Caspase-3 staining in the OB of animals that had been electroporated with the same CRISPRi knockdown constructs at four days post electroporation. The density of cells that were double positive for GFP and Caspase-3 did not vary significantly between groups (Fig 4.9, D). Moreover, there was no significant difference in the proportion of total GFP+ cells in the OB that were co-expressing Caspase-3 (Fig 4.9, E). Example immunohistochemistry is shown in Figure 4.9, F.

Taken together these data on mKi67 and Caspase-3 in both the V-SVZ and OB at 4 days post electroporation suggest that the effect of *Casc15* knockdown on the number of GFP+ cells in the OB is not due to changes in cell proliferation or death. The observed increase in the number of GFP+mKi67+ cells may account for a small part of the increase in GFP+ cells in the OB, but the difference in the absolute number of cycling cells is not sufficient to explain the difference in observed cell density at 14dpe (Fig 4.5).

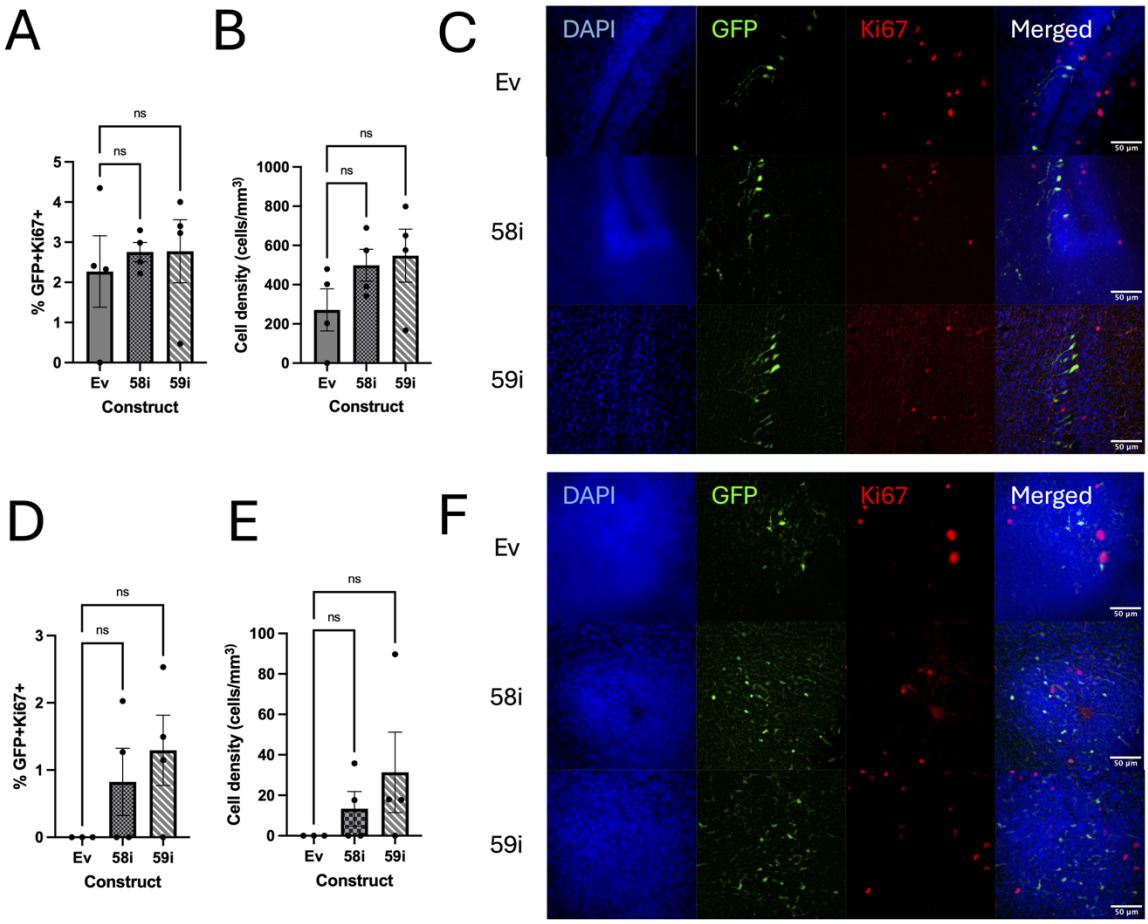

Figure 4.8 Knockdown of Casc15 does not significantly alter proliferation in the V-SVZ or OB at 4 days post electroporation. ***A)*** *The proportion of GFP+ cells that were positive for Ki67 at 4dpe in the V-SVZ.* ***B)*** *The density of GFP+Ki67+ cells at 4dpe in the V-SVZ.* ***C)*** *Example IHC showing DAPI (blue), GFP (green) and Ki67 (red) in the V-SVZ at 4dpe.* ***D)*** *The proportion of GFP+ cells that were positive for Ki67 at 4dpe in the OB.* ***E)*** *The density of GFP+Ki67+ cells at 4dpe in the OB* ***F)*** *Example IHC showing DAPI (blue), GFP (green) and Ki67 (red) in the OB at 4dpe.* ***See Table 4.1 for details of statistical tests.***

Error Bars = SEM, Scale bars = 50µm. Abbreviations: GFP - Green fluorescent protein; 4dpe - 4 days post electroporation; V-SVZ - Ventricular-subventricular zone;, IHC – Immunohistochemistry; OB - Olfactory bulb.

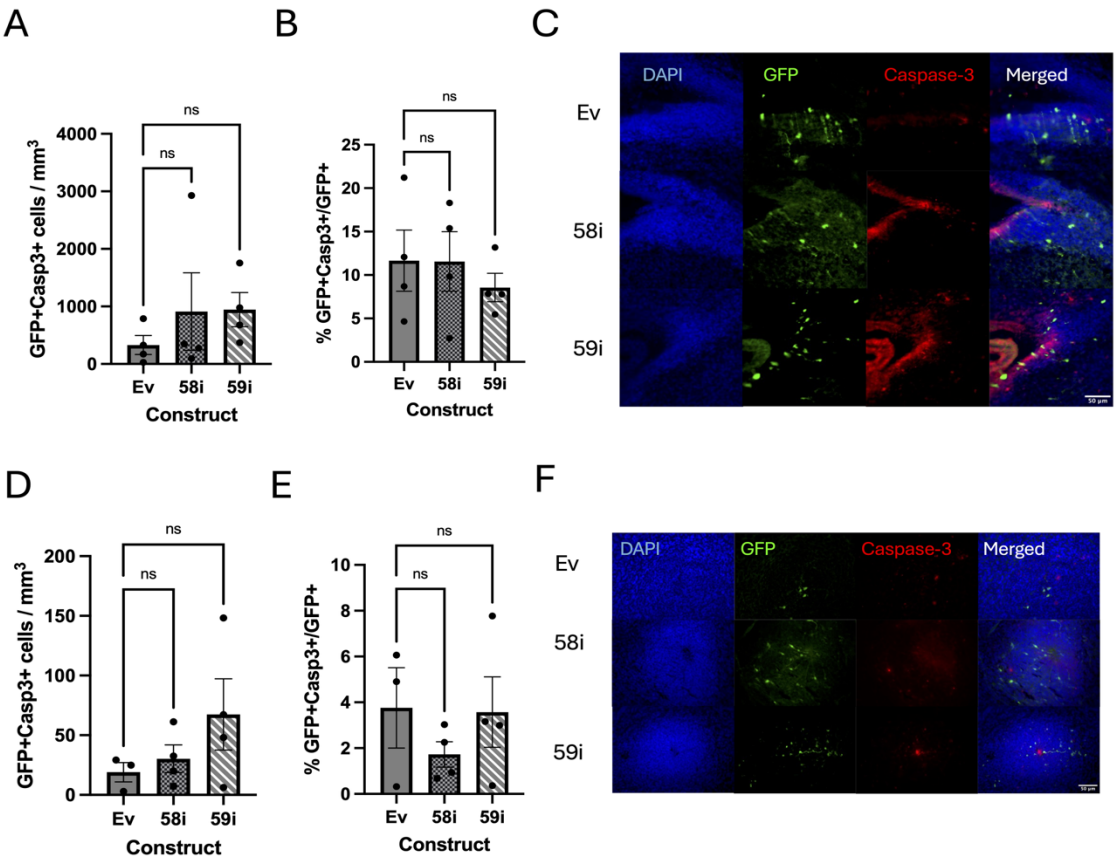

Figure 4.9 Knockdown of Casc15 does not significantly alter cell death in the V-SVZ or OB at 4 days post electroporation ***A)*** *Density of GFP+Casp3+ cells in the V-SVZ of animals 4 days after electroporation with different CRISPRi constructs.* ***B)*** *Percentage of GFP+ cells that are positive for Caspase-3 in the V-SVZ of animals 4 days after electroporation with different CRISPRi constructs* ***C)*** *Example IHC showing DAPI (blue), GFP (green), and Caspase-3 (red) in the V-SVZ at 40x magnification.* ***D)*** *Density of GFP+Casp3+ cells in the OB of animals 4 days after electroporation with different CRISPRi constructs* ***E)*** *Percentage of GFP+ cells that are positive for Caspase-3 in the OB of animals 4 days after electroporation with different CRISPRi constructs.* ***F)*** *Example IHC showing DAPI (blue), GFP (green), and Caspase-3 (red) in the V-SVZ at 40x magnification.* ***See Table 4.1 for details of statistical tests.***

Error bars = standard error of the mean. Scale bars = 50µm. V-SVZ - Ventricular-subventricular zone; OB - Olfactory bulb.

4.2.vii *Casc15* modulates the orientation of newborn OB interneurons *in vivo*

Upon examination of the numbers of mature interneurons in different layers of the olfactory bulb of animals with electroporated CRISPRi constructs I noted an unusual cell morphology that appeared to be predominantly found in animals with *Casc15* knockdown. A typical morphology for OB GCL interneurons would be a cell body closer to the centre of sections/the RMS, and a long primary dendrite ending in extensive branching radially outward. However I

observed a number of cells that did not show this morphology – which I termed “misoriented”. Cells showing this novel “misoriented” morphology have a cell body in the appropriate location and a long primary dendrite reaching radially outward. However, this primary dendrite does not then brand outwards; the majority of dendritic arborisation of these cells is at the opposite pole and close to the cell body and centre of sections. These cells still show appropriate radial symmetry. Characteristic cell morphologies are illustrated in Figure 4.11, A.

When examining the total number of GFP+ cells that show this orientation, knockdown groups 58i and 59i show a significant increase relative to controls in the overall percentage of cells that show this abnormal morphology (Fig 4.11, B). Notably this it is a very small proportion of total GFP+ cells that show this morphology.

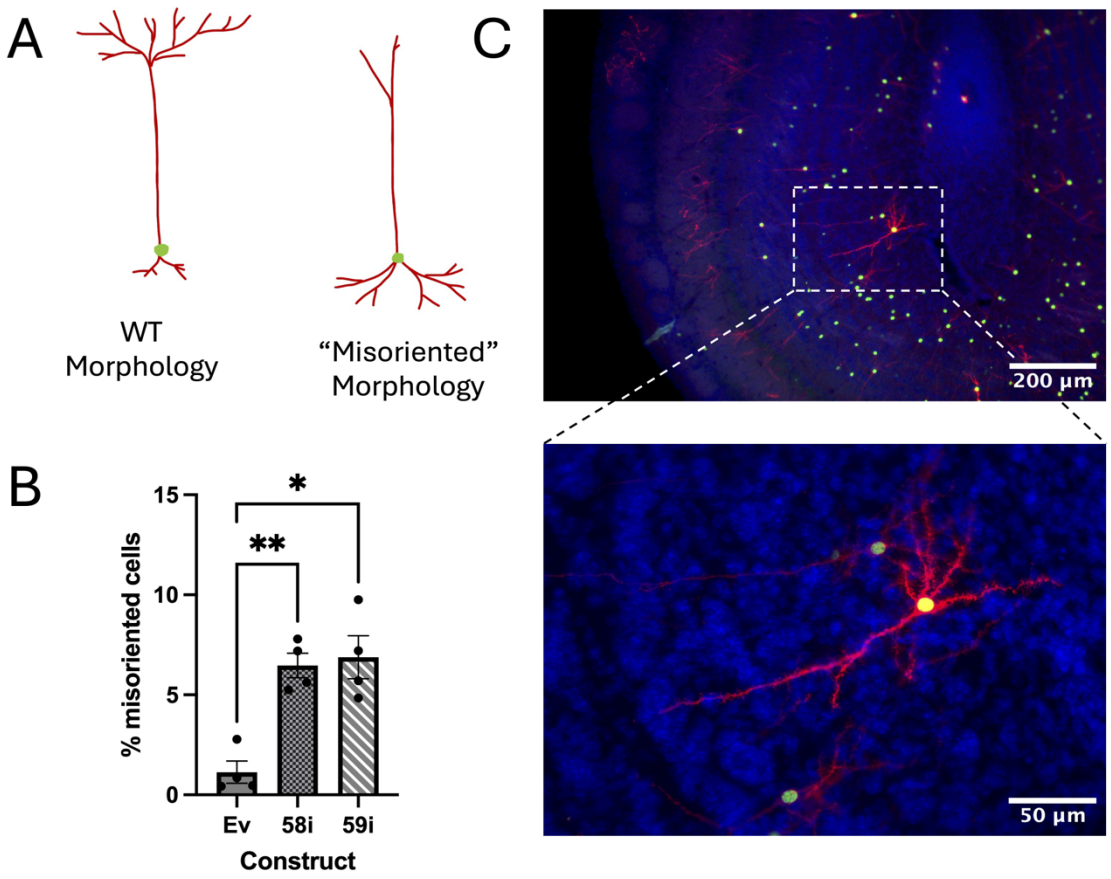

Figure 4.10 Knockdown of Casc15 causes GCL cells to show a misoriented morphology A) *Illustration of canonical wild type morphology and "misoriented" morphology for GCL interneurons generated in the postnatal period.* ***B)*** *Percentage of GCL GFP+ cells that show this misoriented morphology.* ***C)*** *Example images showing a well-defined cell with misoriented morphology in a 58i animal. Cell membranes are highlighted by tdTomato (red) and the nucleus with GFP (green). Nuclei are stained with DAPI (blue).* ***See Table 4.1 for details of statistical tests.***

Error bars = SEM. Scale bars represent 200µm and 50µm in the upper and lower panels respectively. Panel A drawn in Adobe Procreate.

4.2.vi *Casc15* modulates the location of mature newborn OB interneurons *in vivo*

I next examined whether newly generated neurons were maturing in the correct layer of the OB. Interneurons derived from the postnatal V-SVZ typically will stop and mature/differentiate in either the granule cell layer (GCL) or glomerular layer (GL) of the olfactory bulb (Altman, 1969). These layers can be easily distinguished by DAPI staining (nuclei) as they show characteristic morphology and distribution of cells, these layers are highlighted in Figure 4.10, A. I defined "misplaced" cells as those that showed mature morphology (two or more dendritic bifurcations) and whose cell body was located outside of the GCL or GL. Knockdown of

Casc15 significantly increased the density of misplaced cells in the OB with either knockdown construct when compared to controls (Fig 4.10, B).

While this is a statistically significant result, it must be noted that misplaced cells only account for <2% total GFP+ cells.

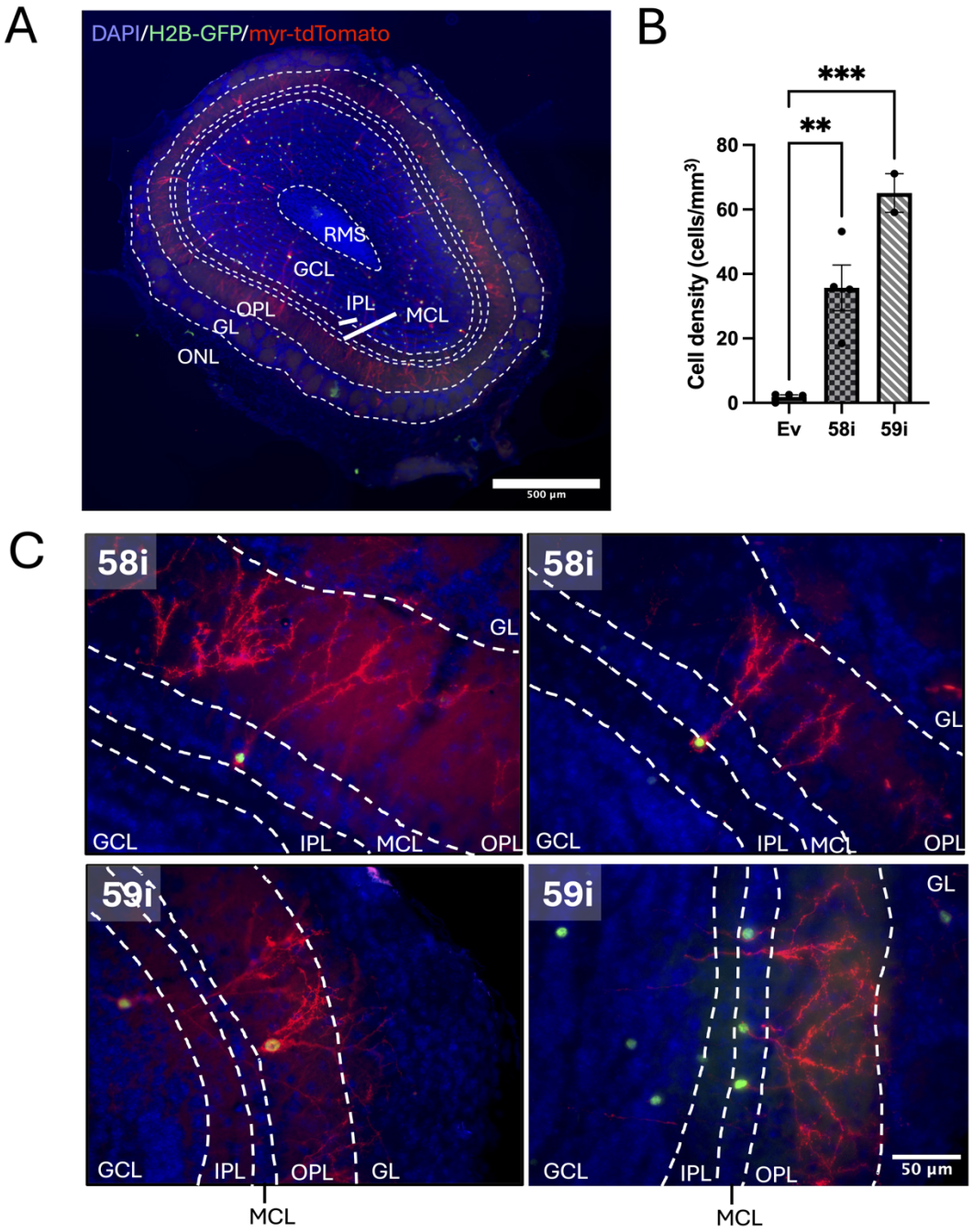

Figure 4.11 Casc15 knockdown causes an increase in cells maturing outside of the GL and GCL A) *Anatomy of the murine olfactory bulb at postnatal day 14, stained for DAPI (blue) and H2B-GFP (green)/myr-tdTom (red) expressing constructs. Layers of the olfactory bulb are delineated with dotted white lines and are labelled in white. Abbreviations: RMS (rostral migratory stream) GCL (granule cell layer) IPL (inner plexiform layer) MCL (mitral cell layer) OPL (outer plexiform layer) GL (glomerular layer) ONL (olfactory nerve layer).* ***B)*** *density of cells showing mature morphology with cell body located outside canonical V-SVZ target layers.* ***C)*** *Higher magnification images of "misplaced" cells.* ***See Table 4.1 for details of statistical tests.***

Error bars represent SEM, scale bar = 500µm ***(A),*** *and 50µm* ***(C).***

4.2.viii *Casc15* modulates the structure of newborn OB interneurons *in vivo*

My next question was whether the additional cells migrating from the V-SVZ to the OB were able to develop the appropriate structure. I quantified the length of the primary dendrite (distance between the centre of the cell body and the first bifurcation) in OB interneurons that showed a mature morphology, using the same definition of maturity as in section 4.2.vi. I measured the length of primary dendrites in cells where I could clearly identify a GFP+ cell body in the granule cell layer, as well as clear dendritic arborisation. I found that knockdown of *Casc15* caused a decrease in the average length of primary dendrites. (Figure 4.12, A). Examples of GCL interneurons are highlighted in Figure 4.12 B-D.

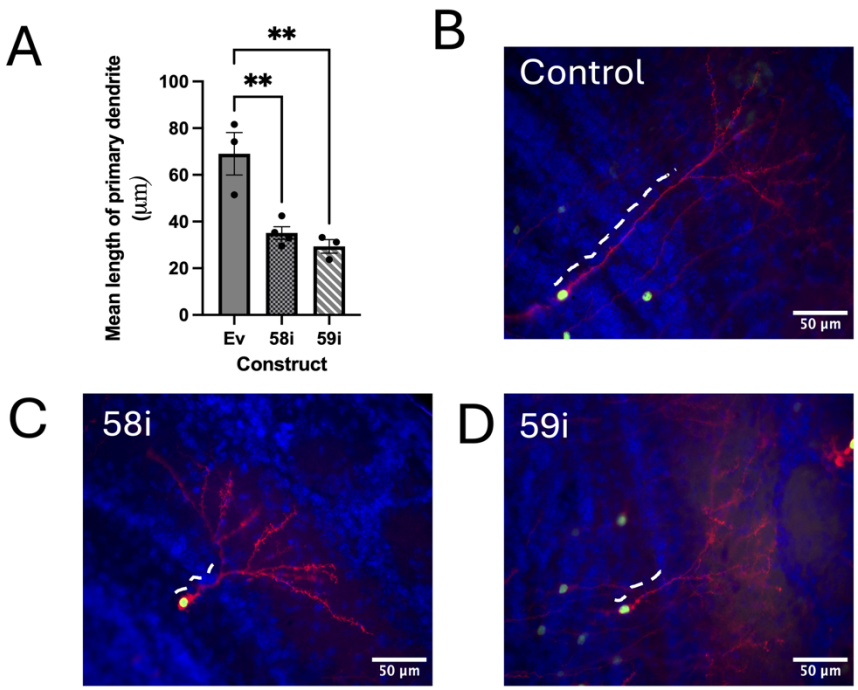

Figure 4.12 Casc15 knockdown causes truncation of GCL interneuron primary dendrites. ***A)*** *mean length of primary dendrites for GCL interneurons between knockdown conditions (µm).* ***B-D)*** *Example images of control and CRISPRi Casc15 depleted interneurons. Images are displayed with DAPI (blue), GFP (green), and tdTom (red), and the length of the primary dendrite is highlighted with a white dashed line in each case.* ***See Table 4.1 for details of statistical tests.***

Error bars = SEM. scale bars represent 50µm

4.2.ix *Casc15* knockdown does not impact dendritic spine density in the OB

Dendritic spines are a characteristic feature of GCL interneurons in the OB. They are small protrusions from the cell that are able to form contacts and synapses with other cells (Shepherd et al., 2007). A reduced density of dendritic spines in postnatally born GCL interneurons leads to decreased inhibition of mitral cells, thus increasing odour-invoked responses in the OB (Reshef et al., 2017).

Animals that were electroporated with CRISPRi constructs and left to recover for 14 days post electroporation (14dpe) expressed a myristoylated-tdTomato that was incorporated into cell membranes, clearly highlighting cell morphology (Trichas et al., 2008). I used high magnification imaging (100x) at 0.05µm z spacing to examine the density of dendritic spines in GCL interneurons. I chose interneurons with cell bodies in the GCL (see Figure 4.10) and wild-type orientation (see Figure 4.11). I chose three cells per animal with cell bodies at similar depths in the GCL, and examined all dendrite branches.

This revealed no difference between control, 58i, or 59i treated animals (Figure 4.13, A). Examples of maximum intensity Z-projections highlighting dendritic spines are shown in Fig 4.13, B.

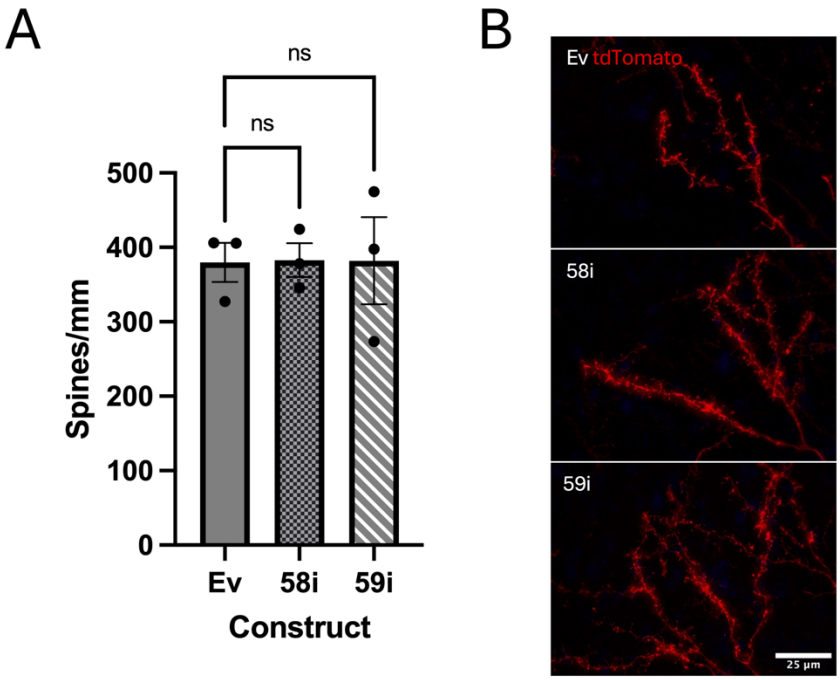

Figure 4.13 Casc15 CRISPRi knockdown does not alter dendritic spine density in the OB at 14dpe A) *The density of dendritic spines does not significantly vary between Ev-, 58i-, and 59i- treated animals at 14 days post electroporation.* ***B)*** *Example Z-projections at 100x magnification showing myr-tdTomato-positive dendrites in the OB.* ***See Table 4.1 for details of statistical tests.***

Error bars = SEM, scale bars = 25µm. Abbreviations: OB – olfactory bulb

4.3 Discussion

4.3.i Transcriptional changes upon *Casc15* depletion

The data illustrated here strongly suggest that *Casc15* knockdown regulates migration via inducing an altered transcriptional program in V-SVZ-derived NSCs, thus biasing them to be more migratory. This bias may be achieved by relief of inhibition, as suggested by downregulation of gene ontologies association with the suppression of migration. The large number of differentially expressed genes upon *Casc15* depletion suggest that it may be participating in a number of parallel mechanisms to regulate gene expression.

For initial gene ontology analysis, an approach built on the python GoEnrich package was chosen. This method returns a list of gene ontologies that are changed, rather than specifically up- or downregulated. This approach is more sensitive to loss of regulation control, whereas other methods that more strictly segregate data by up- or downregulation of genes are better for assessing concerted alterations in transcriptional programmes. Examination of specific pathways in a directional manner is addressed in Chapter 5.

Importantly, this bulk RNAseq was performed on neurospheres: free-floating, proliferative cells derived from the NSCs of the V-SVZ. Neurospheres are heterogeneous spheres of cells, containing a mixture of lineages. Neurospheres contain cells that are positive for the neuroblast markers DCX and TUBB3, as well as large numbers of GFAP+ astrocytes and neural stem-like cells, and O4/OLIG2+ oligodendrocyte precursors (Eunhyuk Chang, unpublished data). Cells expressing all of these markers are present in RMS-derived tissue used for spheroid migration and explant migration assays, although at different ratios. The most important difference between neurospheres and the RMS tissue for explant assays is that neurospheres

are cultured with EGF and FGF, which results in them being highly proliferative and restrains differentiation. Upon withdrawal of growth factors, migratory cells can be derived from neurospheres. In contrast, RMS explants and spheroids are cultured in the absence of growth factors, and as such have very low levels of proliferation highlighted by small numbers of mKi67+ cells in the core of explants (data not shown). Neurospheres therefore represent an earlier point in the V-SVZ neurogenic lineage than RMS spheroids or explants.

For studies of the V-SVZ it is typically inferred that transcriptional changes in neurospheres are able to approximate changes that would be observed *in vitro*, but any extrapolation of *in vitro* results must be approached with caution. Notably, scRNAseq studies (such as Cebrian-Silla et al., 2021) suggest that *Casc15* expression is highest in neuroblasts and slightly lower in the NSCs that are closer in identity to neurospheres. As a result the impact of *Casc15* depletion may be different between these different, but related, cell types.

An important note when considering lncRNAs is that the RNA sequencing we performed used short paired-end reads. Using short reads of this type means that it is almost impossible to determine changes in splicing patterns or the production of any specific isoforms. It is a documented feature of lncRNA that their function can be modulated not by altering the net number of transcripts produced, but by shifting the bias of splicing one isoform over another (Ulicevic et al., 2024; Wright et al., 2022b). This phenomenon has been observed in studies of *CASC15* in human cell lines, with the expression of "CASC15 new transcript 1" (*CANTI)* being suggested as the key pathology-driving isoform of *CASC15* (Ni et al., 2020; Xing et al., 2017). However, the two papers that document this effect have both claimed to have discovered *CANT1* and also state that there are three or fewer isoforms of *CASC15,* which has been disproven by data from Wright et al (2022). Notably a literature search for investigations into

Casc15 reveals 55 studies, 7 of which have been withdrawn (~13%); this is significantly higher than the overall rate of retraction for scientific papers overall (~0.2%) (Van Noorden, 2023).

An important caveat with any bulk RNA sequencing is that by pooling entire cell populations together, we are obscuring any potential heterogeneity within the culture. The V-SVZ is highly heterogeneous in terms of cell types and transcriptional signatures, and while cell culture conditions promote the survival of some cell types over others this will never result in a pure population when we are using primary cells. This sort of heterogeneity could be examined using a single cell technique such as scRNAseq or snRNAseq, but in this context our aim was to examine whether there are broad transcriptional changes in response to *Casc15* knockdown rather than to dissect the minutiae of cell-level regulatory networks. Furthermore the expression of *Casc15* is fairly limited to neuroblasts and to a certain extent ependymal cells, and their distinct functions are relatively easy to delineate. For future studies, now that we have established that there are indeed significant changes in response to *Casc15* depletion, single-cell RNAseq *in vivo* may be able to lend high resolution insight into cell-type-specific regulatory changes.

4.3.ii *Casc15* lncRNA restrains V-SVZ neurogenesis

While there are a few studies examining the roles that lncRNAs such as *Paupar* (Pavlaki et al., 2018a) can play in the regulation of neurogenesis from the V-SVZ, there is no data regarding *Casc15* in this context. Until this point, cancer susceptibility locus 15 has unsurprisingly only been studied in the context of cancer and malignant metastasis. Although these studies examine a role for *CASC15* in a non-physiological context they are able to elucidate some facets of *CASC15* action. A feature that is important to consider is a context specific role of *CASC15* in regulation of migration and metastasis – it appears that in neural-like cells, such as

neuroblastoma, *CASC15* does indeed act to suppress migration, whereas in somatic lineages such as melanoma, it has an opposite role. These studies show conflicting and tissue-type dependent effects of *CASC15* knockdown or overexpression, although all papers examining migration in neuroblastoma cells found that *CASC15* did indeed act to restrain cell migration, consistent with the data I have shown here (Figure 4.1, Table 4.2). From bioinformatic analysis it is clear that *Casc15* is highly conserved and expressed at a high level in V-SVZ neuroblasts, and plays a heretofore unknown role in regulating cell migration in this context. I therefore set out to examine whether *Casc15* is important in homeostatic postnatal neurogenesis in the murine brain.

My key finding was an approximately inverse correlation between the degree of *Casc15* knockdown achieved and indirect measures of migration in V-SVZ derived neuroblasts.

I first illustrated this using a spheroid migration assay in which primary cells are dissected from the RMS, dissociated and electroporated with knockdown constructs, before being plated and embedded in Matrigel (Ducker et al., 2020a). This is the highest throughput of the migration assays I used, and by generating a relatively homogenous cell suspension as the input I can ensure a near-identical starting point for each replicate of this assay. However, due to small numbers of cells (5000) used per technical replicate, it is vulnerable to influence from environmental fluctuations. Namely, any aberration in plasticware as a result of dissection could give rise to tiny fragments of plastic in the cell suspension, impairing formation of spheroids. Furthermore, the inclusion of ependymal cells from the V-SVZ in the initial cell isolation inhibited the formation of spheroids. Importantly this meant that only cells in the more anterior portions of the RMS could be used. Therefore any knockdown phenotype that might have originated from defects at the level of the V-SVZ would be obscured in this assay, and

any phenotype must be arising from aberrations in actively migrating cells; this feature is both a strength and limitation - while V-SVZ-level effects may be obscured this also ensures that by restricting the window of development that is examined, I am able to narrow down the point in the lineage that I am examining this phenotype.

I next examined neuroblast migration using an explant migration assay, in which small explants are dissected from the V-SVZ and RMS and plated directly in a 3D droplet of Matrigel without dissociation. V-SVZ and RMS-derived neuroblasts move using chain migration, and a vital feature of this assay is that these longitudinal arrays are preserved, as cells are not dissociated. However, because cells are not dissociated I was not able to nucleofect as I had done for the spheroid assay, and cells were simply exposed to siRNA constructs in the media and suspended in Matrigel. The siRNA constructs used were very small (21 nucleotides) and so are able to pass across plasma membranes without the need to nucleofect. This can be less efficient than nucleofection, but I have shown using neurospheres that it is sufficient to induce a significant reduction in *Casc15* lncRNA levels. However, the assessment of the efficacy was carried out in a single cell suspension where all cells were exposed to the siRNA, whereas in the explant assay only the most exterior cells were exposed to the siRNA. This may explain why the impact of *Casc15* knockdown was less strong in this assay as in the spheroid migration assay.

This assay used cells derived from the posterior portions of the RMS and anterior portions of the V-SVZ, so it was important to confirm the identify of migrating cells. The regions dissected contain predominantly neuroblasts, but also other cell types including astrocytes and immune cells. I therefore used immunohistochemistry to confirm that migratory cells were indeed TUBB3+ neural progenitors, and that GFAP+ astrocytic cells remained in the body of the explant.

After observing a pattern of dose dependence between *Casc15* levels and the surface area occupied by neuroblasts I moved to *in vivo* examinations of neurogenesis. While there do exist methods to examine the rate of neuroblast migration in live animals (Sun et al., 2022) these remain technically challenging. Knockdown and GFP+ constructs were electroporated into the V-SVZ, and these GFP expressing cells then migrated via the RMS to the OB. I therefore used the density of GFP+ cells in the OB as an indicator for the relative amount of neurogenesis that had occurred. Consistent with the findings from *in vitro* assays, I found that there was an increase in the number of labelled cells reaching the OB.

From these experiments, it cannot be conclusively stated that the observed changes are due solely to changes in cell migration. In the spheroid assay, the volume of space occupied by cells is used as an indication of migration, but this will be strongly influenced by any changes in proliferation or apoptosis – as is also the case for the explant migration assay. *In vivo* alterations in the number of mature OB interneurons can be impacted by migration, but similarly to *in vitro* assays there can be a strong influence of cell survival and proliferation. Immunohistochemical examinations of mKi67 (proliferation) and CASP3 (apoptosis) suggest that this is likely not the case, however. From the data presented here it is likely that *Casc15* depletion does indeed cause an increase in the rate of migration, concurrent with a subtler increase in the rate of proliferation, thus giving rise to a greater density of GFP+ cells in the OB of CRISPRi-treated animals. Based on the RNAseq data, it is likely that migration is indeed the most strongly affected facet of neurogenesis upon *Casc15* depletion, although the RNAseq experiment and migration assays were perfoemd using cells from different points in the neurogenic lineage.

An important consideration when examining these data collectively is the different constructs used; for RNA sequencing and *in vitro* migration assays ASO and siRNA were used respectively, whereas CRISPRi constructs were used for the *in vivo* assays. ASO (antisense oligonucleotides) and siRNA (short interfering RNA) both are small RNA based constructs that target lncRNA transcripts. Fundamental differences lie in the fact that ASOs are delivered as single stranded molecules which directly anneal to their target mRNA, whereas siRNA are delivered as annealed double stranded RNA that are incorporated into RISC/AGO complexes and direct target RNA degradation in this way (Kole et al., 2012). Both ASO and siRNA give rise to rapid but often short-lived depletion in the levels of their target transcripts. For long-term studies this can be prohibitive, but the *in vitro* migration assays used here all ran for less than 48h before being terminated. *In vivo*, however, cells must migrate over much longer distances (a maximum distance of approximately 500μm in explant assays versus >5000μm migration distance from the V-SVZ to the most anterior OB) and longer time courses, so a method that induces a much more sustained knockdown was necessary. CRISPR inhibition (CRIPSRi) targets the locus from which a gene is transcribed, rather than the transcript itself, and induces stable epigenetic repressive marks at the target locus (Qi et al., 2013). This allows knockdown to be maintained continuously for a longer period of time than can be achieved with short-RNA based depletion alone. Despite these differences in the method and timescale of *Casc15* depletion, the same effect is observed repeatedly, in which depletion of *Casc15* transcripts gives rise to a dose-dependent increase in migration of V-SVZ-derived neural progenitors. By showing this impact with multiple ASOs, multiple siRNAs, and multiple CRISPRi gRNAs I can confidently assert that the observed phenotypes are due to the loss of *Casc15* expression, and not an off-target effect or a side effect of the exact technique used.

Particularly important to consider in the context of lncRNA biology is the impact of the functional transcript itself, versus the impact of transcription. Some lncRNAs exert their functionality via the mature transcript; whereas the act of transcribing a lncRNA may be the important factor, where competition between transcriptional units depletes the availability of polymerase complexes. siRNA and ASO approaches primarily degrade the transcript, whilst leaving the transcription from the DNA locus largely untouched, conversely CRISPRi will deplete the transcript as a result of targeting the DNA locus. This is a pertinent consideration with respect to the *Casc15* locus, where transcription through the entire body of the gene will alter the 3D architecture and thus function of multiple enhancer regions, thereby potentially modulating the efficacy of these enhancers without the need for the actual lncRNA to exert this function. For future studies perhaps this could be addressed using multiple parallel approaches. siRNA alone would deplete the *Casc15* transcript while the *Casc15* gene locus remained active; CRISPRi targeting the *Casc15* promoter would suppress transcription-dependent effects, but mature *Casc15* transcripts could be supplied exogenously from a plasmid, thus allowing transcript-dependent mechanisms to continue; siRNA and CRISPRi could be used together to suppress both transcript- and transcription-dependent mechanisms of action. This would require delicate tailoring of the *Casc15*-expressing plasmid to ensure that expression of *Casc15* was approximately equivalent to endogenous levels.

The use of multiple assays *in vitro* and *in vivo* illustrating the same effect strengthens the suggestion that *Casc15* may act as a suppressor of neuroblast migration. Based on similar observations when *Casc15* is depleted via degradation of the transcript (siRNA, ASO) and via suppression of expression (CRISPRi), I theorise that *Casc15* exerts its effect on neurogenesis through the mature lncRNA transcript rather than the act of transcription alone.

4.3.iii *Casc15* lncRNA knockdown does not give rise to an overt V-SVZ phenotype

A change in the behaviour of neuronal stem cells or an alteration in the neurogenic niche could theoretically impact the number of neuroblasts reaching and maturing in the olfactory bulb, so I next examined the V-SVZ of animals that had been electroporated with *Casc15*-targeting CRISPRi constructs. I started by examining the number of cells labelled with marker constructs in each animal to assess whether, for example, *Casc15* knockdown caused an increase in proliferation or perhaps a resistance to apoptosis that gave rise to increased numbers of cells migrating to the OB. There was no statistically significant difference in the density of GFP+ cells in the V-SVZ of brains 4dpe, although this may be due to this particular experiment being underpowered. The plotted data suggest an increase in GFP+cells/mm^3 at 4dpe (Fig 4.6, A), but the data for the 58i treated group of animals are quite variable; this variability may be obscuring a biologically meaningful effect. I did not expect a significant phenotype as scRNAseq data suggests that *Casc15* is dominantly expressed in neuroblasts, rather than the NSCs or ependymal cells in the V-SVZ (Figure 3.5).

I next set out to clarify whether there was a V-SVZ phenotype using immunohistochemical markers for proliferation (mKi67) and apoptosis (Caspase-3), where I did not find any significant differences between constructs. It is notable that there does appear to be a slight, but statistically insignificant, decrease in the proportion of GFP+ cells that are Casp3+ upon *Casc15* knockdown; however, the pattern of this trend differs from the observed trend in migration, and thus differences in migration between knockdown constructs cannot be attributed to this difference. Furthermore, while there was no statistical difference in the density GFP+mKi67+ cells between groups, there did appear to be a trend that mirrored the degree of *Casc15* knockdown. However, the total number of GFP+mKi67+ cells detected per animal was

very low (<10 cells detected per animal), and likely cannot account for the differences observed in the total number of GFP+ cells in the OB of these animals.

While the majority of V-SVZ derived cells in the postnatal brain migrate via the RMS to the OB, a small proportion will migrate into the striatum where they typically will differentiate into glial cells (Al-Dalahmah et al., 2020; Levison and Goldman, 1993). I did not find that the proportion of labelled cells entering the striatum changed upon *Casc15* knockdown, but those that did enter the striatum migrated further from the V-SVZ when *Casc15* was depleted. This was consistent with my expectation, given the observed increase in migration of RMS-neuroblasts. While there was increased migration into the striatum under these conditions, labelled cells were only observed along previously described canonical routes of V-SVZ progenitor migration, there was no aberrant migration observed. As there were no cells observed taking ectopic routes of migration, I inferred that the key phenotype is an increase in the rate of migration, and not an alteration in directional guidance of cells.

4.3.iv Structural defects

Serendipitously when quantifying the density of GFP+ cells in the OB of animals treated with different knockdown constructs I noticed that some cells in the knockdown groups showed an unusual and unanticipated morphology. Postnatally generated olfactory bulb interneurons can be identified by several features, firstly, a characteristic morphology location of the cell body typically in either the granule cell layer or the glomerular layer, and extensive dendritic arborisations.

I next examined cells which appeared to adopt a novel “misoriented” morphology within the GCL, suggestive of a powerful disruption of apicobasal polarity. Typically a mature GCL interneuron will have a cell body positioned more centrally within the GCL, and a single long

primary dendrite which then arborises radially outward towards the glomerular layer. I identified through immunohistochemistry a small population of GCL cells in knockdown conditions that show this morphology but flipped along the radial axis, with arborisations towards the inner/central portions of the GCL. Again, this phenotype accounted for a small overall proportion of cells, but was significantly increased upon depletion of *Casc15* lncRNA. As migration and differentiation are distinct events for OB interneurons it is likely that this phenotype arises through a separate set of molecular events from the migration phenotype.

V-SVZ derived interneurons migrate from the V-SVZ via the RMS to defined layers of the olfactory bulb, namely the granule cell layer (GCL) and the glomerular layer (GL). These layers can be clearly distinguished anatomically using the pattern and distribution of DAPI+ nuclei. V-SVZ neuroblasts will migrate through other layers of the OB en-route to their target destination, but they will show a characteristic migrating morphology here (Nam et al, 2007), and will adopt a clear mature morphology once they have arrived at their destination in the GL or GCL of the OB. However, upon depletion of *Casc15* lncRNA I found cells that were adopting a mature morphology outside of the canonical target layers of the OB for postnatal neurogenesis. I set out defined criteria for how I would distinguish "mature" morphology – i.e. two or more bifurcations and no leading process – and quantified the layer of the OB that the cell body was in. This revealed a striking increase in the number of cells maturing in non-target layers of the OB, increasing with the degree of *Casc15* knockdown. It must be noted, that these cells with misplaced soma accounted for a small percentage of total GFP+ cells. There are rare occasions in which the bias of postnatal neurogenesis towards the GCL of the OB is shifted, notably in the post-partum period. There is a significant increase in the number of V-SVZ-derived cells that integrate into the mitral cell layer (MCL), concurrent with a drop in oestrogen levels (Chaker et al., 2023).

Interneurons in the granule cell layer are the most numerous cells in the OB and are unusual in that they do not possess axons, and instead form dendro-dendritic synapses (Rall et al., 1966); therefore the length of available dendrite is important for the amount of potential connectivity. I measured the mean length of the primary dendrite – from the centre of the cell body to the first bifurcation – of mature GCL interneurons between different conditions, and found that upon *Casc15* depletion, these primary dendrites were significantly shorter. These cells therefore may be able to make fewer dendrodendritic synapses.

Perhaps the fact that maturation in the incorrect layer and the "misoriented" morphology is only seen in a small number of cells illustrates that neuroblasts typically have mechanisms in place to adjust to an altered speed of migration. Perhaps they in some way some account for the altered rate of migration and ensure "normal" location and differentiation, despite changes in migration and gene expression.

Both the discovery of cells in the "incorrect" layer of the OB and truncation of dendrites may be explained by an increased rate of migration upon *Casc15* depletion *in vitro,* as illustrated in Figure 4.14. The cells described show morphology characteristic of granule cell layer interneurons, and for the purpose of discussion are assumed to be GCL interneurons. In Figure 4.14 I have illustrated how this might occur.

In the first row a cell migrates radially for three units of time (t) before extending a process at t4 and maturing by t5. In the second row the cell migrates again for three units of time, but at a higher rate than the cell in the first row, indicated by two blue arrows. Therefore the nucleus is located in the upper GCL, and the length of its primary dendrite is stunted. In the third row,

the cell migrates again for three units of time as before, but at an even higher rate, shown by three blue arrows – therefore it overshoots the GCL and matures with its cell body in the mitral cell layer, but retains the dendritic morphology of a typical GCL interneuron.

An alternative explanation for the alteration of soma positioning and the length of primary dendrites is a shift in cell fate. Granule cell (GC) interneurons can be subdivided on the basis of morphology and position within the granule cell layer; some, such as superficial GCs (Type III granule cells) have a cell body at the outer edge of the GCL and a short primary dendrite, whereas deep GCs (Type II granule cells) have a cell body deeper in the GCL (closer to the RMS) and a much longer primary dendrite (Takahashi et al., 2018). Furthermore, shrub GCs (Type V granule cells), have a cell body in the mitral cell layer (MCL) of the OB, although these cells are dominantly embryonic-born. Altered positioning or morphological characteristics of cells upon *Casc15* depletion could be explained as a shift in the generation of different GC subtypes – for example the observed reduction in primary dendrite length could be due to a bias towards generating a larger proportion of superficial GCs compared to deep GCs. This could be addressed by a more in-depth analysis and classification of cell morphologies coupled with marker expression profiles for GFP+ cells in the OB of *Casc15*-knockdown animals.

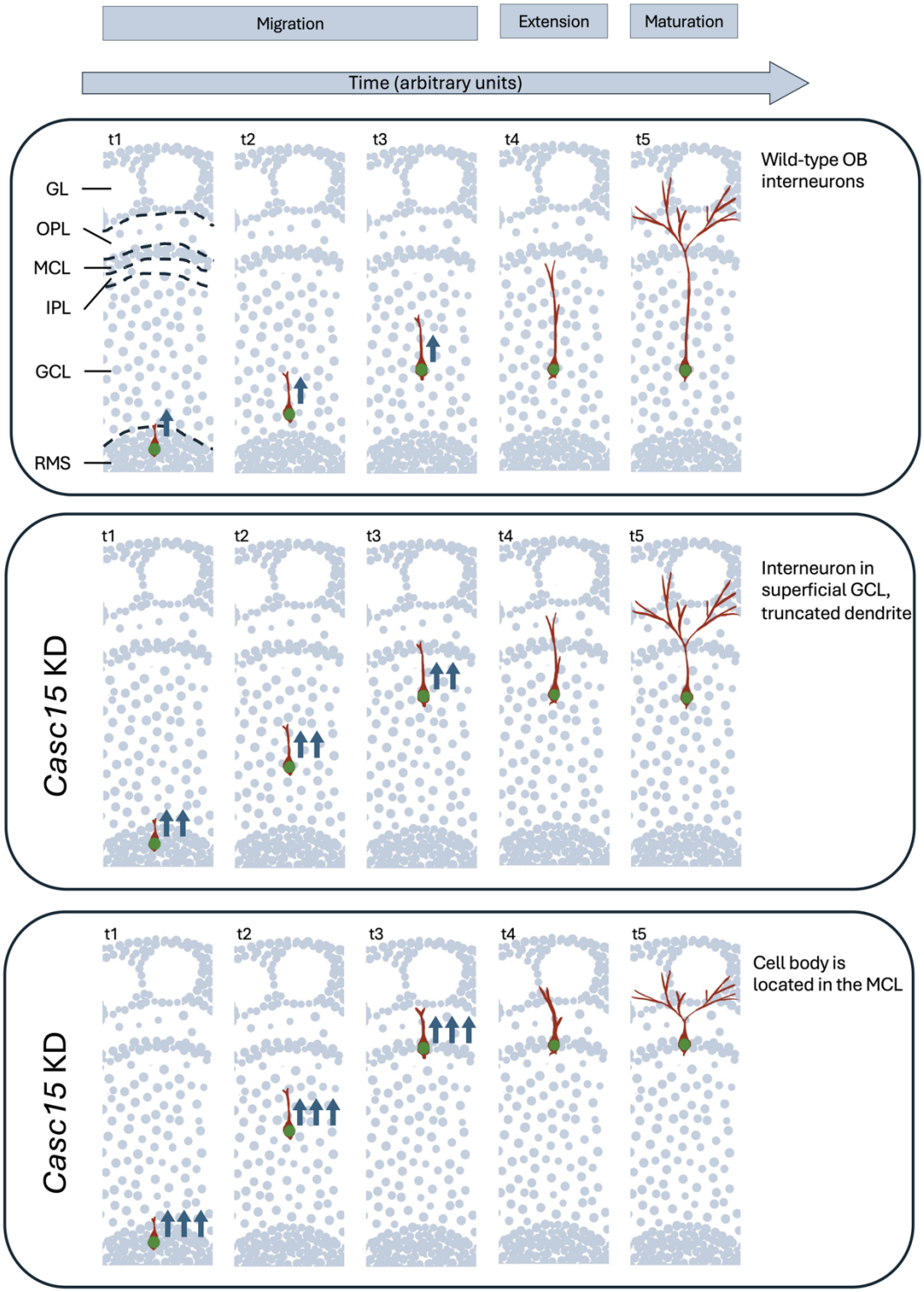

Figure 4.14 A model for the generation of abnormal interneurons

Abbreviations: GL – Glomerular layer; OPL – Outer plexiform layer; MCL – Mitral cell layer; IPL – Inner plexiform layer; GCL – Granule cell layer; RMS – Rostral migratory stream; OB – Olfactory bulb; KD – Knockdown. Illustration drawn in Adobe Procreate.

Together these observations show that while some cells do show marked defects in terms of their location and structure, this is a small population of cells. This suggests that despite dramatic changes in the rate of migration, the majority of cells affected by the knockdown in fact are able to maintain targeting to their canonical regions of the OB and show a canonical structure.

Further investigation into these abnormal OB interneurons should focus on electrochemical properties and connectivity to ascertain whether these are functional interneurons, and whether they integrate into existing OB circuitry.

4.4 Conclusions

Overall, these data indicate that the *Casc15* lncRNA plays a role in regulating olfactory bulb neurogenesis, and that this may be achieved by increasing the rate of neuroblast migration. I have demonstrated that *Casc15* knockdown leads to a dysregulation of genes that typically regulate migration, and that indirect measures of migration are increased both *in vitro* and *in vivo* upon knockdown.

Chapter 5: *Casc15* lncRNA and metabolism

5.1 Introduction

5.1.i lncRNA in metabolic regulation

There is no known precedent for lncRNA regulation of cholesterol synthesis in the brain. At the time of writing, a literature search in Scopus for ("cholesterol biosynthesis") AND ("lncRNA OR long noncoding RNA") reveals only 31 primary research articles, not one of which examines cholesterol in the brain.

5.1.ii Prenylation

When Geranyl-PP and Farnesyl-PP are generated they can be used to generate squalene, or can be used as posttranslational modifications in a process called prenylation (see Figures 1.5 & 1.7). Prenylation is an umbrella term referring to the addition of a farnesyl (farnesylation) or geranylgeranyl group (geranylgeranylation) as a post-translational modification. Farnesylation is performed by the farnesyltransferase (FTase) complex, whereas geranylgeranylation can be performed by three different geranylgeranyltransferase complexes (GGTase I, II, and III). The key effect of prenylation is to allow association of prenylated proteins with cell membranes, which is fundamental to the function of many of these proteins.

5.1.iii Pharmacological inhibitors of mevalonate and prenylation enzymes

The mevalonate and prenylation pathways are highly conserved and have been studied extensively, leading to the development of multiple small molecule inhibitors that inhibit different enzymes. Figure 5.1 illustrates the mevalonate pathway and subsequent prenylation and cholesterol biosynthetic pathways, with the enzymes that specific inhibitors act upon. Four

different inhibitors are used in this study: Simvastatin (Fig 5.1, B), YM53601 (Fig 5.1, C), FTI-277 (Fig 5.1, D), and GGTI-298 (Fig 5.1, E). See Table 5.2 for further details.

Simvastatin is widely prescribed in the UK, with nearly 13 million (12,721,486) Simvastatin prescriptions issued between October 2023 and September 2024, accounting for approximately 13% of total lipid lowering drugs issued through the NHS (Bennet Institude for Applied Data Science, University of Oxford, 2024). Simvastatin was selected over other statins as it crosses the blood brain barrier, and has been found to have a higher concentration in the CNS of acutely treated mice than other statins (Johnson-Anuna et al., 2005). Moreover chronic simvastatin treatment has been found to have a stronger effect on cortical cholesterol levels than other similar statins such as Lovastatin and Pravastatin (Johnson-Anuna et al., 2005). Simvastatin acts as a reversible competitive inhibitor of HMGCR, the rate limiting enzyme in the mevalonate pathway, by mimicking the structure of its substrate HMG-CoA (Istvan and Deisenhofer, 2001).

YM-53601 is a relatively novel inhibitor of squalene synthase, initially developed as a potential cholesterol-lowering drug that had fewer off-target effects than statins. It is not yet clinically available, although Phase-2 trials are in progress (Global Drug Intelligence Database, 2024). It is a rapidly acting reversible inhibitor of squalene synthase (SQS) that has been effective across multiple species (Ugawa et al., 2000, 2002). The lipophilicity and precise molecular mechanism of how YM-53601 acts on SQS have yet to be clarified.

FTI-277 is a peptidomimetic that resembles the CaaM motif recognised by the FTase complex, where C is cysteine, aa is any two aliphatic amino acid residues, and M is Methionine (Lerner et al., 1995). At lower concentrations it inhibits FTase alone, and at higher levels additional

inhibits the structurally similar complex GGTase-I, with approximately 100-fold selectivity for FTase over GGTase-I (Lerner et al., 1995; McGuire et al., 1996). FTI-277 is currently being investigated in preclinical trials for neoplasms (Global Drug Intelligence Database, 2025a).

Similarly, GGTI-298 is also a peptidomimetic, and resembles the CaaL motif that is recognised by the GGTase-I complex, where C is cysteine, aa is any two aliphatic amino acid residues, and L is Leucine (Qian et al., 1998). At low concentrations it inhibits GGTase-I alone, and inhibits FTase as well at higher concentrations, although it is less specific for its target than FTI-277 with only a four-fold selectivity for GGTase-I over FTase (McGuire et al., 1996). GGTI-298 is currently being investigated in preclinical trials for neoplasms (Global Drug Intelligence Database, 2025b).

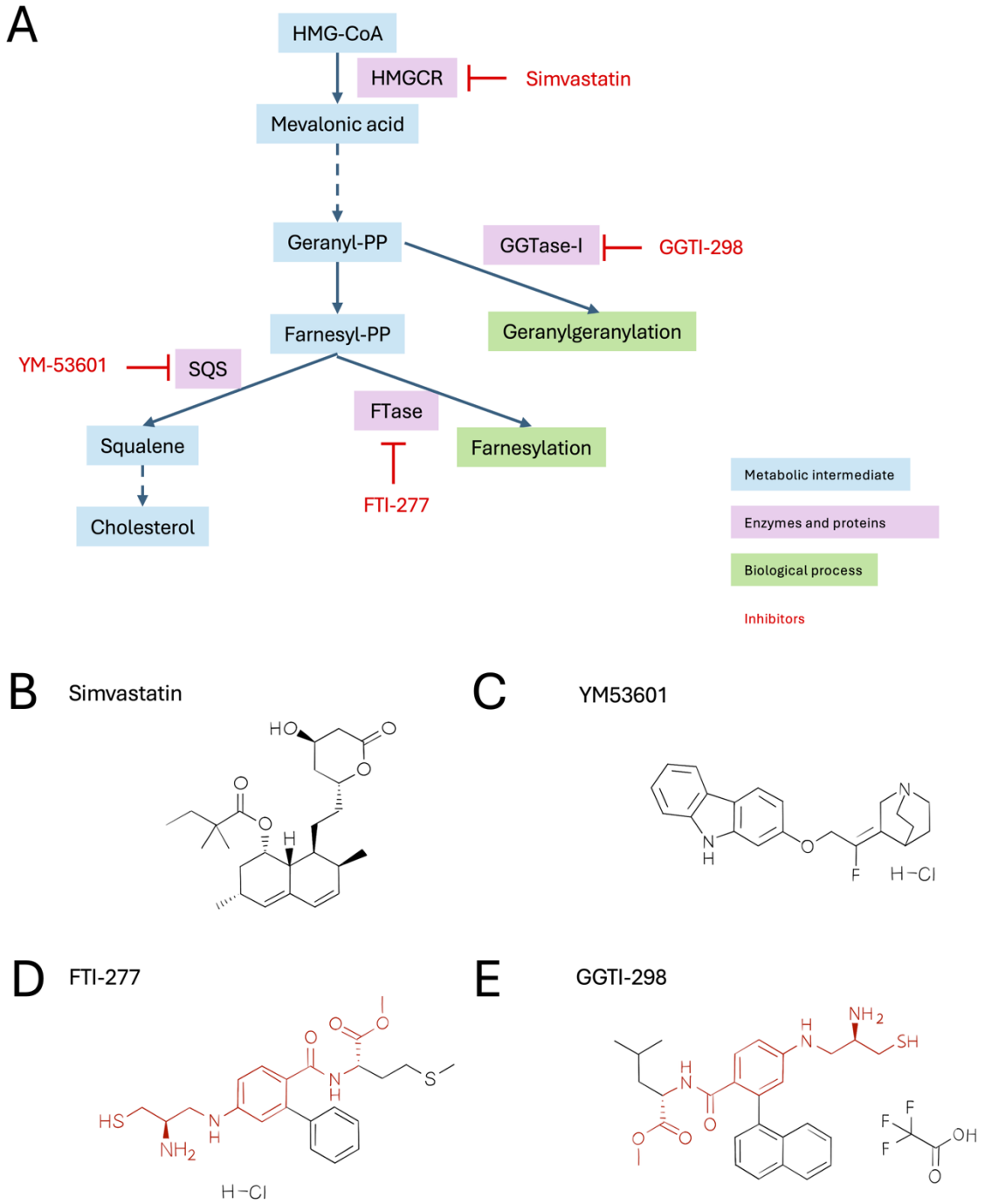

Figure 5.1 Pharmacological inhibitors of mevalonate and prenylation pathways. ***A)*** *Simplified schematic of the mevalonate pathway highlighting the targets of different inhibitors. Pink boxes indicate enzymes and proteins; blue boxes indicate metabolic intermediates; green boxes represent broad pathways and processes.* ***B)*** *Chemical structure of Hmgcr inhibitor Simvastatin.* ***C)*** *Chemical structure of Squalene Synthase inhibitor YM53601.* ***D)*** *Chemical structure of FTase inhibitor FTI-277.* ***E)*** *Chemical structure of GGTase Inhibitor GGTI-298.* ***D & E)*** *Identical parts of the chemical structures of FTI-277 and GGTI-298 are shown in red.* ***See Table 5.2 for more detail.***

Abbreviations: HMGCR - 3-hydroxy-3-methylglutaryl coenzyme A reductase; GGTase - Geranylgeranlytransferase; FTase - Farnesyl transferase; SQS - Squalene Synthase.

5.2 Results

5.2.i *Casc15* regulates mevalonate pathway genes *in vitro*

Pathway analysis

In order to understand in more detail the effect of *Casc15* on transcription I performed Ingenuity Pathway Analysis (IPA) to examine pathway-level changes and identify potential upstream regulators. This analysis was conducted on the same dataset discussed in Chapter 4, Figure 4.2, examining the effect of *Casc15* depletion in V-SVZ-derived neurospheres. This revealed that the pathway that was most significantly increased upon *Casc15* depletion was Cholesterol Biosynthesis (Figure 5.2, A) (Table 5.3). A number of other cholesterol-related terms were increased, such as “Superpathway of cholesterol biosynthesis:, “Cholesterol biosynthesis I”, “Cholesterol biosynthesis II”, among others. Another notable upregulated pathway was the "Warburg effect signalling pathway”; the Warburg effect is a stereotypical shift in metabolism observed in cancer cells (Coleman and Parlo, 2021; Vander Heiden et al., 2009).

Pathways associated with WNT, SHH, Ephrin, and ROBO/SLIT signalling pathways, all of which regulate axon guidance and/or neuronal progenitor migration, were decreased in the pathway analysis results. Other pathways that were significantly decreased included Epithelial to Mesenchymal Transition (EMT) as well as many terms associated with Oestrogen signalling and mitotic cell cycle regulation. Finally, there were decreases in the signalling pathways of Interleukins 4, 6, 8, 10, 13, 17, and 33 (Table 5.3).

Upstream regulator analysis

Upstream regulator analysis was performed to examine whether the transcriptional changes observed upon *Casc15* depletion in neurospheres mimicked known transcriptional changes upon specific interventions. This revealed a predicted activation of SREBP2, the master regulator for the cholesterol biosynthesis pathway, consistent with significant upregulation of 23 of its target genes upon *Casc15* depletion (Table 5.4). Key decreased upstream regulators included EHPA2, Beta-estradiol, and TP53 (Table 5.4)

Targeted gene expression analysis

Based on this I used qPCR to examine changes in *Srebp2* levels in comparison to *Casc15* upon acute *Casc15* depletion by siRNA knockdown in tertiary neurospheres (Fig 5.2, B). I found that both *Casc15* knockdown construct siRNA11 and siRNA12 caused a significant increase in *Srebp2* expression at 72h after electroporation (Fig 5.2, C), consistent with the bulk RNAseq data after ASO-mediated knockdown.

In order to see whether there was any interaction between *Casc15* expression levels and the concentration of the downstream products of the mevalonate pathway I added squalene (20μM) to neurosphere cell cultures and examined *Casc15* expression after 24h. This revealed a significant reduction in *Casc15* expression, suggesting that it is able to regulate the expression of mevalonate pathway enzymes *in vitro* and is in turn regulated by the molecules that these enzymes produce (Fig 5.2, D).

I next examined the expression of several subunits of the FTase and GGTase complexes in neurospheres to see whether they changed in expression upon *Casc15* depletion using the constructs in Fig 5.2, B (see Figure 1.7). ***Fnta***, a subunit of FTase and GGTase-I did not significantly change in relative expression upon *Casc15* knockdown with siRNA12 or

siRNA11(Fig 5.2, E). ***Pggt1b***, a subunit of GGTase-I did not change in relative expression upon *Casc15* depletion (Fig 5.2, F). ***Rabggtb***, a subunit of GGTase-II and GGTase-III did not change in relative expression (Fig 5.2, G). ***Ptar1***, a subunit found only in GGTase-III similarly did not show any statistically significant change in relative expression upon *Casc15* depletion (Fig 5.2, H). *Rabggtb* and *Ptar1* do appear to show a trend in expression change that mirrors that of *Casc15* expression; whilst this is a statistically non-significant result, the variability of the data may be obscuring a biologically meaningful effect. This could be addressed by repeating the experiment with greater numbers of replicates.

Together the data illustrated in Figure 5.2 suggest that *Casc15* depletion causes an upregulation of mevalonate pathway genes via relief of SREBP2 inhibition in neurospheres. Furthermore, *Casc15* expression can be regulated by the addition of squalene, the downstream product of the mevalonate pathway. Additionally, this indicates that *Casc15* depletion with siRNA likely does not cause a significant change in the availability of enzyme complexes that catalyse prenylation reactions. If there is an alteration in prenylation this could be due instead to alterations in the availability of the raw materials for prenylation such as GGPP and FPP (Fig 5.1).

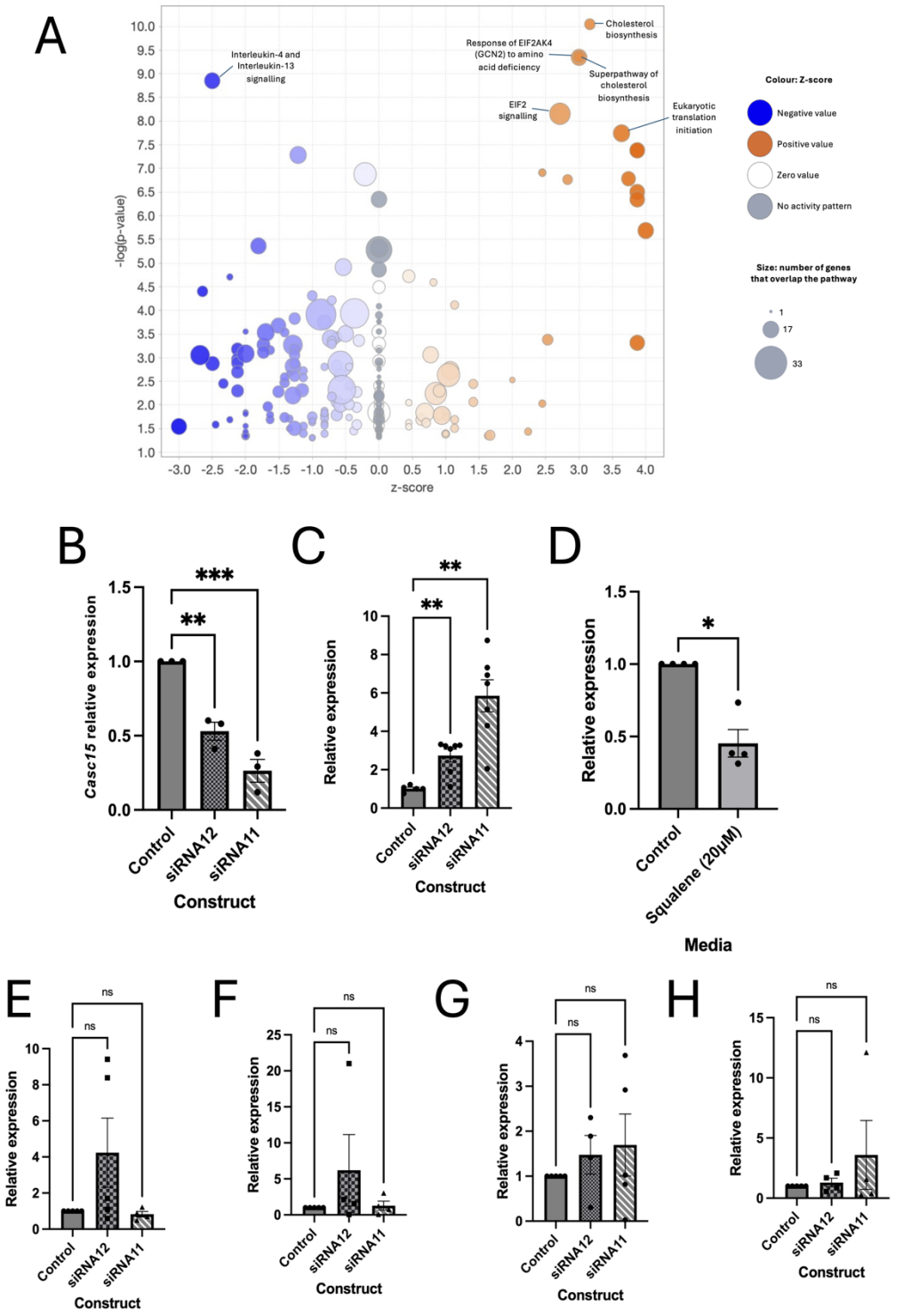

Figure 5.2 Further transcriptional effects of Casc15 knockdown A) *Gene Ontology analysis of genes that are upregulated by Casc15 depletion.* ***B)*** *Effect of siRNA11 or siRNA12 on the relative expression of Casc15.* ***C)*** *Effect of Casc15 depletion with either siRNA11 or siRNA12 on the expression of Srebp2.* ***D)*** *Effect of 20μM squalene on Casc15 relative expression.* ***E-H)*** *Effect on prenylation complex subunits of Casc15 depletion with either siRNA11 or siRNA12. See Figure 1.7 for subunit composition of each complex.* ***See Table 5.1 for details of statistical tests, and Tables 5.3 and 5.4 for further details.***

Error bars = SEM.

5.2.ii *Casc15* interacts with PRC2 to target the *Srebp2* locus

Casc15 interacts with PRC2 – Native RIP

Interaction with the epigenetic repressor polycomb repressor complex 2 (PRC2) is a characterised mechanism for many different lncRNAs and PRC2 has been previously shown to be important for the regulation of V-SVZ neurogenesis (Sun et al., 2018). The inverse relationship between *Casc15* expression and *Srebp2* expression suggests that *Casc15* depletion acts as a relief of inhibition of *Srebp2* . Therefore I next examined whether *Casc15* could be interacting with PRC2 at the *Srebp2* locus. Native RNA immunoprecipitation (RNA-IP) was performed in tertiary neurospheres derived from the postnatal V-SVZ. IP was carried out using the PRC2 subunit EZH2, with a nonspecific IgG as a negative control. Initial pulldown was performed by Dr Bin Sun, with subsequent PCR performed by both myself and Dr Sun. *Casc15* was probed for in all of these pulldown fractions, as well as the *Gapdh* mRNA as a negative control, and the lncRNA *Xist* which is known to interact with PRC2 (Zhao et al., 2008).

Native RNA immunoprecipitation revealed that *Casc15* was significantly more enriched in the EZH2 -pulldown than the IgG pulldown, suggesting that it preferentially interacts with EZH2 (Figure 5.3, A,) *Gapdh* mRNA in contrast was not significantly enriched in the EZH2 fraction compared to IgG, indicating that this enrichment of *Casc15* is not due to a generic RNA-binding feature of EZH2 (Fig 5.3, A,). Moreover, comparing the enrichment of *Casc15* versus *Gapdh* mRNA in the EZH2 pulldown reveals that *Casc15* is significantly enriched in contrast to *Gapdh* (Fig 5.3 A,). The lncRNA *Xist* does appear to show a trend towards increased enrichment in the EZH2 pulldown compared to IgG, but this did not reach statistical significance (Fig 5.3, A).

These data suggest together that *Casc15* interacts specifically and preferentially with the PRC2 subunit EZH2 in neurospheres.

Casc15 depletion effect on H3K27Me3 deposition at the _Srebp2_ promoter

To establish whether the inverse correlation between the expression of *Srebp2* and *Casc15* could be mediated by specific targeting of PCR2 I next examined the epigenetic "mark", or product of PRC2 activity: H3K27Me3. H3K27Me3 is a repressive epigenetic mark deposited at regulatory sequences, typically promoters (Boyer et al., 2006).

Chromatin immunoprecipitation (ChIP) was performed by Dr Bin Sun using V-SVZ-derived tertiary neurospheres that were electroporated with either control or *Casc15*-targeting antisense oligonucleotide (ASO) constructs (Evaluated in Figure 4.2). Antibodies against H3K27Me3 were used, as well as IgG as a negative control. I conducted qPCR with primers targeting the *Srebp2* promoter, and found that H3K27Me3 deposition at this locus was significantly reduced upon *Casc15* depletion by ASOs (Fig 5.3, B,). Further qPCR was conducted examining an intron from the Actin gene and the promoter of *Ngn2*, revealing no alteration or trend in the levels of H3K27Me3 at either of these locations. *Ngn2* was used as a negative control as little/no *Ngn2* is expressed in the postnatal V-SVZ and it did not change in expression upon *Casc15* knockdown, suggesting that it is transcriptionally repressed in all samples.

This suggests that the *Casc15* lncRNA is required for the deposition of high levels of H3K27Me3 at the promoter of *Srebp2 in vitro* . There still is H3K27Me3 deposition at this locus upon *Casc15* knockdown, and it cannot be asserted whether this is due to an incomplete depletion of *Casc15* or, more likely, H3K27Me3 being targeted to the *Srebp2* promoter by another mechanism.

Casc15 depletion effect on global H3K27Me3 deposition

In order to establish whether this is a mechanism specific to the *Srebp2* locus or *Casc15* caused a global disruption of H3K27Me3 deposition by PRC2 I performed immunohistochemical staining of *Casc15* depleted cells *in vivo*. The same animals were used as in Chapter 4, Results 2, in which CRISPRi constructs targeting the *Casc15* locus were electroporated into the V-SVZ of P0 C57BL6 mice (see Figure 4.5). IHC was performed 4 days post electroporation, staining for GFP to mark electroporated cells, and H3K27Me3 to mark PRC2 activity. DAPI staining was not possible in these sections due to the HCl antigen retrieval protocol used, which inhibits DAPI intercalation into DNA (Moshi et al., 2023). High magnification fluorescence microscopy at 100x followed by deconvolution can reveal sub-nuclear localisation of H3K27Me3.

In control animals, H3K27Me3 staining can be seen across the whole nucleus, with bright puncta representing regions of dense heterochromatin (Fig 5.3, C). This same pattern of immunoreactivity is observed in both 58i and 59i CRISPRi knockdown animals. This would not be observed if *Casc15* depletion had caused a depletion of PRC2 or a global disruption of its activity, suggesting that the loss of H3K27Me3 at the *Srebp2* promoter is due to a highly specific loss of PRC2 targeting.

Taken together, the data in Figure 5.2 and 5.3 suggest that *Casc15* targets PRC2 activity to the promoter of *Srebp2*, and that loss of *Casc15* causes a reduction in PRC2-medicated H3K27Me3 deposition at this locus. The loss of PRC2-mediated transcriptional repression could explain the relationship between *Casc15* and *Srebp2* expression as seen in Figure 5.2.

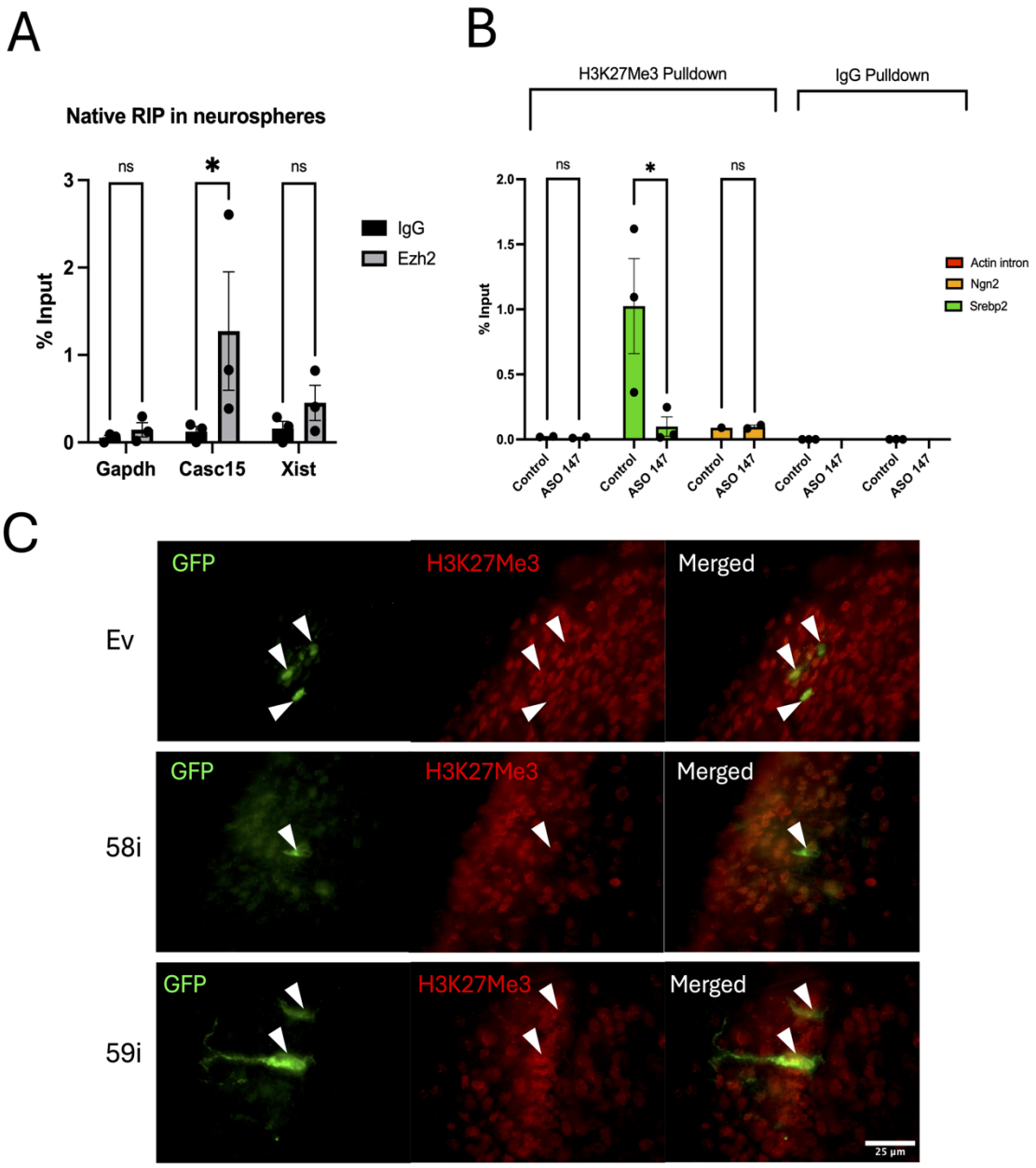

Figure 5.3 Casc15 targets PRC2 to the Srebp2 locus A) *Native RNA-immunoprecipitation in neurospheres.* ***B)*** *ChIP-qPCR examining the effects of Casc15 depletion by ASO 147 on H3K27Me3 deposition.* ***C)*** *Example immunohistochemistry showing H3K27Me3 (red) in GFP+ (green) cells.* ***See Table 5.1 for details of statistical tests.***

Error bars=SEM. Scale bar= 25µm.

5.2.iii Effect inhibiting of HMGCR on neuroblast assays

As SREBP2 is the master transcriptional regulator for the mevalonate pathway, I next began by inhibiting different components of the pathway and its downstream effectors. I began by using the commercially available Cholesterol-lowering drug Simvastatin.

In a spheroid migration model of RMS neuroblast migration I found that the addition of 20μM simvastatin to cell culture media significantly reduced the volume occupied by neuroblasts when compared to controls Figure 5.4, A,B.

I had previously shown using this model that *Casc15* depletion increases the volume of these spheroids (See Fig 4.3), so I next asked whether *Casc15* depletion could rescue the impact of simvastatin. When culturing in control media, *Casc15* depletion with siRNA11 caused a significant increase in volume occupied by cells, but this was not observed when treating with simvastatin (Fig 5.4, C). A particular challenge of this assay was that it requires culture plates to be chilled on ice which caused simvastatin to precipitate out of solution occasionally giving rise to large crystals. This meant that large numbers of technical replicates were used, as spheroids did not form when simvastatin crystals were present.

Therefore I repeated the evaluation of simvastatin on neuroblast migration instead using an explant assay that did not require the same incubation on ice, in order to circumvent the issue of simvastatin crystallisation. I observed an identical pattern in an explant migration assay whereby *Casc15* siRNA knockdown significantly increased the migration ratio when culturing with control media (Fig 5.4,.D, see Fig 4.4, A for calculation). Once again this effect was obscured by the addition of Simvastatin, which significantly reduced the migration ratio. There

was no difference in the surface area occupied by neuroblasts in simvastatin treated explants irrespective of *Casc15* knockdown (Fig 5.4, D).

In both spheroids and explants treated with simvastatin cells showed a rounded morphology and lacked the leading processes characteristic of migrating neuroblasts. This did not appear to be a complete abolition of migration as cells had clearly moved from either the spheroid/explant into the surrounding matrix. Together, these data suggest that simvastatin is a powerful inhibitor of neurogenesis. It cannot be determined from this experiment whether simvastatin acts upstream of *Casc15*, thus obscuring its effect on migration, or whether simvastatin causes acute toxicity to these cells and prevents migration in this manner.

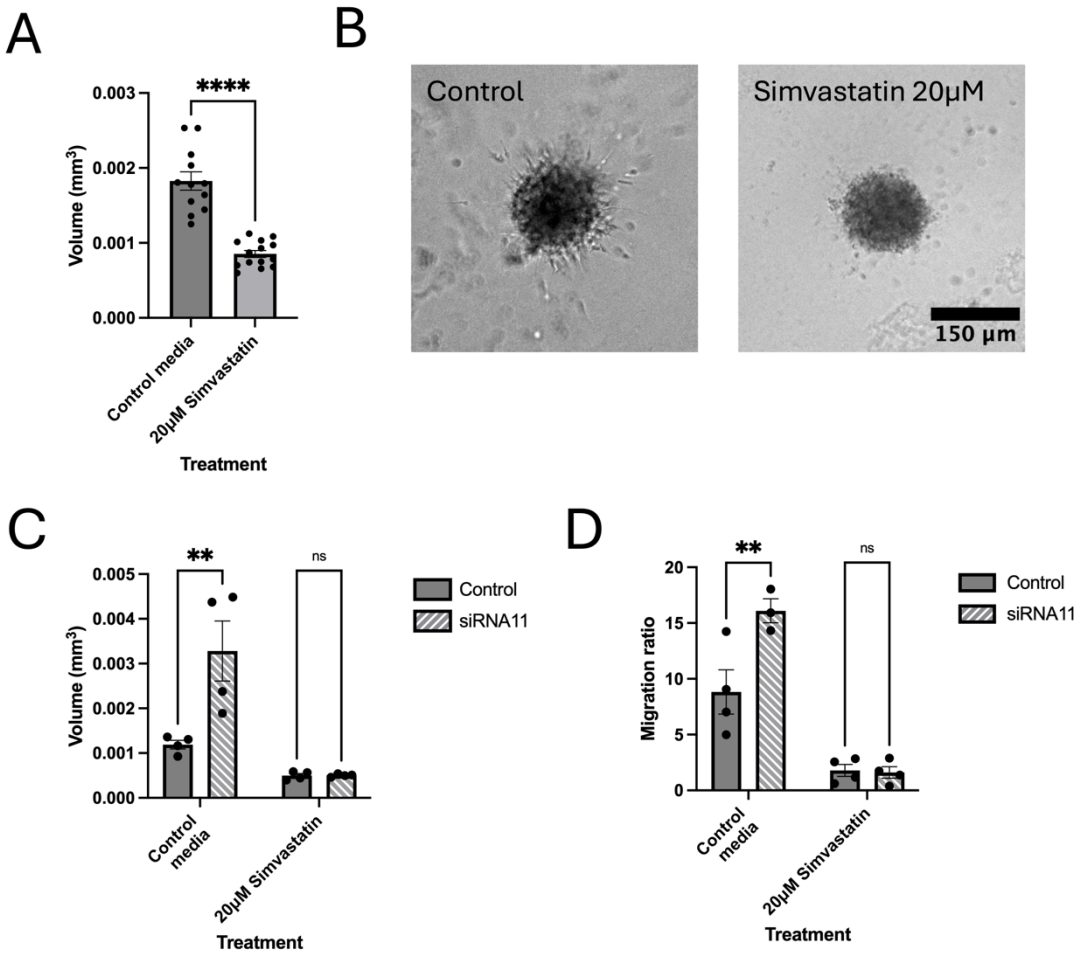

Figure 5.4 Effects of simvastatin on neuroblast assays A) *Effect of Simvastatin (20μM) administration on spheroid migration assay.* ***B)*** *Example images of statin-treated spheroids.* ***C)*** *Effect of Simvastatin (20μM) and Casc15 siRNA knockdown on spheroids.* ***D)*** *Effect of simvastatin (20μM) and Casc15 siRNA knockdown on explants.* ***See Table 5.1 for details of statistical tests.***

Error bars = SEM. Scale bars = 150μm.

5.2.iv Effect of modulating squalene synthesis and availability on RMS explants

I next decided to study if molecules further down the mevalonate pathway affect migration. I therefore repeated migration assays using one of the end-products: squalene and a squalene synthase inhibitor YM53601.

As shown previously, *Casc15* depletion significantly increased the migration ratio in control media (Figure 5.5, A). The addition of squalene (20μM) to media caused an increase in migration ratio. There was a statistically significant difference between knockdown and control

samples when treating with squalene. Administration of the squalene synthase inhibitor YM53601 caused an exceptionally strong suppression of migration ratio, obscuring the effect of *Casc15* depletion (Fig 5.5, A, B).

No significant morphological differences were observed between control and squalene treated explants, and this was not impacted by the siRNA11-mediated knockdown of *Casc15*. YM53601-treated cells however showed a rounded morphology, without any of the extending processes that are characteristic of actively migrating neuroblasts (Fig 5.5, C).

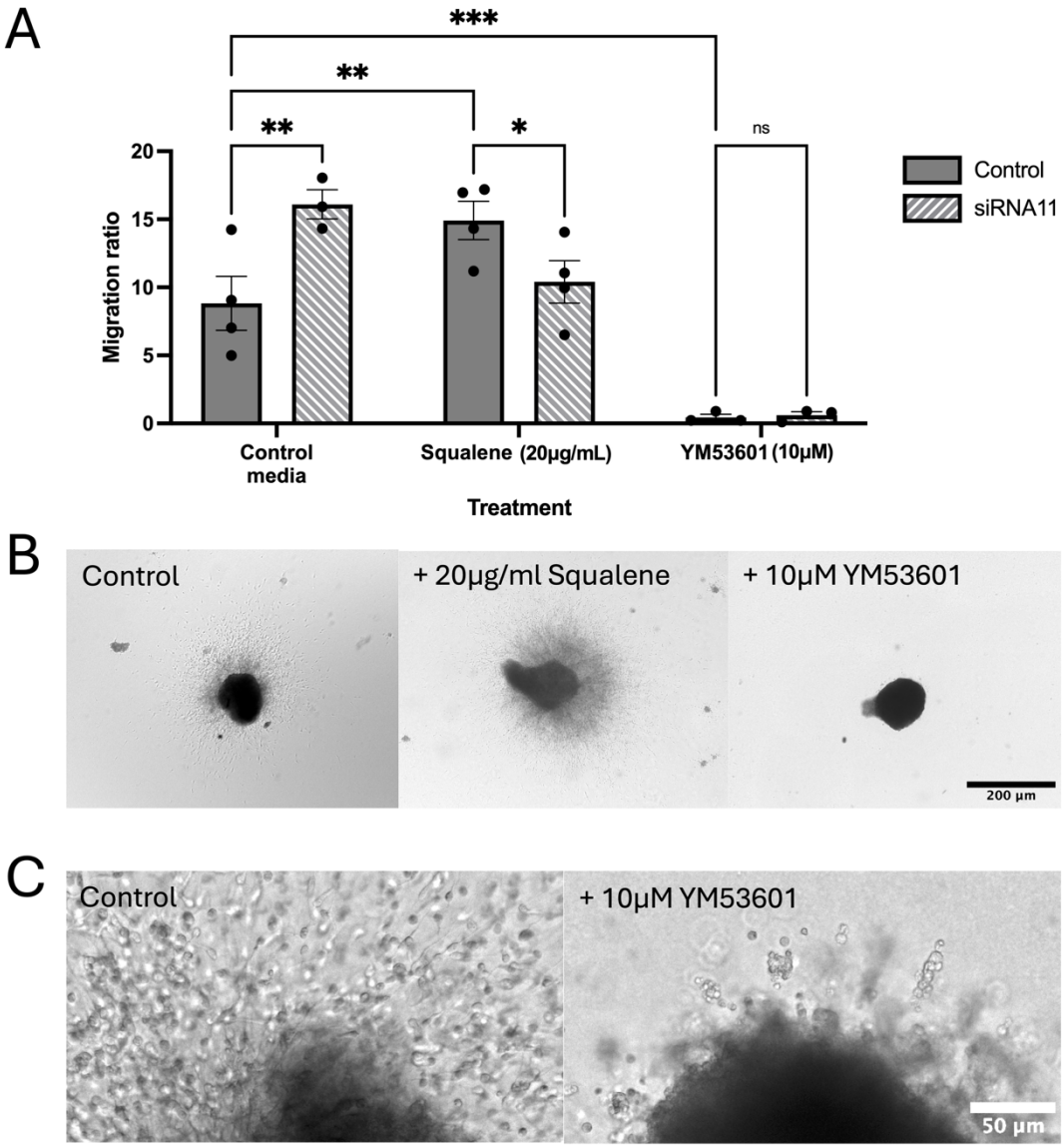

Figure 5.5 Effect of modulating squalene synthesis and availability on an explant assay A) *Effects of adding squalene (20µM) or the squalene synthase inhibitor YM53601 (10µM) to explants, with or without Casc15 siRNA knockdown.* ***B)*** *Low magnification brightfield images of explants under different conditions.* ***C)*** *Higher magnification brightfield images showing morphological characteristics of control (left) and YM53601 (right) treated cells.* ***See Table 5.1 for details of statistical tests.***

Error bars = SEM. Scale bars = 200µm ***(B)****, 50µm* ***(C)****.*

5.2.v Effect of modulating prenylation on RMS explants

Geranyl-PP generated from the mevalonate pathway has one of three fates: used as a substrate for geranylgeranylation, converted to farnesyl-PP for farnesylation, or used to generate

squalene (Figure 5.1). Therefore I next set out to examine the effects of modulating geranylgeranylation and farnesylation on neuroblast migration.

PART 1: Prenylation enzymes

I performed an explant model of neuroblast migration, examining the impact of the prenylation inhibitors FTI-277 and GGTI-298, with concurrent knockdown of *Casc15*. FTI-277 was reconstituted directly in cell culture media, and GGTI-298 in DMSO. A low concentration of FTI-277 (1μM) was used based on similar studies, as this concentration should be low enough to significantly inhibit the FTase complex with minimal effects on GGTase-I (see Table 5.3).

The data generated from this set of explant migration assays is very variable – the control samples treated with 1μM FTI-277 for example show a very large standard error (Figure 5.6, A). Furthermore, sufficiently-powered statistical analysis was not possible due to the small number of samples. Additional replicates might be able to address these issues, but these are currently not possible due to supply issues with FTI-277 and GGTI-298. A tentative interpretation suggests that GGTI-298 is a robust inhibitor of neurogenesis, and that this effect is not modified by *Casc15* depletion.

After 48h of migration neither DMSO (2%) nor FTI-277 (1μM) had given rise to a clear morphological phenotype, and this was not altered by the depletion of *Casc15* by siRNA11 (Fig 5.6, B). Cells that were treated with GGTI-298 (10μM) however showed a clear morphological difference relative to DMSO (2%) controls. GGTI-298-treated cells were small and rounded, with no clear extending processes that are characteristic of migrating neuroblasts. This was not a complete inhibition of migration, shown by cells that had migrated out from the explant. This morphological phenotype was reminiscent of the appearance of cells after treatment with 20μM simvastatin or YM53601 (Figs 5.5, B, 5.6, B).

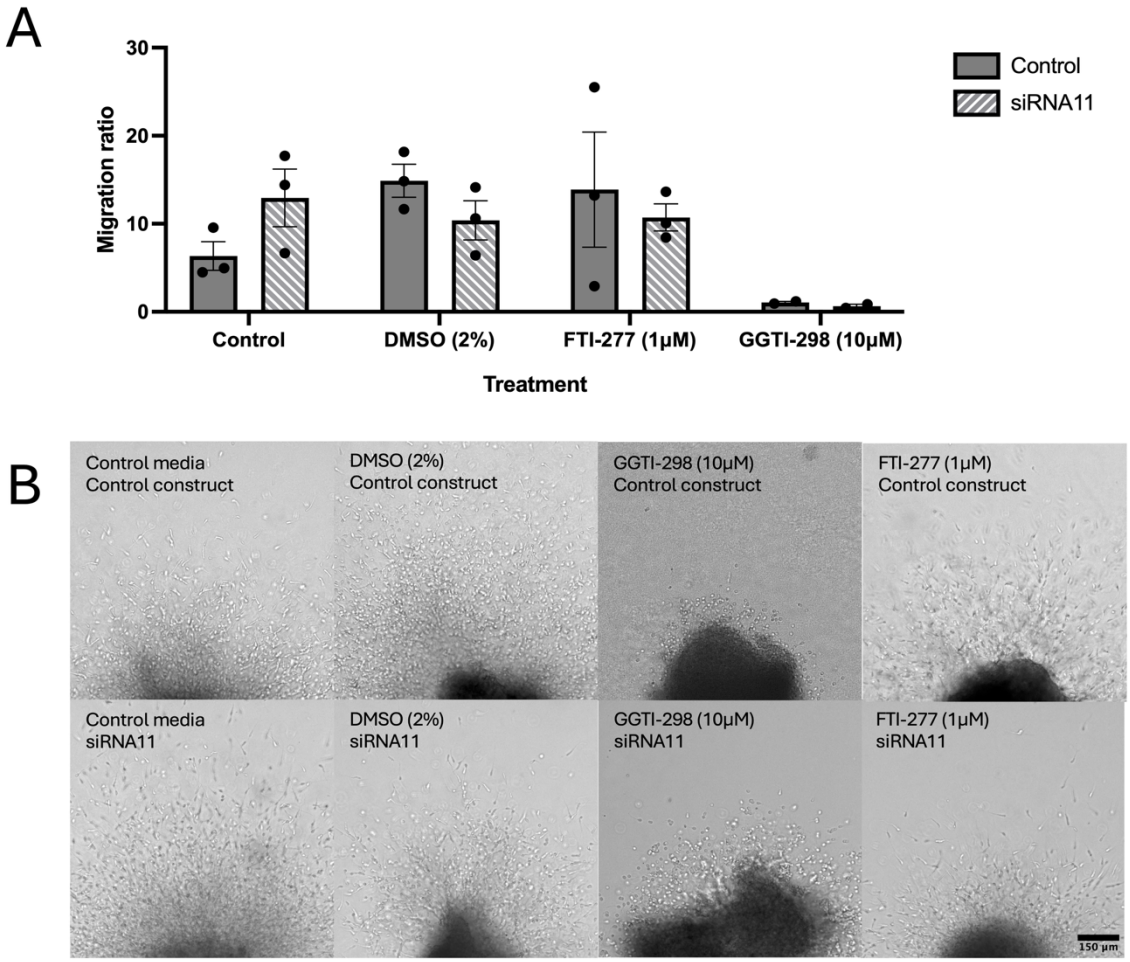

Figure 5.6 Effect of prenylation inhibitors on an explant assay. A) *Effect of DMSO (2%), GGTI-298 (10μM), FTI-277 (1μM) on an explant migration assay with or without Casc15 siRNA depletion.* ***B)*** *Example brightfield images showing morphology of cells migrating from explants treated with DMSO (2%), GGTI-298 (10μM), FTI-277 (1μM), with or without Casc15 depletion.* ***See Table 5.1 for details of statistical tests.***

Error bars = SEM. Scale bars = 150μm

PART 2: High dose FTI-277

Repeating the explant migration assay with a higher dose of FTI-277 (10μM) gave a strong morphological/differentiation phenotype. The 10μM dose of FTI-277 should be sufficient to significantly inhibit the activities of both FTase and GGTase-I. In control groups, neuroblasts migrated from explants with a morphology characteristic of V-SVZ-derived neuroblasts (Figure 5.7, A). However, upon treatment with 10μM FTI-277, cells sent very long (some >2mm long) processes out into the culture dishes (Fig 5.7, B). These explants were imaged at

30 minute intervals for 48h, so the convergence of processes to form bundles can be clearly seen. The FTI-277-treated cells formed a morphology that appeared extremely similar to the axonal growth cone, and extended processes away from the explants that strongly resembled axons, indicating that while their cell bodies weren't moving, they were still capable of forming a growth cone. These processes then proceeded to undergo fasciculation, forming bundles (Fig 5.7, B & D). This phenotype was observed uniquely in FTI-277 10μM treated samples. The neuronal identity of these cells is highlighted in Fig 5.7 C & D by staining for the neuroblast marker Beta-III-Tubulin (TUBB3). This phenotype was observed in approximately 70% of FTI-277 (10μM) treated explants.

This phenotype was unexpected, as the large majority of V-SVZ-derived neuroblasts form granule cell layer GABAergic interneurons which are unusual in their communication via dendro-dendritic synapses, and lack of axons (Aghvami et al., 2022; Price and Powell, 1970). Moreover, fasciculation does not typically occur in these cells. This is therefore not premature differentiation of these cells, but instead *de novo* formation of an atypical structure given their origin. Notably, many of the processes formed in FTI-277 (10μM) treated explants were longer than the entire diameter of the murine OB.

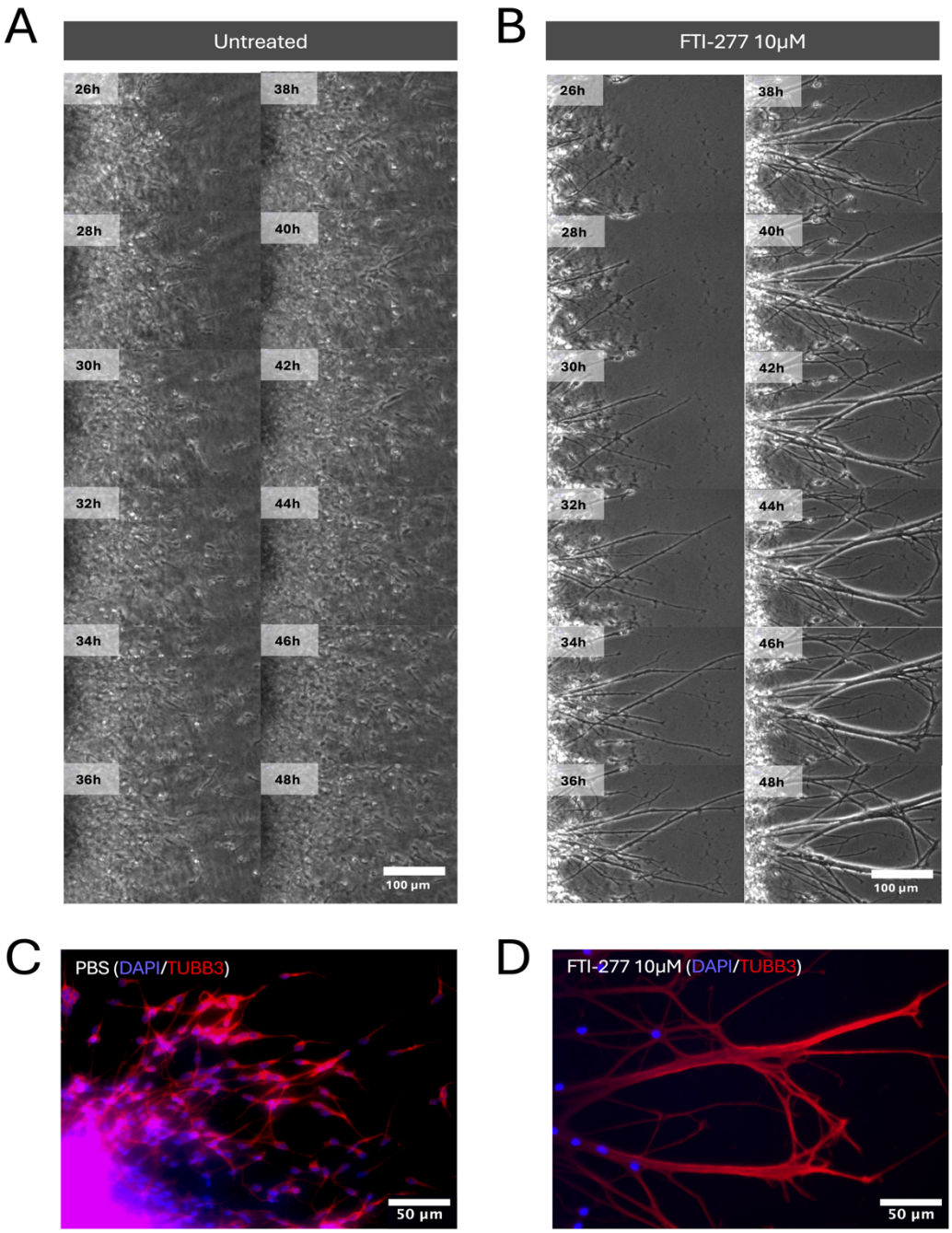

Figure 5.7 Effect of a high dose prenylation inhibitor on neuroblast morphology. *A & B) single frame phase contrast images of cells migrating from RMS-derived explants at 2 hour intervals. The timestamp at the top left of each frame indicates the length of time that cells had been in culture after dissection. C & D) The neuronal identity of migrating cells and processes is confirmed by staining with DAPI (blue) and TUBB3 (red).* ***See Table 5.1 for details of statistical tests.***

Scale bars represent 100µm (A & B); 50µm (C & D)

5.3 Discussion

5.3.i Transcriptional impact of *Casc15* depletion

Initial Gene Ontology analysis of *Casc15* ASO knockdown in tertiary neurospheres revealed significant associations with regulation of cell migration and axonogenesis (Figure 4.2, G). However, re-examination of this data to clarify differentially regulated pathways revealed a strong increase in cholesterol biosynthetic pathways (Figure 5.2, A). There are two key differences between the previous gene ontology analysis (Chapter 4) and this pathway analysis: firstly, the pathway analysis accounts for directionality of change, showing up- and downregulated pathways and thus is better suited to highlight coordinated changes in gene regulation, whereas the previously described GO analysis is better suited to highlight dysregulated gene expression. Secondly, pathway analysis is better for revealing how DE genes function together in broader, defined, networks. A key weakness of both approaches is that they rely on pre-defined gene sets and lists, and therefore can only highlight patterns of gene expression change that have already been described.

Many enzymes of the cholesterol biosynthetic pathway are co-regulated by a single transcriptional regulator: SREBP/F2 – which I subsequently found to be increased in neurospheres where *Casc15* was depleted with siRNA (Figure 5.2, C). These initial results suggested that *Casc15* acted to suppress the expression of enzymes in the cholesterol biosynthetic pathway. Adding squalene, one of the products of the mevalonate pathway (Figures 1.5, and 5.1) suppressed *Casc15* expression *in vitro*. This theoretically causes a relief of *Casc15*-dependent inhibition of *Srebp2*, thus increasing the expression of other mevalonate pathway and cholesterol biosynthesis enzymes. This may be a mechanism to increase the expression of enzymes that utilise squalene to take advantage of its increased availability.

However, qPCR for *Casc15* expression after addition of squalene was conducted 24h after the addition of squalene – in this time delay there could have been multiple oscillations of the entire regulatory network, as shifts in metabolism occur on relatively short timescales. Expanding this analysis to examine multiple time points and concentrations of squalene would be able to clarify this problem. Furthermore, all of these changes were observed in neurospheres, therefore examination of the same gene regulatory networks *in vivo* is necessary to clarify whether or not this is a phenomenon specific to neurospheres.

Further decreased pathways included those that are known to regulate the migration of neuronal precursors and axon guidance, such as ROBO/SLIT and Ephrin signalling (Andrews et al., 2008; Conover et al., 2000). It is likely however that Ephrin signalling is not responsible for the observed phenotype of increased GFP+ cells in the OB, as disruptions to Ephrin signalling in V-SVZ derived cells inhibit migration to the OB. Homozygous knockout of EPH receptor A4 (*Epha4*) -/- decreases cell migration to the OB *in vivo*, similarly truncation of EPH receptor B2 (*Ephb2*) in *in vitro* and *in vivo* disrupts migration (Conover et al., 2000; Katakowski et al., 2005; Todd et al., 2017).

If there was an increase in the enzymes of the mevalonate pathway, I theorised that there must be a concurrent increase in the production of Geranyl-PP and Farnesyl-PP, the substrates for prenylation. I therefore examined the expression of different prenylation complex subunits in neurospheres that had been depleted of *Casc15* (Figure 5.2, E-H). The data shown are highly variable and did not show any statistically significant changes, although there appears to be a trend towards increased expression of *Rabggtb* (a subunit of GGTase II and III) and *Ptar1* (Subunit of GGTase III). I struggled to detect mRNA for the other prenylation complex subunits *Fntb* and *Rabggta* by RT-qPCR. scRNAseq of the murine V-SVZ suggests that the

homeostatic expression of these subunits is low, which could explain the poor detection (Cebrian-Silla et al., 2021a).

Without a comprehensive examination of protein expression levels and the levels of each metabolic intermediate, some doubt may remain as to whether *Casc15* KD induced transcriptional changes truly lead to changes in metabolism. However, the concerted regulation of so many genes in the same pathway suggest that there may be metabolic consequences to *Casc15* depletion.

5.3.ii PRC2 targeting to the *Srebp2* locus

The relationship between *Casc15* depletion and *Srebp2* expression suggest that *Casc15* could act as a direct or indirect inhibitor of *Srebp2* expression. The data presented here strongly suggest that this is achieved through epigenetic silencing by PRC2, in a mechanism that is somehow mediated by *Casc15* lncRNA. *Casc15* may be acting as a scaffold, facilitating the interaction between PRC2 and the *Srebp2* promoter, a mechanism that has been established for a number of different lncRNA. However, it has been postulated that this mechanism is in fact a technical artefact brought about by the relative "stickiness" of PRC2 itself – which has found to interact with over 9000 lncRNAs (Davidovich et al., 2013; Zhao et al., 2010)

It is important to note that the phenotype of *Casc15* depletion on migration and cellular phenotypes in V-SVZ derived cells cannot be solely due to relief of *Srebp2* inhibition. This is highlighted by examining RNAseq data after *Casc15* depletion (as shown in figures 4.2, G and 5.2, A in chapters 4 and 5) where there are many of the genes that change their expression after *Casc15* depletion that are not direct targets of SREBP2. Additionally, if PRC2-mediated H3K27Me3 deposition was the only mechanism of action of *Casc15*, then I would anticipate that the phenotype of *Casc15* knockdown might mirror that of *Srebp2* overexpression.

Unfortunately there do not appear to be any available data examining *Srebp2* overexpression in a similar cell type. Therefore subsequent studies of *Casc15* mechanism of action will need to examine a *Srebp2* overexpression model to ascertain whether the morphological and migration based phenotypes seen in *Casc15* CRISPRi animals can be ascribed to upregulation of *Srebp2*.

5.3.iii Blocking with statins

The powerful effect of simvastatin on *in vitro* assays could not be rescued by *Casc15* depletion, suggesting that simvastatin acts upstream of *Casc15*. These experiments were technically challenging due to poor solubility of simvastatin in cell culture media. The spheroid migration and explant migration assays both required chilling solutions on ice as Matrigel was used, which caused simvastatin to precipitate out of solution and form large crystals if left on ice for more than ~3 minutes. Statins are widely prescribed, so any potential impact on brain function must be deeply examined, as there could be broad reaching implications for the millions of patients prescribed these medications.

Therefore, I have followed this study up with an *in vivo* examination of simvastatin administration in mice. This analysis has not yet been completed, but will provide insight into the impact of oral simvastatin treatment on neurogenesis in adult mice.

5.3.iv Modulation of squalene synthesis and availability

In a similar manner to statins, there were technical challenges associated with the solubility of Squalene in cell culture media. This was mostly overcome by sonication of squalene stock solutions in NBA+ before addition of growth factors, but remains an imperfect method. An important question that remains is to what extent does the addition of squalene mimic the *Casc15* knockdown phenotype? The only *in vitro* phenotype of *Casc15* KD and squalene

addition that matches is an increase in migration ratio and decrease in the expression of *Casc15*. Future studies should be conducted *in vivo* either through the administration of squalene (orally or via intraventricular injection) or overexpression of the *Sqs* gene in the V-SVZ.

5.3.v Modulation of prenylation

The data presented in Figure 5.6 and 5.7 indicate a strong impact of GGTI-298 and 10μM FTI-277 on the migration and maturation of V-SVZ-derived progenitors. However, it is not possible at this stage to assess which prenylation target is the key, or even which prenylation complex. Due to the structural similarity of the prenylation inhibitors GGTI-298 and FTI-277 (Figure 5.1) it is impossible to inhibit FTase or GGTase-I exclusively with these tools. Furthermore, both complexes have such a large number of targets (Figure 1.7), some of which overlap, that even if the inhibitors had 100% specificity it would not be possible to determine which prenylation target was responsible for the phenotype. To understand which prenylation target was responsible, a series of knockdown screen could be performed, depleting each of the targets one at a time.

Unfortunately, it was only possible to perform two replicates of the explant migration assay using GGTI-298 due to supply issues with this drug. Further mechanistic clarification should take the form of either knockout or knockdown of the different enzymes within the prenylation complexes, as this would allow greater specificity of targeting. Additionally, examining the prenylation state of different target proteins would be greatly informative.

All of the migration assays using simvastatin, YM53601, and GGTI-298 that show cells with a rounded morphology should be repeated with a live-dead assay. From the data presented here it cannot be determined whether the cells show a rounding phenotype and decrease migration, or are simply undergoing apoptosis.

5.4 Conclusion

5.4.i Model

Based on the above data and discussion I propose a mechanism of action for the lncRNA *Casc15* as illustrated below (Figure 5.8). In this model *Casc15* participates in a regulatory feedback loop, linking the expression of mevalonate pathway enzymes with the availability of their downstream product. I have shown that *Casc15* preferentially interacts with the EZH2 subunit of PRC2 compared to other proteins (Fig 5.3, A). PRC2 acts upon the *Srebp2* promoter to deposit H3K27Me3, and this interaction is dependent on the presence of *Casc15* – illustrated by the loss of H3K27Me3 deposition upon *Casc15* depletion (Fig 5.3, B). This is an effect limited to a small number of loci including the *Srebp2* promoter and is not a global disruption of PRC1/2 activity, demonstrated by H3K27Me3 immunoreactivity in *Casc15*-depleted cells (Fig 5.3, C). The expression of *Casc15* is linked to the overall activity of the mevalonate pathway, as acute addition of squalene to cell culture media suppresses the expression of *Casc15* (Fig 5.2, D)

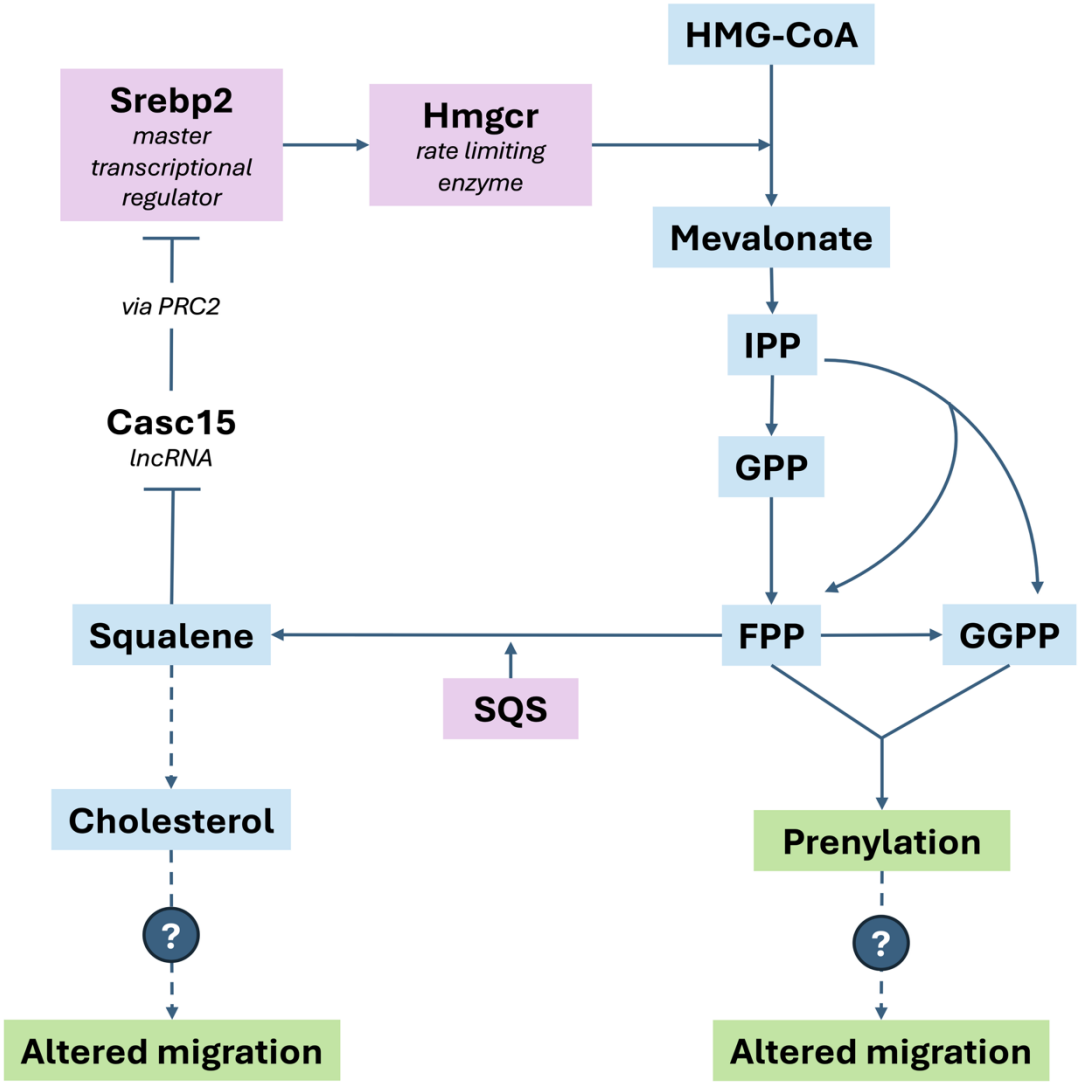

Figure 5.8 A possible mechanism of Casc15 action. *Individual proteins/enzymes are show in pink, metabolic intermediates in blue, and broader processes in green.*

Chapter 6: Discussion

6.1 Overview

6.1.i lncRNAs in the V-SVZ

The first part of my research aimed to evaluate patterns of lncRNA expression within the neurogenic lineage of the postnatal V-SVZ. Previously, Ramos et al found 2,108 lncRNA transcripts uniquely expressed in the neurogenic lineages of the V-SVZ, OB, and DG (data not separated by region) (Ramos et al., 2013a).

I first performed a literature search to identify all studies that used scRNAseq in the V-SVZ, and compared key features such as sequencing platform and average gene coverage per cell (Table 3.2). This revealed that there is a lack of consistency between studies, as well as significant issues regarding transparency of reporting. As summarised in Table 3.2, some studies failed to report the sex or age of animals used, as well as the region of the V-SVZ used for sequencing – not a single study reported all of the metrics that I attempted to examine (Age, Sex, Strain, region of V-SVZ, genes covered per cell, number of cells, average reads per cell, sequencing method, scRNAseq platform). This could introduce issues when attempting a quantitative comparison of these datasets, so I developed my own qualitative approach to comparing results.

My key goal was in understanding cell-type specific patterns of lncRNA expression. I took the results from the Seurat function FindAllMarkers from each paper, which provided a list of genes that were found to be statistically enriched in each cell type within the V-SVZ (e.g. Neural stem cells, transit amplifying progenitors, neuroblasts). I used these results to assign

scores to each lncRNA, with the cumulative score for each lncRNA indicating the number of times it had been found to be enriched within a given cell type. While this is a relatively crude approach, it provided a rapid method requiring low computational power to assess patterns of lncRNA expression across different cell types in the V-SVZ, and is translatable to other cell types and tissues. This approach revealed consistent enrichment of lncRNAs such as *Meg3* with known roles in neural development and differentiation, thereby validating my approach. It additionally was able to recapitulate some of the results of Ramos et al (2013), such as high expression of the lncRNA *C130071C03Rik* in NSCs and TAPs.

In a typical analysis of protein coding gene expression the next step after identifying a list of enriched genes would be to conduct a gene ontology or gene set enrichment analysis, However, as the function of many lncRNAs is poorly understood this was not possible. I used a dataset from Kalamakis et al for a "proof of concept" examination of what I named an "indirect gene ontology" examination of lncRNA expression (Kalamakis et al., 2019). This analysis was based not on the function of the lncRNAs, but on the transcription factors that regulate their expression. I used annotated transcription factor binding sites in the promoter of each lncRNA to infer which processes these genes may be regulated in concert with. This revealed that the majority of these lncRNAs were bound by transcription factors associated with changes in metabolism and biosynthesis.

My analysis of cell-type enrichment revealed a number of lncRNAs that were elevated in neuroblasts, and based on their enrichment and conservation I selected the lncRNA *2610307P16Rik* to examine further. For clarity, *2610307P16Rik* is referred to as *Casc15*, the name of the human homolog. I had found that *Casc15* was enriched with CO of 4 in Neuroblasts, and that its sequence was unusually highly conserved. Both my qualitative

approach and Ramos et al (2013) identified *Casc15* as being enriched in neuroblasts – they found that *Casc15* showed a 19.951-fold enrichment in neuroblasts relative to neural stem cells, although the gene was not annotated in the mouse genome at the time of their study's publication, and was listed as a novel transcript.

Serendipitously Dr Bin Sun, previous DPhil student and postdoctoral researcher with the Szele lab, had independently identified *Casc15* as a candidate for regulation of V-SVZ neurogenesis. Taken together, the results from Ramos et al, my own analysis, and analysis by Dr Sun strongly encouraged me to examine the potential function of *Casc15* in more detail.

Key information that was lacking from the available data was expression of different *Casc15* isoforms. There are a large number of isoforms annotated for *Casc15* in the Ensembl database that could be generated by alternative splicing, with varying levels of data supporting their existence (Howe et al., 2021). For many lncRNAs, it is not a change in the total number of copies of the transcript within a cell that can trigger a developmental change, but instead a shift in the ratio of different isoforms that are expressed. This is very likely to also be the case for *Casc15*; I examined long read RNAseq data from a study looking at the differentiation of SH-SY5Y cells into neurons (Wright et al., 2022a). In this data only 5 out of an annotated 326 possible splice isoforms were described, with the transcript *CASC15-207* accounting for the bulk of *CASC15* expression. Many lncRNAs are also able to adopt circular conformations, but due to their circular nature, there is no poly-Adenylation signal on these molecules and therefore they will not be isolated by "standard" RNAseq library prep methods that selectively enrich for poly(A). In order to address the issue of variations in splicing and the generation of circular isoforms, RNAseq should be performed using long read methods (such as Oxford Nanopore) or a specialised circular RNAseq approach.

6.1.ii *Casc15* lncRNA and migration

Historically, the non-protein coding regions of the genome have been dismissed as junk, and long noncoding RNAs as transcriptional noise. More recently, some have been acknowledged as subtle molecular regulators, which serve to modulate the function of much more important protein coding genes. However, the data illustrated in Chapter 4 Results 2 Migration reveal a possible role for the lncRNA *Casc15* in regulation of migration.

I have shown that using multiple different assays for neuroblast migration, and using multiple different modalities of *Casc15* depletion that the outcome remains the same: *Casc15* depletion increases readouts of neuroblast migration. The "readouts" of migration examined for *in vitro* assays examine the volume (spheroids) or surface area (explants) that actively migrating cells expand to occupy, and are proportional to the overall rate of cell migration. However, these readouts are sensitive to non-migratory effects, which may obscure biologically meaningful changes. For example, high levels of cell proliferation in a spheroid assay will lead to an increase in the volume occupied by cells, alternatively a reduction in cell death/apoptosis could cause a similar effect. Thus there are confounding factors that warrant significant consideration when interpreting the results from these assays. If the *in vitro* results from the explant and spheroid assays were due to cell proliferation, for example, I would anticipate an increase in the proportion of cells that are immunoreactive formKi67 in the brains of animals that were treated with *Casc15* CRISPRi knockdown constructs. Indeed while there is not a statistically meaningful effect of *Casc15* depletion on cell proliferation *in vivo*, I did observe a trend in both the density and proportion of GFP+mKi67+ cells in both the V-SVZ and OB, suggestive of an increase in proliferation. This could be clarified by repeating this stain using a mitotic marker such as MCM2 which is expressed for a longer period of time that mKi67 in the cell cycle.

A decrease in cell death following *Casc15* CIRPSRi knockdown could also lead to an increased number of cells reaching the OB. Upon staining for CASP3 I did not find any notable changes or trends, but there remains a possibility that cell death is affected. Importantly cells were marked with GFP, which has been found to be significantly reduced in cells that are underdoing apoptosis (Strebel et al., 2001). Therefore it is likely that dead and dying cells that were depleted of *Casc15* were not identified due to very low levels of GFP fluorescence. A more successful approach may be to use a marker protein for an earlier step in apoptosis such as a marker of apoptosis **initiation** rather than CASP3, an effect of apoptosis.

In vivo, loss of *Casc15* expression lead to an increased number of labelled cells reaching the OB at 14 days post electroporation. Although more cells reach the OB after *Casc15* depletion some of these show unusual phenotypes, two of which could be explained by increased migration speed. As illustrated in Figure 4.14, if we assume that the amount of time a cell migrates for is fixed and the key difference between cells is the **speed** of migration, the "misplaced" cells observed in Figure 4.11 and the truncated dendrites in Figure 4.12 can be explained. Altered speed of migration cannot account for the abnormal morphology described in Figure 4.10. Timelapse studies of neuroblasts indicate that speed of migration in the RMS is highly heterogeneous and that cells even turn back on themselves, although the net movement is towards the OB (Martinez-Molina et al., 2011; Nam et al., 2007). Perhaps the effect of *Casc15* could be achieved not through making cells migrate faster than they do under control conditions, but through shifting the bias of cells to turn back on themselves,. Alternatively this could be achieved through pushing a population of cells migrating at heterogeneous speeds to instead all migrate at the higher speed. This could be addressed by time-lapse microscopy in acute brain slices from control and knockdown mice.

An important question when examining altered OB neurogenesis is at which point in the lineage the phenotype arises. When examining the V-SVZ for the number of cells, cell death, and cell proliferation I did not find any clear phenotype, although the variation between animals (and subsequent SEM) was quite large, suggesting that this part of my study was perhaps underpowered. However, as illustrated in Figure 3.5, *Casc15* is most highly expressed in neuroblasts, which are found in the dorsal horn of the V-SVZ but are predominantly within the RMS and OB. Therefore is it likely that the phenotype observed upon *Casc15* depletion is due to its role in neuroblasts in the RMS and OB, rather than an effect on NSCs in the V-SVZ that then persists through the lineage. This is reinforced by the observation that gene expression changes after *Casc15* knockdown are predominantly associated with cell migration and metabolism, rather than NSC proliferation and homeostasis. It must be noted however that there is both cell autonomous and non-cell autonomous regulation of V-SVZ neurogenesis, so there may be a phenotype in non-nucleofected cells that was not captured by the data presented here (Ocbina et al., 2006).

The V-SVZ can contribute cells to the striatum, and although I did not find a difference on the overall number of labelled cells migrating into the striatum, those that were present moved further from the V-SVZ when *Casc15* had been depleted. The labelled cells found in the striatum showed a morphology stereotypical of striatal astrocytes. This suggested that the effect of *Casc15* depletion on cell migration was not unique to neuroblasts, and that in fact *Casc15* plays a role in the migration of glial precursors. This is consistent with studies that examine the role of *CASC15* in human cancers – an effect of *CASC15* knockdown on migration was found in a range of different tumour types and cells lines (Figure 4.1).

6.1.iii *Casc15* lncRNA and metabolism

In order to examine the broader cellular effects of *Casc15* knockdown I expanded my analysis of my bulk RNAseq data, derived from tertiary neurospheres, to include pathway analysis and upstream regulator analysis. Pathway analysis revealed a predicted increase in the superpathway of cholesterol biosynthesis, and upstream regulator analysis predicted that this was due to an increase in transcriptional activation by SREBP2. I then confirmed the increase in *Srebp2* expression in neurospheres by qPCR. This suggested that the effect of *Casc15* KD on these genes was via their regulator SREBP2, rather than a direct effect of *Casc15* on each gene (Figure 5.2). These SREBP2-regulated genes were enzymes in the Mevalonate Pathway, a metabolic pathway that produces the precursors for cholesterol (see Figure 1.5). Addition of one of these precursors, Squalene, to cell culture media suppressed the expression of *Casc15*. The observation that *Casc15* regulates expression of mevalonate pathway enzymes, and is in turn regulated by the product of these same enzymes suggests that it may be participating in a feedback loop, coupling the rate of the pathway (via enzyme expression) to its final product (squalene).

I next asked how *Casc15* might be regulating *Srebp2*, examining interactions with the repressive epigenetic modifier PRC2 *in vitro*. These data suggested that *Casc15* interacts with PRC2 to target it to the *Srebp2* promoter. This was reinforced by the observation that *Casc15* KD reduced H3K27Me3 deposition at the *Srebp2* promoter, but did not cause a global loss in H3K27Me3 – suggesting that this is a more specific effect than generic destabilisation of PRC2-target interactions. However, it must be emphasised that physical interactions between PRC2 and lncRNAs are still controversial due to intrinsic features of PRC2 itself (Davidovich et al., 2013; G Betancur and Tomari, 2015). The catalytic subunit EZH2 interactions with RNA in a nonspecific manner, with a preference for longer RNA. The promiscuity of PRC2 and

RNA is such that whole “interactomes” can be isolated and sequenced due to the sheer number of RNAs that it interacts with. It is unlikely that all observed PRC2-lncRNA interactions are functional, so my RIP results must be interpreted conservatively. This is particularly true for data generated in this thesis, where the variability in the amount of *Casc15* pulled down with EZH2 is very high (see Figure 5.3, A).

I next examined how different enzymes and products of the mevalonate pathway regulated neuroblast migration, and how these effects interacted with *Casc15* KD. Blocking the mevalonate pathway with Simvastatin, a drug that inhibits the rate limiting enzyme HMGCR resulted in a sharp reduction in neuroblast migration that could not be rescued by *Casc15* knockdown, suggesting that that if *Casc15* exerts its effects on migration via alterations in the mevalonate pathway, the key effector is downstream of HMGCR.

I next looked at supplementing squalene in the culture media of neurospheres and alternatively inhibiting squalene synthase (SQS). Supplementation of squalene caused an increase in neuroblast migration, perhaps mimicking the effect of *Casc15* siRNA by inhibiting its expression. One challenge with supplementing squalene in cell culture media is that it is nonpolar, and thus has poor solubility in cell culture media. One approach that will be used in future studies of squalene is using a modified squalene that is more soluble in aqueous solution (Zhang et al., 2024). Inhibition of SQS with YM53601 blocked migration, and this effect was not rescued by depletion of *Casc15*. This phenotype is perhaps unsurprising as mutations in the *SQS* gene cause embryonic lethality in mice and severe disruptions of brain development in humans (Fig 1.5).

Initial migration data examining the impact of prenylation inhibitors suggested a profound role for prenylation in the V-SVZ and neuroblasts. However, as discussed the inhibitors used were not sufficiently specific, to determine whether the observed cellular phenotype was due to changes in one prenylation of one particular target, or the combined effect of altering prenylation in dozens of targets simultaneously. Further investigation with these inhibitors was unfortunately not possible due to supply issues, leading to a >8 month lead time.

Examining the available literature for a lncRNA with a similar phenotype regarding cholesterol biosynthesis revels the highly conserved lncRNA small nucleolar host gene 6 (*SNHG6*) (Liu et al., 2022). The *SNHG6* depletion phenotype is a striking mirror of that described for *Casc15* – *SNHG6* KD decreases the expression of cholesterol biosynthetic enzymes and *Srebp2*, whereas *Casc15* KD increases these same genes. *SNH6* expression is induced by the addition of one of the products of this pathway (cholesterol), while *Casc15* is repressed by the addition of Squalene, the first committed precursor to cholesterol. These results taken with the results of the present study has opened the possibility that a great network of lncRNAs regulate cholesterol biosynthesis in the brain.

6.2 Limitations

6.2.i Technical

A key limitation of the gene expression data particularly is that the RNAseq data and many of the qPCR results were generated using neurospheres. Neurospheres are derived from the V-SVZ and possess both similarities to and differences from *in vivo* V-SVZ (Pastrana et al., 2011). Importantly in the neurosphere assay, only proliferative cells will form spheres, so any effect on quiescent NSCs will be obscured. Moreover, these proliferative NSCs occur before neuroblasts in the V-SVZ neurogenic lineage, and so may not be an accurate representation of

regulatory networks that occur in neuroblasts. There is a great spatial heterogeneity within the V-SVZ, which is lost when dissociating cells for preparation of neurospheres (Cebrian-Silla et al., 2021a). In order to strengthen the conclusions made regarding the regulation of *Srebp2* and the mevalonate pathway, many of these gene expression experiments should be repeated *in vivo* either using a knockout mouse or through electroporation of NSCs lining the lateral ventricles.

Live imaging was performed when carrying out *in vitro* migration. The migration dynamics and patterns of movement of neuroblasts within the RMS *in vivo* are stereotypical and tractable, and can be tracked in live animals using 3-Photon (3-P) imaging (Sun et al., 2022). In order to expand upon the migratory phenotype observed and to confirm that the increase in OB GFP+ cells is due to altered migration, 3-P live-imaging of GFP labelled cells in the RMS would be a beneficial approach to assess *Casc15* knockdown.

As discussed previously, a key weakness of the experiments focussing on prenylation and its inhibition is the specificity of the pharmacological inhibitors used. This is predominantly because the enzyme complexes FTase and GGTase-I have overlapping targets, and the inhibitors FTI-277 and GGTI-298 mimic their targets. This could be resolved in part if the complexes were specifically depleted, rather than inhibited. The depletion could be achieved using the same methods described for the depletion of *Casc15*. Each prenylation complex (FTase, GGTase-I – III) has one subunit that is unique to that particular complex (see Figure 1.7, A). Thus depletion by CRISPRi, for example, could be used to reduce the expression of one specific complex and subsequently reduce that complex's activity.

Another prenylation-specific weakness is that these experiments do not show functional changes in prenylation. The assumption is made based on previous studies describing these inhibitors that there is a reduction in prenylation, but this reduction is not characterised in Chapter 5. The process of assessing prenylation can be technically challenging, and would likely need to be addressed one target at a time. A typical approach would be to supplement cells with [^{3}H] labelled FPP, GGPP, or Mevalonate and allow their incorporation as posttranslational modifications. This would be followed by separation of proteins by SDS-PAGE and visualisation by autoradiography (Elam et al., 2005). Alternatively, the prenyl group can be subjected to methyl idodide cleavage and resolved via High-Performance Liquid Chromatography (HPLC) (Whyte et al., 1997).

6.2.ii Species

Another key limitation of the data discussed here is that all functional experiments were performed using murine cells and tissues. While the sequence of *Casc15* is conserved, this is not sufficient to state that its function is as well. One study has found that overexpression of either the human or murine gene yielded the same phenotype in a mouse pre-B cell line (Fernando et al., 2017). Whether this is also the case for V-SVZ neurogenesis has yet to be clarified. Conservation of *Casc15* in this study has been assessed at the level of the entire locus. However, whether there are particularly well conserved motifs within this locus or functional structural signatures has yet to be elucidated; this analysis is currently ongoing.

6.3 Future directions

6.3.i Mouse functional outcomes

A key feature that is missing from this investigation is functional outcomes. I have demonstrated an increase in new neurons in the OB, but this is not a meaningful change unless

it demonstrably impacts OB-dependent behaviour. Ideally this would be assessed by the generation of a conditional knockout mouse, a proposal for which is illustrated in Figure 6.1.

For example, with loxP sites surrounding the *Casc15* locus, and Cre-recombinase under the control of the *Dcx* promoter to limit the KO to neuroblasts and their progeny, the layout of a potential transgene is shown in Figure 6.1. The conditional knockout of *Casc15* would be achieved by flanking the *Casc15* locus with lox-P sites that would recombine upon addition of tamoxifen in cre-recombinase expressing cells. Cre recombinase itself would be under the control of the *Dcx* promoter (*pDcx*), thus limiting the knockout to neuroblasts. The successful induction and activity of the cre recombinase would be assessed using two reporters. The first uses the same *GFP-H2B/myr-tdTom* transgene used in CRIPSRi studies in this thesis, with a premature stop codon flanked by Lox-P sites – upon treatment with tamoxifen this stop signal would be removed, allowing expression of GFP and tdTomato. A second reporter would be used: *YFP* under the control of the *Dcx* promoter, with the entire sequence flanked by LoxP sites. This would ensure expression of YFP under control conditions, and loss of yellow fluorescence in DCX+ cells upon tamoxifen treatment. The murine *Dcx* gene is encoded on the X-chromosome, so these transgenes would be inserted into a different chromosome to avoid accidental silencing by X-chromosome inactivation in female animals (NCBI, 2025). These mice would feature yellow fluorescence in DCX+ cells prior to tamoxifen administration. After tamoxifen, the majority of cells that are **both** YFP- *and* GFP/tdTom positive would represent neuroblasts which had had their *Casc15* locus deleted. A possible complication of this approach is that the V-SVZ is not the only source of DCX+ cells in the brain, so tamoxifen administration would also cause knockout of *Casc15* in the SGZ.

With an inducible knockout model for *Casc15* it would be possible to observe the impact of KO by injecting tamoxifen at different developmental stages. All of the functional work

described here used postnatal mice in a narrow developmental window (P0 to P6). Electroporation of knockdown constructs to target the V-SVZ in adult mice is possible, but at this stage the majority of electroporated cells will be non-migratory ependymal cells (Bin Sun, unpublished data). Additionally, when electroporating as described here in P0 mice, the skull is soft and flexible enough to push a glass needle through the skin and skull without having to make an incision or hole. In an adult animal however, a small hole would need to be drilled in the skull to allow the needle through. Using transgenic mice (as described in Fig 6.1) could allow investigation of *Casc15* function in DCX+ progenitors across the lifespan of animals, and limit technical variability introduced by electroporating at different developmental stages.

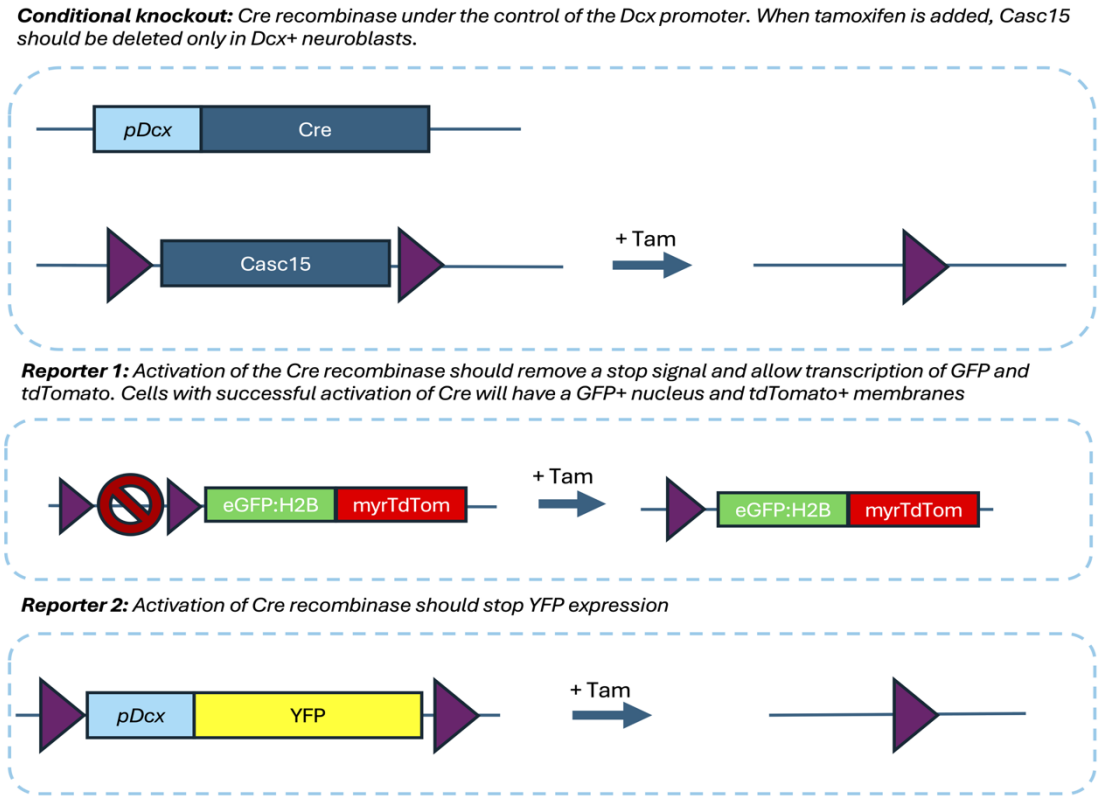

Figure 6.1 Schematic for a conditional knockout of Casc15*. The schematic shows four transgenes: 1) Cre recombinase under the control of the Dcx promoter, 2) Casc15 flanked Lox-P sites, 3) GFP and TdTomato with an upstream STOP signal flanked by Lox-P sites, 4) YFP under the control of the Dcx promoter, flanked by Lox-P sites.*

The data presented focus on the V-SVZ, the largest postnatal stem cell niche in the murine brain. However, the V-SVZ is not the sole stem cell niche. Further investigation should also

examine the impact of *Casc15* depletion on stem cells and neurogenesis in the subgranular zone (SGZ) of the hippocampus. However, DCX+ cells generated in the SGZ are non-migratory, so the profound impact of *Casc15* on migration observed in V-SVZ-derived cells may not be observed – assuming that *Casc15* plays the same role in both the V-SVZ and SGZ. Spatial transcriptomics in Figure 3.6 suggests that *Casc15* is indeed expressed in the SGZ. Hippocampal SGZ progenitors, when transplanted heterotopically into the RMS, migrate to the OB where they differentiate to form both GCL and GL interneurons (Suhonen et al., 1996). This suggests that there could be similar regulatory mechanisms at play in both the V-SVZ and SGZ, so *Casc15* may still be able to exert an effect in the hippocampus.

6.3ii Long term survival of newborn neurons

The data presented in Chapter 4 illustrate an increase in the density of GFP+ cells in the olfactory bulbs of animals at 14 days post electroporation. An important feature of these cells that was not analysed was their long term survival. Observations in both juvenile and adult mice have previously revealed that not all newborn GCL neurons survival long term, and that up to 50% may undergo apoptosis (Chaker et al., 2023; Petreanu and Alvarez-Buylla, 2002). In order to assess whether the *Casc15*-depletion induced increase in cells in the OB is maintained, these experiments should be repeated and the brains of animals examined at later time points.

6.3.iii *CASC15* in the human brain

The sequence and expression pattern of *Casc15* is conserved between mice and humans – *CASC15* is highly expressed in neural progenitors in the human V-SVZ and is positively correlated with Dcx expression across all developmental stages (Bonine et al., 2024; Cebrian-Silla et al., 2021a; Sunkin et al., 2013) (see Figure 4.1). Given the conservation of both sequence and expression, it is likely that *CASC15* may regulate migration of human neuronal

precursors, as well as neuronal-like cancer cells. Work is currently in progress to acquire human V-SVZ samples in order to establish robust protocols for assessing migration, before examining the effect of *CASC15* depletion.

6.3.ii Cholesterol and metabolomics

Data presented here has examined the changes in gene expression of key regulators and enzymes. However, I have not examined the levels of individual metabolic intermediates or total cholesterol content in the cells examined. Based on changes in gene expression the assumption has been made that there is an alteration in protein production, enzyme activity, and finally the rate of the mevalonate pathway as a whole. In order to validate the model proposed in Figure 5.8, an ideal approach would be to leverage newly developed single-cell metabolomic and lipidomic approaches to more robustly interrogate alterations in the mevalonate pathway and cholesterol biosynthesis.

In order to validate the relationship between *Casc15*, SREBP2, and migration (Figure 5.8), I will overexpress (OE) *Srebp2* in the postnatal V-SVZ and compare the phenotype of *Sbrep2*-OE cells with *Casc15*-KD cells (as described in chapter 4 & 5). An identical phenotype might indicate that the entire *Casc15* phenotype is due to alterations in *Srebp2* expression, but this is likely to not be the case as many genes that regulate migration and neurogenesis – but are not *Srebp2* targets - (such as *Robo2*) are altered in the *Casc15* KD RNAseq data (Table 4.3). The production and validation of *Srebp2*-OE constructs is currently in progress.

6.3 Final overview

Together, these data present a first insight into the role of the lncRNA *Casc15* in the V-SVZ. In Chapter 3 I have illustrated the consistencies (and inconsistencies) between studies using the same methods to interrogate the same tissue, and how we can leverage this data to learn

about lncRNAs. In Chapter 4 *Casc15* depletion had a robust and highly reproducible effect on migration assays of V-SVZ-derived progenitor cells. It is currently unclear what the role of *Casc15* is in other neurogenic niches, or even in other non-neural migratory progenitors. The precise mechanism of how *Casc15* may regulate migration on a molecular basis has yet to be elucidated, but data in Chapter 5 indicate that the effect of *Casc15* is exerted at least in part via alterations in cholesterol biosynthesis. I have proposed a mechanism of action, that places *Casc15* in the centre of a highly conserved and tightly regulated metabolic network. This mechanism, even if incorrect, provides a framework that can be interrogated in future experiments.

Appendices

These appendices entail experiments performed in collaboration with other groups that do not fit under the title “The missing lnc: long noncoding RNA in neuroblast migration”.

Appendix 1: Nutraceuticals and cytogenesis in a model of Alzheimer’s Disease

Alzheimer’s Disease (AD) is a neurodegenerative disease that represents a significant global disease burden, with an 55 million people affected by dementia, with AD accounting for an estimated 60-70% of these cases (WHO, 2025). AD is characterised by progressive loss of brain volume in concert with neuronal death and the accumulation of toxic protein plaques (Fischl et al., 2002; Serrano-Pozo et al., 2011; Shankar et al., 2008). A hallmark of AD is cell death and atrophy in the hippocampus, a region critical for memory and cognition. The hippocampus is host to the subgranular zone (SGZ) neurogenic niche (Kempermann et al., 2015). Decreased neurogenesis in the SGZ is associated with AD pathology, therefore it is theorised that artificially increased SGZ neurogenesis could alleviate some AD-induced defects (Scopa et al., 2020; Sung et al., 2020).

AD occurs in both sporadic (late onset) and familial (early onset) cases. Familial AD accounts for ~5% of all cases, while the bulk of AD cases are sporadic (~95%) (Ulaganathan and Pitchaimani, 2023). In the present study, the Senescence Accelerated Mouse Prone-8 (SAMP8) mouse is used to model sporadic AD, these mice show an accelerated aging phenotype and develop AD-like pathology at a relatively young age (Ong et al., 2025). In contrast, the Senescence Accelerated Mouse Resistant-1 (SAMR1) mouse is used as a control, and does not show the same accelerated aging phenotype.

In collaboration with the laboratory of Professor Hiroko Isoda in the University of Tsukuba I have been investigating the impact of naturally derived compounds and extracts on SGZ cytogenesis. One such extract is Rosemary Extract (RME), derived from the rosemary plant (*Rosmarinus officinalis L*) which is high in the anti-inflammatory compound Rosemarinic Acid (Andrade et al., 2018). RME administration and behavioural tests were performed by Dr Kazunori Sasaki at the University of Tsukuba, before perfusion-fixation and dissection of brains. Brain sectioning, immunohistochemistry, and analyses were performed at the University of Oxford by myself, Jun Ong, Sabina Ciaghi, and Ayano Sugiyama-Finnis.

RME at a dose of 20mg/kg or 50mg/kg (or water) was administered by oral gavage for a period of 30 days, the final 9 of which BrdU (1mg/mL) was provided in drinking water (Figure A1.1, A). Examining escape latency in the Morris Water Maze (MWM) test revealed that SAMP8 mice showed increased escape latency relative to SAMR1 controls in the absence of any treatment (Fig A1.1, B). However, this deficit was rescued by the administration of RME at 20mg/kg or 50mg/kg. This pattern is seen when examining the number of platform crossings in the MWM (Fig A1.1, C) and time spent in the target zone (A1.1, D), wherein SAMP8 water-treated mice show a deficit relative to SAMR1s, but this is rescued by treatment with RME.

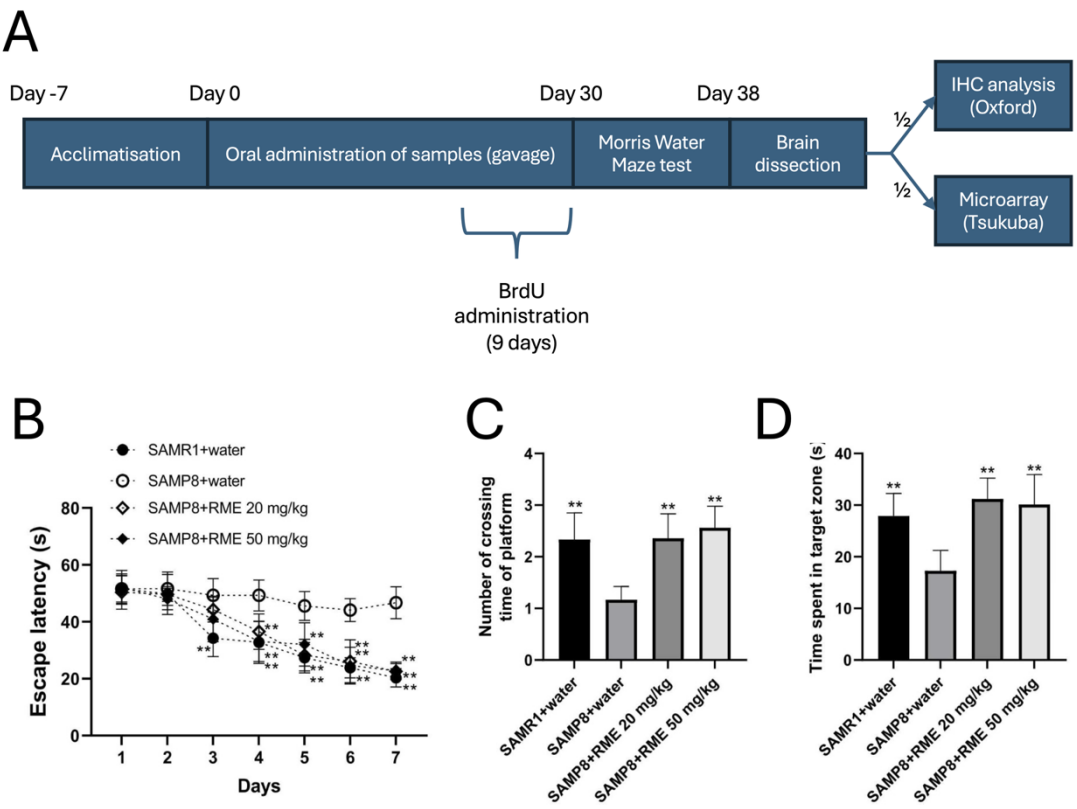

Appendix 1 Figure A1.1 Effect of Rosemary extract (RME) on Morris Water Maze performance A) *Schematic for administration of treatment (water, RME 20mg/kg, or RME 50mg/kg) in 30 week old SAMR1 and SAMP8 mice.* ***B)*** *Escape latency of animals in the MWM test as measured over 7 days.* ***C & D)*** *show the effect of RME on* ***C)*** *the numbers of crossings of platform and* ***D)*** *the time spent in the target quadrant by probe test. Data and analysis by Dr Kazunori Sasaki.*

Error bars represent SEM

Performance in the MWM test is strongly inluenced by hippocampal function, thus we set out to examine whether the phenotypic rescue was due to alterations in neurogenesis or oligodendrogenesis in the SGZ (Gage et al., 1988).

Doublecortin (DCX) is used as a marker of neuroblasts (Fig 1.2) in the SGZ as well as in the V-SVZ. There was no significant difference observed between the total density of DCX+ cells between treatment groups (Figure A1.2, A, E). Examining a later state of the neurogenic lineage by staining for BrdU to mark newly generated cells and NeuN for mature neurons (Fig 1.2, B) revealed cells that had been generated and matured in the dentate gyrus. No statistically significant changes in the density of BrdU+NeuN+ cells were observed between treatment

groups or strains (Fig A1.2, B, F). Taken together, these data suggest that the behavioural alterations observed in RME-treated SAMP8 mice cannot be attributed to changes in neurogenesis in the hippocampus.

We next examined non-neural cytogenesis using GFAP and OLIG2. GFAP is used as a marker of astrocytes, although it can mark both astrocytes and radial glia-like neural stem cells (RGL-NSCs) so cannot be used to delineate astrocytes and RGL-NSCs with absolute confidence (Doetsch et al., 1999). OLIG2 is typically used as a marker for differentiation of the oligodendrogenic lineage, but is expressed in a subset of NSCs and astrocytes (del Águila et al., 2022). No significant changes were observed in the number of newborn astrocytes (A1.1, C, F) or oligodendrocytes (A1.2, D, G).

Together the data presented in Figure A1.2 suggest that the impact of RME administration on MWM performance in SAMP8 mice cannot be attributed to changes in cytogenesis in the SGZ. These results are now published as Sasaki et al (Sasaki et al., 2024).

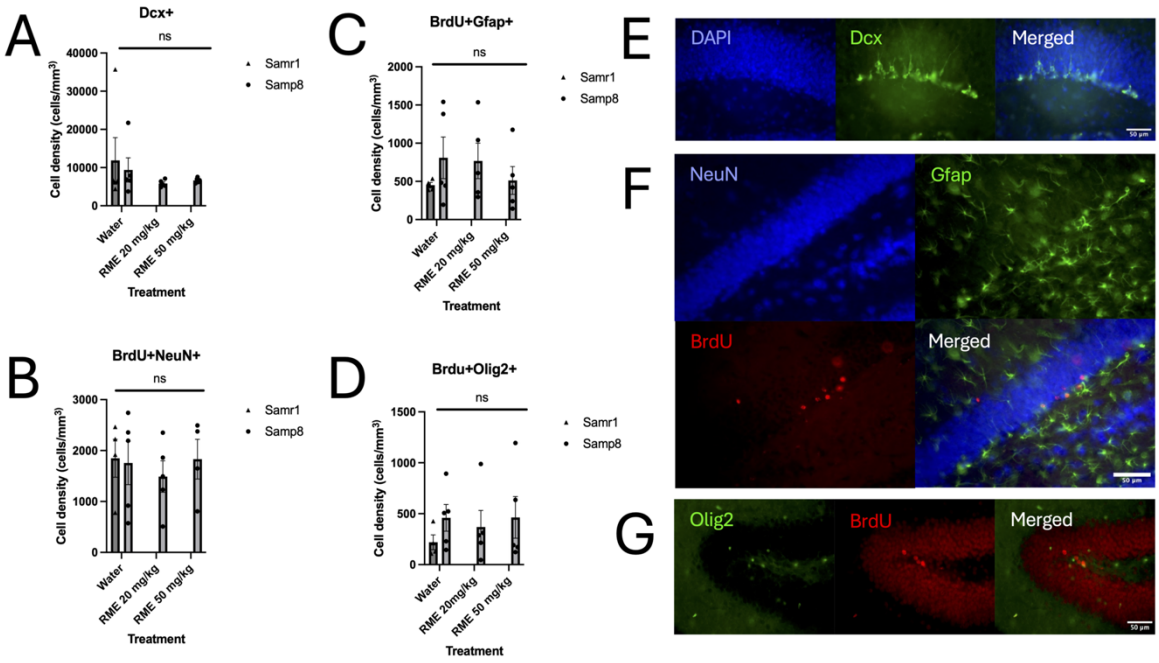

Appendix 1 Figure A1.2 Effect of Rosemary extract (RME) on cytogenesis in the SGZ. A-D) *There was no statistically significant effect of strain or treatment on the density of* ***A)*** *Dcx+ neuroblasts,* ***B)*** *BrdU+NeuN+ newborn neurons,* ***C)*** *BrdU+Gfap+ newborn astrocytes, or* ***D)*** *Brdu+Olig2+ newborn oligodendrocytes.* ***E)*** *Example IHC showing DAPI (blue) and Dcx (green) in the dentate gyrus.* ***F)*** *Example IHC showing NeuN (blue), Gfap (green), and BrdU (red) in the dentate gyrus.* ***G)*** *example IHC showing Olig2 (green) and BrdU (red) in the dentate gyrus.* ***See Table A.1 for detail of statistical tests.***

Error bars represent SEM, scale bars represent 50µm. IHC = Immunohistochemistry

Appendix 2: Impact of pregnancy on hippocampal neurogenesis

Pregnancy and parturition are associated with significant changes in cognition and behaviour (Hillerer et al., 2014; Russell et al., 2001). In mice changes have been found in neurogenesis in the postpartum period, with a peak of V-SVZ neurogenesis in the 7th day after animals have given birth (Chaker et al., 2023; Shingo, 2003). Aberrations in neurogenesis have also been found in rodent models of depression (Siopi et al., 2016). Taking the impact of both depression and pregnancy on neurogenesis, it is likely that targeting neurogenesis may be an effective approach to treating postpartum depression and other associated psychiatric conditions in humans, a concept which is supported by preliminary data (García-Baos et al., 2022).

I set out to examine the impact of pregnancy on neural stem cells and neurogenesis in the hippocampal SGZ in the first week after parturition. I compared age-matched nulliparous (animals that have never been pregnant) and primiparous (animals that have just had their first pregnancy) mice, having administered BrdU at 7 days post parturition (Figure A2.1).

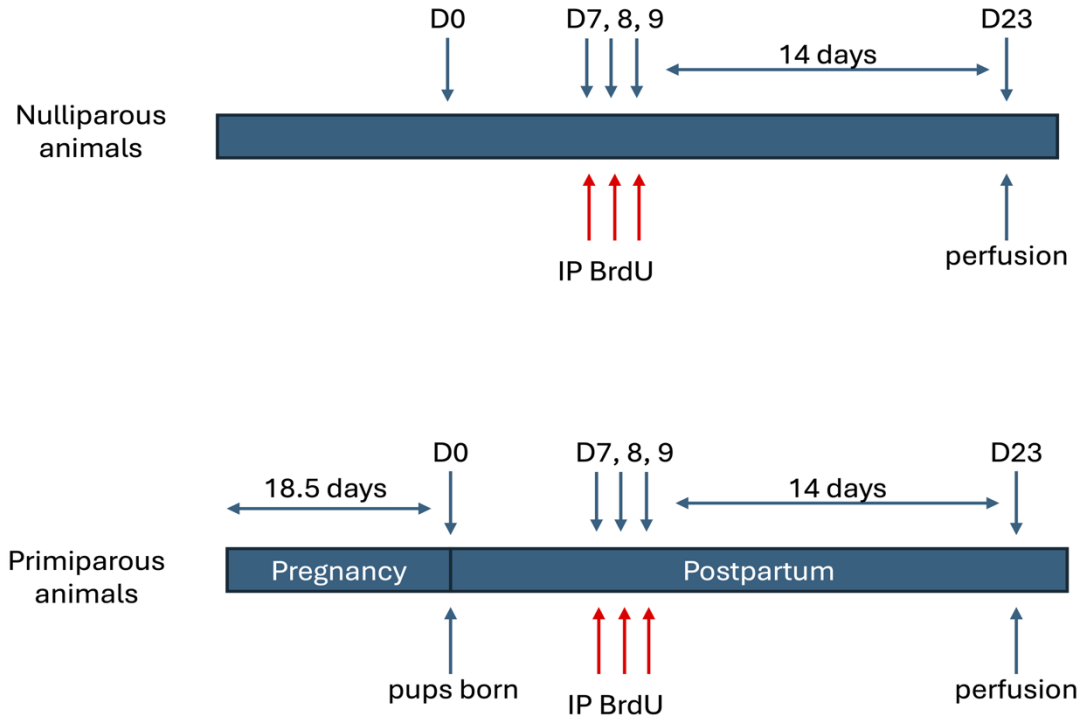

Appendix 2 Figure A2.1 Schedule for investigation in postpartum animals. *Two groups of animals were compared: nulliparous (having had no pregnancies), and primiparous (animals on their first pregnancy). BrdU was injected intraperitoneally once daily for three days at 7 days post parturition (or at equivalent age in nulliparous controls). After two weeks animals were euthanised by perfusion fixation for immunohistochemical studies.*

I first examined the impact of pregnancy on neural stem cells using a combination of the markers BrdU, GFAP, and SOX2. BrdU+ cells represent newborn cells that passed through S-phase during the period of BrdU administration, and significantly decreased in primiparous vs nulliparous animals (Figure A2.2, A). GFAP+BrdU+ cells likely represent a mixed population comprised predominantly of astrocytes, as well as some neural stem-like cells. There was no change in these cells (Figure A2.2, B). SOX2+Brdu+ cells represent predominantly NSCs, as well as some astrocytes and showed a slight but non-significant decrease (A2.2, C). GFAP+BrdU+ SOX2+ cells also will represent a heterogeneous population of astrocytes and NSC-like cells and showed no change with parity (A2.2, D). GFAP+BrdU+ SOX2- cells are dominantly astrocytes, and showed no change with parity (A2.2, E). GFAP-BrdU+ SOX2+ cells are predominantly newborn NSCs and showed a significant decrease with parity (A2.2, E), although it is important to note that no Gfap-BrdU+ SOX2+ cells were detected in 3 out of

4 primiparous animals. These initial data suggest that there is a decrease in cytogenesis in the SGZ in the first week after parturition, and that this decrease is restricted to the neurogenic lineage.

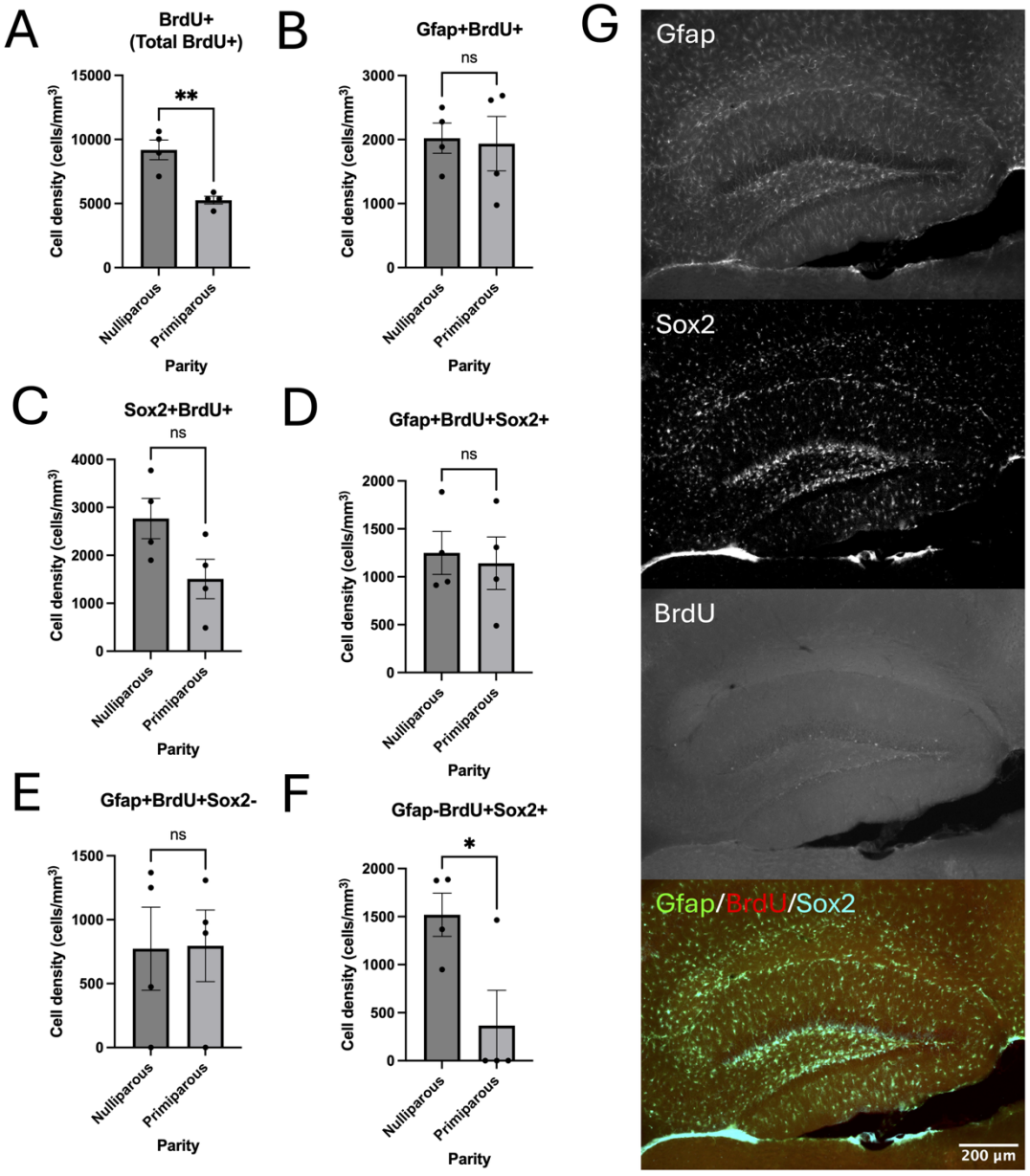

Figure A2.2 Impact of pregnancy on neural stem cells in the SGZ. A)-F) *Comparison of BrdU+ cells in the dentate gyrus of nulliparous animals or primiparous animals.* ***G)*** *Example IHC showing the entire dentate gyrus, with the merged image highlighting Gfap (green), BrdU (red) and Sox2 (cyan).* ***See Table A.1 for detail of statistical tests.***

Error bars represent SEM, scale bar represents 200µm

In order to verify whether the proposed decrease in neurogenesis after pregnancy translates to a reduced number of mature neurons I stained for BrdU to indicate newborn cells and NeuN to mark mature neurons. These BrdU+NeuN+ cells represent cells that passed through S-phase during BrdU administration and subsequently matured in the DG. I observed a significant decrease in the density of BrdU+NeuN+ cells in primiparous animals compared to nulliparous animals (Figure A2.3, A). This is consistent with the decrease in BrdU+Sox2+ cells observed in Fig A2.2.

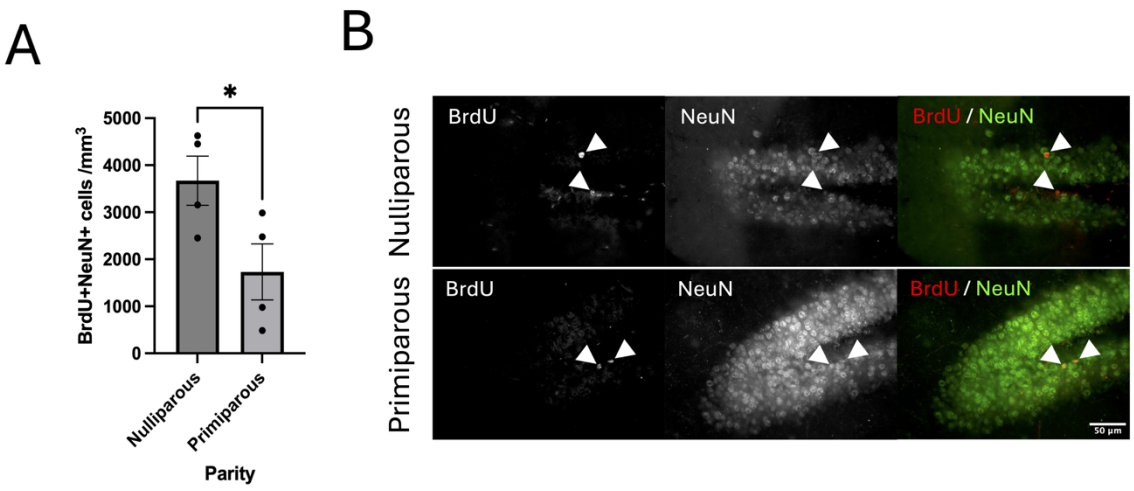

Appendix 2 Figure A2.3 Impact of pregnancy on neurogenesis in the SGZ. A) *Parity caused a significant decrease in the number of BrdU+NeuN+ cells per mm³ in the dentate gyrus.* ***B)*** *Representative IHC at 40x showing BrdU, NeuN, and merged images with BrdU shown in red and NeuN in green. Arrows indicate BrdU+NeuN+ cells.* ***See Table A.1 for detail of statistical tests.***

The scale bar indicates 50µm. Error bars represent SEM.

Together these observations suggest that there is a decrease in hippocampal neurogenesis at 7-9 days post parturition in the mouse brain.

Appendix 3: *Paupar* lncRNA and KAP1 regulation of the V-SVZ

Paupar is a V-SVZ expressed lncRNA that has been extensively investigated in the Szele lab (Alammari et al., 2025; Pavlaki et al., 2018a). *Paupar* interacts with the transcriptional regulator KAP1 to regulate neurogenesis in the V-SVZ. In collaboration with Dr Keith Vance in the University of Bath and Dr Farah Alammari in the King Abdullah International Medical Research Center I have been investigating the mechanism by which *Paupar* and KAP1 regulate neurogenesis.

We identified the *Kap1* and *Paupar* regulated gene sets in P3-P5 SVZ-derived neurospheres. Reduction of *Kap1* levels in SVZ-derived neurospheres using shRNA nucleofection led to changes greater than 1.2-fold (5% false discovery rate FDR), in the expression of 1,905 genes (Figure A3.1, A, C, Table A.2). 977 (51%) of these genes were down-regulated and 928 (49%) were up-regulated. Gene Ontology enrichment analysis showed that KAP1 predominantly regulates genes involved in regulation of the cell cycle, cell division, DNA replication, and mitotic chromosome condensation (Fig A3.1, D, Table A.3). I expanded this analysis to examine pathways that were dysregulated upon KAP1 depletion revealed significant changes in multiple pathways associated with the mitotic cell cycle and cell cycle checkpoints (Fig A3.1,E, Table A.4). In addition, there was also a downregulation of genes associated with the activation of formins by Rho GTPases, suggesting a link between KAP1 expression and regulation of cytoskeleton dynamics. Further examination of upstream regulators revealed a predicted activation of TP53 function (Table A.5).

We next performed transcriptome profiling of P3-P5 SVZ-derived neurospheres in which *Paupar* levels had been reduced using transient transfection of a *Paupar*-targeting shRNA expression vector. This resulted in significant changes in the expression levels of 157 genes

(False Discovery Rate [FDR] < 5%), including 8 lncRNAs, compared to a non-targeting control (Fig A3.1, B, F, Table A.6). 101 (64%) of the transcripts were down-regulated and 56 (35%) were up-regulated. Gene Ontology enrichment analysis of *Paupar*-regulated genes did not reveal any significantly enriched categories most likely attributable to the relatively low number of genes (Table A.7). However, pathway analysis of *Paupar*-regulated genes did show a significant decrease in pathways associated with beta catenin-independent WNT signalling, as well as molecular mechanisms of cancer – suggesting a role in cell migration or proliferation (Fig A3.1,G, Table A.8). Moreover there was an overall increase in genes associated with Gap Junction signalling pathways, which are known to facilitate communication between GFAP+ cells in the V-SVZ (Fig A3.1,G). Moreover, multiple genes involved in ion channel function such as *Gria1*, *Gabrb1*, *Gabra4* and *Grik1*, were found to be regulated by *Paupar* KD (Table A.6).

Finally, investigation of the intersection of KAP1 and *Paupar* transcriptional targets identified 33 genes whose levels are affected by both *Paupar* and *Kap1* knockdown in SVZ-derived neurospheres, 8 of which were upregulated, and 25 were downregulated (Fig A3.1, H & I). Most of these genes had expression changes in the same direction upon *Paupar* or *Kap1* knockdown. Interestingly *Dcx* expression was decreased after both *Kap1* and *Paupar* knockdown. DCX, a microtubule-associated protein, is not just a neuroblast marker, but is also necessary for neuroblast migration (Koizumi *et al*, 2006; Ocbina *et al*, 2006).

These transcriptomic data suggest a role for KAP1 in regulation of cell cycle dynamics and a role for *Paupar* in cytoskeletal arrangement. Deeper conclusions cannot be drawn from this data regarding the function of *Paupar* in the V-SVZ due to the small number of differentially expressed genes. This data and the associated article, is now published as Alammari *et al.,* (2025).

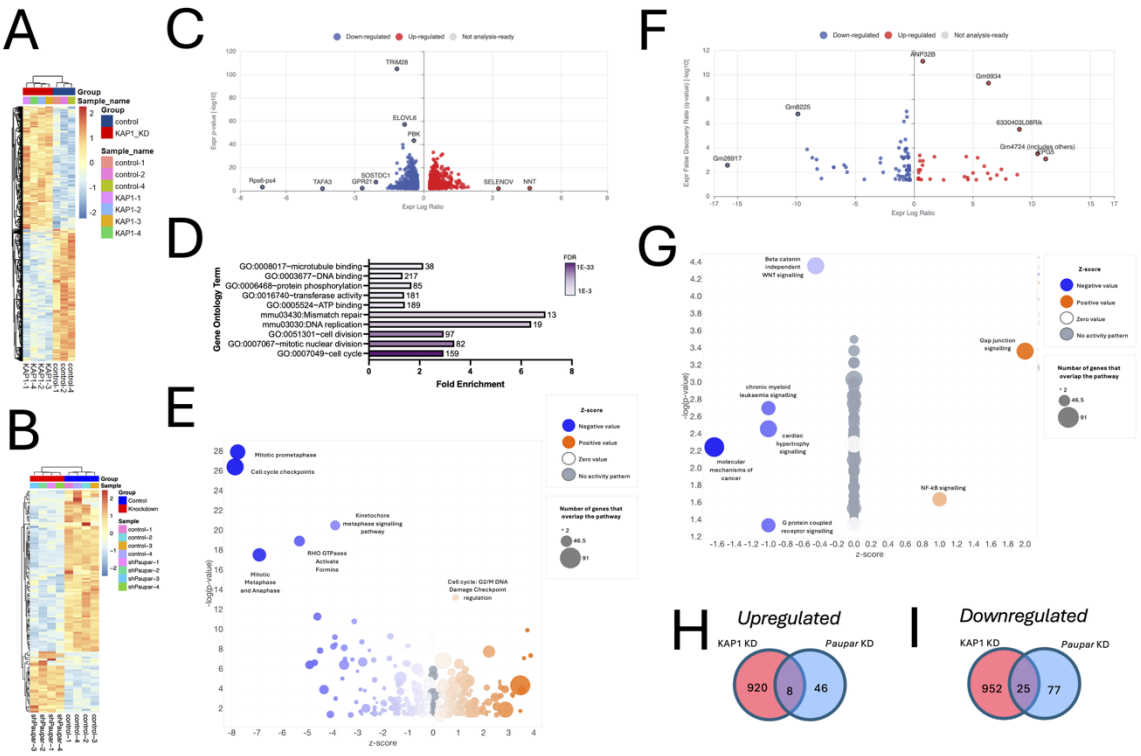

Appendix 3 Figure A3.1 Transcriptional analysis of Paupar and Kap1 knockdowns A) *Kap1 knockdown induces statistically significant changes in gene expression (greater than 1.2-fold, 5% FDR). We used three samples for Kap1 control and four samples for Kap1 KD.* ***B)*** *Paupar knockdown induces statistically significant changes in gene expression in neurospheres (5% FDR). We used four samples each for Paupar control and Paupar KD* ***C)*** *Volcano plot of differentially expressed genes after Kap1 knockdown, with highly differentially expressed genes manually labelled.* ***D)*** *Significant Gene Ontology enrichment analysis of KAP1-regulated genes was performed using GOToolBox. The top 10 most significantly enriched categories were selected from a hypergeometric test with a Benjamini–Hochberg-corrected P-value threshold of 0.05. Bars are coloured by Benjamini–Hochberg-corrected P-value, and annotations indicate the gene count in each category.* ***E)*** *Ingenuity Pathway Analysis of differentially expressed genes following Kap1 knockdown revealed significant downregulation of genes associated with mitotic prometaphase and cell cycle checkpoints.* ***F)*** *Volcano plot of differentially expressed genes after Paupar knockdown, with highly differentially expressed genes manually labelled.* ***G)*** *Ingenuity Pathway Analysis of differentially expressed genes following Paupar knockdown, highlighting downregulation of beta-catenin independent WNT signalling.* ***H)*** *Intersection of genes that are upregulated after Kap1 or Paupar knockdown (KD) reveals common target genes whose expression is controlled by both transcripts in neurospheres.* ***I)*** *Intersection of genes that are downregulated after Kap1 or Paupar knockdown (KD) reveals common target genes whose expression is controlled by both transcripts in neurospheres.* ***See Tables A.2-A.8 for more details.***

Abbreviations: KD – Knockdown; FDR – False discovery rate.

Appendix 4: Refined animal handling for administration of simvastatin

As a continuation of the data presented in Figure 5.4 I set out to examine the *in vivo* effects of simvastatin. As simvastatin (or a control) would need to be administered to all experimental animals on a daily basis, I designed a habituation protocol for these animals. It has been found in previous studies that refinement to handling techniques can reduce measures of anxiety and aversive behaviours in laboratory animals (Davies et al., 2022; Stuart and Robinson, 2015). Furthermore, unpublished data from the laboratory of Prof. Emma Robinson at the University of Bristol has suggested that 10% condensed milk in water is an exceptionally effective reward for positive conditioning of rodents.

I therefore planned a schedule of habituation for one week before the start of animal experiments with a cohort of 7 mice. Initially, animals were introduced to a 1mL syringe (with no needle) containing 10% condensed milk in water through the lid of their cage and allowed to freely interact with it. After this, the lid was removed and I allowed them to lick from the syringe in their home cage. Finally, I scruffed mice and gave them a drop of the 10% condensed milk whilst restrained before returning them to the home cage. A schematic of this process and images are shown in Figure A4.1. After repeating this process daily for seven days I found that animals were very willing to drink from the syringe, and tried to pull it from my hand. I found that they came willingly to stand in my palm. The most important observation was that during scruffing, animals would not urinate, vocalise, or defecate when restrained – all of which are stereotypical signs of distress . Furthermore, mice did not instantly run away when returned to the home cage, and indeed often came back to my hand.

These initial qualitative observations suggest that repeated handling coupled with positive reinforcement can greatly reduce stress for experimental animals as well as the experimenter.

However, this process is time consuming, spending approximately 20 minutes which each mouse each day, and so is not scalable for a single researcher working with large cohorts of mice.

After one week of daily handling and habituation, I began treatment with simvastatin for 14 days, the first three of which I injected BrdU intraperitoneally (Figure A4.2, A). Simvastatin was administered orally at a dose of 25mg/kg, and was provided in suspension with 10% condensed milk in water which animals received voluntarily (See Figure A4.1, B). After simvastatin treatment I performed the Elevate Plus Maze (EPM) test to evaluate anxiety-like behaviours, a social interaction test to measure aggression towards an unfamiliar mouse, and a splash test to examine self-neglect and grooming behaviours. Unfortunately data was not able to be captured for the EPM due to a failure of both the primary and backup cameras.

In the splash test animals are sprayed twice on the back with a 10% sucrose solution and then filmed for 5 minutes. Subsequently videos were blinded and grooming behaviour was manually scored. From this analysis no changes were observed in grooming behaviour after 14 days of simvastatin treatment, both in terms of the total time spent grooming and number of grooming episodes (Fig A4.2, B & C). In social interaction tests mice were place in a three-chambered box, one of which contained an empty cage, one which contained an identical cage with an unfamiliar mouse, and one which was completely empty (Shown in Fig A4.2, D). The unfamiliar mouse, or “stranger”, was a juvenile female C57BL6, so as to minimise potential aggression from the test mouse. Movement of the test animal was automatically tracked by AnyMaze software for 10 minutes. No significant effects of simvastatin on social interaction between test mice and stranger mice were observed (Fig A4.2, E-H)

After the conclusion of behavioural tests animals were sacrificed by IP injection of pentobarbital followed by perfusion fixation. Their brains are currently being analysed to detect any changes in neurogenesis.

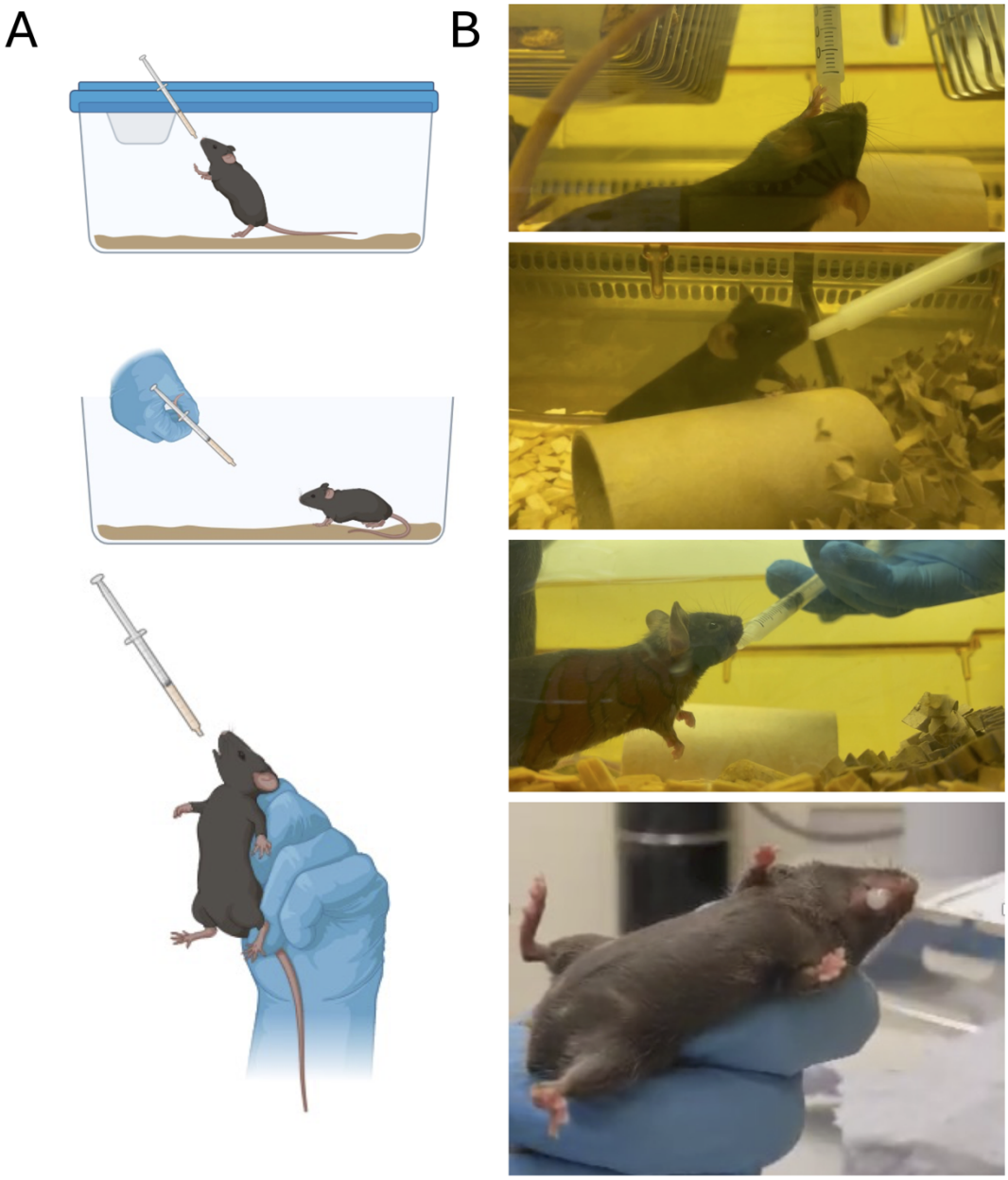

Appendix 4 Figure A4.1 A refined approach to drug administration. ***A)*** *Illustrated is the gradual approach to habituation for animals that will have repeated drug administrations or will be handled extensively for behavioural experiments. Firstly, animals are introduced to a reward through the lid of the cage, next they are introduced to the reward with no cage lid. Finally for those that will be restrained (e.g., for intraperitoneal injections), animals are scruffed and given their reward.* ***B)*** *Example images of C57BL6 mice during the habituation process, prior to the start of behavioural testing. Images were captured on an iPhone 12 mini with the permission of the facility. Panel A generated in BioRender.*

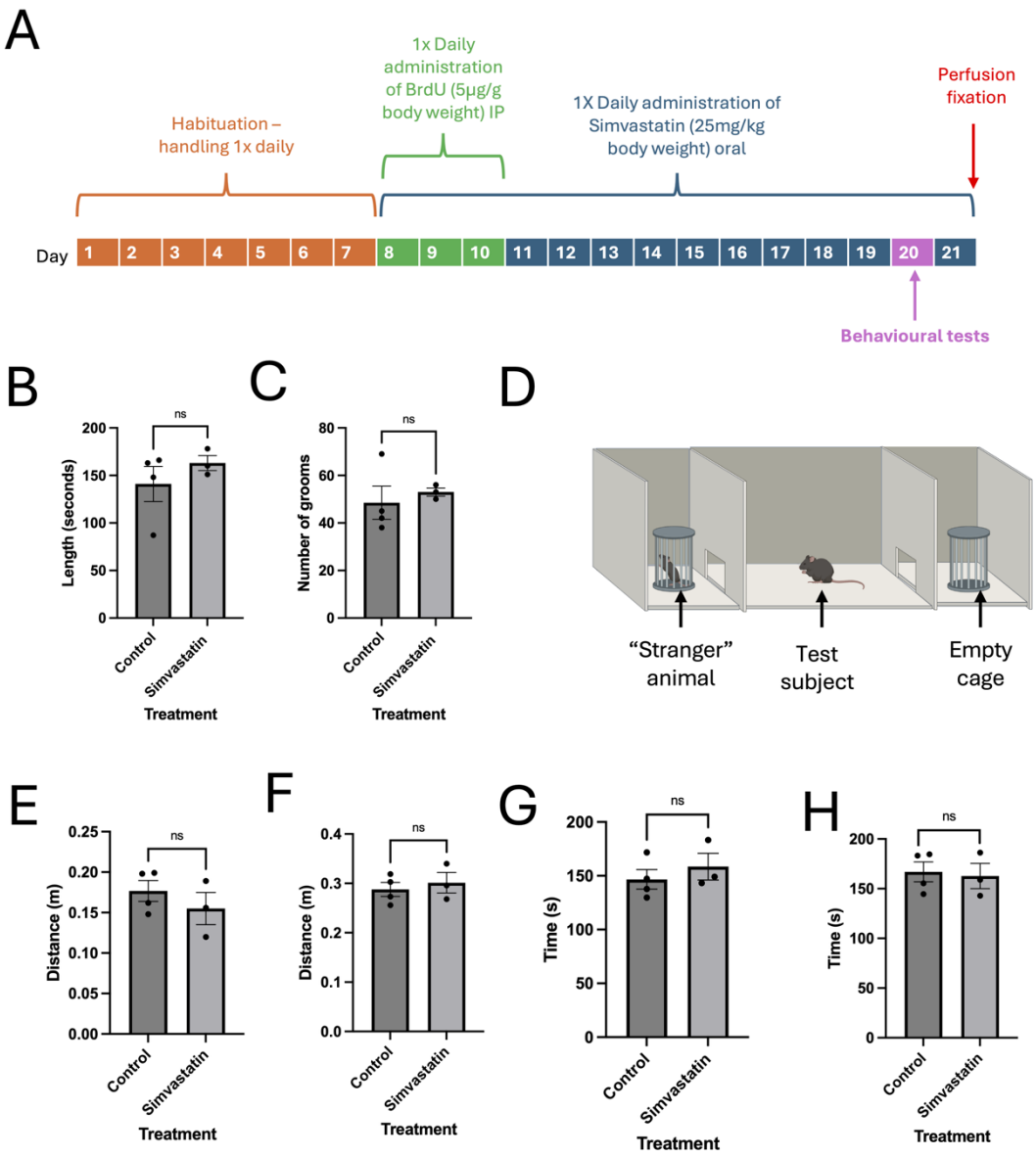

Appendix 4 Figure A4.2 Effect of simvastatin administration on grooming and social interaction in female mice. A) *Timeline for drug administration and behavioural experiments.* ***B)*** *Total length of time spent grooming.* ***C)*** *Number of grooming episodes.* ***D)*** *Setup of the social interaction test.* ***E)*** *Average distance from the stranger (m).* ***F)*** *Average distance from the empty cage* ***G)*** *Time spent moving towards the stranger (s).* ***H)*** *Time spend moving towards the empty cage (s).* ***See Table A.1 for detail of statistical tests.***

Error bars indicate SEM. Panel D generated in BioRender.

References

Ables, J.L., Breunig, J.J., Eisch, A.J., and Rakic, P. (2011). Not(ch) just development: Notch signalling in the adult brain. Nat Rev Neurosci *12*, 269–283. https://doi.org/10.1038/nrn3024.

Afshordel, S., Kern, B., Clasohm, J., König, H., Priester, M., Weissenberger, J., Kögel, D., and Eckert, G.P. (2015). Lovastatin and perillyl alcohol inhibit glioma cell invasion, migration, and proliferation - Impact of Ras-/Rho-prenylation. Pharmacological Research *91*, 69–77. https://doi.org/10.1016/j.phrs.2014.11.006.

Aghvami, S.S., Kubota, Y., and Egger, V. (2022). Anatomical and Functional Connectivity at the Dendrodendritic Reciprocal Mitral Cell–Granule Cell Synapse: Impact on Recurrent and Lateral Inhibition. Front. Neural Circuits *16*. https://doi.org/10.3389/fncir.2022.933201.

del Águila, Á., Adam, M., Ullom, K., Shaw, N., Qin, S., Ehrman, J., Nardini, D., Salomone, J., Gebelein, B., Lu, Q.R., et al. (2022). Olig2 defines a subset of neural stem cells that produce specific olfactory bulb interneuron subtypes in the subventricular zone of adult mice. Development *149*, dev200028. https://doi.org/10.1242/dev.200028.

Aguilera, A., and García-Muse, T. (2012). R Loops: From Transcription Byproducts to Threats to Genome Stability. Molecular Cell *46*, 115–124. https://doi.org/10.1016/j.molcel.2012.04.009.

Alammari, F., Becker, J., Sun, B., Hoerder-Suabedissen, A., Vance, K.W., and Szele, F.G. (2025). The KAP1 chromatin regulator and *Paupar* long non-coding RNA control subventricular zone neural stem cell maintenance and neurogenesis. Stem Cell Reports *20*, 102630. https://doi.org/10.1016/j.stemcr.2025.102630.

Al-Dalahmah, O., Campos Soares, L., Nicholson, J., Draijer, S., Mundim, M., Lu, V.M., Sun, B., Tyler, T., Adorján, I., O'Neill, E., et al. (2020). Galectin-3 modulates postnatal subventricular zone gliogenesis. Glia *68*, 435–450. https://doi.org/10.1002/glia.23730.

Altman, J. (1969). Autoradiographic and histological studies of postnatal neurogenesis. IV. Cell proliferation and migration in the anterior forebrain, with special reference to persisting neurogenesis in the olfactory bulb. Journal of Comparative Neurology *137*, 433–457. https://doi.org/10.1002/cne.901370404.

Altschul, S.F., Gish, W., Miller, W., Myers, E.W., and Lipman, D.J. (1990). Basic local alignment search tool. Journal of Molecular Biology *215*, 403–410. https://doi.org/10.1016/S0022-2836(05)80360-2.

Alvarez-Buylla, A., and García-Verdugo, J.M. (2002). Neurogenesis in Adult Subventricular Zone. J. Neurosci. *22*, 629–634. https://doi.org/10.1523/JNEUROSCI.22-03-00629.2002.

Andrade, J.M., Faustino, C., Garcia, C., Ladeiras, D., Reis, C.P., and Rijo, P. (2018). *Rosmarinus officinalis* L.: an update review of its phytochemistry and biological activity. Future Sci. OA *4*. https://doi.org/10.4155/fsoa-2017-0124.

Andrews, W., Barber, M., Hernadez-Miranda, L.R., Xian, J., Rakic, S., Sundaresan, V., Rabbitts, T.H., Pannell, R., Rabbitts, P., Thompson, H., et al. (2008). The role of Slit-Robo

signaling in the generation, migration and morphological differentiation of cortical interneurons. Developmental Biology *313*, 648–658. https://doi.org/10.1016/j.ydbio.2007.10.052.

Arab, K., Karaulanov, E., Musheev, M., Trnka, P., Schäfer, A., Grummt, I., and Niehrs, C. (2019). GADD45A binds R-loops and recruits TET1 to CpG island promoters. Nat Genet *51*, 217–223. https://doi.org/10.1038/s41588-018-0306-6.

Banka, S., Bennington, A., Baker, M.J., Rijckmans, E., Clemente, G.D., Ansor, N.M., Sito, H., Prasad, P., Anyane-Yeboa, K., Badalato, L., et al. (2022). Activating *RAC1* variants in the switch II region cause a developmental syndrome and alter neuronal morphology. Brain *145*, 4232–4245. https://doi.org/10.1093/brain/awac049.

Bardella, C., Al-Dalahmah, O., Krell, D., Brazauskas, P., Al-Qahtani, K., Tomkova, M., Adam, J., Serres, S., Lockstone, H., Freeman-Mills, L., et al. (2016). Expression of Idh1R132H in the Murine Subventricular Zone Stem Cell Niche Recapitulates Features of Early Gliomagenesis. Cancer Cell *30*, 578–594. https://doi.org/10.1016/j.ccell.2016.08.017.

Basak, O., Krieger, T.G., Muraro, M.J., Wiebrands, K., Stange, D.E., Frias-Aldeguer, J., Rivron, N.C., van de Wetering, M., van Es, J.H., van Oudenaarden, A., et al. (2018). Troy+ brain stem cells cycle through quiescence and regulate their number by sensing niche occupancy. Proceedings of the National Academy of Sciences *115*, E610–E619. https://doi.org/10.1073/pnas.1715911114.

Becker, J., Sun, B., Alammari, F., Haerty, W., Vance, K.W., and Szele, F.G. (2022). What has single-cell transcriptomics taught us about long non-coding RNAs in the ventricular-subventricular zone? Stem Cell Reports *0*. https://doi.org/10.1016/j.stemcr.2022.11.011.

Belenguer, G., Duart-Abadia, P., Jordán-Pla, A., Domingo-Muelas, A., Blasco-Chamarro, L., Ferrón, S.R., Morante-Redolat, J.M., and Fariñas, I. (2021). Adult Neural Stem Cells Are Alerted by Systemic Inflammation through TNF-α Receptor Signaling. Cell Stem Cell *28*, 285-299.e9. https://doi.org/10.1016/j.stem.2020.10.016.

Bennet Institude for Applied Data Science, University of Oxford (2024). OpenPrescribing.net.

Bishop, N.A., Lu, T., and Yankner, B.A. (2010). Neural mechanisms of ageing and cognitive decline. Nature *464*, 529–535. https://doi.org/10.1038/nature08983.

de Boer, C.G., Vaishnav, E.D., Sadeh, R., Abeyta, E.L., Friedman, N., and Regev, A. (2020). Deciphering eukaryotic gene-regulatory logic with 100 million random promoters. Nat Biotechnol *38*, 56–65. https://doi.org/10.1038/s41587-019-0315-8.

Bonine, N., Zanzani, V., Van Hemelryk, A., Vanneste, B., Zwicker, C., Thoné, T., Roelandt, S., Bekaert, S.-L., Koster, J., Janoueix-Lerosey, I., et al. (2024). NBAtlas: A harmonized single-cell transcriptomic reference atlas of human neuroblastoma tumors. Cell Reports *43*, 114804. https://doi.org/10.1016/j.celrep.2024.114804.

Borrett, M.J., Innes, B.T., Jeong, D., Tahmasian, N., Storer, M.A., Bader, G.D., Kaplan, D.R., and Miller, F.D. (2020). Single-Cell Profiling Shows Murine Forebrain Neural Stem Cells Reacquire a Developmental State when Activated for Adult Neurogenesis. Cell Reports *32*, 108022. https://doi.org/10.1016/j.celrep.2020.108022.

Boutin, C., Diestel, S., Desoeuvre, A., Tiveron, M.-C., and Cremer, H. (2008). Efficient In Vivo Electroporation of the Postnatal Rodent Forebrain. PLOS ONE *3*, e1883. https://doi.org/10.1371/journal.pone.0001883.

Bovetti, S., Hsieh, Y.-C., Bovolin, P., Perroteau, I., Kazunori, T., and Puche, A.C. (2007). Blood Vessels Form a Scaffold for Neuroblast Migration in the Adult Olfactory Bulb. J. Neurosci. *27*, 5976–5980. https://doi.org/10.1523/JNEUROSCI.0678-07.2007.

Boyer, L.A., Plath, K., Zeitlinger, J., Brambrink, T., Medeiros, L.A., Lee, T.I., Levine, S.S., Wernig, M., Tajonar, A., Ray, M.K., et al. (2006). Polycomb complexes repress developmental regulators in murine embryonic stem cells. Nature *441*, 349–353. https://doi.org/10.1038/nature04733.

Breton-Provencher, V., Lemasson, M., Peralta, M.R., and Saghatelyan, A. (2009). Interneurons Produced in Adulthood Are Required for the Normal Functioning of the Olfactory Bulb Network and for the Execution of Selected Olfactory Behaviors. J. Neurosci. *29*, 15245–15257. https://doi.org/10.1523/JNEUROSCI.3606-09.2009.

Broad Institude (2019). Picard Toolkit.

Buhaescu, I., and Izzedine, H. (2007). Mevalonate pathway: A review of clinical and therapeutical implications. Clinical Biochemistry *40*, 575–584. https://doi.org/10.1016/j.clinbiochem.2007.03.016.

Buniello, A., MacArthur, J.A.L., Cerezo, M., Harris, L.W., Hayhurst, J., Malangone, C., McMahon, A., Morales, J., Mountjoy, E., Sollis, E., et al. (2019). The NHGRI-EBI GWAS Catalog of published genome-wide association studies, targeted arrays and summary statistics 2019. Nucleic Acids Res *47*, D1005–D1012. https://doi.org/10.1093/nar/gky1120.

Cabili, M.N., Trapnell, C., Goff, L., Koziol, M., Tazon-Vega, B., Regev, A., and Rinn, J.L. (2011). Integrative annotation of human large intergenic noncoding RNAs reveals global properties and specific subclasses. Genes Dev. *25*, 1915–1927. https://doi.org/10.1101/gad.17446611.

Canard, B., and Sarfati, R.S. (1994). DNA polymerase fluorescent substrates with reversible 3′-tags. Gene *148*, 1–6. https://doi.org/10.1016/0378-1119(94)90226-7.

Carelli, S., Giallongo, T., Rey, F., Latorre, E., Bordoni, M., Mazzucchelli, S., Gorio, M.C., Pansarasa, O., Provenzani, A., Cereda, C., et al. (2019). HuR interacts with lincBRN1a and lincBRN1b during neuronal stem cells differentiation. RNA Biology *16*, 1471–1485. https://doi.org/10.1080/15476286.2019.1637698.

Carver, J.J., He, Y., and Zhu, Y. (2021). Delay in primordial germ cell migration in adamts9 knockout zebrafish. Sci Rep *11*, 8545. https://doi.org/10.1038/s41598-021-88024-x.

Casarosa, S., Fode, C., and Guillemot, F. (1999). Mash1 regulates neurogenesis in the ventral telencephalon. Development *126*, 525–534. https://doi.org/10.1242/dev.126.3.525.

Cebrian-Silla, A., Nascimento, M.A., Redmond, S.A., Mansky, B., Wu, D., Obernier, K., Romero Rodriguez, R., Gonzalez-Granero, S., García-Verdugo, J.M., Lim, D.A., et al. (2021). Single-cell analysis of the ventricular-subventricular zone reveals signatures of dorsal and ventral adult neurogenesis. eLife *10*, e67436. https://doi.org/10.7554/eLife.67436.

Cerezo, M., Sollis, E., Ji, Y., Lewis, E., Abid, A., Bircan, K.O., Hall, P., Hayhurst, J., John, S., Mosaku, A., et al. (2025). The NHGRI-EBI GWAS Catalog: standards for reusability, sustainability and diversity. Nucleic Acids Research *53*, D998–D1005. https://doi.org/10.1093/nar/gkae1070.

Chaker, Z., Segalada, C., Kretz, J.A., Acar, I.E., Delgado, A.C., Crotet, V., Moor, A.E., and Doetsch, F. (2023). Pregnancy-responsive pools of adult neural stem cells for transient neurogenesis in mothers. Science *382*, 958–963. https://doi.org/10.1126/science.abo5199.

Chammas, P., Mocavini, I., and Di Croce, L. (2020). Engaging chromatin: PRC2 structure meets function. Br J Cancer *122*, 315–328. https://doi.org/10.1038/s41416-019-0615-2.

Chang, E.H., Adorjan, I., Mundim, M.V., Sun, B., Dizon, M.L.V., and Szele, F.G. (2016). Traumatic Brain Injury Activation of the Adult Subventricular Zone Neurogenic Niche. Front Neurosci *10*, 332. https://doi.org/10.3389/fnins.2016.00332.

Chen, F., Zhang, L., Wang, E., Zhang, C., and Li, X. (2018). LncRNA GAS5 regulates ischemic stroke as a competing endogenous RNA for miR-137 to regulate the Notch1 signaling pathway. Biochemical and Biophysical Research Communications *496*, 184–190. https://doi.org/10.1016/j.bbrc.2018.01.022.

Chen, X., Xue, G., Zhao, J., Zhang, Y., Zhang, S., Wang, W., Li, Y., Yuan, J., He, L., Chan, C.Y., et al. (2022). Lockd promotes myoblast proliferation and muscle regeneration via binding with DHX36 to facilitate 5′ UTR rG4 unwinding and Anp32e translation. Cell Reports *39*, 110927. https://doi.org/10.1016/j.celrep.2022.110927.

Chesler, A.T., Pichon, C.E.L., Brann, J.H., Araneda, R.C., Zou, D.-J., and Firestein, S. (2008). Selective Gene Expression by Postnatal Electroporation during Olfactory Interneuron Neurogenesis. PLOS ONE *3*, e1517. https://doi.org/10.1371/journal.pone.0001517.

Cheung, M., Abu-Elmagd, M., Clevers, H., and Scotting, P.J. (2000). Roles of Sox4 in central nervous system development1. Molecular Brain Research *79*, 180–191. https://doi.org/10.1016/S0169-328X(00)00109-1.

Chillón, I., and Marcia, M. (2020). The molecular structure of long non-coding RNAs: emerging patterns and functional implications. Critical Reviews in Biochemistry and Molecular Biology *55*, 662–690. https://doi.org/10.1080/10409238.2020.1828259.

Clark, M.B., Johnston, R.L., Inostroza-Ponta, M., Fox, A.H., Fortini, E., Moscato, P., Dinger, M.E., and Mattick, J.S. (2012). Genome-wide analysis of long noncoding RNA stability. Genome Res *22*, 885–898. https://doi.org/10.1101/gr.131037.111.

Clemson, C.M., Hutchinson, J.N., Sara, S.A., Ensminger, A.W., Fox, A.H., Chess, A., and Lawrence, J.B. (2009). An Architectural Role for a Nuclear Noncoding RNA: *NEAT1* RNA Is Essential for the Structure of Paraspeckles. Molecular Cell *33*, 717–726. https://doi.org/10.1016/j.molcel.2009.01.026.

Coleman, P.S., and Parlo, R.A. (2021). Warburg's Ghost—Cancer's Self-Sustaining Phenotype: The Aberrant Carbon Flux in Cholesterol-Enriched Tumor Mitochondria via Deregulated Cholesterogenesis. Frontiers in Cell and Developmental Biology *9*. .

Coman, D., Vissers, L.E.L.M., Riley, L.G., Kwint, M.P., Hauck, R., Koster, J., Geuer, S., Hopkins, S., Hallinan, B., Sweetman, L., et al. (2018). Squalene Synthase Deficiency: Clinical, Biochemical, and Molecular Characterization of a Defect in Cholesterol Biosynthesis. The American Journal of Human Genetics *103*, 125–130. https://doi.org/10.1016/j.ajhg.2018.05.004.

Conover, J.C., Doetsch, F., Garcia-Verdugo, J.-M., Gale, N.W., Yancopoulos, G.D., and Alvarez-Buylla, A. (2000). Disruption of Eph/ephrin signaling affects migration and proliferation in the adult subventricular zone. Nat. Neurosci. *3*, 1091–1097. https://doi.org/10.1038/80606.

Courtès, S., Vernerey, J., Pujadas, L., Magalon, K., Cremer, H., Soriano, E., Durbec, P., and Cayre, M. (2011). Reelin controls progenitor cell migration in the healthy and pathological adult mouse brain. PLoS ONE *6*. https://doi.org/10.1371/journal.pone.0020430.

Cremer, H., Lange, R., Christoph, A., Plomann, M., Vopper, G., Roes, J., Brown, R., Baldwin, S., Kraemer, P., Scheff, S., et al. (1994). Inactivation of the N-CAM gene in mice results in size reduction of the olfactory bulb and deficits in spatial learning. Nature *367*, 455–459. https://doi.org/10.1038/367455a0.

D'Arcangelo, G., Miao, G.G., Chen, S.-C., Scares, H.D., Morgan, J.I., and Curran, T. (1995). A protein related to extracellular matrix proteins deleted in the mouse mutant reeler. Nature *374*, 719–723. https://doi.org/10.1038/374719a0.

Davidovich, C., Zheng, L., Goodrich, K.J., and Cech, T.R. (2013). Promiscuous RNA binding by Polycomb repressive complex 2. Nat Struct Mol Biol *20*, 1250–1257. https://doi.org/10.1038/nsmb.2679.

Davies, J.R., Purawijaya, D.A., Bartlett, J.M., and Robinson, E.S.J. (2022). Impact of Refinements to Handling and Restraint Methods in Mice. Animals *12*, 2173. https://doi.org/10.3390/ani12172173.

Davy, A., Gale, N.W., Murray, E.W., Klinghoffer, R.A., Soriano, P., Feuerstein, C., and Robbins, S.M. (1999). Compartmentalized signaling by GPI-anchored ephrin-A5 requires the Fyn tyrosine kinase to regulate cellular adhesion. Genes Dev *13*, 3125–3135. https://doi.org/10.1101/gad.13.23.3125.

Deligiannidis, K.M., Meltzer-Brody, S., Gunduz-Bruce, H., Doherty, J., Jonas, J., Li, S., Sankoh, A.J., Silber, C., Campbell, A.D., Werneburg, B., et al. (2021). Effect of Zuranolone vs Placebo in Postpartum Depression. JAMA Psychiatry *78*, 1–9. https://doi.org/10.1001/jamapsychiatry.2021.1559.

Derrien, T., Johnson, R., Bussotti, G., Tanzer, A., Djebali, S., Tilgner, H., Guernec, G., Martin, D., Merkel, A., Knowles, D.G., et al. (2012). The GENCODE v7 catalog of human long noncoding RNAs: Analysis of their gene structure, evolution, and expression. Genome Res. *22*, 1775–1789. https://doi.org/10.1101/gr.132159.111.

Dey, B.K., Pfeifer, K., and Dutta, A. (2014). The H19 long noncoding RNA gives rise to microRNAs miR-675-3p and miR-675-5p to promote skeletal muscle differentiation and regeneration. Genes Dev *28*, 491–501. https://doi.org/10.1101/gad.234419.113.

Dietschy, J.M., and Turley, S.D. (2004). *Thematic review series: Brain Lipids.* Cholesterol metabolism in the central nervous system during early development and in the mature animal. Journal of Lipid Research *45*, 1375–1397. https://doi.org/10.1194/jlr.R400004-JLR200.

Doetsch, F., García-Verdugo, J.M., and Alvarez-Buylla, A. (1997). Cellular Composition and Three-Dimensional Organization of the Subventricular Germinal Zone in the Adult Mammalian Brain. J. Neurosci. *17*, 5046–5061. https://doi.org/10.1523/JNEUROSCI.17-13-05046.1997.

Doetsch, F., Caillé, I., Lim, D.A., García-Verdugo, J.M., and Alvarez-Buylla, A. (1999). Subventricular Zone Astrocytes Are Neural Stem Cells in the Adult Mammalian Brain. Cell *97*, 703–716. https://doi.org/10.1016/S0092-8674(00)80783-7.

Ducker, M., Millar, V., Ebner, D., and Szele, F. (2020). A Semi-automated and Scalable 3D Spheroid Assay to Study Neuroblast Migration. Stem Cell Reports *15*, 789–802. https://doi.org/10.1016/j.stemcr.2020.07.012.

Dyer, S.C., Austine-Orimoloye, O., Azov, A.G., Barba, M., Barnes, I., Barrera-Enriquez, V.P., Becker, A., Bennett, R., Beracochea, M., Berry, A., et al. (2025). Ensembl 2025. Nucleic Acids Research *53*, D948–D957. https://doi.org/10.1093/nar/gkae1071.

Eddy, S.R. (2013). The ENCODE project: Missteps overshadowing a success. Current Biology *23*, R259–R261. https://doi.org/10.1016/j.cub.2013.03.023.

Elam, C., Hesson, L., Vos, M.D., Eckfeld, K., Ellis, C.A., Bell, A., Krex, D., Birrer, M.J., Latif, F., and Clark, G.J. (2005). RRP22 Is a Farnesylated, Nucleolar, Ras-Related Protein with Tumor Suppressor Potential. Cancer Research *65*, 3117–3125. https://doi.org/10.1158/0008-5472.CAN-04-0749.

ENCODE Project Consortium (2004). The ENCODE (ENCyclopedia Of DNA Elements) Project. Science *306*, 636–640. https://doi.org/10.1126/science.1105136.

Falconer, D.S. (1951). Two new mutants, 'trembler' and 'reeler', with neurological actions in the house mouse (Mus musculus L.). Journ. of Genetics *50*, 192–205. https://doi.org/10.1007/BF02996215.

Fan, B., Pan, W., Wang, X., Wei, M., He, A., Zhao, A., Chopp, M., Zhang, Z.G., and Liu, X.S. (2020). Long noncoding RNA mediates stroke-induced neurogenesis. Stem Cells *38*, 973–985. https://doi.org/10.1002/stem.3189.

Feierstein, C., Lazarini, F., Wagner, S., Gabellec, M.-M., De Chaumont, F., Olivo-Marin, J.-C., Boussin, F., Lledo, P., and Gheusi, G. (2010). Disruption of Adult Neurogenesis in the Olfactory Bulb Affects Social Interaction but not Maternal Behavior. Frontiers in Behavioral Neuroscience *4*. .

Fernández, M.E., Croce, S., Boutin, C., Cremer, H., and Raineteau, O. (2011). Targeted electroporation of defined lateral ventricular walls: a novel and rapid method to study fate specification during postnatal forebrain neurogenesis. Neural Development *6*, 13. https://doi.org/10.1186/1749-8104-6-13.

Fernando, T.R., Contreras, J.R., Zampini, M., Rodriguez-Malave, N.I., Alberti, M.O., Anguiano, J., Tran, T.M., Palanichamy, J.K., Gajeton, J., Ung, N.M., et al. (2017). The lncRNA

CASC15 regulates SOX4 expression in RUNX1-rearranged acute leukemia. Mol Cancer *16*, 126. https://doi.org/10.1186/s12943-017-0692-x.

Fischl, B., Salat, D.H., Busa, E., Albert, M., Dieterich, M., Haselgrove, C., van der Kouwe, A., Killiany, R., Kennedy, D., Klaveness, S., et al. (2002). Whole Brain Segmentation: Automated Labeling of Neuroanatomical Structures in the Human Brain. Neuron *33*, 341–355. https://doi.org/10.1016/S0896-6273(02)00569-X.

Foronda, M., Martínez, P., Schoeftner, S., Gómez-López, G., Schneider, R., Flores, J.M., Pisano, D.G., and Blasco, M.A. (2014). Sox4 Links Tumor Suppression to Accelerated Aging in Mice by Modulating Stem Cell Activation. Cell Reports *8*, 487–500. https://doi.org/10.1016/j.celrep.2014.06.031.

Freundlieb, N., François, C., Tandé, D., Oertel, W.H., Hirsch, E.C., and Höglinger, G.U. (2006). Dopaminergic Substantia Nigra Neurons Project Topographically Organized to the Subventricular Zone and Stimulate Precursor Cell Proliferation in Aged Primates. J. Neurosci. *26*, 2321–2325. https://doi.org/10.1523/JNEUROSCI.4859-05.2006.

Fünfschilling, U., Jockusch, W.J., Sivakumar, N., Möbius, W., Corthals, K., Li, S., Quintes, S., Kim, Y., Schaap, I.A.T., Rhee, J.-S., et al. (2012). Critical Time Window of Neuronal Cholesterol Synthesis during Neurite Outgrowth. J. Neurosci. *32*, 7632–7645. https://doi.org/10.1523/JNEUROSCI.1352-11.2012.

G Betancur, J., and Tomari, Y. (2015). Cryptic RNA-binding by PRC2 components EZH2 and SUZ12. RNA Biol *12*, 959–965. https://doi.org/10.1080/15476286.2015.1069463.

Gage, F.H., Chen, K.S., Buzsaki, G., and Armstrong, D. (1988). Experimental approaches to age-related cognitive impairments. Neurobiology of Aging *9*, 645–655. https://doi.org/10.1016/S0197-4580(88)80129-5.

García-Baos, A., Gallego-Landin, I., Ferreres-Álvarez, I., Puig-Reyne, X., Castro-Zavala, A., Valverde, O., and Martín-Sánchez, A. (2022). Effects of fast-acting antidepressant drugs on a postpartum depression mice model. Biomedicine & Pharmacotherapy *154*, 113598. https://doi.org/10.1016/j.biopha.2022.113598.

Global Drug Intelligence Database (2024). Delving into the Latest Updates on YM-53601 with Synapse.

Global Drug Intelligence Database (2025a). FTI-277 - Global Drug Intelligence Database.

Global Drug Intelligence Database (2025b). GGTI-298 - Global Drug Intelligence Database.

Gonda, K., Watanabe, T.M., Ohuchi, N., and Higuchi, H. (2010). *In Vivo* Nano-imaging of Membrane Dynamics in Metastatic Tumor Cells Using Quantum Dots*. Journal of Biological Chemistry *285*, 2750–2757. https://doi.org/10.1074/jbc.M109.075374.

Grote, P., Wittler, L., Hendrix, D., Koch, F., Währisch, S., Beisaw, A., Macura, K., Bläss, G., Kellis, M., Werber, M., et al. (2013). The Tissue-Specific lncRNA *Fendrr* Is an Essential Regulator of Heart and Body Wall Development in the Mouse. Developmental Cell *24*, 206–214. https://doi.org/10.1016/j.devcel.2012.12.012.

Guttman, M., Amit, I., Garber, M., French, C., Lin, M.F., Feldser, D., Huarte, M., Zuk, O., Carey, B.W., Cassady, J.P., et al. (2009). Chromatin signature reveals over a thousand highly conserved large non-coding RNAs in mammals. Nature *458*, 223–227. https://doi.org/10.1038/nature07672.

Hack, I., Bancila, M., Loulier, K., Carroll, P., and Cremer, H. (2002). Reelin is a detachment signal in tangential chain-migration during postnatal neurogenesis. Nat. Neurosci. *5*, 939–945. https://doi.org/10.1038/nn923.

Hajar, R. (2011). Statins: Past and Present. Heart Views *12*, 121–127. https://doi.org/10.4103/1995-705X.95070.

Hao, Y., Hao, S., Andersen-Nissen, E., Mauck, W.M., Zheng, S., Butler, A., Lee, M.J., Wilk, A.J., Darby, C., Zager, M., et al. (2021). Integrated analysis of multimodal single-cell data. Cell *184*, 3573-3587.e29. https://doi.org/10.1016/j.cell.2021.04.048.

Hao, Y., Stuart, T., Kowalski, M.H., Choudhary, S., Hoffman, P., Hartman, A., Srivastava, A., Molla, G., Madad, S., Fernandez-Granda, C., et al. (2024). Dictionary learning for integrative, multimodal and scalable single-cell analysis. Nature Biotechnology *42*, 293–304. https://doi.org/10.1038/s41587-023-01767-y.

Hezroni, H., Koppstein, D., Schwartz, M., Avrutin, A., David P. Bartel, and Ulitsky, I. (2015). Principles of Long Noncoding RNA Evolution Derived from Direct Comparison of Transcriptomes in 17 Species. Cell Reports 1110–1122. http://dx.doi.org/10.1016/j.celrep.2015.04.023.

Hillerer, K.M., Jacobs, V.R., Fischer, T., and Aigner, L. (2014). The Maternal Brain: An Organ with Peripartal Plasticity. Neural Plasticity *2014*, 1–20. https://doi.org/10.1155/2014/574159.

Hitoshi, S., Maruta, N., Higashi, M., Kumar, A., Kato, N., and Ikenaka, K. (2007). Antidepressant drugs reverse the loss of adult neural stem cells following chronic stress. Journal of Neuroscience Research *85*, 3574–3585. https://doi.org/10.1002/jnr.21455.

Holstein, S.A., and Hohl, R.J. (2004). Isoprenoids: Remarkable diversity of form and function. Lipids *39*, 293–309. https://doi.org/10.1007/s11745-004-1233-3.

Hong, S.E., Shugart, Y.Y., Huang, D.T., Shahwan, S.A., Grant, P.E., Hourihane, J.O., Martin, N.D.T., and Walsh, C.A. (2000). Autosomal recessive lissencephaly with cerebellar hypoplasia is associated with human RELN mutations. Nat Genet *26*, 93–96. https://doi.org/10.1038/79246.

Horton, J.D., Shah, N.A., Warrington, J.A., Anderson, N.N., Park, S.W., Brown, M.S., and Goldstein, J.L. (2003). Combined analysis of oligonucleotide microarray data from transgenic and knockout mice identifies direct SREBP target genes. Proc. Natl. Acad. Sci. U.S.A. *100*, 12027–12032. https://doi.org/10.1073/pnas.1534923100.

Horvat, S., Mcwhir, J., and Rozman, D. (2011). Defects in cholesterol synthesis genes in mouse and in humans: lessons for drug development and safer treatments. Drug Metabolism Reviews *43*, 69–90. https://doi.org/10.3109/03602532.2010.540580.

Howe, K.L., Achuthan, P., Allen, J., Allen, J., Alvarez-Jarreta, J., Amode, M.R., Armean, I.M., Azov, A.G., Bennett, R., Bhai, J., et al. (2021). Ensembl 2021. Nucleic Acids Research *49*, D884–D891. https://doi.org/10.1093/nar/gkaa942.

Hu, H. (1999). Chemorepulsion of Neuronal Migration by Slit2 in the Developing Mammalian Forebrain. Neuron *23*, 703–711. https://doi.org/10.1016/S0896-6273(01)80029-5.

Hu, H., and Rutishauser, U. (1996). A Septum-Derived Chemorepulsive Factor for Migrating Olfactory Interneuron Precursors. Neuron *16*, 933–940. https://doi.org/10.1016/S0896-6273(00)80116-6.

Ihrie, R.A., and Álvarez-Buylla, A. (2011). Lake Front Property: A Unique Germinal Niche by the Lateral Ventricles of the Adult Brain. Neuron *70*, 674–686. https://doi.org/10.1016/j.neuron.2011.05.004.

Inta, D., Lima-Ojeda, J.M., Lau, T., Tang, W., Dormann, C., Sprengel, R., Schloss, P., Sartorius, A., Meyer-Lindenberg, A., and Gass, P. (2013). Electroconvulsive Therapy Induces Neurogenesis in Frontal Rat Brain Areas. PLOS ONE *8*, e69869. https://doi.org/10.1371/journal.pone.0069869.

Istvan, E.S., and Deisenhofer, J. (2001). Structural Mechanism for Statin Inhibition of HMG-CoA Reductase. Science *292*, 1160–1164. https://doi.org/10.1126/science.1059344.

Johnson-Anuna, L.N., Eckert, G.P., Keller, J.H., Igbavboa, U., Franke, C., Fechner, T., Schubert-Zsilavecz, M., Karas, M., Müller, W.E., and Wood, W.G. (2005). Chronic Administration of Statins Alters Multiple Gene Expression Patterns in Mouse Cerebral Cortex. The Journal of Pharmacology and Experimental Therapeutics *312*, 786–793. https://doi.org/10.1124/jpet.104.075028.

Jung, H.-J., Nobumori, C., Goulbourne, C.N., Tu, Y., Lee, J.M., Tatar, A., Wu, D., Yoshinaga, Y., De Jong, P.J., Coffinier, C., et al. (2013). Farnesylation of lamin B1 is important for retention of nuclear chromatin during neuronal migration. Proceedings of the National Academy of Sciences of the United States of America *110*, E1923–E1932. https://doi.org/10.1073/pnas.1303916110.

Kalamakis, G., Brüne, D., Ravichandran, S., Bolz, J., Fan, W., Ziebell, F., Stiehl, T., Catalá-Martinez, F., Kupke, J., Zhao, S., et al. (2019). Quiescence Modulates Stem Cell Maintenance and Regenerative Capacity in the Aging Brain. Cell *176*, 1407-1419.e14. https://doi.org/10.1016/j.cell.2019.01.040.

Karnovsky, M.J., Kleinfeld, A.M., Hoover, R.L., and Klausner, R.D. (1982). The concept of lipid domains in membranes. The Journal of Cell Biology *94*, 1–6. https://doi.org/10.1083/jcb.94.1.1.

Katakowski, M., Zhang, Z., DeCarvalho, A.C., and Chopp, M. (2005). EphB2 induces proliferation and promotes a neuronal fate in adult subventricular neural precursor cells. Neurosci. Lett. *385*, 204–209. https://doi.org/10.1016/j.neulet.2005.05.060.

Kato, M. (2015). Genotype-phenotype correlation in neuronal migration disorders and cortical dysplasias. Front. Neurosci. *9*. https://doi.org/10.3389/fnins.2015.00181.

Kato, K., Cox, A.D., Hisaka, M.M., Graham, S.M., Buss, J.E., and Der, C.J. (1992). Isoprenoid addition to Ras protein is the critical modification for its membrane association and transforming activity. Proc. Natl. Acad. Sci. U.S.A. *89*, 6403–6407. https://doi.org/10.1073/pnas.89.14.6403.

Kempermann, G., Song, H., and Gage, F.H. (2015). Neurogenesis in the Adult Hippocampus. Cold Spring Harb Perspect Biol *7*, a018812. https://doi.org/10.1101/cshperspect.a018812.

Keniry, A., Oxley, D., Monnier, P., Kyba, M., Dandolo, L., Smits, G., and Reik, W. (2012). The H19 lincRNA is a developmental reservoir of miR-675 that suppresses growth and Igf1r. Nature Cell Biology *14*, 659–665. https://doi.org/10.1038/ncb2521.

Kent, W.J. (2002). BLAT—The BLAST-Like Alignment Tool. Genome Res *12*, 656–664. https://doi.org/10.1101/gr.229202.

Kino, T., Hurt, D.E., Ichijo, T., Nader, N., and Chrousos, G.P. (2010). Noncoding RNA Gas5 Is a Growth Arrest and Starvation-Associated Repressor of the Glucocorticoid Receptor. Sci Signal *3*, ra8. https://doi.org/10.1126/scisignal.2000568.

Kirschenbaum, B., Doetsch, F., Lois, C., and Alvarez-Buylla, A. (1999). Adult Subventricular Zone Neuronal Precursors Continue to Proliferate and Migrate in the Absence of the Olfactory Bulb. J. Neurosci. *19*, 2171–2180. https://doi.org/10.1523/JNEUROSCI.19-06-02171.1999.

Kishi, K., Peng, J.Y., Kakuta, S., Murakami, K., Kuroda, M., Yokota, S., Hayakawa, S., Kuge, T., and Asayama, T. (1990). Migration of bipolar subependymal cells, precursors of the granule cells of the rat olfactory bulb, with reference to the arrangement of the radial glial fibers. Arch Histol Cytol *53*, 219–226. https://doi.org/10.1679/aohc.53.219.

Kolde, R. (2019). pheatmap: Pretty Heatmaps.

Kole, R., Krainer, A.R., and Altman, S. (2012). RNA therapeutics: beyond RNA interference and antisense oligonucleotides. Nat Rev Drug Discov *11*, 125–140. https://doi.org/10.1038/nrd3625.

Kriska, J., Janeckova, L., Kirdajova, D., Honsa, P., Knotek, T., Dzamba, D., Kolenicova, D., Butenko, O., Vojtechova, M., Capek, M., et al. (2021). Wnt/β-Catenin Signaling Promotes Differentiation of Ischemia-Activated Adult Neural Stem/Progenitor Cells to Neuronal Precursors. Frontiers in Neuroscience *15*. .

Krute, C.N., Carroll, R.K., Rivera, F.E., Weiss, A., Young, R.M., Shilling, A., Botlani, M., Varma, S., Baker, B.J., and Shaw, L.N. (2015). The disruption of prenylation leads to pleiotropic rearrangements in cellular behavior in Staphylococcus aureus. Mol Microbiol *95*, 819–832. https://doi.org/10.1111/mmi.12900.

Kuchay, S., Wang, H., Marzio, A., Jain, K., Homer, H., Fehrenbacher, N., Philips, M.R., Zheng, N., and Pagano, M. (2019). GGTase3 is a Newly Identified Geranylgeranyltransferase Targeting a Ubiquitin Ligase. Nat Struct Mol Biol *26*, 628–636. https://doi.org/10.1038/s41594-019-0249-3.

Kuhn, H.G., Winkler, J., Kempermann, G., Thal, L.J., and Gage, F.H. (1997). Epidermal Growth Factor and Fibroblast Growth Factor-2 Have Different Effects on Neural Progenitors

in the Adult Rat Brain. J. Neurosci. *17*, 5820–5829. https://doi.org/10.1523/JNEUROSCI.17-15-05820.1997.

Kuleshov, M.V., Jones, M.R., Rouillard, A.D., Fernandez, N.F., Duan, Q., Wang, Z., Koplev, S., Jenkins, S.L., Jagodnik, K.M., Lachmann, A., et al. (2016). Enrichr: a comprehensive gene set enrichment analysis web server 2016 update. Nucleic Acids Res *44*, W90-97. https://doi.org/10.1093/nar/gkw377.

Lai, K., Kaspar, B.K., Gage, F.H., and Schaffer, D.V. (2003). Sonic hedgehog regulates adult neural progenitor proliferation in vitro and in vivo. Nat Neurosci *6*, 21–27. https://doi.org/10.1038/nn983.

Langmead, B., Trapnell, C., Pop, M., and Salzberg, S.L. (2009). Ultrafast and memory-efficient alignment of short DNA sequences to the human genome. Genome Biology *10*, R25. https://doi.org/10.1186/gb-2009-10-3-r25.

Larner, J., Jane, J., Laws, E., Packer, R., Myers, C., and Shaffrey, M. (1998). A phase I-II trial of lovastatin for anaplastic astrocytoma and glioblastoma multiforme. American Journal of Clinical Oncology: Cancer Clinical Trials *21*, 579–583. https://doi.org/10.1097/00000421-199812000-00010.

Larson, J., Hoffman, J.S., Guidotti, A., and Costa, E. (2003). Olfactory discrimination learning deficit in heterozygous reeler mice. Brain Research *971*, 40–46. https://doi.org/10.1016/S0006-8993(03)02353-9.

Latos, P.A., Pauler, F.M., Koerner, M.V., Şenergin, H.B., Hudson, Q.J., Stocsits, R.R., Allhoff, W., Stricker, S.H., Klement, R.M., Warczok, K.E., et al. (2012). Airn Transcriptional Overlap, But Not Its lncRNA Products, Induces Imprinted Igf2r Silencing. Science *338*, 1469–1472. .

Lau, W.-M., Qiu, G., Helmeste, D.M., Lee, T.M.C., Tang, S.-W., So, K.-F., and Tang, S.-W. (2007). Corticosteroid decreases subventricular zone cell proliferation, which could be reversed by paroxetine. Restorative Neurology and Neuroscience *25*, 17–23. https://doi.org/10.3233/RNN-2007-00348.

Lee, J.H., Lee, J.E., Kahng, J.Y., Kim, S.H., Park, J.S., Yoon, S.J., Um, J.-Y., Kim, W.K., Lee, J.-K., Park, J., et al. (2018). Human glioblastoma arises from subventricular zone cells with low-level driver mutations. Nature *560*, 243–247. https://doi.org/10.1038/s41586-018-0389-3.

Leisegang, M.S., Warwick, T., Stötzel, J., and Brandes, R.P. (2024). RNA-DNA triplexes: molecular mechanisms and functional relevance. Trends in Biochemical Sciences *49*, 532–544. https://doi.org/10.1016/j.tibs.2024.03.009.

Lemmon, C.A., Chen, C.S., and Romer, L.H. (2009). Cell Traction Forces Direct Fibronectin Matrix Assembly. Biophysical Journal *96*, 729–738. https://doi.org/10.1016/j.bpj.2008.10.009.

Lerner, E.C., Qian, Y., Blaskovich, M.A., Fossum, R.D., Vogt, A., Sun, J., Cox, A.D., Der, C.J., Hamilton, A.D., and Sebti, S.M. (1995). Ras C*AAX* Peptidomimetic FTI-277 Selectively Blocks Oncogenic Ras Signaling by Inducing Cytoplasmic Accumulation of Inactive Ras-Raf Complexes (*). Journal of Biological Chemistry *270*, 26802–26806. https://doi.org/10.1074/jbc.270.45.26802.

Levental, I., Lingwood, D., Grzybek, M., Coskun, Ü., and Simons, K. (2010). Palmitoylation regulates raft affinity for the majority of integral raft proteins. Proc Natl Acad Sci U S A *107*, 22050–22054. https://doi.org/10.1073/pnas.1016184107.

Levison, S.W., and Goldman, J.E. (1993). Both oligodendrocytes and astrocytes develop from progenitors in the subventricular zone of postnatal rat forebrain. Neuron *10*, 201–212. https://doi.org/10.1016/0896-6273(93)90311-E.

Li, Z., Liu, L., Feng, C., Qin, Y., Xiao, J., Zhang, Z., and Ma, L. (2022). LncBook 2.0: integrating human long non-coding RNAs with multi-omics annotations. Nucleic Acids Res *51*, D186–D191. https://doi.org/10.1093/nar/gkac999.

Lim, D.A., Cha, S., Mayo, M.C., Chen, M.-H., Keles, E., VandenBerg, S., and Berger, M.S. (2007). Relationship of glioblastoma multiforme to neural stem cell regions predicts invasive and multifocal tumor phenotype. Neuro Oncol *9*, 424–429. https://doi.org/10.1215/15228517-2007-023.

Ling, K.-H., Hewitt, C.A., Tan, K.-L., Cheah, P.-S., Vidyadaran, S., Lai, M.-I., Lee, H.-C., Simpson, K., Hyde, L., Pritchard, M.A., et al. (2014). Functional transcriptome analysis of the postnatal brain of the Ts1Cje mouse model for Down syndrome reveals global disruption of interferon-related molecular networks. BMC Genomics *15*, 624. https://doi.org/10.1186/1471-2164-15-624.

Liu, F., Tian, T., Zhang, Z., Xie, S., Yang, J., Zhu, L., Wang, W., Shi, C., Sang, L., Guo, K., et al. (2022). Long non-coding RNA SNHG6 couples cholesterol sensing with mTORC1 activation in hepatocellular carcinoma. Nat Metab *4*, 1022–1040. https://doi.org/10.1038/s42255-022-00616-7.

Llorens-Bobadilla, E., Zhao, S., Baser, A., Saiz-Castro, G., Zwadlo, K., and Martin-Villalba, A. (2015). Single-Cell Transcriptomics Reveals a Population of Dormant Neural Stem Cells that Become Activated upon Brain Injury. Cell Stem Cell *17*, 329–340. https://doi.org/10.1016/j.stem.2015.07.002.

Lois, C., and Alvarez-Buylla, A. (1994). Long-Distance Neuronal Migration in the Adult Mammalian Brain. Science *264*, 1145–1148. https://doi.org/10.1126/science.8178174.

Lombard, J., and Moreira, D. (2011). Origins and Early Evolution of the Mevalonate Pathway of Isoprenoid Biosynthesis in the Three Domains of Life. Molecular Biology and Evolution *28*, 87–99. https://doi.org/10.1093/molbev/msq177.

Lorent, J.H., Diaz-Rohrer, B., Lin, X., Spring, K., Gorfe, A.A., Levental, K.R., and Levental, I. (2017). Structural determinants and functional consequences of protein affinity for membrane rafts. Nat Commun *8*, 1219. https://doi.org/10.1038/s41467-017-01328-3.

Love, M.I., Huber, W., and Anders, S. (2014). Moderated estimation of fold change and dispersion for RNA-seq data with DESeq2. Genome Biology *15*, 550. https://doi.org/10.1186/s13059-014-0550-8.

Luo, J., Daniels, S.B., Lennington, J.B., Notti, R.Q., and Conover, J.C. (2006). The aging neurogenic subventricular zone. Aging Cell *5*, 139–152. https://doi.org/10.1111/j.1474-9726.2006.00197.x.

Luo, J., Hu, X., Zhang, L., Li, L., Zheng, H., Li, M., and Zhang, Q. (2014). Physical exercise regulates neural stem cells proliferation and migration via SDF-1α/CXCR4 pathway in rats after ischemic stroke. Neuroscience Letters *578*, 203–208. https://doi.org/10.1016/j.neulet.2014.06.059.

Ma, B., Tromp, J., and Li, M. (2002). PatternHunter: faster and more sensitive homology search. Bioinformatics *18*, 440–445. https://doi.org/10.1093/bioinformatics/18.3.440.

Maeda, N. (2015). Proteoglycans and neuronal migration in the cerebral cortex during development and disease. Front. Neurosci. *9*. https://doi.org/10.3389/fnins.2015.00098.

Mamber, C., Kozareva, D.A., Kamphuis, W., and Hol, E.M. (2013). Shades of gray: The delineation of marker expression within the adult rodent subventricular zone. Progress in Neurobiology *111*, 1–16. https://doi.org/10.1016/j.pneurobio.2013.07.003.

Mancini-DiNardo, D., Steele, S.J.S., Levorse, J.M., Ingram, R.S., and Tilghman, S.M. (2006). Elongation of the Kcnq1ot1 transcript is required for genomic imprinting of neighboring genes. Genes Dev *20*, 1268–1282. https://doi.org/10.1101/gad.1416906.

Marshall, C.A.G., Novitch, B.G., and Goldman, J.E. (2005). Olig2 Directs Astrocyte and Oligodendrocyte Formation in Postnatal Subventricular Zone Cells. J Neurosci *25*, 7289–7298. https://doi.org/10.1523/JNEUROSCI.1924-05.2005.

Martinez-Molina, N., Kim, Y., Hockberger, P., and Szele, F.G. (2011). Rostral migratory stream neuroblasts turn and change directions in stereotypic patterns. Cell Adhesion & Migration *5*, 83–95. https://doi.org/10.4161/cam.5.1.13788.

Mattick, J.S., Amaral, P.P., Carninci, P., Carpenter, S., Chang, H.Y., Chen, L.-L., Chen, R., Dean, C., Dinger, M.E., Fitzgerald, K.A., et al. (2023). Long non-coding RNAs: definitions, functions, challenges and recommendations. Nat Rev Mol Cell Biol *24*, 430–447. https://doi.org/10.1038/s41580-022-00566-8.

McGuire, T.F., Qian, Y., Vogt, A., Hamilton, A.D., and Sebti, S.M. (1996). Platelet-derived Growth Factor Receptor Tyrosine Phosphorylation Requires Protein Geranylgeranylation but not Farnesylation*. Journal of Biological Chemistry *271*, 27402–27407. https://doi.org/10.1074/jbc.271.44.27402.

Meng, L., Person, R.E., Huang, W., Zhu, P.J., Costa-Mattioli, M., and Beaudet, A.L. (2013). Truncation of Ube3a-ATS Unsilences Paternal Ube3a and Ameliorates Behavioral Defects in the Angelman Syndrome Mouse Model. PLOS Genetics *9*, e1004039. https://doi.org/10.1371/journal.pgen.1004039.

Meyer, M., and Kircher, M. (2010). Illumina Sequencing Library Preparation for Highly Multiplexed Target Capture and Sequencing. Cold Spring Harb Protoc *2010*, pdb.prot5448. https://doi.org/10.1101/pdb.prot5448.

Miyamoto, T., Kuboyama, K., Honda, M., Ohkawa, Y., Oki, S., and Sawamoto, K. (2025). High spatial resolution gene expression profiling and characterization of neuroblasts migrating in the peri-injured cortex using photo-isolation chemistry. Front. Neurosci. *18*. https://doi.org/10.3389/fnins.2024.1504047.

Miziorko, H.M. (2011). ENZYMES OF THE MEVALONATE PATHWAY OF ISOPRENOID BIOSYNTHESIS. Arch Biochem Biophys *505*, 131–143. https://doi.org/10.1016/j.abb.2010.09.028.

Mizrak, D., Levitin, H.M., Delgado, A.C., Crotet, V., Yuan, J., Chaker, Z., Silva-Vargas, V., Sims, P.A., and Doetsch, F. (2019). Single-Cell Analysis of Regional Differences in Adult V-SVZ Neural Stem Cell Lineages. Cell Rep *26*, 394-406.e5. https://doi.org/10.1016/j.celrep.2018.12.044.

Mizrak, D., Bayin, N.S., Yuan, J., Liu, Z., Suciu, R.M., Niphakis, M.J., Ngo, N., Lum, K.M., Cravatt, B.F., Joyner, A.L., et al. (2020). Single-Cell Profiling and SCOPE-Seq Reveal Lineage Dynamics of Adult Ventricular-Subventricular Zone Neurogenesis and NOTUM as a Key Regulator. Cell Rep *31*, 107805. https://doi.org/10.1016/j.celrep.2020.107805.

Mo, C.-F., Wu, F.-C., Tai, K.-Y., Chang, W.-C., Chang, K.-W., Kuo, H.-C., Ho, H.-N., Chen, H.-F., and Lin, S.-P. (2015). Loss of non-coding RNA expression from the DLK1-DIO3 imprinted locus correlates with reduced neural differentiation potential in human embryonic stem cell lines. Stem Cell Research & Therapy *6*, 1. https://doi.org/10.1186/scrt535.

Mobley, A.K., and McCarty, J.H. (2011). β8 integrin is essential for neuroblast migration in the rostral migratory stream. Glia *59*, 1579–1587. https://doi.org/10.1002/glia.21199.

Mondal, T., Subhash, S., Vaid, R., Enroth, S., Uday, S., Reinius, B., Mitra, S., Mohammed, A., James, A.R., Hoberg, E., et al. (2015). MEG3 long noncoding RNA regulates the TGF-β pathway genes through formation of RNA–DNA triplex structures. Nature Communications *6*, 7743. https://doi.org/10.1038/ncomms8743.

Moshi, J.M., Ummelen, M., Broers, J.L.V., Ramaekers, F.C.S., and Hopman, A.H.N. (2023). Impact of antigen retrieval protocols on the immunohistochemical detection of epigenetic DNA modifications. Histochem Cell Biol *159*, 513–526. https://doi.org/10.1007/s00418-023-02187-4.

Mutschler, H., Taylor, A.I., Porebski, B.T., Lightowlers, A., Houlihan, G., Abramov, M., Herdewijn, P., and Holliger, P. (2018). Random-sequence genetic oligomer pools display an innate potential for ligation and recombination. eLife *7*, e43022. https://doi.org/10.7554/eLife.43022.

Nam, S.C., Kim, Y., Dryanovski, D., Walker, A., Goings, G., Woolfrey, K., Kang, S.S., Chu, C., Chenn, A., Erdelyi, F., et al. (2007). Dynamic features of postnatal subventricular zone cell motility: A two-photon time-lapse study. Journal of Comparative Neurology *505*, 190–208. https://doi.org/10.1002/cne.21473.

NCBI (2025). Dcx doublecortin [Mus musculus (house mouse)] - Gene - NCBI.

Ng, S.-Y., Bogu, G.K., Soh, B.S., and Stanton, L.W. (2013). The long noncoding RNA RMST interacts with SOX2 to regulate neurogenesis. Mol Cell *51*, 349–359. https://doi.org/10.1016/j.molcel.2013.07.017.

Ni, H., Chai, P., Yu, J., Xing, Y., Wang, S., Fan, J., Ge, S., Wang, Y., Jia, R., and Fan, X. (2020). LncRNA CANT1 suppresses retinoblastoma progression by repellinghistone methyltransferase in PI3Kγ promoter. Cell Death and Disease *11*. https://doi.org/10.1038/s41419-020-2524-y.

Nieweg, K., Schaller, H., and Pfrieger, F.W. (2009). Marked differences in cholesterol synthesis between neurons and glial cells from postnatal rats. Journal of Neurochemistry *109*, 125–134. https://doi.org/10.1111/j.1471-4159.2009.05917.x.

Nobes, C.D., and Hall, A. (1995). Rho, Rac, and Cdc42 GTPases regulate the assembly of multimolecular focal complexes associated with actin stress fibers, lamellipodia, and filopodia. Cell *81*, 53–62. https://doi.org/10.1016/0092-8674(95)90370-4.

Ocbina, P.J., Dizon, M.L.V., Shin, L., and Szele, F.G. (2006). Doublecortin is necessary for the migration of adult subventricular zone cells from neurospheres. Mol. Cell. Neurosci. *33*, 126–135. https://doi.org/10.1016/j.mcn.2006.06.014.

Ohashi, K., Osuga, J., Tozawa, R., Kitamine, T., Yagyu, H., Sekiya, M., Tomita, S., Okazaki, H., Tamura, Y., Yahagi, N., et al. (2003). Early Embryonic Lethality Caused by Targeted Disruption of the 3-Hydroxy-3-methylglutaryl-CoA Reductase Gene*. Journal of Biological Chemistry *278*, 42936–42941. https://doi.org/10.1074/jbc.M307228200.

Ohira, K., and Miyakawa, T. (2011). Chronic treatment with fluoxetine for more than 6 weeks decreases neurogenesis in the subventricular zone of adult mice. Molecular Brain *4*, 10. https://doi.org/10.1186/1756-6606-4-10.

O'Keeffe, G.C., Tyers, P., Aarsland, D., Dalley, J.W., Barker, R.A., and Caldwell, M.A. (2009). Dopamine-induced proliferation of adult neural precursor cells in the mammalian subventricular zone is mediated through EGF. Proc. Natl. Acad. Sci. U.S.A. *106*, 8754–8759. https://doi.org/10.1073/pnas.0803955106.

Oliver, P.L., Chodroff, R.A., Gosal, A., Edwards, B., Cheung, A.F.P., Gomez-Rodriguez, J., Elliot, G., Garrett, L.J., Lickiss, T., Szele, F., et al. (2015). Disruption of Visc-2, a Brain-Expressed Conserved Long Noncoding RNA, Does Not Elicit an Overt Anatomical or Behavioral Phenotype. Cerebral Cortex *25*, 3572–3585. https://doi.org/10.1093/cercor/bhu196.

Ong, J., Sasaki, K., Ferdousi, F., Suresh, M., Isoda, H., and Szele, F.G. (2025). Senescence Accelerated Mouse-Prone 8: a Model of Neuroinflammation and Aging with Features of Sporadic Alzheimer's disease. Stem Cells sxae091. https://doi.org/10.1093/stmcls/sxae091.

Ono, K., Tomasiewicz, H., Magnuson, T., and Rutishauser, U. (1994). N-CAM mutation inhibits tangential neuronal migration and is phenocopied by enzymatic removal of polysialic acid. Neuron *13*, 595–609. https://doi.org/10.1016/0896-6273(94)90028-0.

Orona, E., Rainer, E.C., and Scott, J.W. (1984). Dendritic and axonal organization of mitral and tufted cells in the rat olfactory bulb. J Comp Neurol *226*, 346–356. https://doi.org/10.1002/cne.902260305.

Osborne, T.F., Gil, G., Goldstein, J.L., and Brown, M.S. (1988). Operator constitutive mutation of 3-hydroxy-3-methylglutaryl coenzyme A reductase promoter abolishes protein binding to sterol regulatory element. Journal of Biological Chemistry *263*, 3380–3387. https://doi.org/10.1016/S0021-9258(18)69082-9.

Oskouian, B., Lee, J.Y., Asgharzadeh, S., Khan, R., Zhang, M., Weisbrod, J.R., Choi, Y.-J., Puri, L., Aguilar, A.E., Zhao, P., et al. (2024). AF1q is a universal marker of neuroblastoma

that sustains N-Myc expression and drives tumorigenesis. Oncogene *43*, 1203–1213. https://doi.org/10.1038/s41388-024-02980-y.

Pardillo-Díaz, R., Pérez-García, P., Ortego-Domínguez, M., Gómez-Oliva, R., Martínez-Gómez, N., Domínguez-García, S., García-Cózar, F., Muñoz-Miranda, J.P., Hernández-Galán, R., Carrascal, L., et al. (2025). The subventricular zone neurogenic niche provides adult born functional neurons to repair cortical brain injuries in response to diterpenoid therapy. Stem Cell Res Ther *16*, 1. https://doi.org/10.1186/s13287-024-04105-4.

Pastrana, E., Silva-Vargas, V., and Doetsch, F. (2011). Eyes Wide Open: A Critical Review of Sphere-Formation as an Assay For Stem Cells. Cell Stem Cell *8*, 486–498. https://doi.org/10.1016/j.stem.2011.04.007.

Pavlaki, I., Alammari, F., Sun, B., Clark, N., Sirey, T., Lee, S., Woodcock, D.J., Ponting, C.P., Szele, F.G., and Vance, K.W. (2018). The long non-coding RNA Paupar promotes KAP1-dependent chromatin changes and regulates olfactory bulb neurogenesis. The EMBO Journal *37*, e98219. https://doi.org/10.15252/embj.201798219.

Pencea, V., Bingaman, K.D., Wiegand, S.J., and Luskin, M.B. (2001). Infusion of Brain-Derived Neurotrophic Factor into the Lateral Ventricle of the Adult Rat Leads to New Neurons in the Parenchyma of the Striatum, Septum, Thalamus, and Hypothalamus. J Neurosci *21*, 6706–6717. https://doi.org/10.1523/JNEUROSCI.21-17-06706.2001.

Petreanu, L., and Alvarez-Buylla, A. (2002). Maturation and Death of Adult-Born Olfactory Bulb Granule Neurons: Role of Olfaction. J. Neurosci. *22*, 6106–6113. https://doi.org/10.1523/JNEUROSCI.22-14-06106.2002.

Pomaznoy, M., Ha, B., and Peters, B. (2018a). GOnet: a tool for interactive Gene Ontology analysis. BMC Bioinformatics *19*, 470. https://doi.org/10.1186/s12859-018-2533-3.

Pomaznoy, M., Ha, B., and Peters, B. (2018b). GOnet: a tool for interactive Gene Ontology analysis. BMC Bioinformatics *19*, 470. https://doi.org/10.1186/s12859-018-2533-3.

Ponti, G., Obernier, K., Guinto, C., Jose, L., Bonfanti, L., and Alvarez-Buylla, A. (2013). Cell cycle and lineage progression of neural progenitors in the ventricular-subventricular zones of adult mice. Proc. Natl. Acad. Sci. U.S.A. *110*. https://doi.org/10.1073/pnas.1219563110.

Ponti, G., Farinetti, A., Marraudino, M., Panzica, G., and Gotti, S. (2018). Sex Steroids and Adult Neurogenesis in the Ventricular-Subventricular Zone. Front Endocrinol (Lausanne) *9*, 156. https://doi.org/10.3389/fendo.2018.00156.

Price, J.L., and Powell, T.P.S. (1970). The morphology of the granule cells of the olfactory bulb. Journal of Cell Science *7*, 91–122. https://doi.org/10.1242/jcs.7.1.91.

Qi, L.S., Larson, M.H., Gilbert, L.A., Doudna, J.A., Weissman, J.S., Arkin, A.P., and Lim, W.A. (2013). Repurposing CRISPR as an RNA-Guided Platform for Sequence-Specific Control of Gene Expression. Cell *152*, 1173–1183. https://doi.org/10.1016/j.cell.2013.02.022.

Qian, Y., Vogt, A., Vasudevan, A., Sebti, S.M., and Hamilton, A.D. (1998). Selective inhibition of type-I geranylgeranyltransferase in vitro and in whole cells by CAAL peptidomimetics. Bioorganic & Medicinal Chemistry *6*, 293–299. https://doi.org/10.1016/S0968-0896(97)10040-2.

Quan, G., Xie, C., Dietschy, J.M., and Turley, S.D. (2003). Ontogenesis and regulation of cholesterol metabolism in the central nervous system of the mouse. Developmental Brain Research *146*, 87–98. https://doi.org/10.1016/j.devbrainres.2003.09.015.

Rall, W., Shepherd, G.M., Reese, T.S., and Brightman, M.W. (1966). Dendrodendritic synaptic pathway for inhibition in the olfactory bulb. Experimental Neurology *14*, 44–56. https://doi.org/10.1016/0014-4886(66)90023-9.

Ramos, A.D., Diaz, A., Nellore, A., Delgado, R.N., Park, K.-Y., Gonzales-Roybal, G., Oldham, M.C., Song, J.S., and Lim, D.A. (2013a). Integration of Genome-wide Approaches Identifies lncRNAs of Adult Neural Stem Cells and Their Progeny In Vivo. Cell Stem Cell *12*, 616–628. https://doi.org/10.1016/j.stem.2013.03.003.

Ramos, A.D., Diaz, A., Nellore, A., Delgado, R.N., Park, K.-Y., Gonzales-Roybal, G., Oldham, M.C., Song, J.S., and Lim, D.A. (2013b). Integration of Genome-wide Approaches Identifies lncRNAs of Adult Neural Stem Cells and Their Progeny In Vivo. Cell Stem Cell *12*, 616–628. https://doi.org/10.1016/j.stem.2013.03.003.

Raponi, E., Agenes, F., Delphin, C., Assard, N., Baudier, J., Legraverend, C., and Deloulme, J.-C. (2007). S100B expression defines a state in which GFAP-expressing cells lose their neural stem cell potential and acquire a more mature developmental stage. Glia *55*, 165–177. https://doi.org/10.1002/glia.20445.

Raymond, A.A., Fish, D.R., Sisodiya, S.M., Alsanjari, N., Stevens, J.M., and Shorvon, S.D. (1995). Abnormalities of gyration, heterotopias, tuberous sclerosis, focal cortical dysplasia, microdysgenesis, dysembryoplastic neuroepithelial tumour and dysgenesis of the archicortex in epilepsy: Clinical, EEG and neuroimaging features in 100 adult patients. Brain *118*, 629–660. https://doi.org/10.1093/brain/118.3.629.

Reshef, R., Kudryavitskaya, E., Shani-Narkiss, H., Isaacson, B., Rimmerman, N., Mizrahi, A., and Yirmiya, R. (2017). The role of microglia and their CX3CR1 signaling in adult neurogenesis in the olfactory bulb. eLife *6*. https://doi.org/10.7554/elife.30809.

Riss, T.L., O'Brien, M.A., Moravec, R.A., Kupcho, K., and Niles, A.L. (2004). Apoptosis Marker Assays for HTS. In Assay Guidance Manual, S. Markossian, A. Grossman, H. Baskir, M. Arkin, D. Auld, C. Austin, J. Baell, K. Brimacombe, T.D.Y. Chung, N.P. Coussens, et al., eds. (Bethesda (MD): Eli Lilly & Company and the National Center for Advancing Translational Sciences), p.

Roberts, P.J., Mitin, N., Keller, P.J., Chenette, E.J., Madigan, J.P., Currin, R.O., Cox, A.D., Wilson, O., Kirschmeier, P., and Der, C.J. (2008). Rho Family GTPase Modification and Dependence on CAAX Motif-signaled Posttranslational Modification. J Biol Chem *283*, 25150–25163. https://doi.org/10.1074/jbc.M800882200.

Rudolph, J. (2023). jdrudolph/goenrich.

Russell, J.A., Douglas, A.J., and Ingram, C.D. (2001). Brain preparations for maternity - Adaptive changes in behavioral and neuroendocrine systems during pregnancy and lactation. An overview. Progress in Brain Research *133*, 1–38. https://doi.org/10.1016/S0079-6123(01)33002-9.

Safari, M.R., Mohammad Rezaei, F., Dehghan, A., Noroozi, R., Taheri, M., and Ghafouri-Fard, S. (2019). Genomic variants within the long non-coding RNA H19 confer risk of breast cancer in Iranian population. Gene *701*, 121–124. https://doi.org/10.1016/j.gene.2019.03.036.

Saha, B., Peron, S., Murray, K., Jaber, M., and Gaillard, A. (2013). Cortical lesion stimulates adult subventricular zone neural progenitor cell proliferation and migration to the site of injury. Stem Cell Research *11*, 965–977. https://doi.org/10.1016/j.scr.2013.06.006.

Sanger, F., Nicklen, S., and Coulson, A.R. (1977). DNA sequencing with chain-terminating inhibitors. Proc Natl Acad Sci U S A *74*, 5463–5467. .

Sasaki, K., Becker, J., Ong, J., Ciaghi, S., Guldin, L.S., Savastano, S., Fukumitsu, S., Kuwata, H., Szele, F.G., and Isoda, H. (2024). Rosemary extract activates oligodendrogenesis genes in mouse brain and improves learning and memory ability. Biomedicine & Pharmacotherapy *179*, 117350. https://doi.org/10.1016/j.biopha.2024.117350.

Sauvageau, M., Goff, L.A., Lodato, S., Bonev, B., Groff, A.F., Gerhardinger, C., Sanchez-Gomez, D.B., Hacisuleyman, E., Li, E., Spence, M., et al. (2013). Multiple knockout mouse models reveal lincRNAs are required for life and brain development. eLife *2*, e01749. https://doi.org/10.7554/eLife.01749.

Sayers, E.W., Beck, J., Bolton, E.E., Brister, J.R., Chan, J., Connor, R., Feldgarden, M., Fine, A.M., Funk, K., Hoffman, J., et al. (2025). Database resources of the National Center for Biotechnology Information in 2025. Nucleic Acids Res *53*, D20–D29. https://doi.org/10.1093/nar/gkae979.

Schlackow, M., Nojima, T., Gomes, T., Dhir, A., Carmo-Fonseca, M., and Proudfoot, N.J. (2017). Distinctive Patterns of Transcription and RNA Processing for Human lincRNAs. Molecular Cell *65*, 25–38. https://doi.org/10.1016/j.molcel.2016.11.029.

Scholzen, T., and Gerdes, J. (2000). The Ki-67 protein: From the known and the unknown. Journal of Cellular Physiology *182*, 311–322. https://doi.org/10.1002/(SICI)1097-4652(200003)182:3%253C311::AID-JCP1%253E3.0.CO;2-9.

Scopa, C., Marrocco, F., Latina, V., Ruggeri, F., Corvaglia, V., La Regina, F., Ammassari-Teule, M., Middei, S., Amadoro, G., Meli, G., et al. (2020). Impaired adult neurogenesis is an early event in Alzheimer's disease neurodegeneration, mediated by intracellular Aβ oligomers. Cell Death Differ *27*, 934–948. https://doi.org/10.1038/s41418-019-0409-3.

Scott-Solomon, E., and Kuruvilla, R. (2020). Prenylation of Axonally Translated Rac1 Controls NGF-Dependent Axon Growth. Developmental Cell *53*, 691-705.e7. https://doi.org/10.1016/j.devcel.2020.05.020.

Serrano-Pozo, A., Frosch, M.P., Masliah, E., and Hyman, B.T. (2011). Neuropathological Alterations in Alzheimer Disease. Cold Spring Harb Perspect Med *1*, a006189. https://doi.org/10.1101/cshperspect.a006189.

Shankar, G.M., Li, S., Mehta, T.H., Garcia-Munoz, A., Shepardson, N.E., Smith, I., Brett, F.M., Farrell, M.A., Rowan, M.J., Lemere, C.A., et al. (2008). Amyloid-β protein dimers isolated directly from Alzheimer's brains impair synaptic plasticity and memory. Nat Med *14*, 837–842. https://doi.org/10.1038/nm1782.

Shepherd, G.M., Chen, W.R., Willhite, D., Migliore, M., and Greer, C.A. (2007). The olfactory granule cell: From classical enigma to central role in olfactory processing. Brain Research Reviews *55*, 373–382. https://doi.org/10.1016/j.brainresrev.2007.03.005.

Shi, Z., Geng, Y., Liu, J., Zhang, H., Zhou, L., Lin, Q., Yu, J., Zhang, K., Liu, J., Gao, X., et al. (2018). Single-cell transcriptomics reveals gene signatures and alterations associated with aging in distinct neural stem/progenitor cell subpopulations. Protein Cell *9*, 351–364. https://doi.org/10.1007/s13238-017-0450-2.

Shingo, T. (2003). Pregnancy-Stimulated Neurogenesis in the Adult Female Forebrain Mediated by Prolactin. Science *299*, 117–120. https://doi.org/10.1126/science.1076647.

Shirakawa, R., Goto-Ito, S., Goto, K., Wakayama, S., Kubo, H., Sakata, N., Trinh, D.A., Yamagata, A., Sato, Y., Masumoto, H., et al. (2020). A SNARE geranylgeranyltransferase essential for the organization of the Golgi apparatus. EMBO J *39*, e104120. https://doi.org/10.15252/embj.2019104120.

Shuman, S. (2020). Transcriptional interference at tandem lncRNA and protein-coding genes: an emerging theme in regulation of cellular nutrient homeostasis. Nucleic Acids Research *48*, 8243–8254. https://doi.org/10.1093/nar/gkaa630.

Sinensky, M., Fantle, K., Trujillo, M., McLain, T., Kupfer, A., and Dalton, M. (1994). The processing pathway of prelamin a. Journal of Cell Science *107*, 61–67. https://doi.org/10.1242/jcs.107.1.61.

Siopi, E., Denizet, M., Gabellec, M.-M., Chaumont, F. de, Olivo-Marin, J.-C., Guilloux, J.-P., Lledo, P.-M., and Lazarini, F. (2016). Anxiety- and Depression-Like States Lead to Pronounced Olfactory Deficits and Impaired Adult Neurogenesis in Mice. J. Neurosci. *36*, 518–531. https://doi.org/10.1523/JNEUROSCI.2817-15.2016.

Solski, P.A., Helms, W., Keely, P.J., Su, L., and Der, C.J. (2002). RhoA Biological Activity Is Dependent on Prenylation but Independent of Specific Isoprenoid Modification. Cell Growth Differ *13*, 363–373. .

Soto, J.S., Jami-Alahmadi, Y., Chacon, J., Moye, S.L., Diaz-Castro, B., Wohlschlegel, J.A., and Khakh, B.S. (2023). Astrocyte–neuron subproteomes and obsessive–compulsive disorder mechanisms. Nature *616*, 764–773. https://doi.org/10.1038/s41586-023-05927-7.

Strachan, T., and Read, A.P. (1994). PAX genes. Current Opinion in Genetics & Development *4*, 427–438. https://doi.org/10.1016/0959-437X(94)90032-9.

Strebel, A., Harr, T., Bachmann, F., Wernli, M., and Erb, P. (2001). Green fluorescent protein as a novel tool to measure apoptosis and necrosis. Cytometry *43*, 126–133. https://doi.org/10.1002/1097-0320(20010201)43:2%253C126::AID-CYTO1027%253E3.0.CO;2-J.

Struhl, K. (2007). Transcriptional noise and the fidelity of initiation by RNA polymerase II. Nat Struct Mol Biol *14*, 103–105. https://doi.org/10.1038/nsmb0207-103.

Stuart, S.A., and Robinson, E.S.J. (2015). Reducing the stress of drug administration: implications for the 3Rs. Sci Rep *5*, 14288. https://doi.org/10.1038/srep14288.

Stutterd, C.A., and Leventer, R.J. (2014). Polymicrogyria: A common and heterogeneous malformation of cortical development. American Journal of Medical Genetics Part C: Seminars in Medical Genetics *166*, 227–239. https://doi.org/10.1002/ajmg.c.31399.

Südhof, T.C., Russell, D.W., Brown, M.S., and Goldstein, J.L. (1987). 42 bp element from LDL receptor gene confers end-product repression by sterols when inserted into viral TK promoter. Cell *48*, 1061–1069. https://doi.org/10.1016/0092-8674(87)90713-6.

Suhonen, J.O., Peterson, D.A., Ray, J., and Gage, F.H. (1996). Differentiation of adult hippocampus-derived progenitors into olfactory neurons in vivo. Nature *383*, 624–627. https://doi.org/10.1038/383624a0.

Sun, B., Chang, E., Gerhartl, A., and Szele, F.G. (2018). Polycomb Protein Eed is Required for Neurogenesis and Cortical Injury Activation in the Subventricular Zone. Cereb Cortex *28*, 1369–1382. https://doi.org/10.1093/cercor/bhx289.

Sun, B., Wang, M., Hoerder-Suabedissen, A., Xu, C., Packer, A.M., and Szele, F.G. (2022). Intravital imaging of the murine subventricular zone with three photon microscopy. Cereb Cortex *32*, 3057–3067. https://doi.org/10.1093/cercor/bhab400.

Sun, X., Sun, X., Liu, T., Zhao, M., Zhao, S., Xiao, T., Jolkkonen, J., and Zhao, C. (2015). Fluoxetine enhanced neurogenesis is not translated to functional outcome in stroke rats. Neuroscience Letters *603*, 31–36. https://doi.org/10.1016/j.neulet.2015.06.061.

Sung, P.-S., Lin, P.-Y., Liu, C.-H., Su, H.-C., and Tsai, K.-J. (2020). Neuroinflammation and Neurogenesis in Alzheimer's Disease and Potential Therapeutic Approaches. International Journal of Molecular Sciences *21*, 701. https://doi.org/10.3390/ijms21030701.

Sunkin, S.M., Ng, L., Lau, C., Dolbeare, T., Gilbert, T.L., Thompson, C.L., Hawrylycz, M., and Dang, C. (2013). Allen Brain Atlas: an integrated spatio-temporal portal for exploring the central nervous system. Nucleic Acids Res *41*, D996–D1008. https://doi.org/10.1093/nar/gks1042.

Sur, S., and Ray, R.B. (2021). Emerging role of lncRNA ELDR in development and cancer. The FEBS Journal *n/a*. https://doi.org/10.1111/febs.15876.

Sur, S., Nakanishi, H., Steele, R., Zhang, D., Varvares, M.A., and Ray, R.B. (2020). Long non-coding RNA ELDR enhances oral cancer growth by promoting ILF3-cyclin E1 signaling. EMBO Reports *21*, e51042. https://doi.org/10.15252/embr.202051042.

Suzuki, S., Gerhold, L.M., Böttner, M., Rau, S.W., Dela Cruz, C., Yang, E., Zhu, H., Yu, J., Cashion, A.B., Kindy, M.S., et al. (2007). Estradiol enhances neurogenesis following ischemic stroke through estrogen receptors α and β. Journal of Comparative Neurology *500*, 1064–1075. https://doi.org/10.1002/cne.21240.

Szele, F.G., and Chesselet, M.-F. (1996). Cortical lesions induce an increase in cell number and PSA-NCAM expression in the subventricular zone of adult rats. Journal of Comparative Neurology *368*, 439–454. https://doi.org/10.1002/(SICI)1096-9861(19960506)368:3%253C439::AID-CNE9%253E3.0.CO;2-6.

Takahashi, H., Yoshihara, S., and Tsuboi, A. (2018). The Functional Role of Olfactory Bulb Granule Cell Subtypes Derived From Embryonic and Postnatal Neurogenesis. Frontiers in Molecular Neuroscience *11*. .

Talamillo, A., Quinn, J.C., Collinson, J.M., Caric, D., Price, D.J., West, J.D., and Hill, R.E. (2003). Pax6 regulates regional development and neuronal migration in the cerebral cortex. Developmental Biology *255*, 151–163. https://doi.org/10.1016/S0012-1606(02)00046-5.

Tan, A.C., Ashley, D.M., López, G.Y., Malinzak, M., Friedman, H.S., and Khasraw, M. (2020). Management of glioblastoma: State of the art and future directions. CA: A Cancer Journal for Clinicians *70*, 299–312. https://doi.org/10.3322/caac.21613.

Thomas, M., White, R.L., and Davis, R.W. (1976). Hybridization of RNA to double-stranded DNA: formation of R-loops. Proc Natl Acad Sci U S A *73*, 2294–2298. .

Tibbit, C.J., Williamson, C.M., Mehta, S., Ball, S.T., Chotalia, M., Nottingham, W.T., Eaton, S.A., Quwailid, M.M., Teboul, L., Kelsey, G., et al. (2015). Antisense Activity across the Nesp Promoter is Required for Nespas-Mediated Silencing in the Imprinted Gnas Cluster. Noncoding RNA *1*, 246–266. https://doi.org/10.3390/ncrna1030246.

Todd, K.L., Baker, K.L., Eastman, M.B., Kolling, F.W., Trausch, A.G., Nelson, C.E., and Conover, J.C. (2017). EphA4 regulates neuroblast and astrocyte organization in a neurogenic niche. J. Neurosci. *37*, 3331–3341. https://doi.org/10.1523/JNEUROSCI.3738-16.2017.

Torigoe, M., Yamauchi, K., Zhu, Y., Kobayashi, H., and Murakami, F. (2015). Association of astrocytes with neurons and astrocytes derived from distinct progenitor domains in the subpallium. Sci Rep *5*, 12258. https://doi.org/10.1038/srep12258.

Trent, S., Fry, J.P., Ojarikre, O.A., and Davies, W. (2014). Altered brain gene expression but not steroid biochemistry in a genetic mouse model of neurodevelopmental disorder. Molecular Autism *5*, 21. https://doi.org/10.1186/2040-2392-5-21.

Trichas, G., Begbie, J., and Srinivas, S. (2008). Use of the viral 2A peptide for bicistronic expression in transgenic mice. BMC Biology *6*, 40. https://doi.org/10.1186/1741-7007-6-40.

Udaondo, Z., Sittikankaew, K., Uengwetwanit, T., Wongsurawat, T., Sonthirod, C., Jenjaroenpun, P., Pootakham, W., Karoonuthaisiri, N., and Nookaew, I. (2021). Comparative Analysis of PacBio and Oxford Nanopore Sequencing Technologies for Transcriptomic Landscape Identification of Penaeus monodon. Life (Basel) *11*, 862. https://doi.org/10.3390/life11080862.

Ugawa, T., Kakuta, H., Moritani, H., Matsuda, K., Ishihara, T., Yamaguchi, M., Naganuma, S., Iizumi, Y., and Shikama, H. (2000). YM-53601, a novel squalene synthase inhibitor, reduces plasma cholesterol and triglyceride levels in several animal species. Br J Pharmacol *131*, 63–70. https://doi.org/10.1038/sj.bjp.0703545.

Ugawa, T., Kakuta, H., Moritani, H., and Inagaki, O. (2002). Effect of YM-53601, a novel squalene synthase inhibitor, on the clearance rate of plasma LDL and VLDL in hamsters. British Journal of Pharmacology *137*, 561–567. https://doi.org/10.1038/sj.bjp.0704906.

Ulaganathan, S., and Pitchaimani, A. (2023). Spontaneous and familial models of Alzheimer's disease: Challenges and advances in preclinical research. Life Sciences *328*, 121918. https://doi.org/10.1016/j.lfs.2023.121918.

Ulicevic, J., Shao, Z., Jasnovidova, O., Bressin, A., Gajos, M., Ng, A.H., Annaldasula, S., Meierhofer, D., Church, G.M., Busskamp, V., et al. (2024). Uncovering the dynamics and consequences of RNA isoform changes during neuronal differentiation. Molecular Systems Biology 1–32. https://doi.org/10.1038/s44320-024-00039-4.

Van Noorden, R. (2023). More than 10,000 research papers were retracted in 2023 — a new record. Nature *624*, 479–481. https://doi.org/10.1038/d41586-023-03974-8.

Vance, J.E., Pan, D., Campenot, R.B., Bussiere, M., and Vance, D.E. (1994). Evidence that the Major Membrane Lipids, Except Cholesterol, Are Made in Axons of Cultured Rat Sympathetic Neurons. Journal of Neurochemistry *62*, 329–337. https://doi.org/10.1046/j.1471-4159.1994.62010329.x.

Vance, K.W., Sansom, S., Lee, S., Chalei, V., Kong, L., Cooper, S., Oliver, P.L., and Ponting, C.P. (2014). The long non-coding RNA Paupar regulates the expression of both local and distal genes. The EMBO Journal *33*, 296–311. https://doi.org/10.1002/embj.201386225.

Vander Heiden, M.G., Cantley, L.C., and Thompson, C.B. (2009). Understanding the Warburg Effect: The Metabolic Requirements of Cell Proliferation. Science *324*, 1029–1033. https://doi.org/10.1126/science.1160809.

Wang, M., and Casey, P.J. (2016). Protein prenylation: unique fats make their mark on biology. Nat Rev Mol Cell Biol *17*, 110–122. https://doi.org/10.1038/nrm.2015.11.

Wang, C., Duan, Y., Duan, G., Wang, Q., Zhang, K., Deng, X., Qian, B., Gu, J., Ma, Z., Zhang, S., et al. (2020). Stress Induces Dynamic, Cytotoxicity-Antagonizing TDP-43 Nuclear Bodies via Paraspeckle LncRNA NEAT1-Mediated Liquid-Liquid Phase Separation. Molecular Cell *79*, 443-458.e7. https://doi.org/10.1016/j.molcel.2020.06.019.

Whitman, M.C., and Greer, C.A. (2007). Adult-generated neurons exhibit diverse developmental fates. Developmental Neurobiology *67*, 1079–1093. https://doi.org/10.1002/dneu.20389.

WHO (2025). Global Dementia Observatory (GDO).

Whyte, D.B., Kirschmeier, P., Hockenberry, T.N., Nunez-Oliva, I., James, L., Catino, J.J., Bishop, W.R., and Pai, J.-K. (1997). K- and N-Ras Are Geranylgeranylated in Cells Treated with Farnesyl Protein Transferase Inhibitors*. Journal of Biological Chemistry *272*, 14459–14464. https://doi.org/10.1074/jbc.272.22.14459.

Wichterle, H., García-Verdugo, J.M., and Alvarez-Buylla, A. (1997). Direct Evidence for Homotypic, Glia-Independent Neuronal Migration. Neuron *18*, 779–791. https://doi.org/10.1016/S0896-6273(00)80317-7.

Winkler, M., Biswas, S., Berger, S.M., Küchler, M., Preisendörfer, L., Choo, M., Früh, S., Rem, P.D., Enkel, T., Arnold, B., et al. (2020). Autism-like behavior in Pianp-deficient mice is associated with decreased neuronal Erdr1 expression and altered GABAB receptor signaling. Mol Psychiatry *25*, 2645–2645. https://doi.org/10.1038/s41380-020-00900-6.

Winner, B., Cooper-Kuhn, C.M., Aigner, R., Winkler, J., and Kuhn, H.G. (2002). Long-term survival and cell death of newly generated neurons in the adult rat olfactory bulb. European Journal of Neuroscience *16*, 1681–1689. https://doi.org/10.1046/j.1460-9568.2002.02238.x.

Wolda, S.L., and Glomset, J.A. (1988). Evidence for modification of lamin B by a product of mevalonic acid. Journal of Biological Chemistry *263*, 5997–6000. https://doi.org/10.1016/S0021-9258(18)68736-8.

Worman, H.J., Fong, L.G., Muchir, A., and Young, S.G. (2009). Laminopathies and the long strange trip from basic cell biology to therapy. J Clin Invest *119*, 1825–1836. https://doi.org/10.1172/JCI37679.

Wright, D.J., Hall, N.A.L., Irish, N., Man, A.L., Glynn, W., Mould, A., Angeles, A.D.L., Angiolini, E., Swarbreck, D., Gharbi, K., et al. (2022). Long read sequencing reveals novel isoforms and insights into splicing regulation during cell state changes. BMC Genomics *23*, 42. https://doi.org/10.1186/s12864-021-08261-2.

Wu, H., Jiang, H., Lu, D., Xiong, Y., Qu, C., Zhou, D., Mahmood, A., and Chopp, M. (2009). Effect of simvastatin on glioma cell proliferation, migration, and apoptosis. Neurosurgery *65*, 1087–1097. https://doi.org/10.1227/01.NEU.0000360130.52812.1D.

Wu, W., Wong, K., Chen, J., Jiang, Z., Dupuis, S., Wu, J.Y., and Rao, Y. (1999). Directional guidance of neuronal migration in the olfactory system by the protein Slit. Nature *400*, 331–336. https://doi.org/10.1038/22477.

Wyss, J.M., Stanfield, B.B., and Cowan, W.M. (1980). Structural abnormalities in the olfactory bulb of the Reeler mouse. Brain Research *188*, 566–571. https://doi.org/10.1016/0006-8993(80)90056-6.

Xie, X.P., Laks, D.R., Sun, D., Poran, A., Laughney, A.M., Wang, Z., Sam, J., Belenguer, G., Fariñas, I., Elemento, O., et al. (2020). High-resolution mouse subventricular zone stem-cell niche transcriptome reveals features of lineage, anatomy, and aging. Proceedings of the National Academy of Sciences *117*, 31448–31458. https://doi.org/10.1073/pnas.2014389117.

Xie, Z., Bailey, A., Kuleshov, M.V., Clarke, D.J.B., Evangelista, J.E., Jenkins, S.L., Lachmann, A., Wojciechowicz, M.L., Kropiwnicki, E., Jagodnik, K.M., et al. (2021). Gene Set Knowledge Discovery with Enrichr. Current Protocols *1*, e90. https://doi.org/10.1002/cpz1.90.

Xing, Y., Wen, X., Ding, X., Fan, J., Chai, P., Jia, R., Ge, S., Qian, G., Zhang, H., and Fan, X. (2017). CANT1 lncRNA Triggers Efficient Therapeutic Efficacy by Correcting Aberrant lncing Cascade in Malignant Uveal Melanoma. Molecular Therapy *25*, 1209–1221. https://doi.org/10.1016/j.ymthe.2017.02.016.

Yan, L., Yang, S., Yue, C.-X., Wei, X.-Y., Peng, W., Dong, Z.-Y., Xu, H.-N., Chen, S.-L., Wang, W.-R., Chen, C.-J., et al. (2020). Long noncoding RNA H19 acts as a miR-340-3p sponge to promote epithelial-mesenchymal transition by regulating YWHAZ expression in paclitaxel-resistant breast cancer cells. Environmental Toxicology *35*, 1015–1028. https://doi.org/10.1002/tox.22938.

Yang, H.K.C., Sundholm-Peters, N.L., Goings, G.E., Walker, A.S., Hyland, K., and Szele, F.G. (2004). Distribution of doublecortin expressing cells near the lateral ventricles in the adult

mouse brain. Journal of Neuroscience Research *76*, 282–295. https://doi.org/10.1002/jnr.20071.

Yao, Y., Wang, X., and Gao, J. (2020). Lncrna kcnq1ot1 sponges mir-206 to ameliorate neural injury induced by anesthesia via up-regulating bdnf. Drug Design, Development and Therapy *14*, 4789–4800. https://doi.org/10.2147/DDDT.S256319.

Yao, Z., van Velthoven, C.T.J., Kunst, M., Zhang, M., McMillen, D., Lee, C., Jung, W., Goldy, J., Abdelhak, A., Aitken, M., et al. (2023). A high-resolution transcriptomic and spatial atlas of cell types in the whole mouse brain. Nature *624*, 317–332. https://doi.org/10.1038/s41586-023-06812-z.

Ya-Ping, Y., Wen-Fu, H., Ya-Yin, T., Ya-Lin, L., Shan, L.E., Ho-Chiang, H., Yen-Chung, C., Ting-Chun, L., Chang, M., Li, J., et al. (2018). Dlk1-Dio3 locus-derived lncRNAs perpetuate postmitotic motor neuron cell fate and subtype identity. eLife *7*. https://doi.org/10.7554/eLife.38080.

Ye, J., Coulouris, G., Zaretskaya, I., Cutcutache, I., Rozen, S., and Madden, T.L. (2012). Primer-BLAST: A tool to design target-specific primers for polymerase chain reaction. BMC Bioinformatics *13*, 134. https://doi.org/10.1186/1471-2105-13-134.

Zambelli, F., Pesole, G., and Pavesi, G. (2009). Pscan: finding over-represented transcription factor binding site motifs in sequences from co-regulated or co-expressed genes. Nucleic Acids Research *37*, W247–W252. https://doi.org/10.1093/nar/gkp464.

Zamboni, M., Llorens-Bobadilla, E., Magnusson, J.P., and Frisén, J. (2020). A Widespread Neurogenic Potential of Neocortical Astrocytes Is Induced by Injury. Cell Stem Cell *27*, 605-617.e5. https://doi.org/10.1016/j.stem.2020.07.006.

Zeisig, R., Koklič, T., Wiesner, B., Fichtner, I., and Sentjurč, M. (2007). Increase in fluidity in the membrane of MT3 breast cancer cells correlates with enhanced cell adhesion *in vitro* and increased lung metastasis in NOD/SCID mice. Archives of Biochemistry and Biophysics *459*, 98–106. https://doi.org/10.1016/j.abb.2006.09.030.

Zeppilli, S., Ackels, T., Attey, R., Klimpert, N., Ritola, K.D., Boeing, S., Crombach, A., Schaefer, A.T., and Fleischmann, A. (2021). Molecular characterization of projection neuron subtypes in the mouse olfactory bulb. eLife *10*, e65445. https://doi.org/10.7554/eLife.65445.

Zhang, M., Zhao, K., Xu, X., Yang, Y., Yan, S., Wei, P., Liu, H., Xu, J., Xiao, F., Zhou, H., et al. (2018). A peptide encoded by circular form of LINC-PINT suppresses oncogenic transcriptional elongation in glioblastoma. Nat Commun *9*, 4475. https://doi.org/10.1038/s41467-018-06862-2.

Zhang, X.-O., Dong, R., Zhang, Y., Zhang, J.-L., Luo, Z., Zhang, J., Chen, L.-L., and Yang, L. (2016). Diverse alternative back-splicing and alternative splicing landscape of circular RNAs. Genome Res *26*, 1277–1287. https://doi.org/10.1101/gr.202895.115.

Zhang, Y., Bejaoui, M., Linh, T.N., Arimura, T., and Isoda, H. (2024). A novel amphiphilic squalene-based compound with open-chain polyethers reduces malignant melanoma metastasis in-vitro and in-vivo. Cell Communication and Signaling *22*, 437. https://doi.org/10.1186/s12964-024-01813-5.

Zhao, J., Sun, B.K., Erwin, J.A., Song, J.-J., and Lee, J.T. (2008). Polycomb Proteins Targeted by a Short Repeat RNA to the Mouse X Chromosome. Science *322*, 750–756. https://doi.org/10.1126/science.1163045.

Zhao, J., Ohsumi, T.K., Kung, J.T., Ogawa, Y., Grau, D.J., Sarma, K., Song, J.J., Kingston, R.E., Borowsky, M., and Lee, J.T. (2010). Genome-wide Identification of Polycomb-Associated RNAs by RIP-seq. Molecular Cell *40*, 939–953. https://doi.org/10.1016/j.molcel.2010.12.011.

CASC15 cancer susceptibility 15 [Homo sapiens (human)] - Gene - NCBI.